

**Some pages of this thesis may have been removed for copyright restrictions.**

If you have discovered material in Aston Research Explorer which is unlawful e.g. breaches copyright, (either yours or that of a third party) or any other law, including but not limited to those relating to patent, trademark, confidentiality, data protection, obscenity, defamation, libel, then please read our [Takedown policy](#) and contact the service immediately (openaccess@aston.ac.uk)

**PHARMACEUTICAL PROCESS OPTIMISATION OF BULK LYOPHILISATES:  
IMPLICATIONS OF POWDER HANDLING**

**EDMOND PETER EKENLEBIE**

**Doctor of Philosophy**

**ASTON UNIVERSITY**

**August 2014**

**© Edmond Peter Ekenlebie, 2014**

**Edmond Peter Ekenlebie asserts his moral right to be identified as the author of this  
thesis.**

**This copy of the thesis has been supplied on condition that anyone who consults it is  
understood to recognise that its copyright rests with its author and that no quotation  
from the thesis and no information derived from it may be published without  
appropriate permission or acknowledgement.**

**Aston University**

**Pharmaceutical Process Optimisation of Bulk Lyophilisates: Implications of Powder Handling**

Edmond Peter Ekenlebie  
Doctor of Philosophy  
August 2014

**Thesis Summary**

Lyophilisation or freeze drying is the preferred dehydrating method for pharmaceuticals liable to thermal degradation. Most biologics are unstable in aqueous solution and may use freeze drying to prolong their shelf life. Lyophilisation is however expensive and has seen lots of work aimed at reducing cost. This thesis is motivated by the potential cost savings foreseen with the adoption of a cost efficient bulk drying approach for large and small molecules.

Initial studies identified ideal formulations that adapted well to bulk drying and further powder handling requirements downstream in production. Low cost techniques were used to disrupt large dried cakes into powder while the effects of carrier agent concentration were investigated for powder flowability using standard pharmacopoeia methods. This revealed superiority of crystalline mannitol over amorphous sucrose matrices and established that the cohesive and very poor flow nature of freeze dried powders were potential barriers to success. Studies from powder characterisation showed increased powder densification was mainly responsible for significant improvements in flow behaviour and an initial bulking agent concentration of 10-15 %w/v was recommended.

Further optimisation studies evaluated the effects of freezing rates and thermal treatment on powder flow behaviour. Slow cooling (0.2 °C/min) with a -25°C annealing hold (2hrs) provided adequate mechanical strength and densification at 0.5-1 M mannitol concentrations. Stable bulk powders require powder transfer into either final vials or intermediate storage closures. The targeted dosing of powder formulations using volumetric and gravimetric powder dispensing systems were evaluated using Immunoglobulin G (IgG), Lactate Dehydrogenase (LDH) and Beta Galactosidase models. Final protein content uniformity in dosed vials was assessed using activity and protein recovery assays to draw conclusions from deviations and pharmacopoeia acceptance values. A correlation between very poor flowability ( $p < 0.05$ ), solute concentration, dosing time and accuracy was revealed. LDH and IgG lyophilised in 0.5 M and 1 M mannitol passed Pharmacopoeia acceptance values criteria with 0.1-4 while formulations with micro collapse showed the best dose accuracy (0.32-0.4% deviation). Bulk mannitol content above 0.5 M provided no additional benefits to dosing accuracy or content uniformity of dosed units. This study identified considerations which included the type of protein, annealing, cake disruption process, physical form of the phases present, humidity control and recommended gravimetric transfer as optimal for dispensing powder. Dosing lyophilised powders from bulk was demonstrated as practical, time efficient, economical and met regulatory requirements in cases.

Finally the use of a new non-destructive technique, X-ray microcomputer tomography (MCT), was explored for cake and particle characterisation. Studies demonstrated good correlation with traditional gas porosimetry ( $R^2 = 0.93$ ) and morphology studies using microscopy. Flow characterisation from sample sizes of less than 1 mL was demonstrated using three dimensional X-ray quantitative image analyses. A platinum-mannitol dispersion model used revealed a relationship between freezing rate, ice nucleation sites and variations in homogeneity within the top to bottom segments of a formulation.

**Key words/phrases:** Lyophilisation, Bulk drying, Particle characterisation, Flowability, Powder technology.

## ***Dedication***

*This thesis is dedicated to my parents Nana Odeneho Peter Miezah Ekenlebie and Mrs Mary Ethel Ama Ekenlebie who have worked ever so hard all their lives to provide me with the best they never had. I wish to also thank my family, loved ones and friends for being with me every step of the journey.*

## **Acknowledgement**

My outmost gratitude to my supervisor Dr Andrew Ingham and associate supervisor Professor Yvonne Perrie for the academic support and advice provided throughout my research.

Professor Landon of MicroPharm UK is acknowledged for the gift of Ovine Sera. Dr Mike Edkins and Dr Dave Seaward of 3P Innovation Limited are acknowledged for access to their newly developed gravimetric dosing system. I wish to also acknowledge the entire technical team at Aston University especially Mr Jiteen Ahmed and Christine Jakeman for technical support.

# Table of Contents

	Page
Title page .....	1
Thesis Summary.....	2
Dedication .....	3
Acknowledgement.....	4
Table of Contents .....	5
Table of Figures.....	11
List of Tables .....	17
<b>1 INTRODUCTION .....</b>	<b>18</b>
1.1 The Pharmaceutical Industry and Freeze drying .....	18
1.2 Freeze drying system components .....	19
1.2.1 Origin .....	19
1.2.2 Freeze drying process.....	19
1.3 Fundamentals of the freeze dryer .....	22
1.3.1 Refrigeration .....	22
1.3.2 Pumps and vacuum .....	23
1.3.3 Types of freeze dryers .....	24
1.3.4 Temperature measurement.....	24
1.4 Efficient Processing of Lyophilised Formulations .....	25
1.4.1 Morphology .....	26
1.4.2 Activity .....	28

1.4.3	Dissolution .....	30
1.4.4	Long-term Storage .....	31
1.4.5	Cost .....	32
1.5	Current state of the art in freeze drying from the patent landscape .....	35
1.5.1	Container systems .....	35
1.5.2	Continuous flow and traditional tray freeze drying .....	39
1.6	Characterising freeze dried powders.....	41
1.6.1	Flow properties of bulk solids .....	41
1.7	Powder dispensers .....	47
1.8	Material visualisation through tomography .....	47
<b>2</b>	<b>THESIS AIMS AND OBJECTIVES .....</b>	<b>49</b>
<b>3</b>	<b>MATERIALS AND METHODS .....</b>	<b>52</b>
3.1	Preparation of active pharmaceutical ingredient.....	52
3.2	Pre-formulation characterisation .....	52
3.2.1	Collapse point and eutectic melt determination .....	52
3.2.2	Differential scanning calorimetry .....	54
3.3	Lyophilisation process design .....	56
3.4	Post freeze drying characterisation .....	58
3.4.1	Dried sample transfer and moisture control through isolation .....	58
3.4.2	Karl Fischer coulometric analysis .....	59
3.4.3	Helium pycnometry .....	61
3.4.4	Light microscopy .....	62

3.4.5	Mechanical sieving and laser light diffraction.....	63
3.4.6	X-ray powder diffraction .....	64
3.4.7	Bicinchoninic acid assay (BCA).....	65
3.4.8	Lactate dehydrogenase activity assay.....	66
3.4.9	Fluorescence quenching assay.....	67
3.4.10	Flowability characterisation .....	67
3.4.11	Lyophilised powder dispensing.....	72
3.4.12	Micro Computer Tomography.....	74
3.4.13	Statistical analysis.....	75
<b>4</b>	<b>INVESTIGATING THE FLOW BEHAVIOUR OF BULK LYOPHILATES .....</b>	<b>76</b>
4.1	Introduction.....	76
4.2	Aim and Objectives.....	80
4.3	EFFECT OF SOLUTE CONCENTRATION ON FLOWABILITY OF BULK FREEZE DRIED POWDERS.....	81
4.3.1	Materials and Methods.....	81
4.3.2	Results.....	84
4.3.3	Discussion.....	96
4.3.4	Conclusion .....	101
4.4	EFFECT OF FREEZING RATE AND THERMAL TREATMENT ON FLOWABILITY OF BULK FREEZE DRIED POWDERS.....	102
4.4.1	Background.....	102
4.4.2	Materials and Methods.....	102
4.4.3	Results.....	105

4.4.4	Discussion.....	118
4.4.5	Conclusion .....	122
<b>5</b>	<b>DISPENSING OF BULK LYOPHILATES FOR VIAL OR AMPOULE ENCLOSURE .....</b>	<b>123</b>
5.1	Introduction.....	123
5.2	Aim and Objectives.....	125
5.3	VOLUMETRIC AND GRAVIMETRIC DISPENSING USING ACCOFIL AND QUANTOS DOSING SYSTEM .....	126
5.3.1	Materials and Methods.....	126
5.3.2	Results.....	131
5.3.3	Discussion.....	142
5.3.4	Conclusion .....	144
5.4	GRAVIMETRIC DISPENSING OF BULK LYOPHILATES USING THE FILL2WEIGHT™ SYSTEM.....	145
5.4.1	Background.....	145
5.4.2	Materials and Methods.....	145
5.4.3	Results.....	150
5.4.4	Discussion.....	163
5.4.5	Conclusion .....	167
<b>6</b>	<b>X-RAY MICRO COMPUTER TOMOGRAPHY STUDIES OF LYOPHILISED POWDER FOR DETERMINATION OF FLOW CHARACTERISTICS AND DOSE UNIFORMITY OF ACTIVE PHARMAEUTICAL INGREDIENTS .....</b>	<b>169</b>
6.1	Introduction.....	169

6.2 Aims and Objectives .....	171
6.3 STUDY OF POROSITY, PACKING AND MORPHOMETRIC PARAMETERS IN BULK LYOPHILISED POWDERS.....	172
6.3.1 Background.....	172
6.3.2 Materials and Methods.....	172
6.3.3 Results.....	175
6.3.4 Discussion.....	191
6.3.5 Conclusion .....	196
6.4 INVESTIGATIONS INTO LOCALISATION OF ACTIVE PHARMACEUTICALS IN LYOPHILISED FORMULATIONS .....	197
6.4.1 Background.....	197
6.4.2 Materials and Methods.....	198
6.4.3 Results.....	201
6.4.4 Discussion.....	213
6.4.5 Conclusion .....	217
<b>7 FINAL CONCLUSIONS AND IMPLICATIONS .....</b>	<b>218</b>
<b>8 REFERENCES .....</b>	<b>222</b>
<b>Appendix I: Standard operating procedure for IgG purification .....</b>	<b>238</b>
<b>Appendix II: Standard operating procedure for porosity investigation .....</b>	<b>244</b>
<b>Appendix III: Standard operating procedure for lactate dehydrogenase assay.....</b>	<b>248</b>
<b>Appendix IV: Standard operation procedure for optimisation of quenching assay .</b>	<b>252</b>
<b>Appendix V: Standard operating procedure for quenching assay .....</b>	<b>256</b>
<b>Appendix VI: Typical freeze drying cycle plot for samples .....</b>	<b>261</b>

<b>Appendix VII: Cycle plot for samples studied with microcomputer tomography .....</b>	<b>264</b>
<b>Appendix VIII: Typical MDSC thermographs.....</b>	<b>266</b>

## Table of Figures

	<b>Page</b>
Figure 1.1: Phase diagram of water.....	20
Figure 1.2: Schematic of a solution undergoing bulk freeze drying in a tray.....	21
Figure 1.3: Three-dimensional cross-sectional X-ray MCT into packed powders.....	27
Figure 1.4: Schematic of container systems disclosed by GE Healthcare.....	36
Figure 1.5: Schematic of container closures and reconstitution syringe.....	37
Figure 1.6: Schematic of bulk drying containers.....	38
Figure 1.7: Schematic of the types of available flow characterisation methods.....	42
Figure 1.8: Representation of transmission tomography within a single slice.....	48
Figure 3.1: Schematic representation of a freeze drying microscope stage.....	53
Figure 3.2: Laboratory scale Virtis Advantage freeze dryer.....	57
Figure 3.3: Schematic representation of bulk drying tray containers.....	57
Figure 3.4: Schematic of custom designed 2 gloves polyurethane flexible isolator.....	58
Figure 3.5: Schematic representation of a gas multipycnometer.....	61
Figure 3.6: Particle size analysis by mechanical sieving.....	63
Figure 3.7: Typical calibration plot for bovine serum albumin analysed by BCA assay.....	67
Figure 3.8: Schematic of an angle of repose experimental set up.....	69
Figure 3.9: Exploded schematic of shear cell arrangement of a Brookfield flow tester.....	71
Figure 3.10: Experimental set up of Quantos gravimetric dosing system.....	72
Figure 3.11: Schematic of experimental set up using the Accofil volumetric dispensing system.....	73
Figure 3.12: Experimental set up of Fill2weight™ gravimetric dosing system.....	74
Figure 4.1: Section of the hexagonal packing of vials on a typical freeze dryer shelf.....	77

Figure 4.2: Compressibility index and porosity of freeze dried mannitol and sucrose from 1-15 %w/v solutions. ....	85
Figure 4.3: Moisture content (mean $\pm$ SD) of bulk freeze dried mannitol and sucrose powders from 1-15 %w/v solutions.....	87
Figure 4.4: Bulk density (mean $\pm$ SD) of bulk freeze dried mannitol and sucrose powders from 1-15 %w/v solutions. ....	88
Figure 4.5: Cumulative particle oversize distribution of freeze dried mannitol from solutions of 3-15 %w/v and freeze dried sucrose from 10 %w/v and 15 %w/v solutions.	90
Figure 4.6: Light microscope images of freeze dried particles from 1 %w/v mannitol .....	91
Figure 4.7: Light microscope images of freeze dried particles from 5 %w/v mannitol .....	92
Figure 4.8: Light microscope images of freeze dried mannitol from 15 %w/v mannitol .....	93
Figure 4.9: Focal plane stacked light microscope images of fluid bed dried mannitol .....	94
Figure 4.10: Correlation between compressibility index (CI) of powders and Top: moisture content and Porosity. Bottom: Median particle size and Bulk density. ....	95
Figure 4.11: Moisture content for bulk freeze dried mannitol from 0.056-1 M solutions.....	106
Figure 4.12: Effect of freezing rate and thermal treatment on compressibility index of bulk freeze dried mannitol from 0.056-1 M solution .....	107
Figure 4.13 Effect of cooling rate and thermal treatment on angle of repose of bulk freeze dried mannitol from 0.056-1 M solution .....	109
Figure 4.14: Effect of cooling rate and thermal treatment on bulk density of bulk freeze dried mannitol from 0.056-1 M solution. ....	110
Figure 4.15: Effect of freezing rate and thermal treatment on porosity of bulk freeze dried mannitol from 0.056-1 M solution. ....	111
Figure 4.16: Particle sizing analysis of bulk freeze dried mannitol from 0.056 M-1 M solution with varied thermal treatment and powder breaking .....	112

Figure 4.17: Median particle sizes of bulk freeze dried mannitol from 0.056-1 M solution with varied thermal treatment and powder breaking .....	113
Figure 4.18: Schematic of disruption process of sections of bulk freeze dried mannitol cake dried from solution with varied cooling rates and thermal treatment. ....	113
Figure 4.19: Light microscope images at x100 magnification for powders freeze dried from mannitol solutions .....	114
Figure 4.20: Typical stress data for bulk lyophilised mannitol from 1 M solution at a slow cooling rate of 0.2 °C/min.....	115
Figure 4.21: Flow function curve of bulk lyophilised powders from 1 M mannitol solution at different cooling rates compared to fluid bed dried mannitol and sucrose. ....	116
Figure 4.22: Freeze dried mannitol powder adhered to shear cell.....	117
Figure 5.1: Variation in powder mass transfer using gravimetric dispenser .....	132
Figure 5.2: Left: Mean deviation from the target dose as dispensed with the Quantos system Right: Activity of dosed freeze dried Mannitol IgG.....	133
Figure 5.3: IgG activity recovered (n = 4) of dosed freeze dried Mannitol IgG lyophilised from 15 %w/v solution.....	134
Figure 5.4: Automated dosing time of bulk lyophilised mannitol (MAN), sucrose (SUC), vial lyophilised mannitol with IgG (MAN IgG), sucrose with IgG (SUC IgG) and with beta galactosidase (SUC BGAL) from different %w/v solutions.....	135
Figure 5.5: Variation in powder mass transfer using a volumetric dispenser (Accofil) .....	136
Figure 5.6: Bulk density and porosity of dosed bulk lyophilised mannitol (MAN) and from 1 %w/v and 15 %w/v solutions .....	137
Figure 5.7: Compressibility index (mean $\pm$ SD) of dosed formulations freeze dried from different concentrations (%w/v) of mannitol solution.....	137
Figure 5.8: Total manual operation time of bulk lyophilised mannitol (MAN), sucrose (SUC), IgG and LDH formulations.....	138

Figure 5.9: X-ray powder diffraction of A: IgG freeze dried in mannitol (I) and sucrose (II) solution and fluid bed dried sucrose (B) and mannitol (C). .....	139
Figure 5.10: Appearance of dosed formulations.....	140
Figure 5.11: Gravimetric or mass filled lyophilised powder losses due to sticking to inner walls of dosing head (A) and brim of glass vial (B).....	141
Figure 5.12: Typical images and temperature profile from freeze drying microscopy analysis of LDH in 0.5 M sucrose solution. ....	151
Figure 5.13: Mean deviations from target doses (n = 40) of lyophilised IgG from 0.5 M,1 M mannitol (MAN) and varied molar ratios of mannitol and sucrose solutions containing lactate dehydrogenase (LDH MAN:SUC).....	152
Figure 5.14: Left: Variation in mass of powder transfer. Right: Compressibility index of the same bulk lyophilised formulations (n = 3) of mannitol (MAN) from 1 M solutions containing IgG and LDH.....	152
Figure 5.15: Variation in mass of powder transfer using Fill2weight gravimetric dispenser. ....	153
Figure 5.16: Porosity and bulk density of dosed bulk lyophilised IgG and LDH from 0.5 M,1 M mannitol (MAN) and varied molar ratios of mannitol (MAN) and sucrose (SUC) solutions.....	153
Figure 5.17: Particle size distribution of formulations freeze dried from 1 M mannitol (MAN) and varied molar ratios of mannitol and sucrose (LDH MAN:SUC). ....	155
Figure 5.18: Polarised light microscopy images of F2W gravimetric dispensed powders at x100 magnification A) IgG 0.5 M MAN B) IgG 1 M MAN C) LDH MAN:SUC 1:1 D) Fluid bed dried mannitol. ....	156
Figure 5.19: Polarised light microscopy images of F2W gravimetric dispensed powders at x100 magnification E) LDH 0.5 M MAN F) LDH 1 M MAN G) LDH MAN:SUC (5:1) H) LDH MAN:SUC 5:2 .....	157

Figure 5.20: Polarised light microscopy images of F2W gravimetric dispensed powders ..	158
Figure 5.21: Total protein content with % relative standard deviation .....	159
Figure 5.22: Total protein and activity recovery in mass dosed LDH formulations .....	160
Figure 5.23: Left: Compressibility index of bulk lyophilised formulation prior to mass dispensing. Right: Moisture content of bulk freeze dried formulations and fluid bed dried mannitol and sucrose. ....	161
Figure 6.1: Typical results from MCT scans and 2D morphometric analysis for packed fluid bed dried sucrose .....	175
Figure 6.2: Porosity and particle density of lyophilised mannitol using helium (He) and nitrogen (N <sub>2</sub> ) as pycnometric gases. ....	176
Figure 6.3: Porosity of bulk lyophilised mannitol from solution using X-ray MCT .....	177
Figure 6.4: Porosity correlation study 1. Correlative plot of helium pycnometry and X-ray microcomputer tomography (MCT) porosity measurements for powders from bulk lyophilised mannitol .....	177
Figure 6.5: Three dimensional cross-sectional X-ray MCT into packed powders.....	178
Figure 6.6: Three dimension cross-sectional X-ray MCT images of mannitol lyophilised from solutions .....	180
Figure 6.7: Helium pycnometry and X-ray MCT computer tomography porosity measurements for powders from bulk lyophilised mannitol .....	181
Figure 6.8: Porosity correlation study 2. Correlative plot of helium pycnometry and X-ray MCT porosity measurements for powders from bulk lyophilised mannitol .....	183
Figure 6.9: Cumulative undersize distribution using structure thickness from MCT. ....	184
Figure 6.10: Structural model Index (SMI) investigations into effect of cooling rate and annealing on the morphology of lyophilised mannitol (MAN) powder.....	186
Figure 6.11: Picture of standard shapes used in structural model index morphometric parameter in MCT studies.....	186

Figure 6.12: Three dimension X-ray tomography models .....	187
Figure 6.13: Light microscope images at x100 magnification for powders freeze dried from mannitol solutions .....	189
Figure 6.14: Fragmentation index investigation into effect of cooling rate and annealing on fragmentation index of lyophilised mannitol (MAN) powder. ....	189
Figure 6.15: X-ray microcomputer tomographic investigation into effect of freezing rate and annealing on fractal dimension of lyophilised mannitol (MAN) powder. ....	190
Figure 6.16: Experimental set up for lyophilisation of optimised 1 M mannitol platinum dispersions.....	199
Figure 6.17: Optimisation of platinum dispersion stability for freezing studies with X-ray microcomputer tomography. ....	201
Figure 6.18: X-ray microcomputer tomographic investigation into effect of cooling rate on number of platinum particulate model localisation in lyophilised mannitol (MAN) cake .....	203
Figure 6.19: X-ray microcomputer tomographic investigation into effect of freezing rate on volume of platinum particulate model localisation in lyophilised mannitol (MAN) cake. ....	204
Figure 6.20: X-ray microcomputer tomographic investigation into effect of quench cooling and fast cooling rate on platinum in lyophilised mannitol (MAN) cake .....	210
Figure 6.21: X-ray microcomputer tomographic investigation into effect of medium cooling rate of 1.5°C (Mid) on platinum in lyophilised mannitol (MAN) cake. ....	211
Figure 6.22: Relative volume colour scale distribution of platinum within freeze dried mannitol .....	212

## List of Tables

	<b>Page</b>
Table 4.1: Calculation of the volume of dryer shelf not used when filled using the hexagonal arrangement of vials on different freeze dryer shelves .....	78
Table 4.2: Mannitol and Sucrose powders densities .....	89
Table 4.3: Flow index determined from shear cell measurements of powders bulk lyophilised from 0.5 M mannitol (Man) solution.....	117
Table 5.1: Moisture content of formulations dosed using gravimetric (quantos) and volumetric (accofil) powder dispensing systems.....	131
Table 5.2: Moisture content of vial lyophilised formulations dosed using gravimetric (quantos) powder dispensing system .....	131
Table 5.3: Content uniformity and calculated acceptance values of dosed formulations ..	162
Table 6.1: Bulk and true density measurements of bulk lyophilised mannitol by helium pycnometry in powder packing study 1.....	179
Table 6.2: Median over size distribution of powder measured from analytical sieving and MCT .....	185
Table 6.3: Observed nucleation events and calculated rates for mannitol only and mannitol-platinum dispersions from product freeze drying cycle plots. ....	205

# 1 INTRODUCTION

## 1.1 The Pharmaceutical Industry and Freeze drying

There is continued movement for protein research as potential therapeutics due to progress made in understanding their role in the human body and the ease of production in large volumes (Sarciaux *et al.*, 1995). Most proteins are unstable in aqueous solution and may use freeze drying to prolong their shelf life. Freeze drying or lyophilisation is a drying process used for converting solutions of labile materials into dry solids of sufficient stability for distribution and storage (Pikal, 2007). By the end of 2003, lyophilised biologicals contributed to 46% of all US Food and Drug Administration (FDA) market approvals in the biopharmaceuticals category which include vaccines, proteins and peptides (Costantino and Pikal, 2004). Proteins and peptides are the most rapidly growing class of drugs and had an increased growth rate globally in 2009 of 10.9% (Yang *et al.*, 2009). Formulation strategies for current FDA approved vaccines including those adopting freeze drying to overcome the cold chain have been reviewed (Kumru *et al.*, 2014). Many studies also continue to focus on molecular dynamics in proteins and their freeze drying behaviour in highly concentrated formulations (Geidobler *et al.*, 2013, Xu *et al.*, 2014, Hill *et al.*, 2014).

The demand for freeze drying is not expected to slow over the next decade as many smaller freeze drying entities or contract manufacturers continue to invest time into acquiring intellectual property along wider business themes. The global market for lyophilisation has been forecasted to be worth \$3.25bn by 2015 (Visiongain, 2011).

Freeze drying to date has continued to offer numerous benefits over other drying methods which include evaporative and spray drying processes (Walters *et al.*, 2014). Freeze drying is a widely accepted method for drying of injectable, offering sterility control from fill to finish; it provides the least thermal degradation, controls moisture in the final product as well as allowing easier resolution of scale up problems (Pikal, 2007). Freeze drying is however

financially expensive (Ratti, 2001, Niazi K. Sarfaraz, 2004) and processes targeted at cost reduction are highly welcomed by manufacturers. This has been the motivation of many studies in literature and includes this thesis.

## **1.2 Freeze drying system components**

### **1.2.1 Origin**

Centuries before the term freeze drying or lyophilisation was coined, the Peruvian Incas harnessed the sun's radiative heat energy together with the low pressure afforded at high altitudes to dehydrate frozen meat (Rey and May, 1999). The history of freeze drying or lyophilisation has been discussed (Rey and May, 1999); with much of the pioneering contributions in the early 20<sup>th</sup> century. The term lyophilisation was coined in 1935 and was used for the large scale drying of human plasma during World War 2. Initial reports of success for drying vaccines and antibiotics were also mentioned.

### **1.2.2 Freeze drying process**

The freeze drying process is comprised of three main stages: freezing, primary drying and secondary drying. An equilibration step is often included prior to beginning the freezing process to assure all liquids are at the same temperature. This involves keeping a formulation batch usually at room temperature for a short period before initialising chilling. This is to a lesser extent a measure to minimise batch variation although the control of ice nucleation (control of ice crystal formation and growth) or annealing (thermal hold treatment) in batches will be required to minimise inter and intra batch variation.

The underpinning principle of freeze drying surrounds an understanding of the phase diagram of water (Figure 1.1). A liquid formulation solidifies during freezing which must be complete before a vacuum is pulled to prevent frothing (Aulton, 2007).

A frozen product is then supplied with heat energy (latent heat of sublimation) at the primary drying stage using a vacuum pressure below the triple point of water.

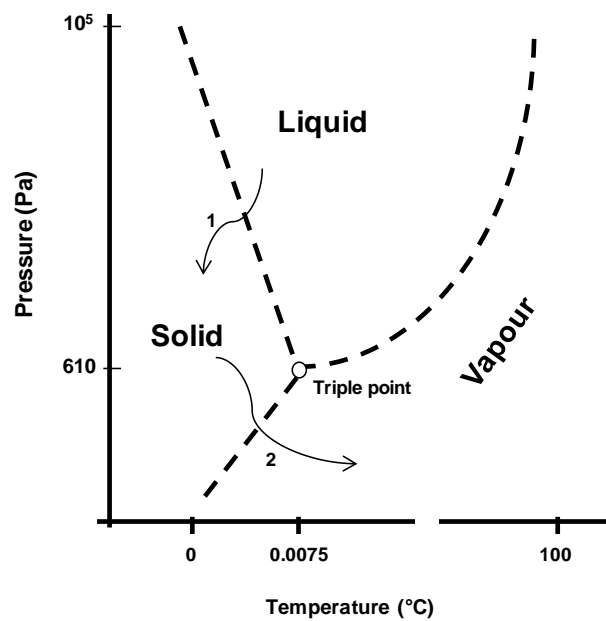


**Figure 1.1: Phase diagram of water. Under reduced pressure below 610Pa, liquid frozen (1) to solid (ice) can be converted to vapour via sublimation (2) by supplying heat energy (heat of sublimation). Image adapted from Aulton (2007).**

For sublimation to occur, the heat of sublimation of ice which is 2900 KJkg<sup>-1</sup> must be supplied (Aulton, 2007). At the end of the sublimation (primary drying stage), all bulk ice is removed and any remaining moisture is removed by desorption during the secondary drying stage which can require higher elevated temperatures. The economics of the freeze drying process are driven largely by the primary drying stage which can be slow and last for long periods depending on the chosen freeze drying cycle parameters.

Sadikoglu and Liapis (1997) modelled primary and secondary drying stages of a bulk solution freeze dried in a tray to describe the transport mechanism of water vapour and inert gases through the pores of a bulk dried layer (Figure 1.2). Experimental and mathematical model showed the major mechanism of mass transfer were the removal of bound water from the solute phase, Knudsen diffusion and bulk diffusion.

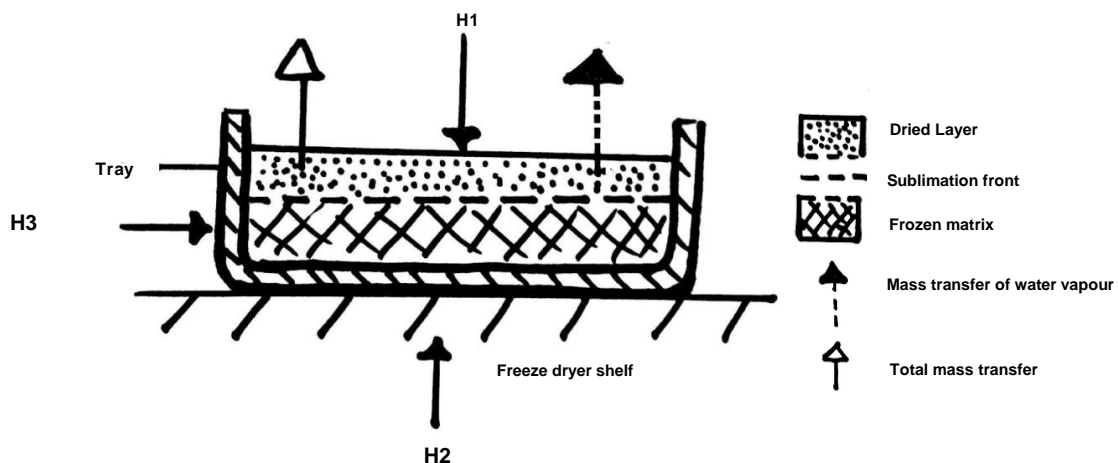


**Figure 1.2: Schematic of a solution undergoing bulk freeze drying in a tray. Heat supplied to the surface of the dried layer (H1) is by conduction, convection or radiation from the gaseous composition in the drying chamber. Thermal transfer from the shelf (H2) is by conduction through the bottom of tray subsequently through the frozen matrix towards the sublimation front. H3 represents the amount of heat in the vertical sides of the tray or thermal transfer between the drying chamber and vertical sides of the tray. Total mass flux is the sum of mass transfer of water vapour and inert gas. H3 is relatively negligible and less than H1 or H2. Image adapted from Sadikoglu and Liapis (1997).**

Lyoprotectant protection of proteins during freeze drying is by either the vitrification or water replacement hypotheses. But neither mechanism in isolation can fully explain lyoprotection (Li *et al.*, 2005). The vitrification hypothesis assumes a rigid glass matrix is formed by excipients and immobilises the protein mechanically. This results in a restriction of translational and relaxation processes capable of protein unfolding and spatial separation between protein molecules thus preventing aggregation (Li *et al.*, 2005). The water

replacement hypothesis proposes that hydrogen bonds are formed between excipients, polar and charged groups on proteins prior to the drying process which replace previous bonds with water. Carpenter and Crowe (1989) showed the  $1583\text{ cm}^{-1}$  band of lysozyme from fourier transform infrared (FTIR) due to hydrogen bonding of water to the carboxylate groups was absent after lyophilisation. Lysozyme however was found to retain the band when dried in the presence of sucrose.

It's important to stress the importance of the choice of formulation components as it influences attributes of the final dried cake because a poor formulation will yield a dried cake of questionable quality.

### **1.3 Fundamentals of the freeze dryer**

Acquisition of freeze drying equipment is a large capital investment. Machine cost together with the man hours and long product drying times make the process expensive. Freeze dryers consist of a refrigeration unit made up of shelves, a condenser and vacuum pump attachment. The drying chamber houses the shelves which hold the products and typically a condenser which may be beneath the shelf or externally positioned.

#### **1.3.1 Refrigeration**

Refrigeration is required for cooling the shelf and process condenser using either compressed gases (conventional refrigeration) or liquid nitrogen options. A conventional refrigeration unit is comprised of a compressor, condenser heat exchanger, capillary or expansion valve and evaporative heat exchanger (Wood, 2000). The refrigerant which is initially a low pressure vapour is compressed by a reciprocating compressor into a high pressure vapour. This is discharged to a condenser heat exchanger where it is condensed

into a high pressure warm liquid before being passed on through a capillary or expansion valve. The latter is responsible for regulating flow to the evaporator and reduces the pressure of the liquid refrigerant. At the evaporative heat exchanger, the now cold low pressure liquid received from the expansion valve is evaporated into a gas. The latent heat of evaporation required is obtained from the freeze dryer's circulating silicone oil within the evaporator which cools the dryer. The vapour is pumped back into the compressor and the refrigeration cycle continues.

The process condenser typically attains extremely low temperatures in the range of  $-70^{\circ}\text{C}$  to  $-75^{\circ}\text{C}$  before the start of primary drying. The resulting temperature differential between the drying chamber and the process condenser is a driver for the collection of sublimed gases onto the condenser surface. The other driver is the lower vapour pressure at the condenser compared to the product. Condenser capacity is usually specified as the maximum amount of water in litres it is capable of holding on its surface, and is referred to as the ice capacity. It may be designed as a coil or plate and found either internal or external to the freeze dryer chamber.

### **1.3.2 Pumps and vacuum**

A vacuum pump is required to attain chamber pressures below the triple point of water where gas, liquid and solid phases exist in equilibrium. Vacuum pumps vary in their mode of operation and can be grouped into two main classes (Umrath, 2007). A class of pumps work using compression stage(s) to remove gas molecules from the chamber followed by ejection using displacement or pulse transfer into the atmosphere. The other class removes the gas molecules by condensation or other means of bonding onto a surface (Umrath, 2007).

A two stage rotary vane pump which is a form of compression pump was used in these studies, capable of pulling vacuums of up to 0.001 mbar. Other types of compression

vacuum pumps include root, turbo molecular and vapour pumps (Umrath, 2007) which may pull greater vacuums but are of specific use typically for small volume systems.

Pirani gauge and capacitance manometers are the commonly used pressure measurement tools (Patel *et al.*, 2010). Both measure pressure with specific limitations. These limitations now form part of a commonly used process analytical tool (PAT) in freeze drying to monitor the process.

### **1.3.3 Types of freeze dryers**

Freeze dryers differ in size, total shelf area, condenser capacity, condenser type (Plate or coil), position of the condenser (external or internal) and can be broadly categorised into bench top, pilot and production scale dryers (SP Scientific, 2014c). Some bench top dryers are often used in research and have condenser ice capacities in the range of 3-9 litres. Bench top dryers support vertical and drum manifolds which are useful for drying materials on tray racks or in flask attachments. Here the condenser is usually internally positioned. Production or commercial scale dryers are considered the largest freeze dryers with predominately externally positioned condensers with ice capacities in excess of 40-800 litres. Pilot dryers are commonly used for production of products during clinical trials and are useful for small entities or small contract manufacturers. The design specification for pilot scale machines is between the bench and production scale dryers.

### **1.3.4 Temperature measurement**

The temperature of the product throughout the freeze drying process is an important variable. Thermocouples are inserted at the bottom of product vials to inform the product temperature during cycles. Thermocouples are made of two different metal alloys connected

at a point called a hot junction (Morris and Langari, 2012, Kerlin and Johnson, 2012). This junction maintains a voltage difference (emf) which is measured at the open end of the thermocouple known as the reference junction (Morris and Langari, 2012, Kerlin and Johnson, 2012)

The American Society for Testing and Materials (ASTM) have standardised letters (J, T, K, E, N, C, S, R, and B) assigned to the various types of metal based on their emf-temperature behaviour and not the alloy composition (Kerlin and Johnson, 2012). K type thermocouples made of nickel and alumel were used in our laboratory together with an eight channel data logger for monitoring the complete temperature profile drying cycles. K type thermocouples are useful across the temperature range of -200 to +1300°C within an accuracy of  $\pm 0.75^{\circ}\text{C}$  (Morris and Langari, 2012). They are not the most accurate at low temperatures but provide the best range for measurement at ambient temperatures and throughout freezing and drying.

Resistive Temperature Detectors (RTDs) and thermistors are resistive temperature measurement devices which use a change in electrical resistance to measure temperature. RTDs show a linear relation for metals such as platinum, nickel and copper over a limited range to produce a measurable change in resistance as a function of temperature (Morris and Langari, 2012). Thermistors are made up of a combination of 2-3 metal oxides in a ceramic with lead wires connected to a semiconductor chip (Wilson, 2005).

#### **1.4 Efficient Processing of Lyophilised Formulations**

Rational approaches and considerations for cost-efficient, short-cycle development with emphasis on bulk freeze drying are next discussed. It must be noted that published work on pharmaceutical freeze drying can be drawn from a variety of backgrounds. This may include

food, vial or spray systems and we aim to draw information from these studies towards these aims.

Material quality is affected across all stages of lyophilisation and has been reviewed extensively; (I) stabilisation (Rathore and Rajan, 2008) (II) freezing (Kasper and Friess, 2011) (III) primary drying (Franks, 2007a, Mellor, 1978) (IV) secondary drying (Franks, 2007b, Pikal *et al.*, 1990) (V) back fill and (VI) product sealing (Gassler, 2004, Chang and Liu, 2011, Zingle and George, 1997).

We characterise quality factors as the term given to the individual priorities developers place on distinct aspects of a formulation to define its final acceptance. We intend to discuss some of the most common quality factors assigned to lyophilized products examining each for its implications and limitations. It is never the case that all factors can be maximised, a rational selection based on the formulation must be achieved. The economics of freeze drying do not allow for both the cost-efficient production and ability to obtain the highest quality score across all descriptors, with a mixture of factors being the most common outcome.

#### **1.4.1 Morphology**

Physical appearance is the most common quality factor for any product. However, its priority with respect to other descriptors is important. It would be important to describe any particular appearance in colour, shape, texture or porosity that is a priority, as during cycle design colour may be lost without affecting taste.

The morphology of a freeze dried cake is often seen to provide reassurance of quality to an end user. In particular, physicians are known to reject materials with poor visual appearance. It is largely a subjective measure but a cake volume representative of the original frozen mass with consistent colouring and minimum surface abnormalities are typically considered ideal freeze dried materials.

To alter morphology, annealing during the freezing step can be adopted. To anneal a formulation it is held frozen at an elevated temperature for an extended period often above the glass transition temperature of the maximally frozen concentrate ( $T_g'$ ) or eutectic temperature. The crystal reorganisation of ice and eutectic phases will often reduce product resistance during sublimation with a resultant decrease in primary drying time (Chang and Patro, 2004).

Processing of freeze dried materials as dried products demands free flowing powders and is found in both food (Mumenthaler and Leuenberger, 1991, Quispe-Condori *et al.*, 2011) and pharmaceutical industries (Garmise *et al.*, 2006, Maa *et al.*, 2003); careful characterization of the morphology is needed to allow processing or packing. Primary drying temperatures above glass transition or collapse are known to significantly affect morphology producing shapes pyramidal in structure or high moisture content film residues. To maintain flow properties a consistent morphology must be demanded (Howard, 2007).

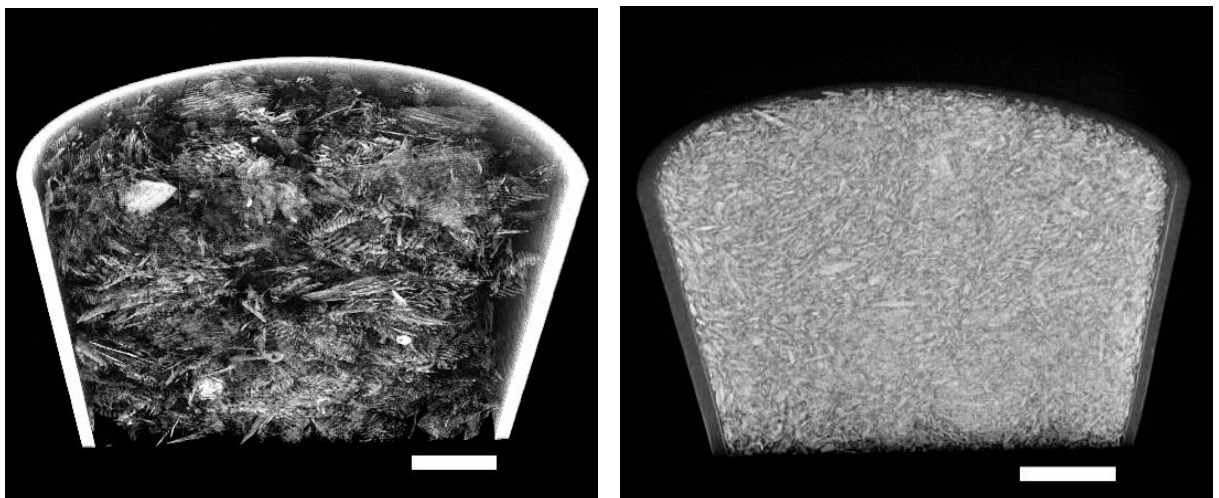


**Figure 1.3: Three-dimensional cross-sectional X-ray MCT into packed powders. Left: Freeze-dried mannitol powder. Right: Fluid bed dried mannitol powder. Scale bar: 1.25 mm**

X-ray micro-computed tomography (X-ray MCT) is allowing the investigation of the micro-structure of lyophilized powders (Figure 1.3) providing data on surface area, particle

orientation and particle size distribution of the freeze dried powders. Parker *et al.* (2010) quantitatively studied the micro-collapse of Bovine Serum Albumin lyophilized cakes, correlating porosity and connectivity with electron microscopy images in freeze dried cakes.

It is suggested that the non-destructive analysis of powders with this technique may expand to allow characterization of characteristics as diverse as flow and dissolution through surface area and geometric modelling. Unlike scanning electron microscopy (SEM) it has the ability to examine the internals of a sample without disruption of the original sample-defining morphology within the highly heterogeneous freeze dried cakes. X-ray MCT is described in more detail in section 3.4.12 and employed in studies later in chapter 6.

#### **1.4.2 Activity**

Intrinsic activity of an Active Pharmaceutical Ingredient (API) will affect the priority of any activity quality factor during cycle design. Although bulk freeze drying is commonly used for small molecules (Baheti, 2010) such as antibacterials (e.g., Azithromycin (Pfizer, 2011), Clarithromycin and anticancer agents e.g. Doxorubicin, Cisplatin (Association of British Pharmaceutical Industry (ABPI), 2008) there have been clear trends to explore larger sensitive bio-molecules.

Small drug molecules are intrinsically robust through primary and secondary drying. Extensive reviews of small molecules (Baheti, 2010), biopharmaceuticals (Costantino, 2004) and their excipients approved over the decades by the Food and Drug Administration (FDA) have been made. Common concerns for small molecules during lyophilisation include avoidance of melt back as a result of change from solid to a liquid state during primary drying (Niazi K. Sarfaraz, 2004).

Protein API's have particular stability issues and require careful control of sublimation below critical processing temperatures ( $T_c$  or  $T_g'$ ) to avoid activity loss (Wang, 2000). The three-

dimensional structure of proteins make them particularly sensitive to over drying or under drying, requiring carefully titrated levels of moisture within the powdered state (Pikal *et al.*, 1990).

Obtaining a frozen matrix of a solution can often determine final activity. During the freezing step high degrees of super cooling affect activity recovery for enzymes with an inverse relationship between the level of super cooling and activity (Cochran and Nail, 2009). The higher interfacial areas between ice and concentrated solute enhance adsorption and have been linked to reduced activity caused by aggregation and protein unfolding (Cochran and Nail, 2009, Strambini and Gabellieri, 1996, Chang *et al.*, 1996, Sarciaux *et al.*, 1999, Webb *et al.*, 2002); however, for other typically smaller APIs the interfacial area is of less significance. Adopting a reproducible ice nucleation process is desirable. Simple and more advanced ice nucleation techniques have been studied using; nucleating agents (Cochran and Nail, 2009, Searles *et al.*, 2001a, Searles *et al.*, 2001b), ultrasound (Kasper and Friess, 2011, Passot *et al.*, 2009), ice fog (Rambhatla *et al.*, 2004, Padilla *et al.*, 2011) and electric field (Petersen *et al.*, 2006) which are discussed by Bursac *et al.* (2009). A more recent approach involves pressurisation of the product chamber with argon gas to 26-28 psig, cooling to a desired nucleation temperature and de pressurising the chamber to 1 psig triggering a precise nucleation point (Konstantinidis *et al.*, 2011). The aim of all nucleation methodologies is to avoid high degrees of super cooling and induce controlled nucleation at high temperatures for production of large ice crystals with minimal batch variation (Searles *et al.*, 2001b). The large ice crystals formed minimise the ice water interface preventing protein adsorption and the consequential denaturation while maximizing recovery (Cochran and Nail, 2009, Passot *et al.*, 2009, Bursac *et al.*, 2009).

### 1.4.3 Dissolution

High dissolution rates for freeze dried materials are common. However, where further enhancement is required, choice of excipients and cycle design may affect a product significantly. Non-reducing sugars are commonly used excipients and the use or optimisation of the differing physical states of a formulation can affect the dissolution as defined in the Noye's Whitney equation (Noyes and Whitney, 1897) as adapted:

$$\left(\frac{dm}{dt}\right) = \left(\frac{D}{h}\right)A(C_s - C_t) \quad (1.1)$$

**Equation 1.1: Where 'D' is the diffusion coefficient (of the active molecule), h is the thickness of the diffusion layer surrounding a surface (A). Cs is the saturation solubility of the drug in the diffusion layer. Ct is the concentration of the drug in the reconstitution medium at time t. dm is the mass change in solution over a period of time (dt).**

Formulations with a high level of nucleation sites produce small ice crystals with a resultant large surface area and porosity. This change in surface area (A) provides a higher dissolution rate (dm/dt) for a short reconstitution time. In contrast, annealing produces large ice crystals with small surface area in the associated phase (A) this increases reconstitution time (dm/dt). This effect was seen as an 18-fold decrease in dissolution rate for recombinant human interferon- $\gamma$  cakes (Webb *et al.*, 2003).

Solutions with high masses of dissolved solute are seen to reduce the level of crystallinity (D) during freezing often forming amorphous disorganised states. Freeze-dried pegylated or high-level sucrose (>50 mg/mL) systems have often been shown to have shortened reconstitution times (Mosharraf *et al.*, 2007). Other approaches have included altering the reconstitution medium (Cs) or resorts to modify the actual API (D) (Costantino, 2004).

#### 1.4.4 Long-term Storage

Storage can be considered effective in even poor freeze drying processes; this is due to degradation rates in powders often being in orders of magnitude less than those of the solution. For bulk freeze dried materials a long-term storage of two years would be a common expectation.

The degradative processes common to lyophilisation are predominated by hydrolysis (Wang, 2000). Careful optimisation of the secondary drying phase (Pikal *et al.*, 1990) can minimise the final water content while avoiding over drying or scorching of a powder.

Selection and control of excipients can extend the shelf life of products. Fully crystallised mannitol was shown to prevent escalation of moisture levels in *Bacillus Calmette-Guérin* (BCG) vaccine on long-term storage (Jin *et al.*, 2011). Conversely, many proteins have been reviewed to show damage when exposed to crystallisation during storage (Wang, 2000). It is of particular note that unstable excipients may release moisture to a system or change on extended storage. An unstable mannitol hydrate required extension of the secondary drying period by 13 hours to transform the powder state for long-term storage (Johnson *et al.*, 2002). In these cases, it is important to have a clear understanding of the degradative stresses for the individual API and control crystallisation through annealing and the regulation of moisture levels.

Exclusion of reducing agents is common; these slow reduction reactions are able to damage API's over extended periods of storage. The Maillard reaction describes when reducing sugars are oxidised by amino acids producing a browning of a formulation over long periods, moisture levels can retard or accelerate such a reaction (Wang, 2000, Kadoya *et al.*, 2010).

### 1.4.5 Cost

Although not a direct factor for a formulation, the economics (Franks, 2007c) of a freeze drying process may override all other quality factors. This is particularly the case for low-value solutions; but may be particularly of concern for re-optimisation of an existing freeze drying cycle or development of a generic pharmaceutical copy. The cost of freeze drying cycles is often dictated by how well optimisation was performed to allow scale up. Scale up of freeze drying cycles has been discussed in depth (Trappler, 2007), with particular importance placed on the monitoring and feedback of this information to the stages of drying. Limitations of the final production machine should be considered, as fast cycles often include high rates of drying requiring equally high condensation rates not available on all systems.

The cost of maintaining high vacuums and providing both low temperatures for condensation and high temperatures for sublimation drives the economic cycle around the batch production of freeze dried items. Labour provides additional expense when a cycle is unable to complete on a convenient daily cycle resulting in driers being active but not productive. Any process that can be adapted to reduce these running times or minimise staff will benefit the associated costs. Bhambhani and Medi (2010) discussed primary packing in detail, while it was clear bulk drying provided the most basic of container system its use can be economical. Bulk freeze drying maximizes shelf area minimizing costs of thermal transfer. Avoiding fill depths in excess of 2 cm is common to prevent product resistance to vapour flow limiting the maximum primary drying rate (Tang and Pikal, 2004). However, products of high solute content may require special attention to prevent significant extension of the primary and secondary drying periods (Tang and Pikal, 2004). High super-cooling rates are to be avoided as production of large numbers of small ice crystals increases final product surface area increasing product resistance to vapour flow during sublimation and increase total running time (Pikal, 2007, Passot *et al.*, 2009). Nucleation at higher temperatures is of

particular use in the production of large contiguous ice crystals suitable for higher sublimation rates (Searles *et al.*, 2001b, Bursac *et al.*, 2009).

The role of controlled ice nucleation on the total length of some newly developed cycles may be self-limiting since any resulting decrease in sublimation time may be offset by an increase in desorption time (Passot *et al.*, 2009). However, practically it appears that controlled nucleation does provide benefit, cycle lengths reducing by between 14-41% (Passot *et al.*, 2009, Konstantinidis *et al.*, 2011, Searles *et al.*, 2001b).

Membrane trays of polypropylene and polytetrafluoroethylene laminate have been proposed which are able to minimise product loss or blow out from trays (Patel and Pikal, 2011) during or at the conclusion of drying (Gassler, 2004). Gassler and Rey attributed the superior heat transfer observed in membrane trays to low thermal inertia. Membranes were associated with a 20-30% reduction in freezing time and have been linked with 20-30% reductions in drying time when compared with stainless tray systems. However, the advantages of stainless steel trays are lost and product transfer may become restricted with less protection from rupture of the container. It is also clear that membrane sealed trays may demand a lowering of the sublimation rate requiring increased cycle lengths due to container resistance (Mayeresse Y. *et al.*, 2009).

The rule of thumb that a 1°C rise in product temperature will decrease primary drying time by about 13% is commonly quoted (Tang and Pikal, 2004) and governed by the sublimation rate defined by (Chang and Patro, 2004):

$$\frac{dm}{dt} \propto \left( \frac{P_o - P_c}{R_s - R_p} \right) \quad (1.2)$$

Where 'dm/dt' is the sublimation rate or mass transfer for water vapour (kg/s), 'P<sub>o</sub>' is vapour pressure of ice at the product temperature (Pa), 'P<sub>c</sub>' is chamber pressure (Pa), R<sub>p</sub> is product resistance (Pa.s/kg) and 'R<sub>s</sub>' is stopper resistance (Pa.s/kg). During sublimation an

increasing thickness of dried layer forms. This layer resists the flow of water vapour through the solidifying cake with no direct proportionality to mass flow. It is unaffected below collapse temperatures but may show dependence to any resistance within the container used.

Defining critical formulation temperatures is key for cost reduction over the long term. By using temperatures close to those for formulation collapse or glass state transition energy transfer is maximized, maintaining the highest sublimation rates possible. These temperatures can be exploited in the process of micro-collapse when the lower resistance of the dry layer between  $T_g'$  and  $T_c$  allows enhanced rates of sublimation to be achieved.

High protein or solute concentration may contribute to alterations in the  $T_g'$  or collapse of a formulation. Increased Bovine serum albumin (BSA) concentration has been found to increase  $T_g'$  and  $T_c$  allowing aggressive drying temperatures (Parker *et al.*, 2010). Despite a low  $-32^\circ\text{C}$   $T_g'$  for sucrose, 5 mg/L and 50 mg/L BSA can be successfully dried with a  $25^\circ\text{C}$  shelf temperature in the presence of sucrose with cakes finally exhibiting 2 year stability profiles in line with those freeze dried at  $-25^\circ\text{C}$  (Parker *et al.*, 2010).

Crystallising agents may provide scaffolds to allow micro-collapse while maintaining macro structure by taking advantage of the high eutectic temperatures of sugars or salts. Mannitol sucrose mixtures have been dried at  $-10^\circ\text{C}$  while avoiding visual signs of macro-collapse, exploiting the high eutectic temperature of mannitol  $-1.5^\circ\text{C}$  (Pikal, 2007). Care, however, must be taken to consider the consequences of incomplete crystallisation for long-term behaviour.

Pharmaceutical scientists who bulk freeze dry need to foremost identify what quality factors are of a priority during cycle development since the economics of freeze drying do not allow for both the cost-efficient production and the ability to obtain the highest quality score across all quality factors. Consider; morphology, activity, dissolution, long-term storage, packaging and cost.

## **1.5 Current state of the art in freeze drying from the patent landscape**

It is often the case for advances in research to be protected by initial intellectual property; usually patented before disclosure in general literature. The 18 months lag between filling of patents and publication means most novelty is hidden or unknown for years. This makes the patent literature a useful source for industrial trends. The patent literature has been examined (unpublished data) for expiring patents and current (2010 – 2013) trends in freeze drying. The patents of relevance are discussed in the context of this thesis to highlight trends.

### **1.5.1 Container systems**

As a batch process freeze drying for parenteral applications has typically focused on a container or vessel within which the material is freeze dried. GE Healthcare UK Limited (2013) recently disclosed a series of container systems (Figure 1.4) suitable for small volume drying which suggested a focus on diagnostic uses. Proposing an application for polymerase chain reaction (PCR) reagents, the plastic containers made of polycarbonate, polypropylene or polystyrene form bottle necks or 'collars' (Figure 1.4A). The collar separates the container into upper and lower sections retaining powdered material by locking it into a fixed position. The presence of angular prongs with textured surfaces (Figure 1.4B) increase adhesion of the dried cake to the container. Individual containers can be arranged in a plastic tray with a sealing membrane of flexible foil or poly laminate covering analogous to the well-known lyoguard trays by Gore (Gassler and Rey, 2004). The combination appears well suited to address the concerns of friable powder volumes if there is sufficient mass to be fixed by the prongs.



**Figure 1.4: Schematic of container systems disclosed by GE Healthcare (GE Healthcare UK Limited, 2013). (A) Vial or 96 well plate system to incorporate a collar to prevent movement of the powdered cake on completion of freeze drying. (B) Larger cakes can be held by angular prongs that hold the powder in position and prevent it from movement if upturned. (C) Small volume system for diagnostic reagent (or similar) that considers the small surface contact area of dried powder for easing reconstitution.**

Regulatory considerations for complete vial closure under grade A would have been a clear focus of the Datwyler container closure for vials (Figure 1.5A) (Datwyler Pharma Packaging International, 2013b). It provides for the sealing and crimping of vials within the grade A (EU GMP) inside the freeze drier (Datwyler Pharma Packaging International, 2013a). While this appears useful, the industry priority for ease of reconstitution by medics or professionals with a reduced skill set has seen the disclosure of a variety of syringe freeze drying combinations which will compete with such technology. Eulysis UK Limited (2013) disclosed a single component vial system where the freeze dried powder is encased within the cap or closure of the vial (Figure 1.5 B). Drying of the API is done in the cap with compression of cap breaking the base of the cap and releasing the API for reconstitution. Glucago and Lyogo LLC disclosed the inner workings of a series of syringes for reconstitution of freeze dried formulations (Bartlett. *et al.*, 2013). In a peculiar version, the seal separating the reconstitution and diluent chambers within the syringe is fused with a thread/wire made of an inert material which runs axially through the attached needle of the device (Figure 1.5 C).



**Figure 1.5: Schematic of container closures and reconstitution syringe. (A) Container closure for vials with the potential for grade A crimping (Datwyler Pharma Packaging International, 2013b). The crimp is shown held in place during drying and with pressure applied from above the outer casing is able to provide a crimp seal to the stopper. (B) Provides for a material freeze dried into an initial stopper to be pressed and break at the point marked; releasing powder into a reconstitution chamber (Eulysis UK Limited, 2013). (C) Two compartment syringe with a separation membrane that can be broken by pulling the plunger with an attached thread. Breaking this separation releases the reconstitution fluid in this case from the upper chamber (Bartlett. *et al.*, 2013).**

The radiative properties of a material can be represented by the emissivity coefficient; glass, stainless steel and PTFE have relative emissivity's of 0.22 0.92 and 0.78 respectively (Middlebeek *et al.*, 2009). Middlebeek *et al.* (2009) reported the use of a black carbon filled polyethylene terephthalate to maximise the emissivity of a plastic for freeze drying heat radiation.

Container patents that have entered an expiry period include the Cryopharm collapsible blood bag (Figure 1.6 A-B). Designed as flexible, polyvinylchloride film plasticised with diethyl hexyly phthalate is reinforced through the insertion of rods to maintain the structure of side walls during freeze drying (Cho *et al.*, 1992). The bag system also provides for disruption of the freeze dried material prior to reconstitution while sealed. This appears intended to provide reduction in shipping or storage volume of the dried material and also direct infusion from bag when hanged.

Boehringer Mannheim GmbH (1994) disclosed a similar bag or tube composed of 0.5-1 mm impermeable resin base with a hermetically sealed membrane (Figure 1.6 B). Sealed with a 0.2  $\mu\text{m}$  semi permeable membrane of cellulose derivatives and polytetrafluoroethylene it appears to provide the same minimal mass flow resistance of current tray systems (Lyoguard™).

The laminated blister packs of Scherer preventing the warping of thin sheets of freeze drying blister trays through incorporation of a 45  $\mu\text{m}$  aluminium sheet within a polyvinylchloride, polypropylene or polyamide combination to provide a similar overall co-efficient of thermal expansion (Scherer Ltd, 1994). These appear to remain significant for continued or future use and indeed relate well into the diagnostic areas of freeze drying previously identified.



**Figure 1.6: Schematic of bulk drying containers. (A-B) A collapsible blood bag for lyophilisation (Cho *et al.*, 1992) capable of been re-enforced with rods. The large circular area is an exit for sublimed materials with a described aseptic consideration. (C) Sealed tray system with semi permeable membrane of practical use in aseptic conditions (Boehringer Mannheim GmbH, 1994). (D) Composite materials described to prevent a tray system warping during freeze drying e.g. Oral dispersible tablets or for very thin bulk drying trays (Scherer Ltd, 1994).**

### 1.5.2 Continuous flow and traditional tray freeze drying

Emerging semi continuous and continuous freeze drying systems are allowing a shift from batch systems to draw on the cost benefits. Traditional tray drying or use of bulk containers are still in use in combination with novel approaches for producing particles for freeze drying.

A recent patent disclosed by Takano and Gayama used stainless steel tray drying for processing dry yeast high in s-adenosyl-L-methionine for its potential use within nutraceuticals (Kentarou Takano and Shinyo Gayama, 2013).

Sanofi has recently reported processing lines capable of semi continuous or continuous freeze drying for terminal powder dispensing (Sanofi Pasteur Sa, 2013b). An atomizing chamber freezes calibrated droplets (200-500  $\mu\text{m}$  range) for aseptic transfer into a rotating drum freeze dryer housed in a vacuum controlled chamber (Sanofi Pasteur Sa, 2013c). Temperature controlled inner walls allow heat transfer for sublimation while an absence of stopper resistance and increased exposed surface area suggests potential decrease in drying times. There are clear concerns for drying homogeneity and powder scorching within rotating drums. Replacing heated walls with a radiation emitter may resolve drawbacks caused by moisture and electrostatics (Sanofi Pasteur Sa, 2013a). Inventors describe a 50% reduction in drying time when using an active radiation emitter.

Middlebeek *et al.* (2009) disclosed a method for freeze drying a frozen bed of particles using a container which is heated beneath by conduction and the top powder surface by radiation from above using two heating plates preferably warmed to the same temperatures. Final product moisture content of less than 1.5% is claimed.

An interesting patent disclosed by Qiagen is built on the disposition for one of two immiscible phases to inherently form a spherical shape when combined (Wende and Jesziorski, 2011). The immiscible phases are either hydrophobic or hydrophilic and either can serve as a solvent for dissolving the API of interest prior to incorporating a second liquid

phase. A continuous application of the invention is also disclosed as a set up with a continuous circular flow of a hydrophobic media. The hydrophilic phase containing the API is injected to form spherical entities.

Lamprecht (2013) reported the spray freeze drying of lysozyme, insulin and Immunoglobulin G (IgG). The patent focused on flowability by engineering spherical mono dispersed particles aimed for different administration routes including oral, buccal and sublingual routes. The invention required a mix of at least a cryoprotectant and a stabilizer with the API to yield porous mono dispersed particles in the 1  $\mu\text{m}$ -1 mm size range. 90% activity was retained after drying 1 %w/v lysozyme, 5 %w/v mannitol with BSA, dextran or PVP at 0.1-10 %w/v. After 6 months, stability of the 10 %w/v solid content was statistically unchanged.

It is envisaged that bulk drying using these combinations of semi continuous and tray drying or continuous flow drying approaches will be best for process economics if final containers are dosed from bulk freeze dried solids. Perhaps the use of tray drying solely could suffice and thus avoid the huge capital investment for new equipment requirements or retrofitting of existing dryers. Dosing from bulk is however hypothesised to be heavily challenged by flowability of the final porous amorphous freeze dried powders.

## 1.6 Characterising freeze dried powders

As previously mentioned, knowledge of the critical temperatures of a formulation is required for a successful drying process. These refer to glass transition temperature of the maximally freeze-concentrated phase ( $T_g'$ ), eutectic temperature ( $T_{eu}$ ) and collapse temperature ( $T_c$ ) (Pyne *et al.*, 2002, Hawe and Friess, 2006b). Thermal analysis techniques such as DSC (differential scanning calorimetry) are available for measuring  $T_g'$ . Freeze drying microscopy can also be used to determine collapse temperatures of formulations prior to drying. During the freezing step, if the solute crystallises it forms a eutectic with ice and the eutectic temperature becomes important (Pyne *et al.*, 2002). Primary drying above the  $T_c$  and  $T_{eu}$  of a material will lead to cake collapse and melt back respectively.

### 1.6.1 Flow properties of bulk solids

Flowability of powders is influenced by many properties such as size distribution, moisture, static electricity and density (Lavoie *et al.*, 2002, Jiang *et al.*, 2009, Staniforth and Aulton, 2007, Schneider *et al.*, 2007). History of powder handling could also induce variation in measurements for the same powder. For instance, the number of  $-30^{\circ}\text{C}$  to  $30^{\circ}\text{C}$  freeze-thaw cycles used in preparing microcrystalline cellulose-starch composites increased the angle of repose and Carr's index (Builders *et al.*, 2010).

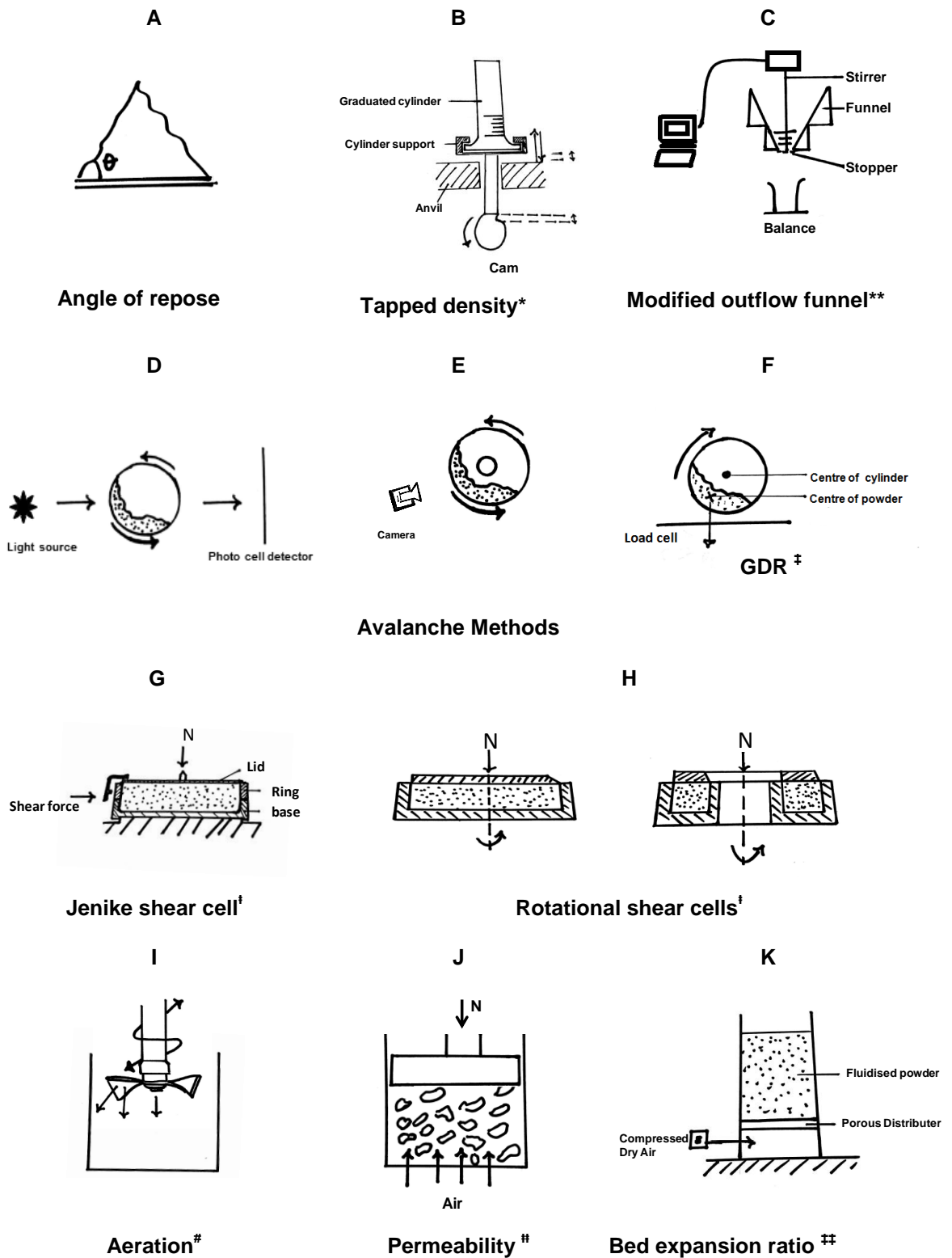


Figure 1.7: Schematic of the types of available flow characterisation methods. Images adapted or drawn from : \* British Pharmacopoeia Commission (2013a) ; \*\* Ruppel *et al.* (2009); † Schwedes (2003); ‡ Faqih *et al.* (2006); # Freeman (2007); †† M. Krantz *et al.* (2009) and # Fu *et al.* (2012). GDR = Gravitational displacement rheometer. N = Normal force

Various methods have been reported for characterising these flow attributes and the main available techniques and some variations of interest are herein introduced (Figure 1.7). Angle of repose, tapped density (Carr's index) and shear cell methods were used in chapter 4 for studies which characterise bulk lyophilised powders.

Methods for characterising the flow of pharmaceutical powders can be categorised into direct and indirect methods (Staniforth and Aulton, 2007, British Pharmacopoeia Commission, 2013c). Indirect methods include angle of repose, bulk density measurements, Hausner's ratio and Carr's index. Direct methods include hopper flow rate and recording flow meter. Tests can alternatively be grouped into static and dynamic tests with the later believed to be most ideal as it mimics the actual intended process.

When a powder is allowed to flow onto a surface, it may form a heap and the angle ( $\theta$ ) which the free surface forms to the horizontal plane (Figure 1.7 A) is referred to as the angle of repose (Howard, 2007). Poured and drained angle of repose methods are the two main types of angle of repose available. The former is the angle measured when a powder pile is poured freely onto a flat surface while the latter is measured on the conical surface of a powder when it is discharged through an orifice onto the base of a flat bottomed vessel (Howard, 2007). More than one angle of repose may be formed by a powder bed making this rather low cost and simple test error prone. Lavoie *et al.* (2002) were challenged with multiple angles for cohesive lactose, malto-dextrin and microcrystalline cellulose. This technique has been described as "crude" or "rough" but useful in early drug development and quality control where new chemical entities are usually available only in small quantities (Staniforth and Aulton, 2007, Howard, 2007).

Shah and Misra (2004) used angle of spatula method to evaluate the flow of lyophilised liposomes of Amikacin dry powder. It involved estimating the angle formed by a heap of powder at the end of a spatula held horizontally.

Vibrating spatula is another modification of the angle of spatula method and deemed as a dynamic method for accessing powder flow (Louey *et al.*, 2004). The apparatus measures the mass of powder falling from a vibrating spatula as a function of time.

Different powders will be consolidated to various extents when compressed and the poorer the flow properties of powder, the more compact it becomes. This powder characteristic is a measure of inter particulate forces (Carr, 1965). Carr's compressibility index and Hausner's ratios are similar methods of accessing flowability based on tapped density and bulk density measurements. Using a graduated cylinder, bulk and tap densities of a powder can be determined (Figure 1.7 B). Hausner's ratio is expressed as a ratio of bulk to tapped density or a ratio of bulk volume to tapped volume (British Pharmacopoeia Commission, 2013a, Howard, 2007). Powders with low inter particulate friction are free flowing and have ratios of approximately 1.2 (Carr, 1965). Both tests require the measurement of bulk density using graduated cylinders and the precise method adopted in pouring the powder into a container has a more profound effect on particle packing variation than on the container sizes used (Brown and Richards, 1970).

A modification of the standard flow through an orifice test method which determines the flow rate of a powder through an orifice (British Pharmacopoeia Commission, 2013c) was reported by Ruppel *et al.* (2009). The "modified outflow funnel" apparatus measures powder flow based on other parameters such as powder arch destruction time and descriptors calculated from the torque used by the stirrer (Figure 1.7 C).

The use of static flow predictions has often being criticised as not informing the complete flow behaviour of a material. Lavoie *et al.* (2002) criticised the flowability predictions made on static beds as unable to inform on the complete flow behaviour of a material and recommended the use of methods of assessment under a dynamic condition of avalanche which was more representative of powder working conditions. These avalanche techniques

use a rotating drum or cylinder in combination with either a light source and detector (Figure 1.7 D) or a camera (Figure 1.7 E) or load cell (Figure 1.7F).

The time between avalanches can be used to characterise the avalanche behaviour which is captured by signals recorded by photocells as powders avalanche (Hancock *et al.*, 2004, Lindberg *et al.*, 2004). Good flowing powders show short reproducible avalanches but powders which adhere to surfaces can interfere with signals meant for the photoelectric detector (Thalberg *et al.*, 2004). Cohesive powders may form aggregates and be erroneously characterised as good flowing if they display short intervals between avalanches. This makes this technique poor in discriminating between more cohesive powders (Thalberg *et al.*, 2004). This setup was commercially available as Aeroflow™ and was discontinued in 2006 (TSI, 2014) perhaps due to lack of patronage or competition from newer techniques on the market.

A camera can be used to monitor the maximum angle formed by a powder before it avalanches (Krantz *et al.*, 2009) which in effect is a dynamic angle of repose. The camera system can be employed to also monitor the avalanche and the signals Fourier transformed to inform flow (unpublished powder flow cascade by J Davies and A. Ingham). A gravitational displacement rheometer (GDR) is a variation of the previously described avalanche apparatus (Figure 1.7 F). It utilises a load cell to investigate the size of avalanches using the change in the centre of a powder's mass (Faqih *et al.*, 2006, Vasilenko *et al.*, 2011).

Different rank order of flowability can be generated by different measurement techniques and emphasises is often made to utilise techniques that is representative of the process (Schneider *et al.*, 2007).

Shear cell testers are particularly useful in measuring cohesion, ranking flowability using flow function and invaluable tools for hopper design since the first introduction of the Jenike Shear cell tester. The various types such as the Jenike or translational (Figure 1.7 G), uniaxial, biaxial and rotational or ring shear cells (Figure 1.7 H) have been comprehensively reviewed (Schwedes, 2003). The main differences surround the application of the normal force (N) in relation to the measured shear force (S) and type of powder receptacle in use. Powder behaviour under a series of different normal stresses and the corresponding shear forces are studied using Mohr circles to rank powders. The underpinning operation principles are the same for all types of shear cells. The background of a ring shear and the application of Mohr circles to characterise flow of lyophilised powders is described in more detail in section 3.4.10.3 on page 70.

A powder rheometer reported by Freeman (2007) is a peculiar apparatus with a stirring rod which can be interchanged from a blade into a flat surfaced piston or shear cell lid making it a versatile powder characterisation tool. A similar apparatus using a helical blade has also been reported (Shah *et al.*, 2008). Freeman's blade performs aeration test (Figure 1.7 I) which measures cohesive strength as "flow energy" as it ploughs through a powder bed. Pistons can be used to measure compressibility or used in combination with supply of air through the powder bed for permeation test (Figure 1.7 J) which informs resistance between powder particles as a function a change in pressure. A similar set up reported as a bed expansion ratio apparatus (Figure 1.7 K) characterises powders based on the ratio of fluidised powder height to settled powder height (Krantz, 2009).

## 1.7 Powder dispensers

The use of powder dispensers is common in solid dose form manufacture such as capsule filling (Jones, 2001, Nalluri *et al.*, 2013). Powder dispensers can be grouped based on their main method of operation into pneumatic, volumetric, gravimetric, screws or augers, electrostatic and vibratory methods (Yang and Evans, 2007). Pneumatic dispensers are a form of volumetric method that dispense powder volumes using a dosing die or aspirating tube. A negative and positive pressure is used to pick and dispense powders. Gravimetric methods rely on the use of a load cell in combination with a suitable powder feed from usually a hopper. A commercially available pneumatic powder dispenser and two different types of gravimetric dispensers are used in studies investigating compatibility with freeze dried powders in chapter 5 on page 123.

## 1.8 Material visualisation through tomography

Tomography is a non-invasive and quantitative description of a section or slice of matter from within a bulky object or material (Baruchel *et al.*, 2000). It has found uses in traditional medical imaging and with the equipment now downsized; found use for analysis in food (Mousavi *et al.*, 2005), tissue engineering (Lin *et al.*, 2013), pharmaceuticals (Monkare *et al.*, 2012) and the wider material science industry (Fu *et al.*, 2005). X-ray and gamma ray tomography are the most widely used in industry. Its simplest form, transmission tomography, provides a map of linear attenuation co-efficient (a measure of X-ray absorbed or scattered) of the object under investigation as a function of its density and atomic number. For a clear separation between density and atomic number, scattered photon tomography is able to relate the ratio of Compton and Rayleigh scattered photons to atomic number with no influence from density while emission tomography is used in the detection of photons emitted by an object which is itself under investigation (Baruchel *et al.*, 2000).

Transmission tomography is based on Beer-Lambert's Law or attenuation law (Equation below):

$$N_1 = N_0 \exp \left[ - \int \mu(x, y) dx \right] \quad (1.2)$$

A reconstruction of the linear attenuation map of a sample can be obtained from several measurements through the same sample slice. This is correlated from the energy of the photon, density and atomic number of the material.  $N_0$  and  $N_1$  are the number of photons emitted and transmitted through a single line across a sample and  $\mu(x, y)$  is the linear attenuation co-efficient at point  $(x, y)$  within the sample (See Figure 1.8).

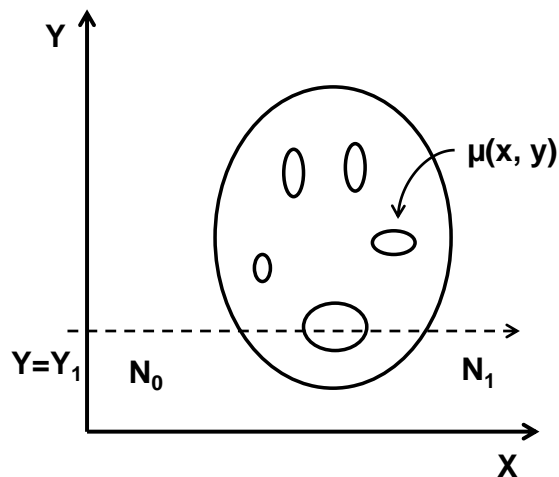


**Figure 1.8:** Representation of transmission tomography within a single slice. The number of photons emitted from the source ( $N_0$ ) and transmitted ( $N_1$ ) through a single line across sample is used to obtain the integral of the attenuation co-efficient ( $\mu$ ) along the path of the X-ray photon.  $\mu(x, y)$  represents linear attenuation co-efficient at point  $(x, y)$ . Redrawn from Baruchel et al. (2000).

Transmission X-ray tomography which uses a cone beam and computer algorithm for image reconstruction was used to study freeze dried powders in chapter 6.

## 2 THESIS AIMS AND OBJECTIVES

Freeze drying is currently an expensive batch process and faces competition from cheaper drying alternatives. There is regulatory pressure to stop the use of batch processing to reduce variability. While there have been attempts to convert it into a continuous process, these are yet to be successful.

Leading pharmaceutical companies including Sanofi and Bayer have disclosed a series of patents in this area (Sanofi Pasteur Sa, 2013a, Sanofi Pasteur Sa, 2013c, Sanofi Pasteur Sa, 2013b, Gehrmann *et al.*, 2010). All strategies for either semi continuous or continuous drying systems require processing of the final bulk lyophilised powders.

The freeze drying tray has been used for bulk purposes mostly for food in the past. Emerging drying and powder transfer technologies provide the opportunity for large bulk tray lyophilisers and accurate (less than 3% RSD) powder dispensers to be combined to reduce the overall mass processed. Harnessing these technologies for high throughput commercial production could have significant economic benefits. However a published knowledge gap exists around bulk formulation requirements that would allow formulations to meet regulatory approval and be designed to maximise the efficiency of such a paradigm shift from traditional vial fill to finish drying.

This thesis is motivated by the potential cost savings associated with bulk drying of small and large molecule pharmaceuticals. It is anticipated that findings would not be limited to bulk tray freeze drying but would also benefit semi-continuous and continuous bulk drying provisions in areas where they too may require handling of final product material outside the freeze dryer.

Tray drying is revisited in the quest for findings expected to be useful for scientists considering manipulation of freeze dried powder using conventional bulk tray drying for parenteral use, direct powder compression or production of process intermediates.

The primary objectives of this thesis are set out here as studied in chapters 4 to 6.

Chapter 4: Assessment of the flow behaviour of bulk lyophilisates.

The aim was to fully characterise bulk freeze dried powders (lyophilisates) for flow behaviour. Flow properties of potential bulking agents were evaluated to identify relationships with variations in solute concentration. An objective was to understand the role of cooling rate and thermal holds during bulk freezing on final cake morphology and powder flow. Identification of a suitable, industrially acceptable and consistent method for disrupting large bulk cakes into loose powder systems for handling was a further objective.

Chapter 5: Investigations into the compatibility of bulk lyophilised powder for vial or ampoule enclosure.

Studies aimed at investigating volumetric and gravimetric methods of freeze dried powder transfer into container closures using both small and large scale commercial dispensers. The objective was to identify the problems associated with dispensing a final patient suitable dose in a market suitable packaging. Evaluation of the regulatory concerns for dose uniformity and identifying the implications of powder flowability to maximise both precise and accurate doses were prioritised objectives due to an absence in literature. Identification and optimisation of formulation properties of significance to allow a standard for successful powder transfer was to be defined.

Chapter 6: X-ray Microcomputer tomography studies for the determination of powder flow characteristics and dose uniformity of freeze dried active pharmaceuticals.

The aim was to explore this new non-destructive technique to identify correlations with traditional methods used for characterising powders for porosity, size and shape. An

objective was to establish the use of small powder volumes for full and reliable freeze dried powder flow characterisation while avoiding incompatibilities associated with freeze dried powders such as its hygroscopic nature. A further objective was to provide a quantitative evaluation of active pharmaceutical ingredient (API) uniformity throughout freeze dried cakes and provide an understanding into the effects of freezing rate on dose uniformity.

## **3 MATERIALS AND METHODS**

### **3.1 Preparation of active pharmaceutical ingredient**

Immunoglobulin G (IgG) was obtained from caprylic acid precipitation of ovine sera and was received as a gift from MicroPharm UK (Polyclonal, Wales, Sheep no. 1363 16/02/94). A detailed description of materials and methodology is outlined in appendix I on page 238.

### **3.2 Pre-formulation characterisation**

#### **3.2.1 Collapse point and eutectic melt determination**

##### **3.2.1.1 Background**

A freeze drying microscope (Lyostat3, Biopharma UK) allows the qualitative identification of collapse and eutectic temperatures of formulations prior to freeze drying (Figure 3.1). Its cryogenic stage is equipped with an imaging station and a silver heating block. The temperature control system utilises a heating element and liquid nitrogen supply to meet temperature in the working range of -196°C to +125°C. A Pt100 temperature probe connected to the stage logs product temperature during drying. The cryogenic stage is also fitted to a vacuum pump which is regulated through pirani gauge feedback. The imaging station is comprised of a camera and lens objective which is capable of real time image capture using Linksys 32 software.

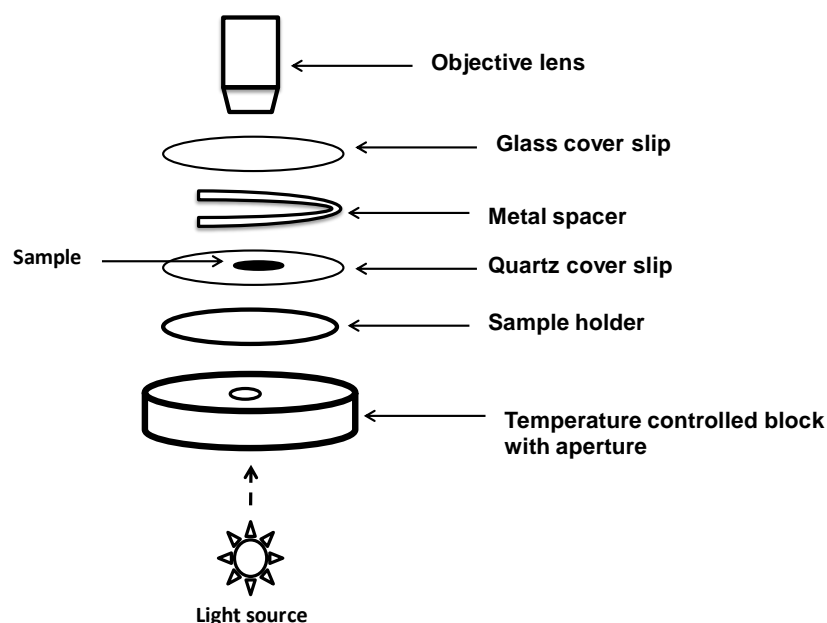


**Figure 3.1: Schematic representation of a freeze drying microscope stage showing sample and stage assembly for identification of collapse temperatures. Redrawn from Ward (2010).**

### **3.2.1.2 Procedure**

The microscope was validated using known collapse temperatures of sucrose at  $-32^{\circ}\text{C}$  and eutectic melt of sodium chloride at  $-21.5^{\circ}\text{C}$ . The lid and stage were unscrewed and opened to allow access to the silver sample block and the fitting of a sample holder. The sample holder ring was fitted onto the sample block and secured. A drop of silicon oil was introduced onto the block within the confines of the sample holder ring and covered with a 16 mm quartz glass with the aid of a vacuum pen. A  $70\ \mu\text{m}$  semi-circular metallic spacer or shim was introduced onto the sample block with forceps. A sample solution of  $1.5\ \mu\text{L}$  was introduced onto the stage and covered with a 13 mm glass slide using a vacuum pen. For easy identification and tracking of the drying front or sublimation interface, the edge of the solution was moved to around the edge of the light source on the stage by adjusting the sample holder ring. The lid was screwed back into place and a nitrogen curtain introduced to prevent condensation during analysis. Sample was frozen and sublimation commenced by

pulling a vacuum. The sublimation interface and samples were observed through the course of drying within temperatures of interest to identify critical temperatures.

A sample of 1-2  $\mu\text{L}$  was frozen using a ramp rate of 20  $^{\circ}\text{C}/\text{min}$  to  $-40^{\circ}\text{C}$  and held isothermal until an amorphous and or crystalline material was completely formed. Vacuum was pulled to 0.369 mbar (36.9 Pa) to commence the sublimation process. Image capture was initially set at a delay of 60 seconds during freezing and initial sublimation. This was reduced to a 5 seconds delay further into sublimation. Onset of collapse was initially identified using a 1  $^{\circ}\text{C}/\text{min}$  temperature ramp and the sample observed for changes in the sublimation interface. Upon initial identification of the collapse temperature, heat-cool cycles were repeated at a slower ramp rate of 0.5  $^{\circ}\text{C}/\text{min}$  to confirm the collapse or eutectic temperature.

### **3.2.2 Differential scanning calorimetry**

#### **3.2.2.1 Background**

Differential scanning calorimetry (DSC) is a form of thermal analysis useful in characterising the thermal properties of solutions or the final dried product. It measures the heat flow changes within a sample in comparison to a reference. Heat flux and power compensation DSC are the two available types (Ford and Timmins, 1989). A heat flux DSC measures the temperature difference between a sample in a DSC pan and a reference (empty pan). The latter measures the heat flow required to maintain the sample and the reference at the same temperature.

A Q200 series MDSC (TA Instruments, USA) with a refrigerated cooling system (RCS 40) capable of  $-40^{\circ}\text{C}$  to  $400^{\circ}\text{C}$  cooling and heating was used to study phase transitions of formulation solution to be freeze dried. Purge nitrogen gas (BOC, UK) supply of 50 mL/min was used at all times.

### **3.2.2.2 Procedure**

#### **3.2.2.2.1 Calibration**

The DSC was initially calibrated before sample analysis using the inbuilt calibration wizard. Tzero aluminium pan, standard and hermetic lids were purchased from Walters UK.

##### **3.2.2.2.1.1 Tzero calibration or baseline calibration**

Runs were performed to generate cell resistance and capacitance. The cells of the DSC were run empty from -40°C to 200°C at a ramp rate of 20 °C/min. A clear (sample) and red sapphire (reference) disc (TA Instruments, USA, Lot 970345.901) both weighing 108.5 mg were placed directly on the cell and the thermal program was initiated. A  $\Delta T$  and  $\Delta T_{zero}$  versus time plots showing no transitions and low noise to signal ratio in both empty and sapphire runs was accepted as ideal. The resulting cell resistance and capacitance was then plotted and saved. Increasing capacitance and a decrease in resistance with temperature was accepted as ideal.

##### **3.2.2.2.1.2 Cell constant and Temperature**

Pre melted indium of 9.8 mg (TA Instruments, P-E P/N 0319-0033) was run from 100°C to 180°C at 10 °C/min to calibrate for cell constant and temperature. A melting point observed at 156.6°C and enthalpy of fusion of 28.457 J/g was deemed acceptable. The cell constant was calculated and logged to file.

##### **3.2.2.2.1.3 Heat capacity (Cp) constant calculation**

Existing values for reversing and total heat cp constants were reset to a value of 1. Sapphire was run from -40 to 200°C at 5 °C/min amplitude of  $\pm 0.1^\circ\text{C}$  using nitrogen gas at 50 mL/min purge and desired period. Values resulting from Cp, reversing Cp and temperature plot were

exported into Microsoft Excel and the Cp calibration constants were calculated from an average of 3 ratios of theoretical to measured Cp values.

#### **3.2.2.2.2 *Sample analysis***

Samples were weighed by difference in a Tzero aluminium pan. A standard lid was used for solid samples while solutions were hermetically sealed using an encapsulating press (TA Instruments, USA). An empty pan was weighed and used as reference. Sample and reference pans were placed in the DSC cell and covered with the cell lid. The thermal program specifying equilibration and temperature range, heating rate, amplitude and period was initiated. Thermographs were analysed for phase transitions and labelled using TA instrument universal analysis 2000 4.5A software.

### **3.3 Lyophilisation process design**

Freeze drying was performed in a Virtis Advantage bench freeze dryer (Figure 3.2) using cycles specified in individual thesis chapters. A stainless steel tray and a custom made three compartment tray (Dense grade polystyrene model foam frame (Trylon, UK) and polyethylene base (Tesco, UK) were used as bulk container systems (Figure 3.3). Conventional vial freeze drying was performed in 10 mL type 1 glass freeze drying vials (Adelphi Healthcare Packaging, UK). K type thermocouples (RS Components, UK) were used to monitor product temperature during the drying process.

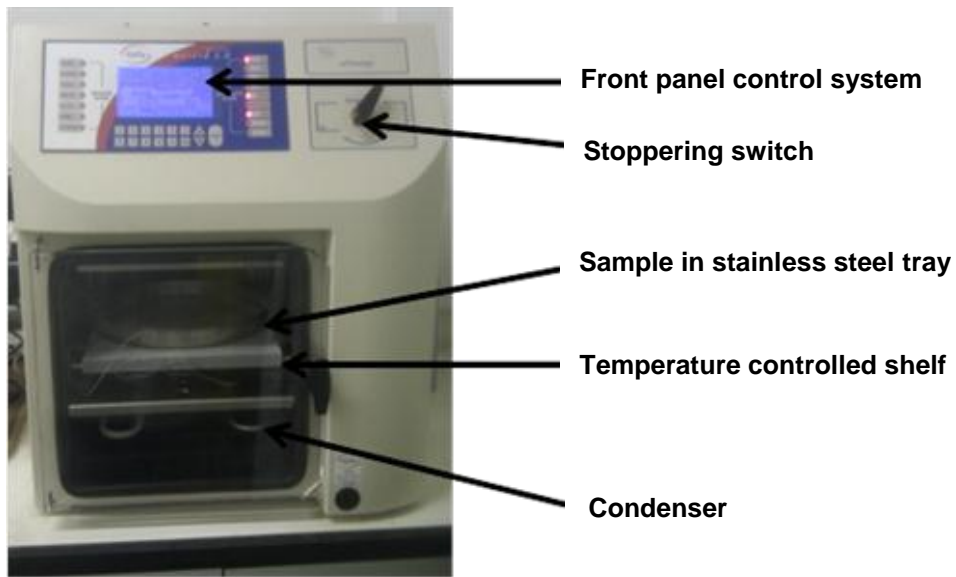


**Figure 3.2: Laboratory scale Virtis Advantage freeze dryer**

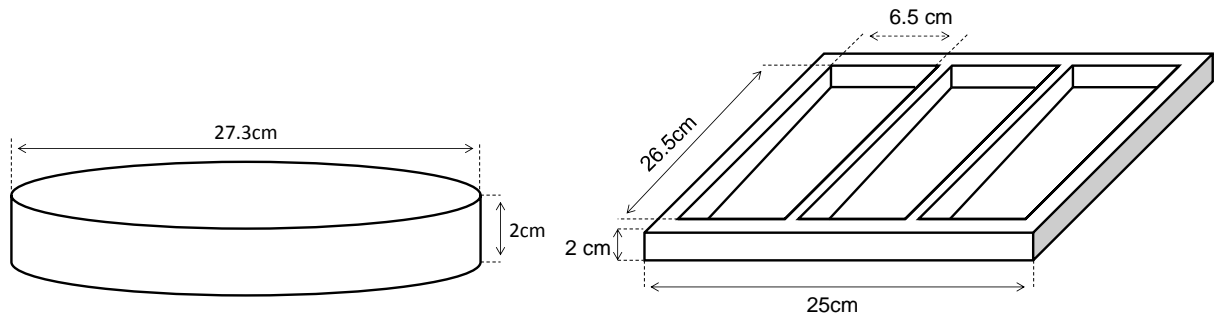


**Figure 3.3: Schematic representation of bulk drying tray containers used in lyophilisation process. Left: Stainless steel tray. Right: Custom made 3 compartment dense grade polystyrene model foam tray system with a polyethylene base.**

### 3.4 Post freeze drying characterisation

#### 3.4.1 Dried sample transfer and moisture control through isolation

Sample trays were transferred from the freeze dryer at the end of drying cycles into a flexible polyurethane isolator (Soloflex, UK) purged with oxygen free dry nitrogen (BOC, UK) to 10-20% relative humidity. Isolator was fastened onto the Virtis advantage freeze dryer using polyurethane (PU) skirt and an O-ring (Figure 3.4).



**Figure 3.4: Schematic of custom designed 2 gloves polyurethane flexible isolator supported on an aluminium frame for dried bulk tray transfer from freeze dryer. Image from Soloflex UK design proposal (Ingham group 2012).**

### 3.4.2 Karl Fischer coulometric analysis

#### 3.4.2.1 Background

The coulometric method of moisture analysis by Karl Fisher is preferred in freeze drying for its lower working range of 0.0001% to 5% of sample. Karl Fischer used equation (3.1) which requires sulphur dioxide in the presence of iodine in a non-aqueous medium to quantify water content (Mettler Toledo, 2009).



Acidic by-products previously eliminated with pyridine were replaced with imidazole ( $CH_3H_4N_2$ ) which is a less toxic base. The use of methanol as solvent results in a 1:1 water to iodine consumption. The standard reaction equation for Karl Fischer moisture determination (Scholz, 1981) is :



The titration cell of a coulometric Karl Fischer houses the anode and cathode electrodes.

The anode or generating electrode electrochemically yields iodine by oxidation according to the half equation:



The 2 electrons liberated at the anode reduce positive hydrogen ions to hydrogen at the cathode. Electrons can be related to current and time using to quantify water content using Faraday's constant (96485 coulombs/mol). From the relation between the molecular mass of water and total current required for anodic iodine production, 1 mg of water requires 10.712 coulomb of electric current. The end point of moisture content titration is determined by biopotentiometric indication which requires the application of a known polarization electric current to the cathode platinum pins and a high voltage to maintain such polarization current

(Mettler Toledo, 2009). At the end point of titration, free iodine will be present in the titration cell and will react with the platinum pins to reduce the voltage required to keep the polarization current constant. The end point is reached when a defined voltage is exceeded and terminates the titration.

### **3.4.2.2 Procedure**

Residual moisture content determinations were performed using a coulometric C20 Karl Fischer titrator (Mettler Toledo, Switzerland). 100 mL of CombiCoulomat fritless (Apura®) Karl Fischer reagent (VWR, UK, Product No: 1.09257.0500) was poured into the titration cell and titrated to dryness. Using a 12 cm hypodermic needle (Sterican, VWR, UK, Product No. 612-0161) and 10 mL syringe, 1 mL of dry reagent was drawn from the titration cell into aluminium crimped sample vials. Sample vials were bath sonicated for 10 minutes to facilitate moisture extraction. An aliquot (1 mL) of sample and anolyte was injected into the cell and titrated to the endpoint. Three replicates were measured per sample and recorded as the total water content (C). Total moisture content in a freeze dried sample was calculated using the equation:

$$R = C \times \left( \frac{M_{sol} + M_{ext}}{M_{ext}} \right) - \left( \frac{M_{sol}}{M_{ext}} \right) \quad (3.4)$$

**Equation 3.4: Where R is water content in the sample; C is the measured total water content; Msol is the amount of solvent (g); Mext is the amount of sample (g) extracted with the solvent.**

### 3.4.3 Helium pycnometry

#### 3.4.3.1 Background

Porosity was calculated from pycnometry determinations of true and bulk density of materials. The principle of gas pycnometry is drawn from Archimedes principle of fluid displacement. The small atomic dimensions of helium which is  $0.90 \pm 0.06$  angstrom (Youxue and Zhengjiu, 1995) makes it an ideal inert displacement gas for exploring inter and intra particulate pores. Using helium as fluid, the particle or true density of samples can be calculated from the resulting pressure difference when helium flows from a known reference cell volume into a sample cell (Figure 3.5).



**Figure 3.5: Schematic representation of a gas multipycnometer (Quantachrome Instruments, 2009).**

### 3.4.3.2 Procedure

A Multipycnometer (Model MUP- 6DCE Quantachrome Instruments, USA) was purged with 10 cycles of helium gas (BOC, UK) and validated using a 2.145 cm<sup>3</sup> micro calibration sphere standard. Powder samples were mechanically agitated through a 1 mm aperture sieve to remove any agglomerates formed on storage. Bulk density was calculated as a ratio of mass to volume obtained from a 10 mL measuring cylinder and an analytical balance. Sample was loaded into a 12.03 cm<sup>3</sup> micro sample cell volume (V<sub>c</sub>) and the 6.397 cm<sup>3</sup> reference cell volume (V<sub>r</sub>) was used. True powder volume (V<sub>p</sub>) and porosity were calculated using the equation:

$$V_p = V_c - V_r \left( \left( \frac{\text{Initial pressure in reference cell}}{\text{Final pressure in sample cell}} \right) - 1 \right) \quad (3.5)$$

Porosity was calculated from the equation (3.6) for an average of three measurements and its standard deviation was reported (Kumar *et al.*, 2001).

$$\text{Porosity} = 1 - \frac{\text{Bulk density}}{\text{Pycnometric density}} \quad (3.6)$$

A detailed standard operating procedure is available in appendix II on page 244 .

### 3.4.4 Light microscopy

Morphology studies were conducted with a light microscope (Carl Zeiss, Scope.A1 Germany) equipped with a polariser, camera system (Axiocam MRM) and imaging software (Axiovision version 4.8). Bottle of stock powder was homogenously mixed by 30 seconds of hand shaking. A small powder sample heap was collected with a metallic spatula onto a glass microscope slide (VWR, UK). Sample was spread uniformly on the slide by gentle tapping on the sides to remove excess powder and was covered with an 18x18 mm glass cover slip (Menzel Glaser, DE). Samples were viewed at magnifications of x10 eyepiece and

x10 or x40 objective lens. Three sets of camera images were taken per sample and focal stacked to create one image where applicable.

### 3.4.5 Mechanical sieving and laser light diffraction

#### 3.4.5.1 Mechanical sieving

The size distribution of powders were measured using a mechanical sieve shaker (Retsch, AS 200 basic, Germany) with a 16 set 38 mm diameter brass sieve stack (Endecotts, UK) with aperture sizes ranging from 1000-63  $\mu\text{m}$ . The mass of test sample used per assessment and maximum allowed residual masses after test was adapted from a published standard which is based on 200 mm diameter sieve area (International Organization for Standardization, 1988). Test samples were shaken at an amplitude of 80 mm at 5 minute intervals. The endpoint of the sieving process was reached when the mass of none of the test sieves was unchanged by more than 5% or 0.1 g of its previous mass (British Pharmacopoeia Commission, 2013d).

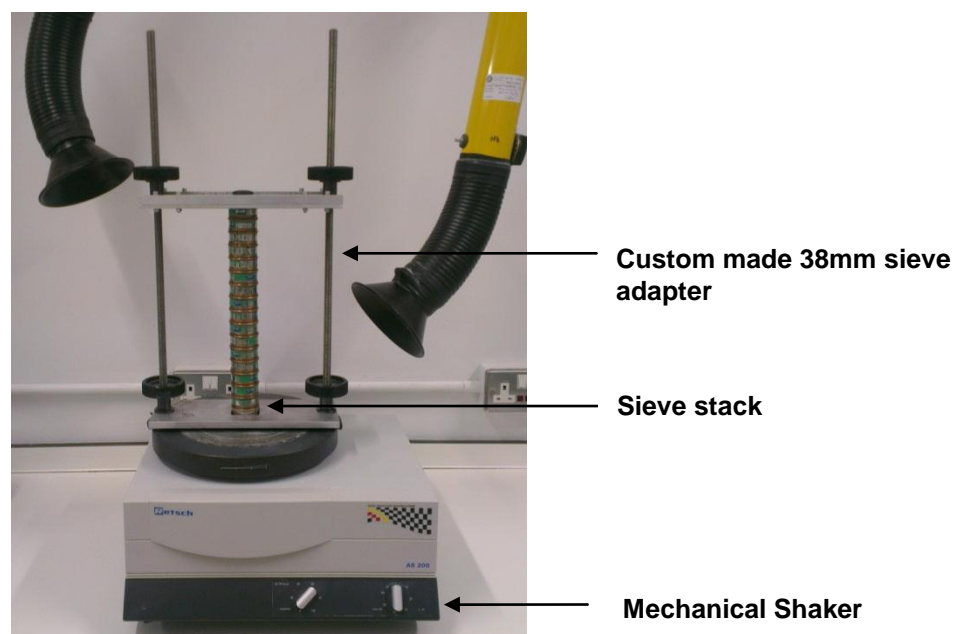


Figure 3.6: Particle size analysis by mechanical sieving.

### **3.4.5.2 Laser light diffraction**

#### **3.4.5.2.1 Background**

Diffraction patterns resulting from directing a laser beam at a particle can be used to obtain its particle size distribution. The laser light diffraction particle sizer utilises light-particle interactions to generate cumulative size distributions from an optics set up of Fourier lens, multi element photo detector and mathematical models. The intensity distribution with angles of diffraction are transferred onto a detector ring of known radius and transformed using Fraunhofer or Mie algorithms (Sympatec, 2013) to produce a size distribution.

#### **3.4.5.2.2 Procedure**

Particle sizing of a sample was measured with the laser light diffractor, Sympatec Helos/BF (Sympatec, DE), with windows 5.4.0 control software. A sensor range of 0.25/0.45-87.5  $\mu\text{m}$  was selected for use with a clean 50 mL optical glass cuvette and magnetic stirrer. Cuvette was filled with 40 mL of ultra-pure water and a reference diffraction measurement was determined at a stirring speed of 200 rpm. A sample volume of 2 mL was transferred with a pipette into the cuvette and a diffraction measurement was made at a particle dispersion speed of 200 rpm. Cumulative size distributions with standard deviation were recorded for 3 replicates per sample.

### **3.4.6 X-ray powder diffraction**

#### **3.4.6.1 Background**

X-ray powder diffraction is used to characterise the physical form of a material. It provides information directly related to the molecular packing within the solid state peak positions and intensities, amorphous and crystalline forms of a material can be differentiated and verified against reference diffraction patterns (Newman, 2011, Raj Suryanarayanan, 1995).

### **3.4.6.2 Procedure**

Samples were analysed with an X-ray powder diffraction (Bruker D2 Phaser, UK) using 30 kV 10 mA 300 W X-ray source.

## **3.4.7 Bicinchoninic acid assay (BCA)**

### **3.4.7.1 Background**

Quantification of total protein content using BCA is based on the colorimetric detection of cuprous ions at 526 nm (Smith *et al.*, 1985). It is based on the biuret reaction which involves the reduction of cupric to cuprous ions by the presence of proteins. Cuprous ions are chelated by two molecules of BCA to form a purple coloured complex caused by the presence of amino acids, peptide bonds and the protein macro structure (Wiechelman *et al.*, 1988).

### **3.4.7.2 Procedure**

Total protein content was determined using a bicinchoninic acid (BCA) assay kit (Thermo scientific, UK) in combination with a Multiskan spectrum plate reader (Thermo scientific). Six standard solutions were prepared with distilled water to prepare a calibration curve. Known standards were either BSA (Bovine serum albumin) or immunoglobulin depending on the type of unknown to be quantified. BCA working reagent was prepared from a 50:1 ratio of reagent A (sodium carbonate, sodium bicarbonate, bicinchoninic acid and sodium tartrate in 0.1 M sodium hydroxide) and reagent B (4% cupric sulphate). A standard of 25  $\mu$ L was transferred into 96 clear flat bottom micro well plates (Greiner Bio-one, UK). Working reagent (200  $\mu$ L) was added to each well with 3 pipette mixing manipulations. Plates were incubated in a plate reader at 37°C for 30 minutes and absorbance was measured at 562

nm. A standard calibration curve from an average of three readings for each standard concentration was drawn for use in the determination of unknowns (Figure 3.7).

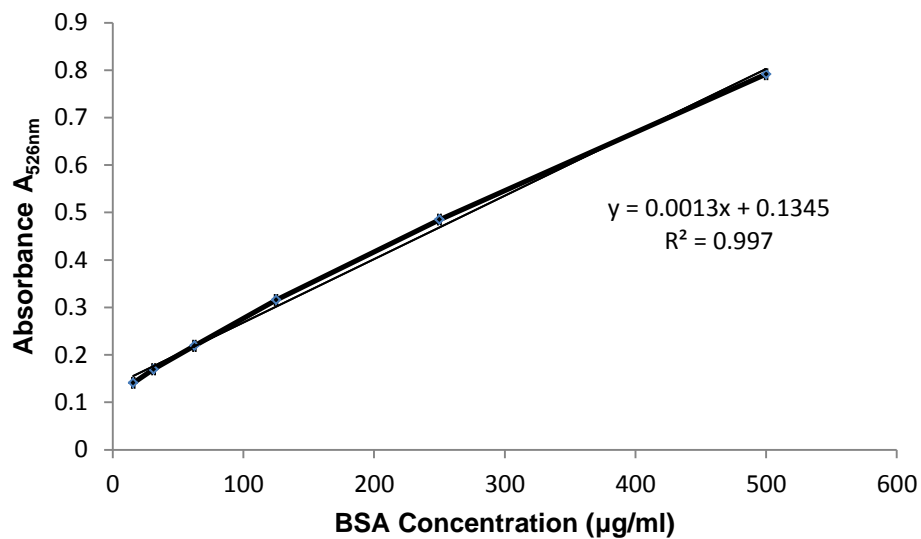


**Figure 3.7: Typical calibration plot for bovine serum albumin standard solutions analysed by BCA assay.**

### **3.4.8 Lactate dehydrogenase activity assay**

#### **3.4.8.1 Background**

LDH activity was determined using a kinetic UV spectroscopy assay conducted at 340 nm on the Multiskan spectrum plate reader (Thermo scientific, USA).

In the presence of NADH (Reduced Nicotinamide Adenine Dinucleotide) and LDH, Pyruvate is converted to lactic acid. Measurement of the absorbance at 340 nm is related to the amount of NADH consumed and is used to quantify the amount of LDH present (Krieg *et al.*, 1967, Grant, 2010).

### **3.4.8.2 Procedure**

A detailed standard operating procedure is available in Appendix III on page 248.

## **3.4.9 Fluorescence quenching assay**

### **3.4.9.1 Background**

A fluorescence quenching assay is a simple analytical method for quantifying proteins. When attached to a protein, fluorescein will fluoresce if exposed to an excitation wave length of 491 nm and subsequently emit at 520 nm. Immunoglobulin G raised against fluorescein isothiocyanate (Anti-FITC IgG) will bind to fluorescein in solution and quench the fluorescence intensity of any fluorescein present.

### **3.4.9.2 Procedure**

The assay was initially optimised for excitation and emission wave lengths of Anti-FITC IgG. The optimised process is available in appendix IV on page 252. The fluorescence quenching assay was performed according to standard operation procedure found in Appendix V on page 256.

## **3.4.10 Flowability characterisation**

### **3.4.10.1 Compressibility index**

#### **3.4.10.1.1 Background**

The extent of compaction exhibited by a powder when compressed provides a measure of its flowability. Good flowing powders are less compressible, have lower compressibility

indices and show low particulate friction (Carr, 1965). The index is calculated from either of the below equations:

$$\text{Compressibility index} = 100 \times \frac{(\text{Tapped Density} - \text{Bulk density})}{\text{tapped density}} \quad (3.7)$$

$$\text{Compressibility index} = \frac{(\text{Bulk volume} - \text{Tapped volume})}{\text{Bulk volume}} \quad (3.8)$$

Hausner's ratio is a variation to compressibility index expressed as a ratio of bulk to tapped density or a ratio of bulk volume to tapped volume (British Pharmacopoeia Commission, 2013c, Howard, 2007). Powders with low inter particulate friction are free flowing with ratios of 1.12-1.18 (Carr, 1965).

#### **3.4.10.1.2 Procedure**

Compressibility index was determined using a tap density apparatus (Sotax FD2, USA). The measurement of bulk density was adapted from the British Pharmacopoeia Commission (British Pharmacopoeia Commission, 2013a) using a 10 mL or 100 mL cylinder dependent on the amount of bulk powder available. Samples were passed through a sieve with 1 mm aperture to remove any agglomerates formed on storage. Using a 200 mL funnel, samples were poured gently into a dry cylinder and the unsettled apparent volume or bulk volume was measured and bulk density was calculated as a ratio of sample weight to bulk volume. The cylinder was transferred to the United States Pharmacopoeia I (USP I) holder to conduct the tap density measurement. The endpoint of the tapped sample was reached when there was no more than a 2 mL change in sample volume. Tapped density was calculated as a ratio of sample weight to tapped volume. Compressibility index was calculated as a percentage of the difference between tapped and bulk density divided by its tapped density. An average of three measurements and its standard deviation was recorded.

### 3.4.10.2 Angle of repose

#### 3.4.10.2.1 Background

Powders allowed to flow onto a surface may form a heap or a stock pile and the three dimensional angle ( $\theta$ ) that its surface forms to the horizontal plane is referred to as the angle of repose (Howard, 2007, British Pharmacopoeia Commission, 2013c). It provides an indirect measure of inter particulate resistance or friction to movement within a powdered mass. Carr (1965) classifies powders with values between 31-35° as “good” and above 66° as “Very very poor”.

#### 3.4.10.2.2 Procedure

Measurements were made using the experimental set up (Figure 3.8) of a 100 mL funnel and retort stand above a flat base. Samples were poured through the funnel and allowed to form a heap with height ( $h$ ) and radius ( $r$ ). The tip of the powder heap was at least 2 cm from the funnel. Angle of repose was calculated as the inverse function of the ratio of height to radius and reported as an average of three replicates with a standard deviation.

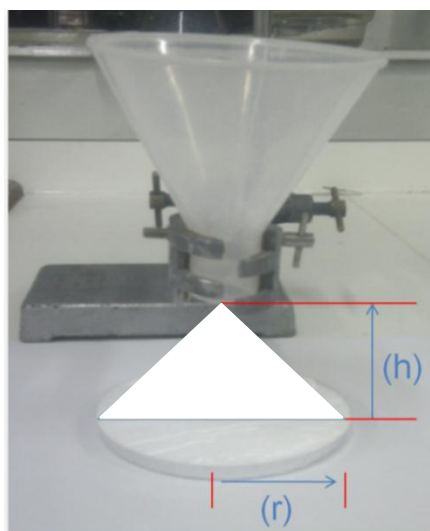


Figure 3.8 : Schematic of an angle of repose experimental set up. The angle of repose is expressed as  $Tan^{-1} \frac{h}{r}$

### **3.4.10.3 Shear Cell**

#### **3.4.10.3.1 Background**

Shear cell testers provide more precise powder flowability assessments and inform the basics for hopper design from both derived and raw determinants such as yield loci, angle of internal friction, unconfined yield strength and tensile strength of a material (BP 2013).

The Brookfield powder flow tester (Figure 3.8) is a shear cell capable of wall friction, bulk density, standard and time consolidated flow function tests.

Applying a shear stress causes a powder to flow and its magnitude is dependent on the bulk density of material which relates to the compacting and normal stresses (Williams, 1990). At different compacting stresses, the vane lid traps powder particles in compartments and are sheared against particles in the sample trough. Different shear stress and normal stresses can be studied to obtain the relationship called the yield locus. In combination with tangentially drawn Mohr circles to the yield locus, the angle of internal friction, unconfined yield strength and principal compacting stress tensile strength of a material can be derived (Schwedes, 2003).

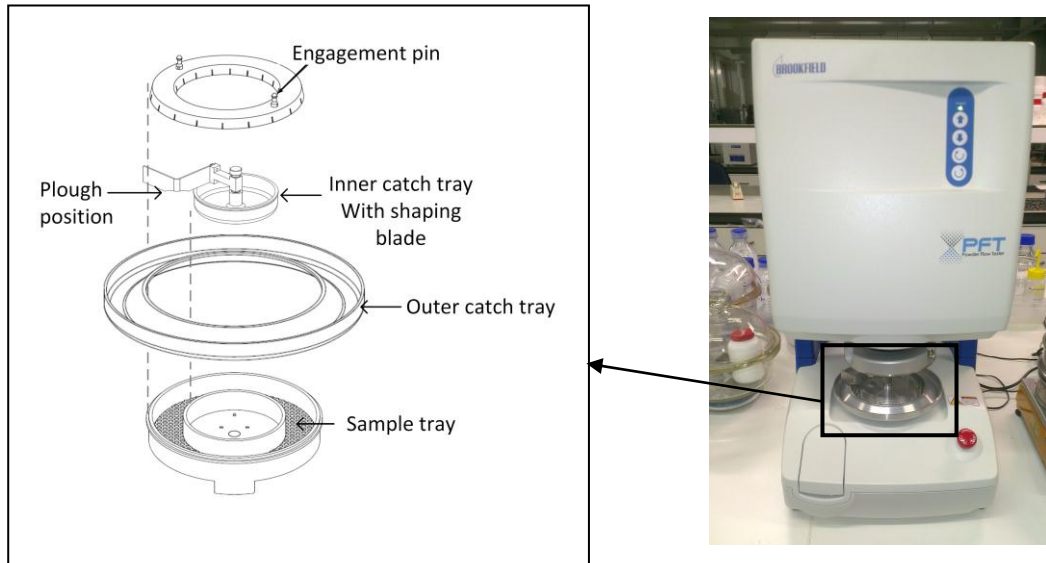


**Figure 3.9: Left: Exploded schematic view of shear cell arrangement of a Brookfield powder flow tester (PFT). Image adapted from operation manual (Brookfield Engineering Laboratories Inc.) Right: Picture of PFT used in research laboratory.**

#### **3.4.10.3.2 Procedure**

Shear cell measurements were obtained using a Brookfield powder flow tester (Brookfield, USA) with Powder Flow Pro V1.2 Build 20 software. Test samples were passed through a 1 mm test sieve to break any agglomerates that may have formed on storage.

Sample was filled into a 6 inch small trough using a powder scoop and sample weight was obtained by difference. Outer and inner catch trays were attached to trap powder overflows during powder levelling and analysis. Powder was levelled by clockwise rotation of the shaping blade in the plough position. The flat shaping blade position was used for powder levelling during wall friction tests in conjunction with a wall friction lid. Type of test, number of consolidation stresses and number of stresses were specified according to 1 of 4 desired assessments as previously described (section 3.4.10.3.1). A refresh sample was used to determine 3 replicates where possible and results recorded.

### 3.4.11 Lyophilised powder dispensing

#### 3.4.11.1 Gravimetric and Volumetric dispensing of non-annealed freeze dried powders

Non annealed freeze dried powders were gravimetric and volumetric dispensed using either a Quantos mass dispenser (Mettler Toledo, UK) or Accofil volume dispensing system (Biopharma, UK) shown in figures below.

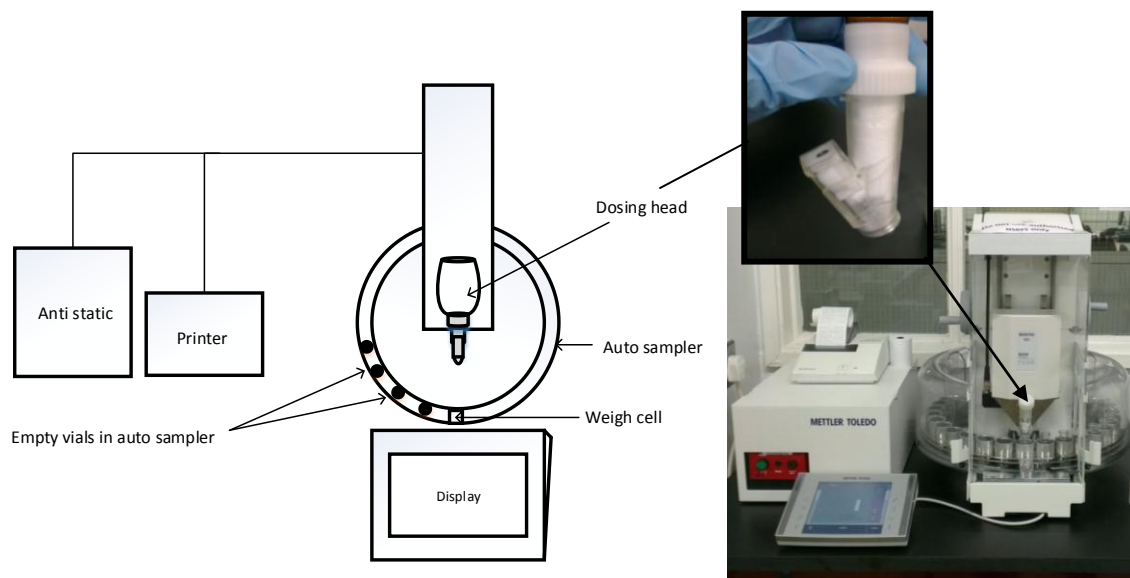


**Figure 3.10: Experimental set up of Quantos gravimetric dosing system. Left: Schematic and Right: Picture Insert: Magnification of dosing head. The dosing head of the Quantos system has a stirrer, dosing pin and a radio frequency identification (RFID) chip for storage of unique sample data.**

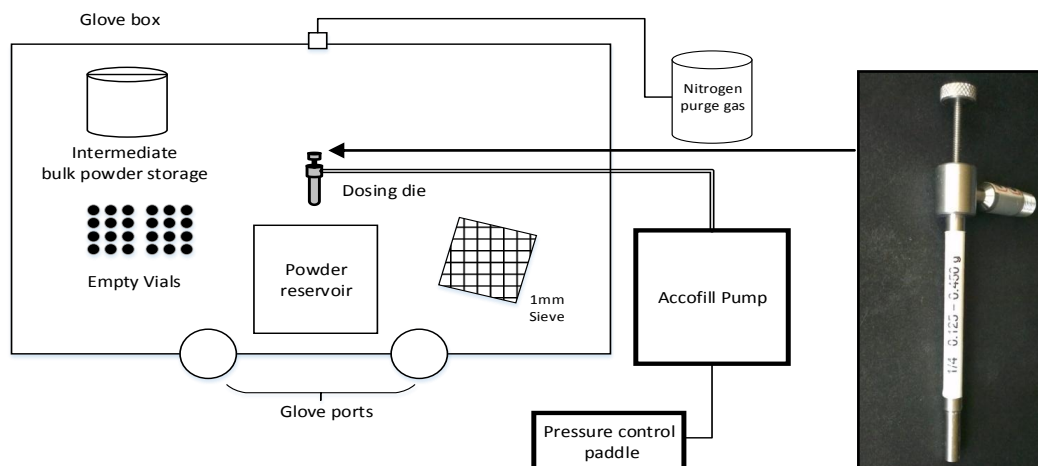


**Figure 3.11: Schematic representation of experimental set up using the Accofill volumetric dispensing system. Insert: Picture of the dosing head or die with die volume adjusting screw top.**

### **3.4.11.2 Gravimetric dispensing of annealed freeze dried powders**

Prior to dosing, samples were passed through a 1 mm aperture sieve to break up aggregates formed on storage before dispensing using a commercial Fill2Weight powder dispensing system by 3P Innovation, UK (Figure 3.11). Powders were conditioned by aeration before dosing. Dosing was performed in a fixed relative humidity (12.8%-14.5%) at a 20°C temperature.

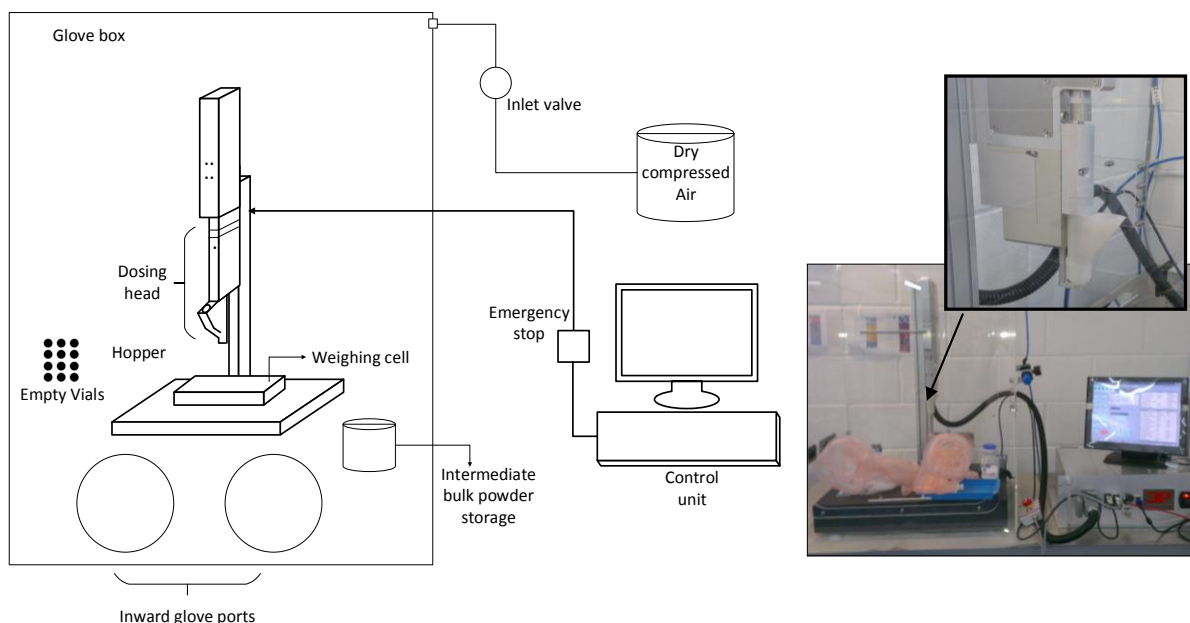


**Figure 3.12: Experimental set up of Fill2weight™ gravimetric dosing system Left: Schematic and Right: Picture Insert: Magnification of dosing head. A powder dosing valve is opened and closed in response to weight feedback from a calibrated weighing cell.**

### 3.4.12 Micro Computer Tomography

#### 3.4.12.1 Back ground

X-ray beams are absorbed or scattered when directed through an object. A detector can capture these attenuated X-rays into corresponding shadow images. X-ray attenuation is influenced by density, atomic number and X-ray energy (Baruchel *et al.*, 2000). Using the Feldkamp cone beam algorithm these shadow images are can be converted into computer tomographic (CT) images which are 2 dimensional slice by slice cross section image representations (Feldkamp *et al.*, 1984). By stacking a series of 2D images, a 3D reconstructed volume can be produced to inform the internal geometry of the object. X-ray microcomputer tomography (Micro CT) analyses were performed using a SkyScan 1172 Micro CT scanner (Bruker, Belgium) equipped with a 20-1000 kV/10 W X-ray source and 11 mega pixel cooled 12 bit charge coupled device (CCD) camera. Analysis chamber housed a

standard object or sample stage capable of angular rotation on its axis. An object with a maximum of 50 mm diameter and 70 mm length could be scanned.

#### **3.4.12.2 Procedure**

Samples were securely mounted upright on the object stage with multipurpose tac or dental beading wax in the analysis chamber. Micro CT analyses were with a 36-60 kV X-ray source with current and power settings which were study dependent. Samples were imaged with 0.2-0.7° object stage rotations. Camera resolution was 3-6 microns with 2-10 images averaged. Samples were confirmed to be upright, remained in the field of view of camera through the entire scan and scan initiated using the Skyscan 1172 control software. Fresh samples were used for replicates were applicable. Resulting X-ray projection images were reconstructed into 2 or 3 dimensional cross sectional images using the Nrecon (local version 1.6.6) software and volume rendered with CTvox (version 2.2). Reconstructed images were analysed to provide information on the structural attributes using CT Analyser (Version 1.12) software.

#### **3.4.13 Statistical analysis**

One way analysis of variance (ANOVA) statistical analysis was performed using Graph pad Prism 6 analysis software. A probability value (P) of less than 0.05 within 95% confidence limits was defined as statistically significant.

## 4 INVESTIGATING THE FLOW BEHAVIOUR OF BULK LYOPHILATES

### 4.1 Introduction

The need to characterise pharmaceutical materials for their powder flow properties is commonplace in pre-formulation studies for tableting and quality control (QC). The powder handling industries characterise powder flow patterns as it influences flow from storage vessels and prior to packaging at processing lines and also informs hopper design.

While many pharmaceuticals powders have been thoroughly characterised for flow, only brief fragments of such studies of freeze dried powders are available in literature. Arguably this area has not caught the attention of freeze drying scientists because the status quo is to dry sterile small molecules and biopharmaceuticals in glass vials. Bulk freeze drying applications which require powder flow characterisation do however exist predominantly in the food industry where sterility is not a concern. Powder characterisation in industry often involves the use of a cost effective and simple aerated methods such as angle of repose, flow through an orifice, tapped density or the non-aerated shear cell method (Guerin *et al.*, 1999, British Pharmacopoeia Commission, 2013c).

The number of times flow properties of lyophilised pharmaceuticals have been reported is very few. Garmise *et al.* (2006) characterised the morphology of lyophilised inactive influenza viruses in lactose and trehalose. Samples were however vial dried and flow properties were measured for milled powders in the 45-125 micron particle size range only. Schiffter *et al.* (2010) measured tap density of spray freeze dried nano suspensions of insulin in trehalose, mannitol and dextran. Sample volumes were limited and a modified pharmacopoeia method using a 5 mL volumetric vessel was used. Generally lessons for flowability of bulk lyophilised formulations cannot be ideally drawn. Kaialy and Nokhodchi (2013) investigated 5 %w/v freeze dried mannitol (63-90  $\mu\text{m}$ ) in comparison with commercial

and spray dried mannitol for its superior pulmonary delivery. The attention given to flow though minimum was the highest fill volume reported in literature that had been dried and investigated for flow properties. Interestingly, a 100 mL initial solution was freeze dried in a 250 mL round bottom volumetric flask at  $-110^{\circ}\text{C}$ . The choice of drying container and cycle temperatures are not desirable and atypical for an optimal bulk freeze drying process.

There is no literature fully characterising flow behaviour of bulk freeze dried powders which can serve as the bench mark for work in this area to harness the cost benefits of bulk tray drying. Such bench mark study will also require a reproducible powder breaking or disruption technique for bulk tray dried cakes into powder capable of further processing.

A hexagonal arrangement of vials on freeze dryer shelves is adopted in industry to maximise the use of shelf space (Figure 4.1).

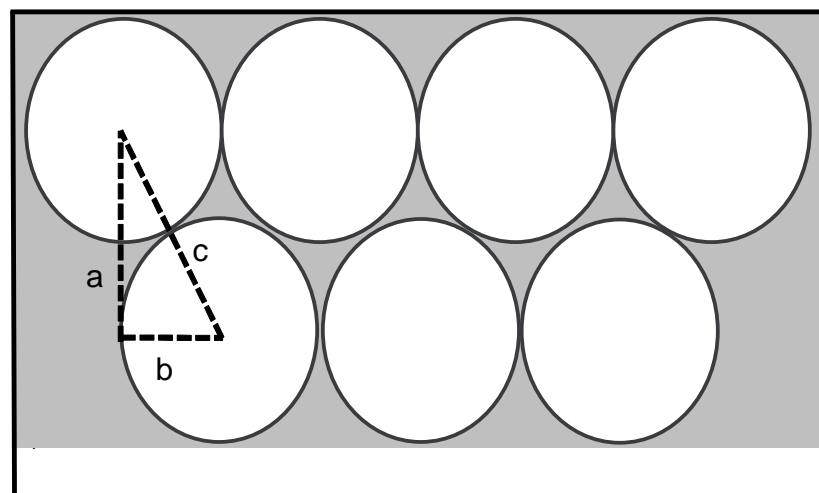


**Figure 4.1: Section of the hexagonal packing of vials on a typical freeze dryer shelf showing dead space (grey area) not in use. From shelf and vial dimensions including wall thickness, the volume not being used can be calculated using trigonometry.**

However comparing vials to bulk drying in a tray held on the same shelf dimensions, 23% to 34.4% of the shelf volume is wasted when a comparison is made. A shelf to be loaded with vials and a fixed volume will require either an increase in fill depth of vials or additional vials

(bigger shelf) to make up the total liquid volume to be dried (See Table 4.1). Any increase in fill depths exceeding 2 cm is not considered ideal due to an expected increase in resistance to mass transfer and a resultant increase in primary drying times.

**Table 4.1: Calculation of the volume of dryer shelf not used when filled using the hexagonal arrangement of vials on different freeze dryer (A-F) shelves. Calculations were based on vial and tray wall thicknesses of 1.5 mm, fill height of 10 mm and an outer vial diameter of 29 mm or 50 mm. Waste is expressed as a percentage volume not used. Alternatives to meeting the short fall is expressed as additional process vials or suggested increase in fill depth.**

<b>Type of freeze dryer and geometry</b>										
Freeze dryer	A	B*	C	D**	E	F	G	H*	E	F**
Shelf width (m)	0.3	0.654	1	1.524	5	10	0.3	0.654	1	1.524
Shelf length (m)	0.6	0.711	3	1.829	7	10	0.6	0.711	3	1.829
Area (m <sup>2</sup> )	0.18	0.46	3	2.79	35	100	0.18	0.46	3	2.79
<b>Drying process</b>										
Vials diameter (mm)	29	29	29	29	29	29	50	50	50	50
Shelf not used (%)	19.6	14.5	13	12.1	10.3	10.2	21.5	15.5	13.2	14.8
Shelf holds (vials)	219	602	3953	3708	47506	136026	72	200	1326	1210
Fill height (mm)	10	10	10	10	10	10	10	10	10	10
<b>Volume not used (%)</b>	<b>34.4</b>	<b>30.7</b>	<b>29.8</b>	<b>29.1</b>	<b>27.9</b>	<b>27.7</b>	<b>29.5</b>	<b>24.7</b>	<b>23</b>	<b>24.4</b>
Increase fill by (mm)	4.22	3.55	3.41	3.30	3.10	3.09	3.71	2.9	2.64	2.85
Process additional (vials)	115	266	1675	1523	18348	52210	30	66	396	391

\* Virtis AdVantage 2.0 bench top freeze dryer. Dryer dimension taken from SP Scientific (2014a). \*\* Hull production freeze dryer model 450FxS800. Dryer dimension taken from SP Scientific (2014b).

The adoption of bulk tray drying is challenged by the difficulty to maintain sterility, sample losses or “blow out” and wapping of stainless trays on the long term (Patel and Pikal, 2011). Commercially available lyoguard trays by Gore (Gassler and Rey, 2004) and a patent disclosed by Bergmann and Brustmann (1994) addressed sample losses using semi permeable membrane tray covers with minimal resistance to vapour flow. Cho *et al.* (1992) also disclosed collapsible blood bags for bulk lyophilisation. Some materials by nature will

only benefit from bulk drying and examples include lyophilised medical wound dressings and lyophilised cidofovir sheets which require moulding (Piette *et al.*, 2013).

Recent advances in technology is allowing aseptic bulk tray drying. An isolated aseptic commercial scale GMP freeze dryer with automated loading and unloading for bulk stainless steel trays has been reported in detail for drying polypeptides from fill to finish (Telstar, 2010). The technology has since being integrated for production lines used in bulk drying of sterile antibiotics in industry (Telstar, 2012).

There is the need to bulk dry either at early stage drug development which requires large amounts of lyophilised API or production of process intermediates for storage in intermediate bulk containers. Bulk drying can also be a final requirement in spray freeze drying approaches. Spray freeze drying techniques continue to utilise bulk drying vessels after atomization, freezing and collection of droplets into final stainless steel tray, bowl (Schiffter *et al.*, 2010) or glass dishes (Costantino *et al.*, 2000) for drying on a standard freeze dryer shelf.

Mannitol was chosen for flowability studies in this chapter because of its common use as bulking agent in freeze drying, diluent in oral disintegration tablets and carrier in dry powder inhalers. Most importantly it can fully crystallise when freeze dried which is desired for final stability. Mannitol has been well studied in literature for its final freeze dried attributes. Freeze dried mannitol provides structural support to produce cakes with an elegant appearance (Pyne *et al.*, 2002). It also provides structural support in the presence of a collapsed amorphous phase; a phenomenon referred to as micro collapse (Johnson *et al.*, 2002). Its high eutectic temperature of  $-1.5^{\circ}\text{C}$  allows the use of both conventional and aggressive high temperature drying (Kim *et al.*, 1998, Hawe and Friess, 2006b, Cao *et al.*, 2006). Mannitol is known for its vial breaking tendency when in the crystalline state can exist as a mixture of both amorphous and crystalline forms as well as a hydrate (Yu *et al.*, 1999,

Cao *et al.*, 2006). Its stabilising effect however deteriorates with increasing crystallinity (Izutsu *et al.*, 1994). The various polymorphs of mannitol and their preparation have also been thoroughly reported (Burger *et al.*, 2000, Yu *et al.*, 1999) and its behaviour in the presence of other co solutes is well known (Torrado, 2002, Hawe and Friess, 2006b).

We hypothesise crystalline components in a freeze dried powder system will be responsible for good flowability rather than amorphous components if present. Poly dispersed powder particles from disrupted bulk freeze dried powders may be produced and will influence flow.

## **4.2 Aim and Objectives**

It is the aim of this chapter to investigate the flow properties of bulk lyophilised mannitol and sucrose as carriers for small molecules and biopharmaceuticals. The effect of total solute content on particle morphology which influence flow properties were investigated using standard pharmacopoeia methods. A further objective was to investigate the role of thermal treatment during the freezing stage of the lyophilisation process on these flow properties. The chapter is concluded with considerations to inform aspects for further processing of bulk lyophilised biopharmaceuticals or small molecules downstream in a production line. It must be emphasised that maintaining aseptic conditions during drying and powder manipulation are not within the scope of this chapter.

## **4.3 EFFECT OF SOLUTE CONCENTRATION ON FLOWABILITY OF BULK FREEZE DRIED POWDERS**

### **4.3.1 Materials and Methods**

Fluid bed dried D-mannitol Ph. Eur. was purchased from Fagron, UK. Fluid bed dried sucrose BP was obtained from Fischer Scientific, UK. CombiCoulomat fritless Karl Fischer reagent was purchased from VWR, UK.

#### **4.3.1.1 Freeze drying**

##### **4.3.1.1.1 Pre-formulation characterisation**

Eutectic melt temperature ( $T_{eu}$ ) for mannitol and glass transition temperature of the maximally frozen solution ( $T_g'$ ) for sucrose were investigated using MDSC as previously described (Section 3.2.2.2). About 20mg of sample was equilibrated at  $-40^{\circ}\text{C}$  with  $\pm 0.5^{\circ}\text{C}$  or  $1^{\circ}\text{C}$  modulation every 50 or 100 seconds. A ramp rate of  $1^{\circ}\text{C}/\text{min}$  to  $20^{\circ}\text{C}$  was used.

##### **4.3.1.1.2 Drying cycle**

Mannitol and sucrose (300 mL, 1-15 %w/v) solutions were freeze dried in a stainless tray (Figure 3.3 page 57) in a Virtis advantage freeze dryer. Samples were shelf loaded and cooled from room temperature to  $-55^{\circ}\text{C}$  with 6 hours hold. Primary drying was performed at  $-30^{\circ}\text{C}$  for 32 hours with secondary drying at an elevated temperature of  $20^{\circ}\text{C}$  for 4 hours. Condenser was at a constant  $-75^{\circ}\text{C}$  with pressure at 200  $\mu\text{bar}$ . Product temperature was monitored using K type thermocouples placed at the centre and edge of trays to monitor product temperature during the freeze drying cycle. Trays containing bulk dried cakes were transferred through a funnel into sealed bottles for storage in a desiccator over moisture indicating dried silica gel.

#### **4.3.1.2 *Cake disruption technique (I)***

Bulk freeze dried cakes were broken down into powder with a British pharmacopeal tablet friabilator (Sotax USP F2, Switzerland) using a fixed 1000 revolutions in simulation of typical handling.

#### **4.3.1.3 *Karl Fischer moisture content determination***

Residual moisture content determinations were performed using a coulometric C20 Karl Fischer titrator, Mettler Toledo, Switzerland as previously described in the materials and methods section 3.4.2.2 on page 60.

#### **4.3.1.4 *Compressibility index***

Compressibility index was calculated from bulk and tapped densities measured using a 100 mL measuring cylinder as described in material and methods chapter section 3.4.10.1 on page 67.

#### **4.3.1.5 *Angle of repose***

Angle of repose was measured by passing samples through a funnel from the calculated tangential inverse function of the ratio of powder height to radius as previously described in material and methods section 3.4.10.2.2 page 69.

#### **4.3.1.6 *Light microscopy***

Morphology studies were conducted with a light microscope (Carl Zeiss, Scope.A1 Germany) equipped with a camera system (Axiocam MRM) and imaging software

(Axiovision version 4.8). Magnifications of x10 eyepiece and x10 or x40 objectives were used.

#### **4.3.1.7 Particle sizing by mechanical sieving**

Particle sizing method (British Pharmacopoeia Commission, 2013d) was performed using a mechanical sieve shaker (Retsch, AS 200 basic, Germany) and 200 mm test sieves with an aperture size range of 1000-75  $\mu\text{m}$ . An amplitude of 60 mm for 5 minutes per run was used until the endpoint of the sieving process was reached as defined by the BP and described in materials and methods section 3.4.5.1 on page 63.

#### **4.3.1.8 Porosity studies**

Porosity measurements were made using a helium gas multipycnometer (Quantachrome, MUP-6DCE, USA). Standard operating procedure for this analysis is available in the appendix II on page 244.

## 4.3.2 Results

### 4.3.2.1 Freeze drying

Pre-formulation characterisation results showed a eutectic melt of  $-1.44^{\circ}\text{C} \pm 0.01$  for mannitol and a  $T_g'$  of  $-31.58^{\circ}\text{C} \pm 0.43$  on the reverse heat flow curve for 15 %w/v sucrose (Appendix VIII). These were in agreement with the published eutectic melt of mannitol of  $-1.4^{\circ}\text{C}$  (Kim et al., 1998). Pikal (2007), Chang and Randall (1992) reported  $T_g'$  of  $-35^{\circ}\text{C}$  and  $-32^{\circ}\text{C}$  for sucrose.

Mannitol and sucrose from 1-15 %w/v solution were freeze dried producing elegant looking bulk dried cakes without product collapse or melt back. Minor cracks were observed in products with lower solute content (1-5 %w/v). Average thermocouple readings indicated that primary drying was completed in all cases, elevated thermocouple reading indicative of reduced sublimation cooling was seen for all dried materials. During primary drying, product temperatures were maintained below the measured eutectic melt of mannitol and the  $T_g'$  of sucrose. A typical cycle thermograph is available in appendix VI Figure A 10.

#### 4.3.2.2 Flow characterisation

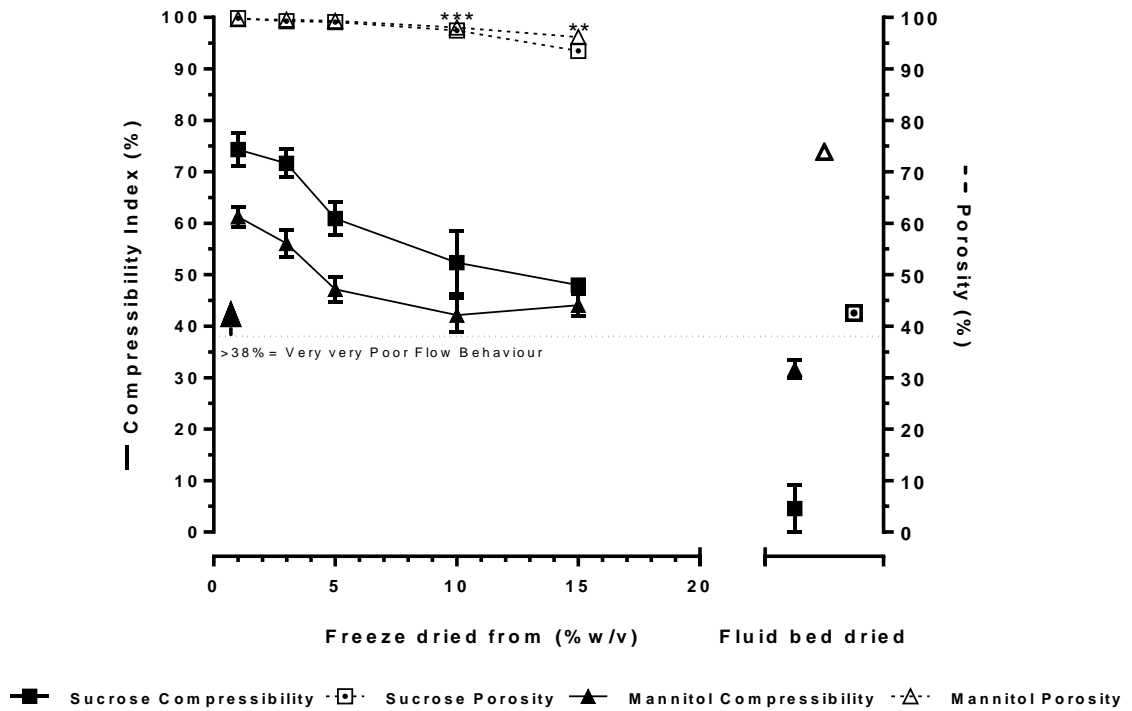


**Figure 4.2: Compressibility index and porosity of freeze dried mannitol and sucrose from 1-15 %w/v solutions. Fluid bed dried = BP grade crystalline powdered mannitol and sucrose (Fagron UK and Fisher UK respectively). \*\* Represents significance at  $P \leq 0.01$  ( $n = 3$ ) ANOVA between mannitol and sucrose porosity. \*\*\* Represents significance of 10 %w/v at  $p < 0.001$  from 15 %w/v in mannitol and sucrose porosity.**

Compressibility index and Hausner ratios were calculated. To avoid duplication in discussion of the interrelated indices, only the compressibility index is discussed.

Freeze drying mannitol and sucrose from a 1-15 %w/v solution produced dried cakes which when broken into powder using technique (I) (Fixed revolutions in a friabilator) produced powders with significantly ( $p \leq 0.01$ ) higher compressibility indices (Figure 4.2). A high compressibility index (Carr's index) value meant powders were very compressible, more cohesive and exhibited poor flow (Carr, 1965). Fluid bed dried sucrose powder had excellent flow, classified as  $4.59 \pm 4.58$  %, in contrast lyophilised sucrose was classified as 'very very

poor' ( $74.31 \pm 3.21$  %) when lyophilised from an initial solution concentration of 1 %w/v. The same comparison could be made for mannitol. An increase in the total solid content of both mannitol and sucrose solutions was found to influence compressibility indices of the final lyophilised powder. Increasing solute concentration correlated with a decrease in compressibility index and an improvement in the assigned flow character within freeze dried batches. Above 5 %w/v, there was no significant decrease ( $P>0.05$ ) in compressibility and no significant improvement in flowability of mannitol in its lyophilised forms.

#### **4.3.2.3 Angle of repose**

The angle of repose assessment based on the recommended British pharmacopoeia method was not possible in cases. Lyophilised powders did not flow and required forcing through funnels using a micro spatula, thus invalidating the measurement. Fluid bed dried samples however required no modification to their assessment method.

The angle of repose for fluid bed dried mannitol and sucrose was  $27.77 \pm 0.52^\circ$  and  $13.13 \pm 0.63^\circ$  respectively which conferred a flowability attribute of "Excellent" (Carr, 1965). Determination of angle of repose for lyophilised mannitol and sucrose were recorded as invalid due to bridging or arching that blocked the funnel.

#### 4.3.2.4 Moisture content determination

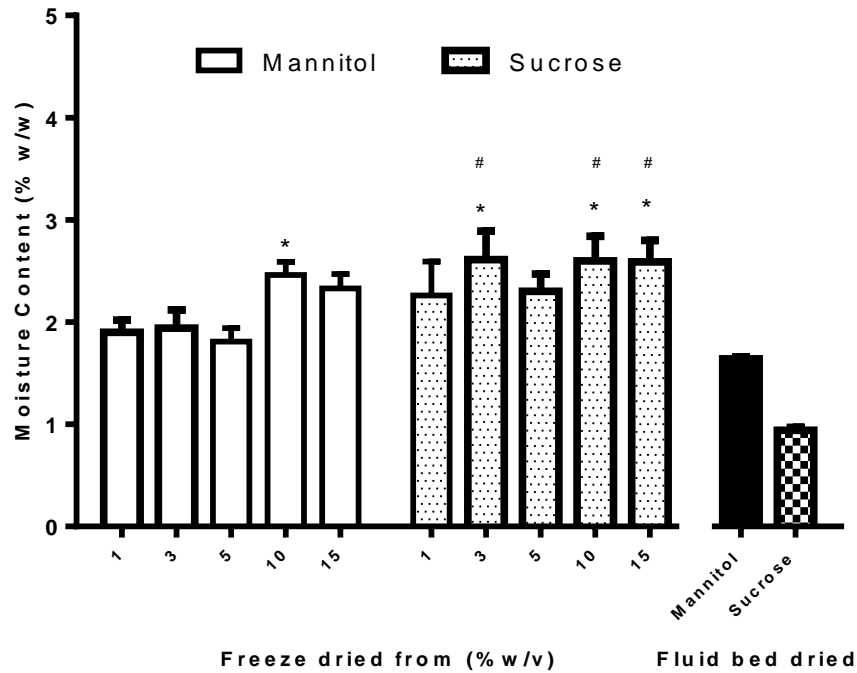


**Figure 4.3: Moisture content (n = 3) of bulk freeze dried mannitol and sucrose powders from 1-15 %w/v solutions. Fluid bed dried = BP grade crystalline powder mannitol and sucrose purchased from Fagron UK and Fisher UK respectively. \* represents significance at  $p < 0.05$  from mannitol lyophilised from 5 %w/v solution. # represents significance at  $p < 0.05$  from mannitol lyophilised from 1% and 3 %w/v solution.**

Moisture content (Figure 4.3) for both bulk dried mannitol and sucrose from 1-15 %w/v solutions were below 2.6 %w/w. Higher moisture content which average 0.4 %w/w was present in corresponding powders of the same solute content.

Moisture content for freeze dried mannitol ranged between 1.8-2.5 %w/w and sucrose ranged between 2.2 %w/w-2.6 %w/w.

There were no significant differences in moisture content within the lyophilised sucrose formulation batch. The same was true within the lyophilised mannitol batch except for powders dried from 5 and 10 %w/v solutions ( $p < 0.05$ ). Other statistical significance at

$p < 0.05$  ( $n = 3$  one way ANOVA) observed between some mannitol and sucrose batches were due to very minute differences in residual moisture of less than 1 %w/w in all cases (Figure 4.3).

Fluid bed dried sucrose recorded the least moisture content of 0.94 %w/w and higher residual moisture of 1.64 %w/w in fluid bed dried mannitol.

#### 4.3.2.5 Porosity studies

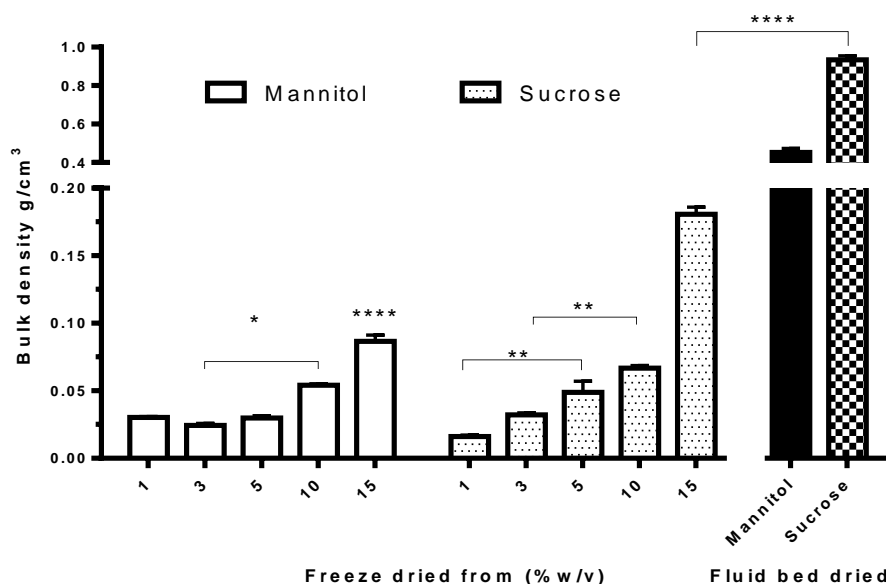


Figure 4.4: Bulk density ( $n = 3$ ) of bulk freeze dried mannitol and sucrose powders from 1-15 %w/v solutions. Fluid bed dried = BP grade crystalline powder mannitol and sucrose (Fagron UK and Fisher UK respectively). \* =  $P < 0.05$ , \*\* =  $P < 0.01$ , \*\*\*\* =  $P < 0.0001$  from all formulations ( $n = 3$  one way ANOVA)

**Table 4.2: Mannitol and Sucrose powders densities. Bulk and true densities (Mean  $\pm$  SD, n = 3) with literature comparison. Values are rounded to two decimal places where appropriate.**

Fluid bed dried Sample	Density (g/cm <sup>3</sup> )		Literature
Mannitol (Ph. Eur.) (Fagron, UK)	Bulk density	0.45 $\pm$ 0.02	0.43 g/cm <sup>3</sup> (Powdered) *
	True density	1.73 $\pm$ 0.02	1.514 g/cm <sup>3</sup> *
Sucrose BP (Fischer Scientific, UK)	Bulk density	0.93 $\pm$ 0.02	0.93 g/cm <sup>3</sup> (crystalline) $\approx$
	True density	1.62 $\pm$ 0.002	1.6 g/cm <sup>3</sup> $\approx$ , 1.586 g/cm <sup>3</sup> $\square$

\* (Armstrong, 2009a)  $\approx$  (Armstrong, 2009b)  $\square$  (Imamura *et al.*, 2008)

Bulk and true density measurements used for calculation of porosity were in agreement with literature values as shown in Table 4.2.

Powders from freeze dried mannitol and sucrose from 1-15 %w/v solution were very porous in nature (Figure 4.2) and calculated from true and bulk densities (Figure 4.4).

Porosity-concentration dependent variation was evident for freeze dried carriers and was skewed towards the production of less porous samples as total solid content increases per formulation. On the average, freeze dried mannitol had a porosity of 98.57% compared to 73.85% observed for its fluid bed dried form. A similar trend is observed in freeze dried sucrose with porosity averaging 97.83% within the batch compared to its fluid bed dried form, 42.58%. This represented a magnitude change of about 2 in total porosity ( $p < 0.001$  n = 3 ANOVA).

Powders from freeze dried mannitol and sucrose from 1-15 %w/v solution were very porous in nature (Figure 1) and porosities were calculated from true and bulk densities (Figure 2).

Porosity-concentration dependent variation is evident for freeze dried carriers and is skewed towards the production of less porous samples as total solid content increase per

formulation. On the average, freeze dried mannitol had a porosity of 98.57% compared to the 73.85% observed for its fluid bed dried form. A similar trend is observed in freeze dried sucrose with porosity averaging 97.83% within the batch compared to its fluid bed dried form, 42.58%. This represented a magnitude change of about 2 in total porosity ( $p < 0.001$   $n = 3$  ANOVA).

Low total solid contents were observed not to significantly yield different final powder porosity in either mannitol or sucrose and the least porous samples resulted from the highest 15 %w/v solute concentrations. No significant differences ( $P > 0.05$ ) in porosity was observed either within lyophilised mannitol powder batch formulated from 1-5 %w/v solutions or sucrose powders originating from an initial solute concentrations of 1-10 %w/v.

#### 4.3.2.6 Particle sizing analysis

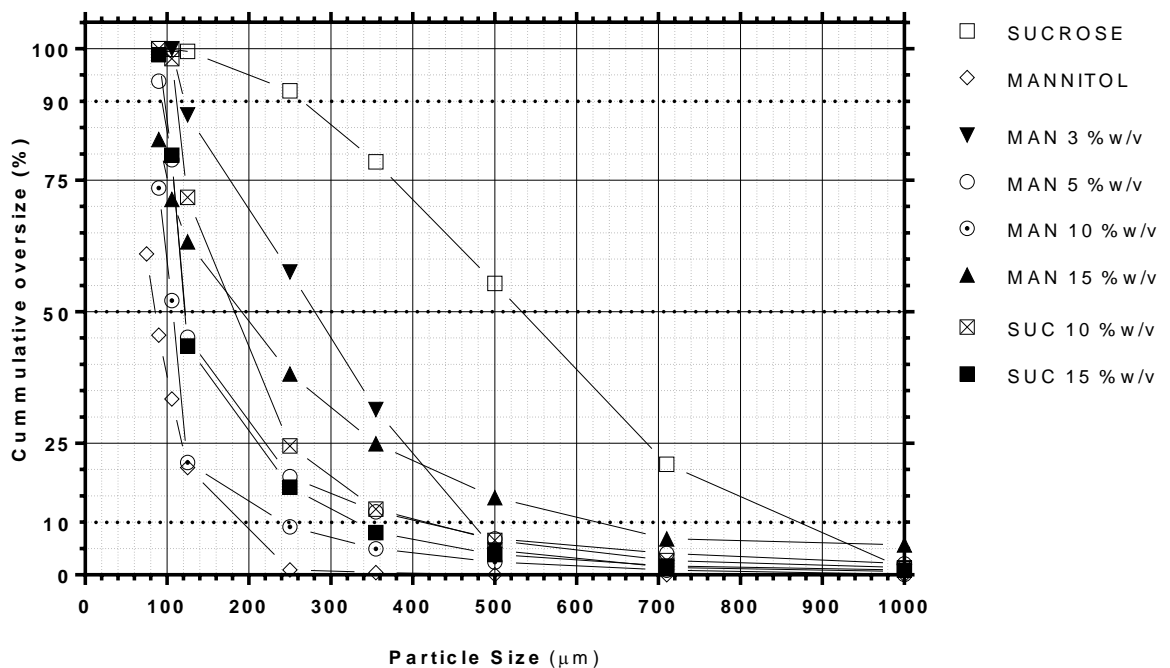
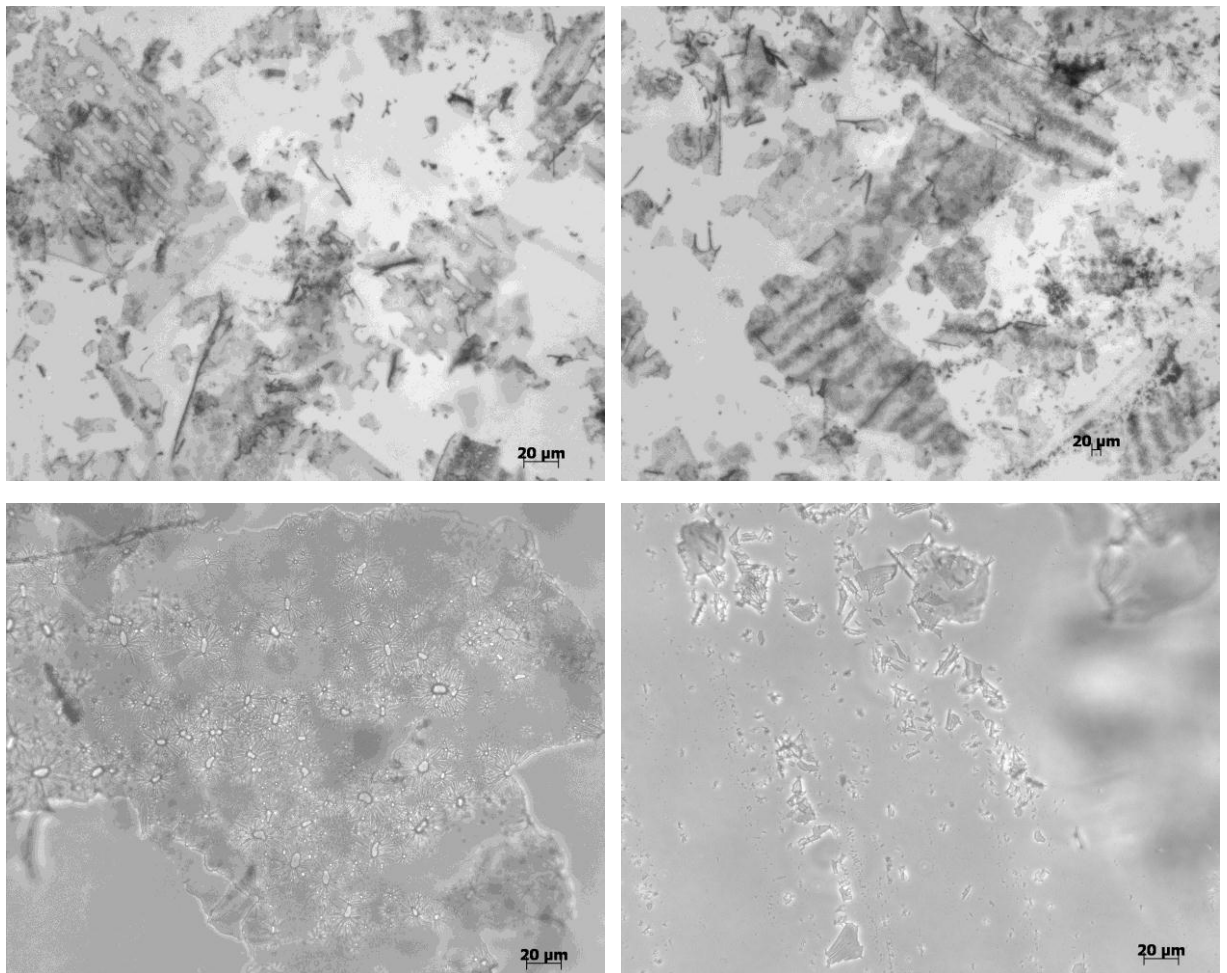


Figure 4.5: Cumulative particle oversize distribution ( $n = 1$ ) of freeze dried mannitol from solutions of 3-15 %w/v and freeze dried sucrose from 10 %w/v and 15 %w/v solutions. Fluid bed dried = BP grade crystalline powder mannitol and sucrose (Fagron UK and Fisher UK respectively). Size distributions collected into a sieving pan were below 75 microns.

There was not enough statistical evidence to suggest a correlation between final particle size distribution and initial concentration of freeze dried solution feed. The median particle size for disrupted freeze dried mannitol (1-15 %w/v) was between 100-280 microns and 120-200 microns in sucrose (10 and 15 %w/v only).

Particle size analysis for 1-5 %w/v freeze dried sucrose was not possible due to the high hydroscopic nature of the powder and moisture uptake during the powder assessment period at room temperature and pressure.

#### **4.3.2.7 Morphology studies by light microscopy**



**Figure 4.6: Light microscope images of freeze dried particles from 1 %w/v mannitol solution using x100 magnification (top row) and x 400 magnification (bottom row).**

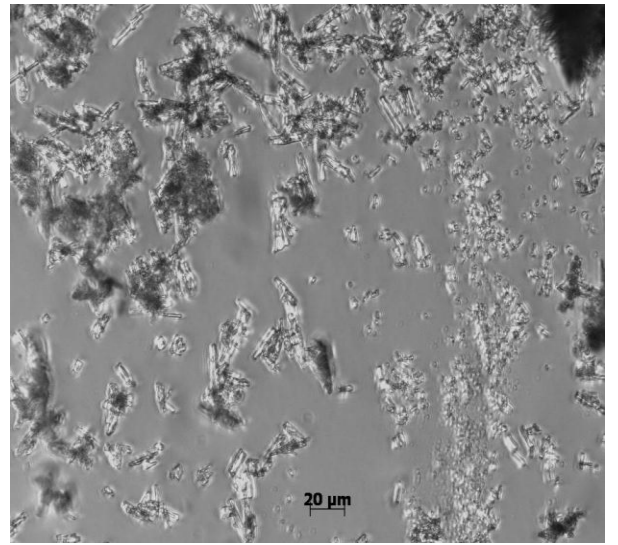
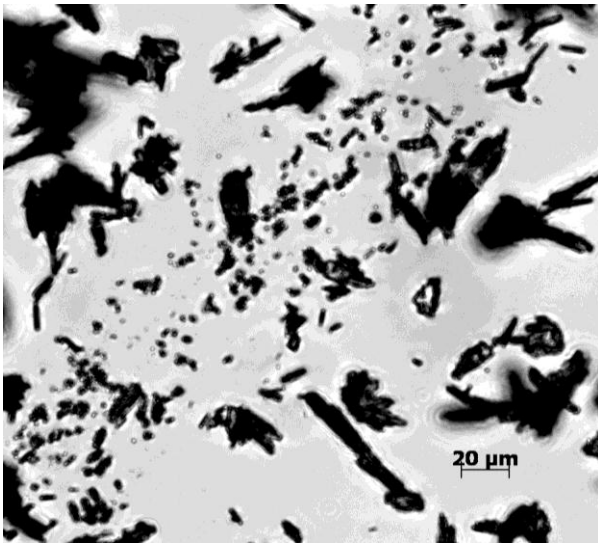
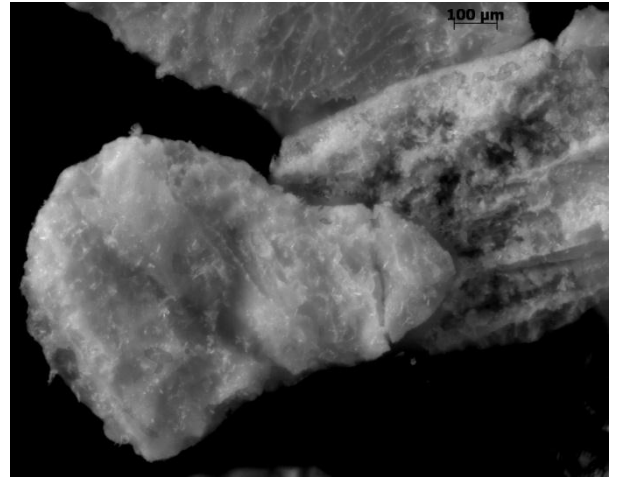
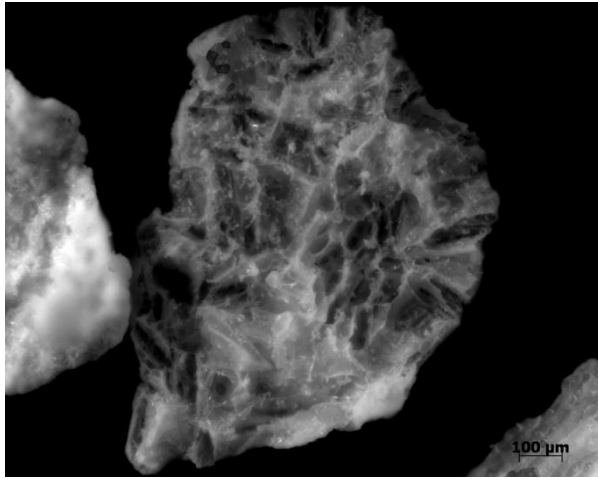


**Figure 4.7: Light microscope images of freeze dried particles from 5 %w/v mannitol solution using x100 magnification (top row, Focal plane stacked) and x400 magnification (bottom row).**

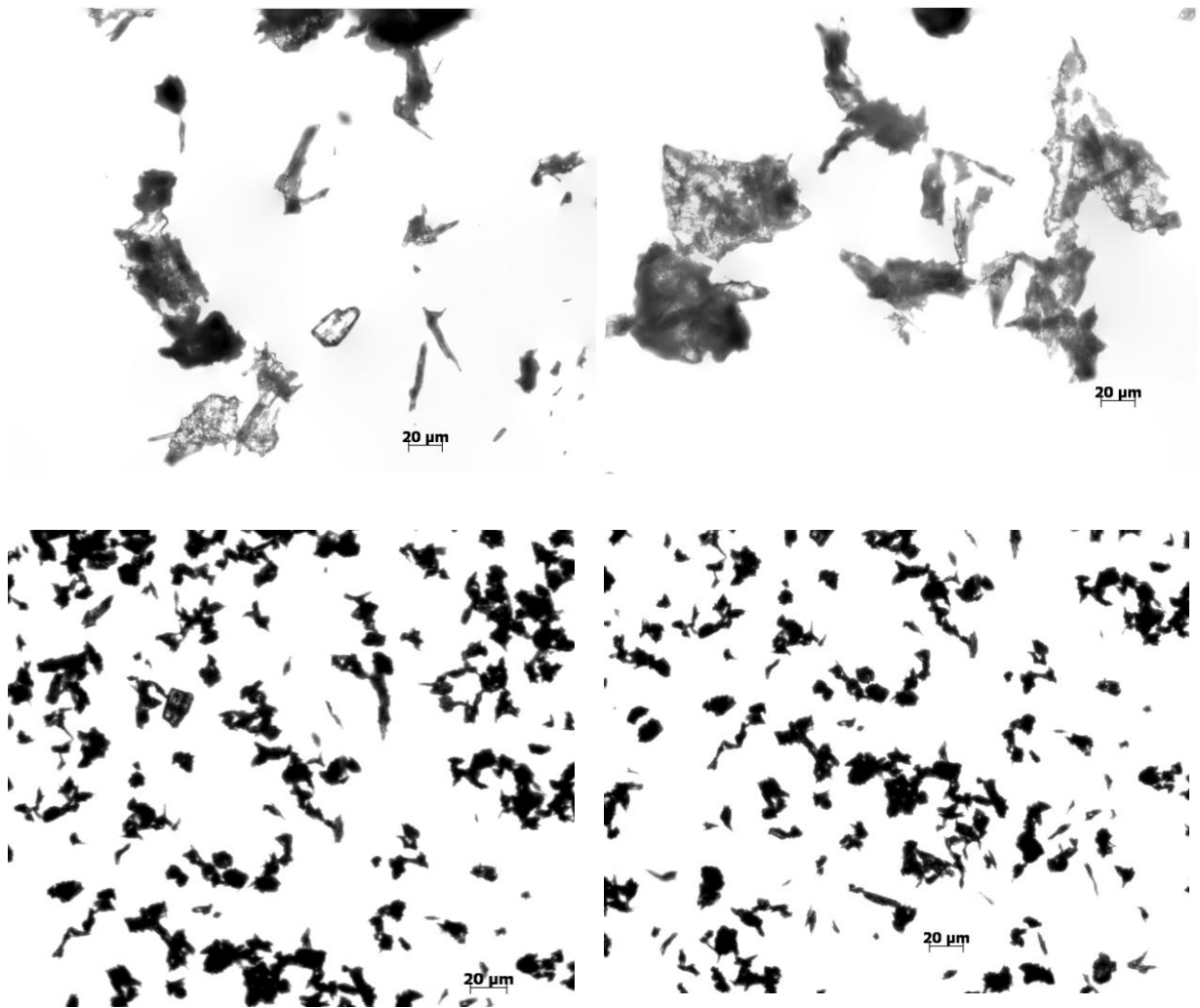


**Figure 4.8: Light microscope images of freeze dried mannitol from 15 %w/v mannitol solution at magnifications Top: x400 and Bottom: x100.**

Freeze dried mannitol (lyophilised from 1 %w/v and 15 %w/v solution) had irregular shapes with rough surfaces (Figure 4.6 to Figure 4.8). Platy and acicular or flaky particulate morphologies were also observed (Figure 4.6). Fluid bed dried sucrose particles were observed as crystalline blocks or masses (Figure 4.8) consistent with the description by Armstrong (2009b). They appeared more prismatic compared to fluid bed dried mannitol. Fluid bed dried mannitol were described by Armstrong (2009) as orthorhombic. In agreement, this study observed various sizes and shapes with some needle like appearance.

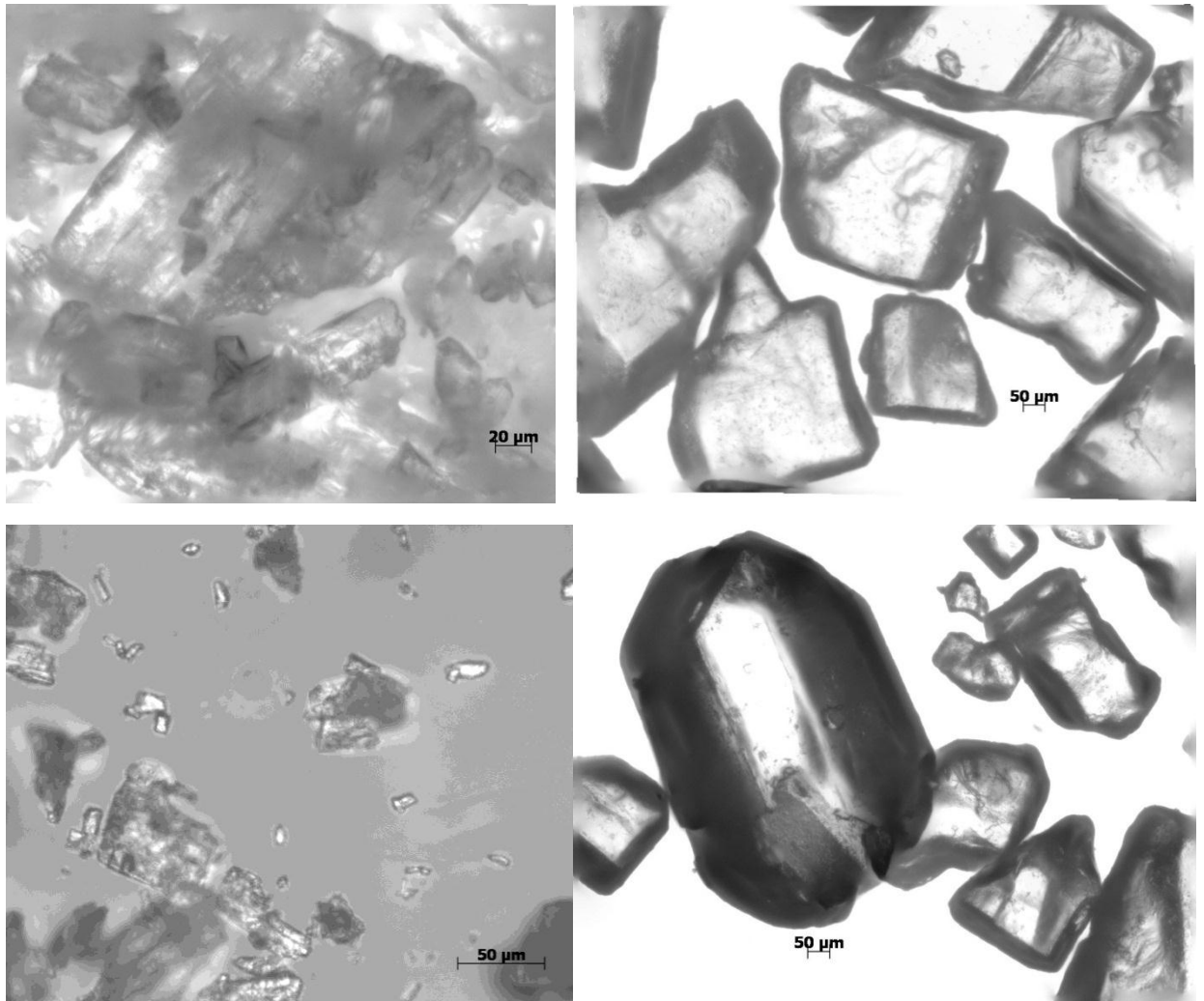


**Figure 4.9: Focal plane stacked light microscope images of fluid bed dried mannitol (x400 magnification, left column) and fluid bed dried sucrose (x100 magnification, right column).**

A correlation was identified between measured compressibility indices and some flow properties investigated (Figure 4.10). A strong relationship between porosity and bulk density of lyophilised mannitol and sucrose formulations exist. The least porous formulations (high bulk densities) showed better compressibility indices across formulations. The same was true in fluid bed dried forms serving as controls in this study.

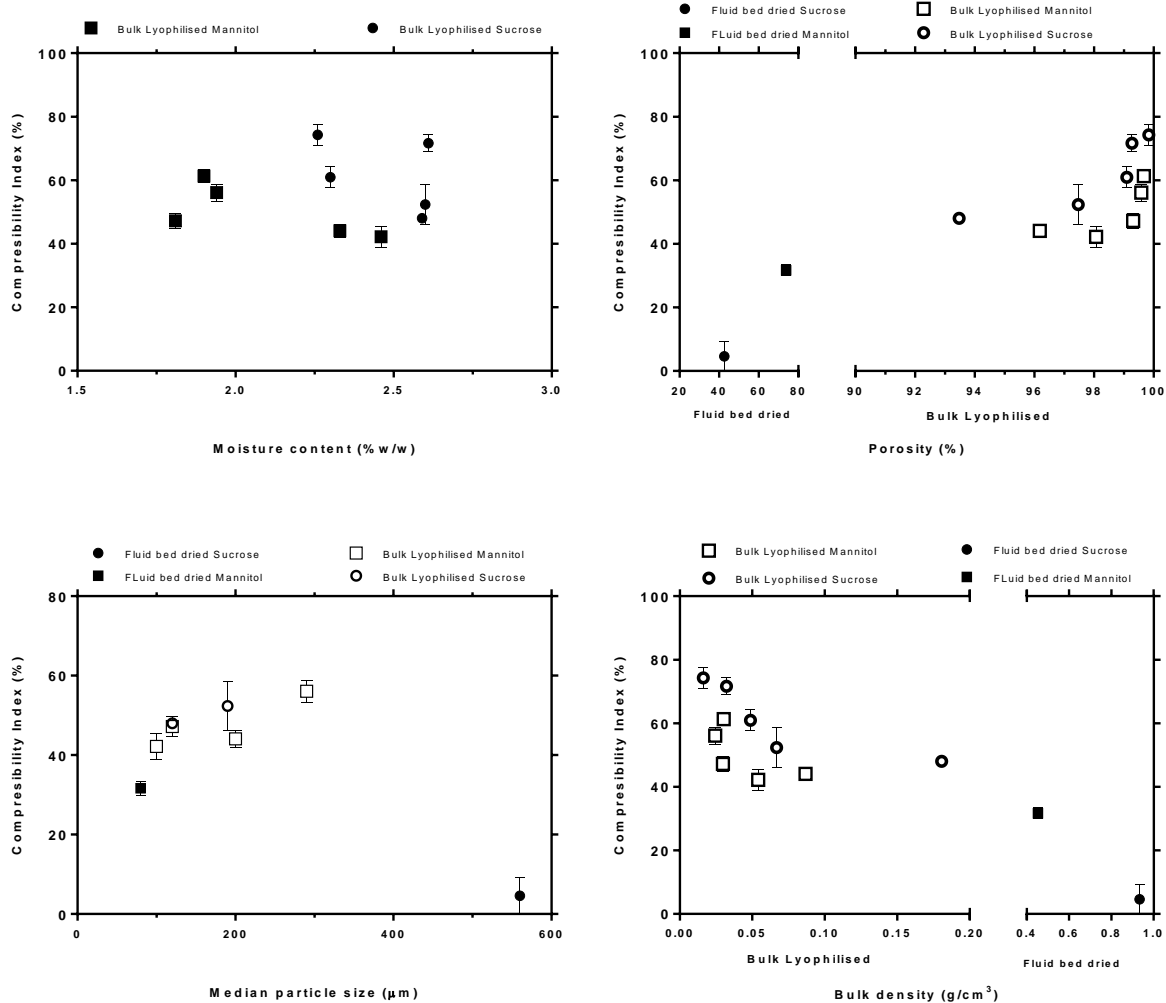


**Figure 4.10: Correlation between compressibility index (CI) of powders and Top: moisture content and Porosity. Bottom: Median particle size and Bulk density. CI (Mean  $\pm$  Standard deviation) is plotted against the mean ( $n = 3$ ) of moisture and porosity. Median particle size was determined from total sample lyophilised. Particle size of sucrose lyophilised from 1-5 %w/v sucrose solution and mannitol lyophilised from 1 %w/v solution are not documented.**

### **4.3.3 Discussion**

#### **4.3.3.1 Flowability**

Compressibility had a strong relationship with; the type of excipients lyophilised and the initial solute content of formulations. Bulk lyophilised mannitol batches were found to exhibit better flow characteristics when compared with sucrose formulations. The high compressibility indices observed in freeze dried sucrose implied it was more compressible than mannitol. For example sucrose freeze dried from 5 %w/v solution was significantly different in flow when compared with a dried mannitol powder from same solute concentration.

The compressibility index value for fluid bed dried sucrose corresponds to an excellent flow character which is in agreement with literature (Armstrong 2009).

Our initial postulation that increasing the solute concentration of a bulk carrier agent would increase the flowability of powders was confirmed true. Increased solute concentration from 1-15 %w/v decreased compressibility indices and improved flow behaviour.

Increasing the solid content of the initial freeze dried solution resulted in powders with a higher bulk density and explains the trend seen with decreasing compressibility indices (Figure 4.10). The extent to which the bulk density can be increased in formulations is however limited by solubility of its excipients. For example the solubility of mannitol and sucrose at 20°C are 1 in 0.5 and 1 in 5.5. Heating on a stirring plate may be required in cases where solubility at room temperature has been exceeded. This would not be ideal for heat labile APIs. A significant second factor is the need to avoid drying of an extra mass which may be unnecessary within the formulation, as this would negatively drive the economics of the lyophilisation process towards longer cycle lengths. Within this study, drying a mass of mannitol or sucrose above any solute concentration not associated with improvement in flowability will be wasteful. The presence of higher solute content results in

higher mass transfer resistance during the sublimation period and primary drying time is prolonged.

High solute content has been seen to provide similar benefits in literature (Maa *et al.*, 2004, Lamprecht, 2013). A high solid content of 20-30% for spray freeze dried influenza vaccine yielded powdered particulates with high “tap densities” was reported by Maa *et al.* (2004). The highest tap density reported was from a mixture of dextran, trehalose and mannitol at 0.79 g/mL; however these were not obtained with standard pharmacopeia methodology. The author’s methodology involved the use of samples in glass vials which were tapped on the bench 20 times and compared to an equivalent volume of water.

Lamprecht (2013) documented that by increasing the concentration of either BSA, dextran or PVP from 0.1 to 1 or 10% in spray freeze dried lysozyme they were able to produce a smooth and uniform lyophilised particle with fewer cracks and increase in mechanical strength from SEM.

#### **4.3.3.2 Moisture and morphology**

No one property can predict the flowability (British Pharmacopoeia Commission, 2013c) but it is controlled by a multitude of flow properties including; moisture, porosity, density, size and morphology.

At the end of primary drying, samples still contain about 5-20% residual moisture dependent on the formulation (Tang and Pikal, 2004). This is due to the presence of unfrozen water in its solute phase and requires elevated drying temperatures during secondary drying for removal by desorption. The typical objective of secondary drying would be to reduce moisture content to a level deemed optimal for the stability of a given formulation which is usually a level of less than 1 %w/w (Tang and Pikal, 2004).

The extent to which flowability of porous cohesive materials are affected by moisture was limited because residual moisture penetrates the core of particulates instead of forming liquid bridges (Howard, 2007). Formation of liquid bridges would negatively affect flow behaviour. Amorphous or crystalline mannitol can be produced depending on the freeze drying process and may exist in one of its polymorphic forms (Yu *et al.*, 1999). In its crystalline form, surface adsorption is the most common route of moisture uptake where water molecules interact at the vapour interface through weak interactive forces and form water mono layers on the crystal surface (Hancock and Shamblin, 1998). This observation is analogous to the behaviour of water insoluble powders which form water vapour or liquid bridges at high humidity (Coelho and Harnby, 1978). In this case it is the relative humidity and not the moisture content that determines whether any moisture present remains in the form of liquid bridges or is adsorbed as water vapour (Coelho and Harnby, 1978). While at low relative humidity (RH) moisture is adsorbed as vapour, formation of liquid bridges are favoured as RH increases after condensation at the particle contact points. It must be noted however that crystalline sucrose can absorb up to 1% moisture and is hygroscopic when finely divided (Armstrong, 2009b).

In this chapter, while tap density measurements were made at RTP, storage and measuring cylinder required for determinations were sealed from ingress of moisture. The effect of any absorbed moisture impacting on the compressibility of hygroscopic freeze dried sucrose (Armstrong, 2009b) can be assumed to have been negligible. Conversely, freeze dried mannitol is non hygroscopic after lyophilisation and has been demonstrated from moisture sorption studies in literature. Fakes *et al.*, (2000) disclosed lyophilised mannitol remained unchanged even at a high relative humidity of 60%. The authors found lyophilised sucrose absorbed up to 4% more moisture at 50% RH and desorbed at 55% RH Amorphous sucrose can absorb moisture and crystallise if poorly stored. Hancock and Dalton (1999) reported the crystallisation of amorphous sucrose after 3 months of storage at 30°C was above 40% RH.

Despite the absence of enough statistics to establish a relationship between size distribution and solid content, the effect of particulate size on lyophilised powder flowability was apparent.

Fluid bed dried mannitol and lyophilised mannitol from 5-10 %w/v solutions had particle fractions below 90 microns collected into the sieving pan. In the absence of the availability of other suitable characterisation methods, it could be assumed these micronised fractions may contain particles below 10 microns which are known to have bulk behaviour when in contact. Powders exhibiting bulk behaviour are cohesive due to the presence of surface energy forces which are strong enough to cause plastic deformation on the surface of particles at the points of contact (Walton *et al.*, 2007). Another difficulty working with very fine particles is the fact that they can become fluidized and may cause flooding (Carr, 1965) which can affect downstream processes or equipment not designed to handle a sudden influx of powder in larger quantities.

Particles above 250 microns are free flowing while below 100 microns flow problems are eminent due to increasing cohesiveness (Staniforth and Aulton 2007). Coarser particles are influenced more by gravitational forces than cohesive forces which negate good flow behaviour. For example freeze dried mannitol from 10% and 15 %w/v solutions, compressibility results show increasing flow behaviour which may be linked to the fact that 15 %w/v contained 38.16% oversize of 250 micron particles compared to 9.13% over size of 250 micron in the former. Freeze dried sucrose which showed excellent flow properties had the largest cumulative oversize distribution with 50% of particles above 540  $\mu\text{m}$ . Notably, 91.97% of particles were sized above 250 microns (Figure 4.5).

Fluid bed dried mannitol was composed of more fines compared to fluid bed dried sucrose although both crystalline in nature. Only 60% of the former was above 80 microns (40% below 80microns) compared to the 90% found greater than 280 microns in the later.

Flaky particles have a high surface to volume ratio and result in poorer flow behaviour (Staniforth and Aulton, 2007). This supports why the poorest flow behaviour was shown by powders with the least solute content, 1 %w/v. The more irregular the shapes of the particles, the poorer its flowability (Howard, 2007).

Similar benefits of both increasing solute concentration, shape and density was reported by Schiffter *et al.*, (2013) who used trehalose, mannitol and dextran with a total solid content of 35 %w/w to yield high density and robust spray freeze dried particles with irregular shape and wrinkled or rough surface morphology. The observed morphology was attributed to collapse of the amorphous phase and concluded to be beneficial for needle free ballistic insulin powder injection. These benefited from increased density and mechanical strength. Whilst a direct comparison cannot be made due to the 5 mL volumetric flask used in the determination of tap density by Schiffter and co-workers, reported Hausners indicate a range of spray freeze dried with fair to poor flowing powders.

The final physical form of a bulking agent or stabiliser is important for final storage. Clearly the use of mannitol in formulations over sucrose is warranted on the basis of its superior flowability over sucrose (Figure 4.1). Mannitol is however not ideal for lyoprotection. Other motivations for the use of mannitol in freeze dried formulations have been the elegant cakes that result and also for being a good bulking agent that will fully crystallise during drying. This prevents the release of moisture on storage that can affect stability of pharmaceuticals (Izutsu *et al.*, 1994). Sucrose is a better lyoprotectant than mannitol and as such the use of mannitol-sucrose mixtures have been investigated in literature (Johnson *et al.*, 2002). It is anticipated that such binary mixtures will be investigated further in this thesis

to identify considerations for bulk drying of pharmaceuticals where powder flowability is of immense importance.

#### **4.3.4 Conclusion**

Dryer shelf volume of 23%-34.4% was wasted when the hexagonal vial arrangement was compared to bulk drying in trays.

Both methods of accessing flow reinforced each other to emphasise the negative impact of freeze drying on powder flow behaviour. Fluid bed dried mannitol and sucrose showed better flow properties than all bulk lyophilised batches. A positive correlation between particle size, bulk density, porosity and freeze dried powder flowability has been found to exist. Increased solute content increases density and improves flow of freeze dried powders up to 15 %w/v. Mannitol as a flow enhancing bulking agent must be used at a concentration not less than 5 %w/v.

## **4.4 EFFECT OF FREEZING RATE AND THERMAL TREATMENT ON FLOWABILITY OF BULK FREEZE DRIED POWDERS.**

### **4.4.1 Background**

From the concentration-flowability studies in section 4.3 of this chapter, it was established that increasing the solute content of initial solution feed of freeze dried powders benefited its flow behaviour after breaking the cake into powder. The freezing step in lyophilisation is the most critical stage when the ice crystal morphology is formed depending on the freezing conditions. The use of a slow freezing rate no higher than 0.5 °C/min is often recommended in industry for the formation of large ice crystals to benefit from shorter primary drying times. Annealing formulations also induce homogeneity in ice morphology and reduce drying times (Searles *et al.*, 2001a). However, higher freezing rates for example when formulations are loaded onto precooled shelves and quench or rapid cooling in liquid nitrogen are occasionally adopted. These higher freezing rates produce smaller ice crystals and are associated with longer drying times. Unlike bulk tray drying, conventional drying in vials using these different freezing rates do not require any further cake processing and as such the flow properties that may be induced is unknown and not of concern.

In the following section of this chapter, the effect of different freezing rates and thermal treatment (Annealing) that could be adopted in bulk tray freeze drying is investigated to identify freezing step considerations for maximum benefits to final bulk dried powder flowability.

### **4.4.2 Materials and Methods**

Fluid bed dried D-mannitol Ph. Eur. was purchased from Fagron, UK. Fluid bed dried sucrose BP was obtained from Fischer Scientific, UK. CombiCoulomat fritless Karl Fischer reagent was purchased from VWR, UK.

#### **4.4.2.1 Freeze drying**

Mannitol solutions (100 mL, 0.056 M-1 M) were freeze dried in a Virtis advantage freeze dryer using a custom made three compartment tray (Dense grade polystyrene model foam frame (Trylon, UK) and polyethylene base (Tesco, UK)) (figure 3.3 in Chapter 3).

Different freezing rates of 0.2 °C/min, 1 °C/min and 5 °C/min were used. Samples chilled at 0.2 °C/min and 1 °C/min were equilibrated on a 25°C shelf for 30 minutes, shelf temperature was ramped to -55°C and held frozen for 6 hours. Samples which required annealing were equilibrated on a 25°C shelf for 30 minutes and chilled to -55°C (0.2 °C/min) with an additional temperature hold at -20°C for 2 hours. Samples which required freezing at 5°C /min were loaded directly onto a -70°C precooled shelf. Primary drying used a -10°C shelf temperature.

A constant -80°C condenser and vacuum of 200 µbar was used. Shelf was subsequently elevated to 20°C for secondary drying over 6 hours. K type thermocouples were placed at the centre and edge of trays to monitor product temperature during the entire freeze drying cycle. Tray containing bulk dried cakes were transferred into polyethylene bags and into a nitrogen purged isolator (Soloflex, UK). Cakes were passed through a funnel into sealed bottles for storage in desiccators over moisture indication dried silica gel.

#### **4.4.2.2 Cake disruption technique (II)**

Freeze dried cakes were broken into powder through mechanical sieving at a vibration amplitude of 80 mm through a 200 mm diameter sieve nest with aperture size range 710-75 µm fixed onto a mechanical sieve shaker (Retsch, AS 200 basic, Germany). Endpoint of the powder breaking process was reached when the mass on any of the test sieves were unchanged by more than 5% or 0.1g of its previous mass (British Pharmacopoeia Commission, 2013d).

#### **4.4.2.3 Karl Fischer moisture content determination**

Residual moisture content determinations were performed using a coulometric C20 Karl Fischer titrator, Mettler Toledo, Switzerland as previously described (Section 3.4.2.2).

#### **4.4.2.4 Light microscopy**

Morphology studies was conducted with a light microscope (Carl Zeiss, Scope.A1 Germany) equipped with a camera system (Axiocam MRM) and an imaging software (Axiovision version 4.8). Magnifications of x10 eyepiece and x10 or x40 objectives were used to capture 3 sets of images per powder sample.

#### **4.4.2.5 Particle sizing by mechanical sieving**

Method for particle sizing (British Pharmacopoeia Commission, 2013d) was performed using a mechanical sieve shaker (Retsch, AS 200 basic, Germany). Ten test sieves with an aperture size range of 1000- 53  $\mu\text{m}$  and base pan were used at an amplitude of 80 mm for 5 minutes per run. Endpoint of the sieving process was reached as previously described.

#### **4.4.2.6 Porosity studies**

Porosity measurements were made using a helium gas multipycnometer (Quantachrome, MUP-6DCE, USA). Standard operating procedure for this analysis can be found in Appendix II.

#### **4.4.2.7 Compressibility index**

Compressibility index was calculated from bulk and tapped densities measured as described in material and methods chapter using a 50 mL measuring cylinder which was sealed with parafilm™.

#### **4.4.2.8 Angle of Repose**

Angle of repose was measured by passing samples along the side of a funnel in small quantities to form a heap of powder. The tangential inverse function of the ratio of powder height to radius calculated as previously described in material and methods section 3.4.10.2.2.

#### **4.4.2.9 Shear cell**

Flow function test was measured using a Brookfield powder flow shear cell tester (Brookfield, USA) as previously described (Section 3.4.10.3.2). A geometric spacing with 4 consolidation levels and 3 stresses up to a maximum of 6.26 kPa was used. The shear tester was set to an axial speed of 1 mm/sec and torsional speed of 1 rev/hr. Sample trough and vane lids of 5 inches in diameter were used. All measurements were performed at room temperature and pressure.

### **4.4.3 Results**

#### **4.4.3.1 Freeze drying**

Formulations were successfully freeze dried and typical freeze drying cycle plots are available in appendix VI (Figure A11-A14, page 261). Thermograms for mannitol freeze

dried confirmed product temperature remained below the eutectic melt of mannitol of  $-1.5^{\circ}\text{C}$  (Kim *et al.*, 1998). Vacuum and condenser temperature remained constant with evidence of sublimation cooling during the primary drying phase. A subsequent elevation in product temperature during primary drying depict the removal of bulk ice and the cycle allowed enough soaking period to guarantee uniformly dried middle and edges of the bulk cake. Freeze dried cakes were elegant in appearance with no visual observation of melt back.

#### 4.4.3.2 Moisture content determination

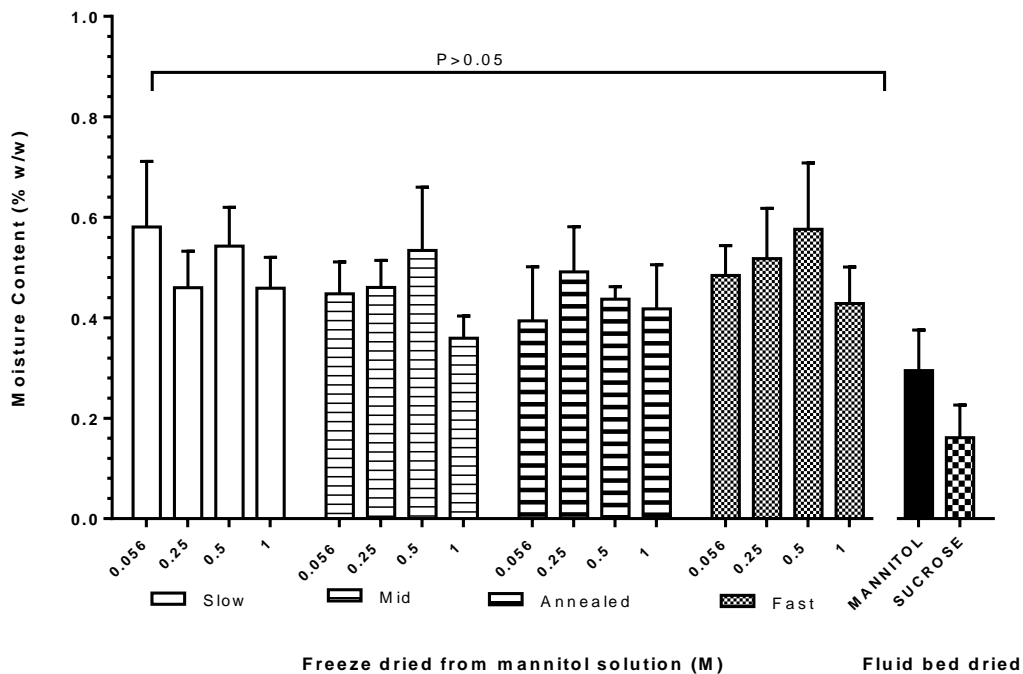


**Figure 4.11: Moisture content (n = 3) for bulk freeze dried mannitol from 0.056-1 M solutions. Slow =  $0.2^{\circ}\text{C}/\text{min}$ . Mid = freezing rate of  $1^{\circ}\text{C}/\text{min}$ . Fast = freezing rate of  $5^{\circ}\text{C}/\text{min}$ .**

All freeze dried samples recorded residual moisture content of less than 0.6 %w/w without significant difference at  $p > 0.05$  (Figure 4.11).

#### 4.4.3.3 Compressibility Index

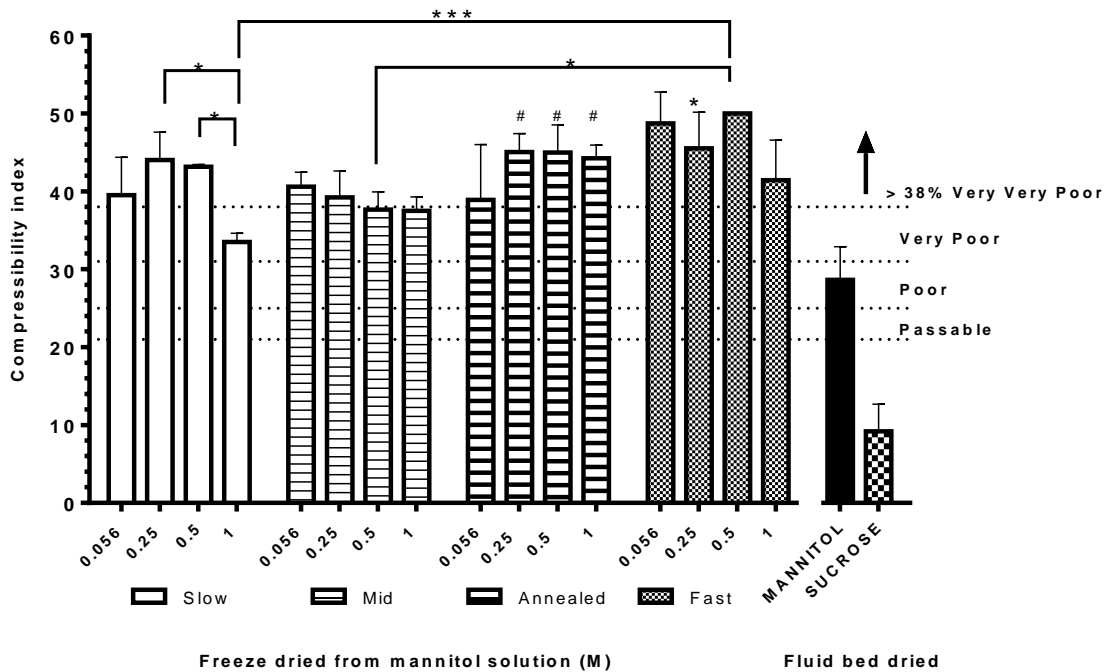


Figure 4.12: Effect of freezing rate and thermal treatment on compressibility index (n = 3) of bulk freeze dried mannitol from 0.056-1 M solution. Slow = 0.2 °C/min. Mid = freezing rate of 1 °C/min. Fast = freezing rate of 5 °C/min. \* = p< 0.05, \*\*\* = p<0.001 and # = p< 0.05 from power lyophilised from 1 M mannitol solution.

The effect of freezing rate and thermal treatment of mannitol lyophilised from 0.056 M-1 M solution revealed some apparent concentration-flowability relationships with statistical evidence in cases. Increasing compressibility values corresponded to a decline in powder flowability. Except for mannitol lyophilised from 1 M solution which was frozen at 0.2 °C/min, freezing solutions at rates of 0.2-5 °C/min or annealing produced powders with no improvement in compressibility index and were classed as "Very very poor" in flowability. Based on same compressibility criteria, the former was classed as very poor. Fluid bed dried mannitol and sucrose however were poor (p<0.05) and excellent (p<0.00001) in flowability respectively.

Total solid content-compressibility index relationship is apparent in powders lyophilised from solutions chilled at 0.2 °C/min and at 5 °C/min ( $p > 0.05$ ). Increasing solute concentration from 0.25 M to 1 M resulted in a marginal improvement in compressibility index with significance  $p < 0.05$  (one way ANOVA). A similar trend was observed when 0.056 M to 1 M mannitol solutions were lyophilised from an initial chilling at 0.2 °C/min without significance ( $P > 0.05$ ).

Freezing samples faster on precooled freeze drying shelves at 5 °C/min yielded no benefit neither did annealing samples at a -20°C (2hours hold) provide benefits from compressibility indices. Majority of the evidence from compressibility indices suggests the use of higher solid content of 0.25 M to 1 M cooled at either 0.2 °C/min or 1 °C/min was beneficial.

#### **4.4.3.4 Angle of Repose**

Angle of repose measurements detected no significant differences between bulk lyophilised powders regardless of their handling history (Figure 4.13). Fluid bed dried mannitol and sucrose were however significantly different from all lyophilised powders with significance at  $p < 0.05$  and  $p < 0.0001$  respectively.

The angle of repose for lyophilised powders ranged from 47.41°-51.07° which corresponded to poor on Carr's flowability scale and therefore classed as materials which require agitation or vibration (Carr, 1965). Fluid bed dried mannitol was measured at 40.18° and classed with a flow property between fair and passable while fluid bed dried sucrose measured at 22.21° was classed as excellent.

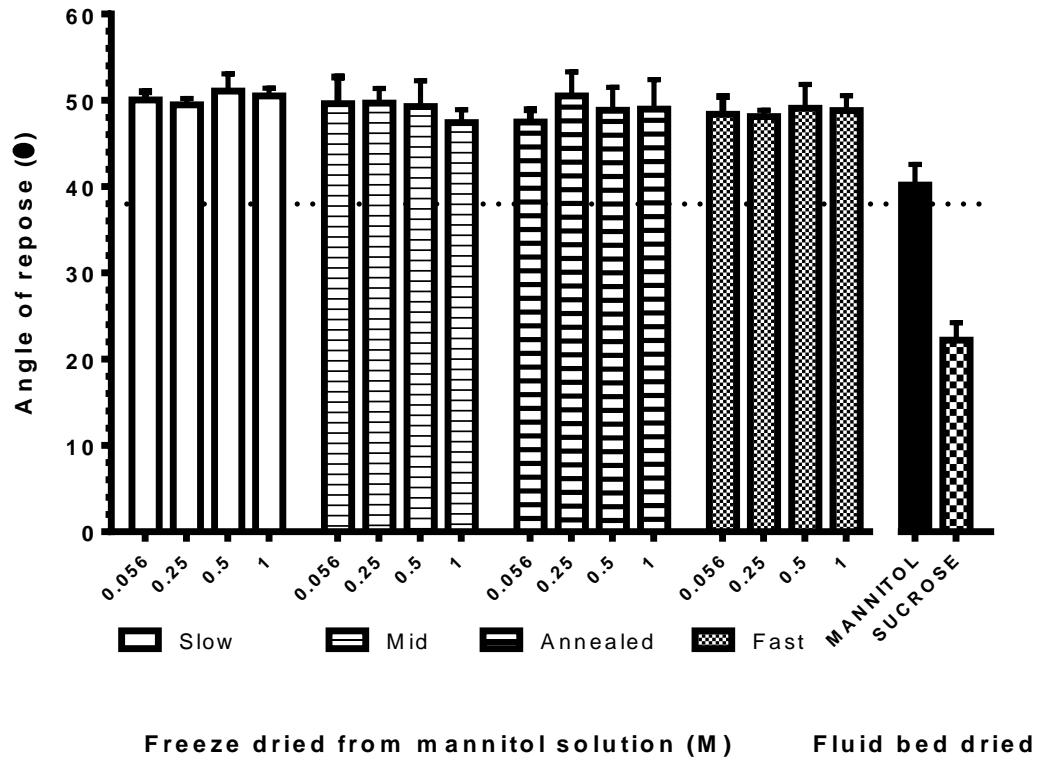


Figure 4.13 Effect of cooling rate and thermal treatment on angle of repose (n = 3) of bulk freeze dried mannitol from 0.056-1 M solution. Slow = 0.2 °C/min. Mid = 1 °C/min. Fast = freezing rate of 5 °C/min.

#### 4.4.3.5 Porosity studies

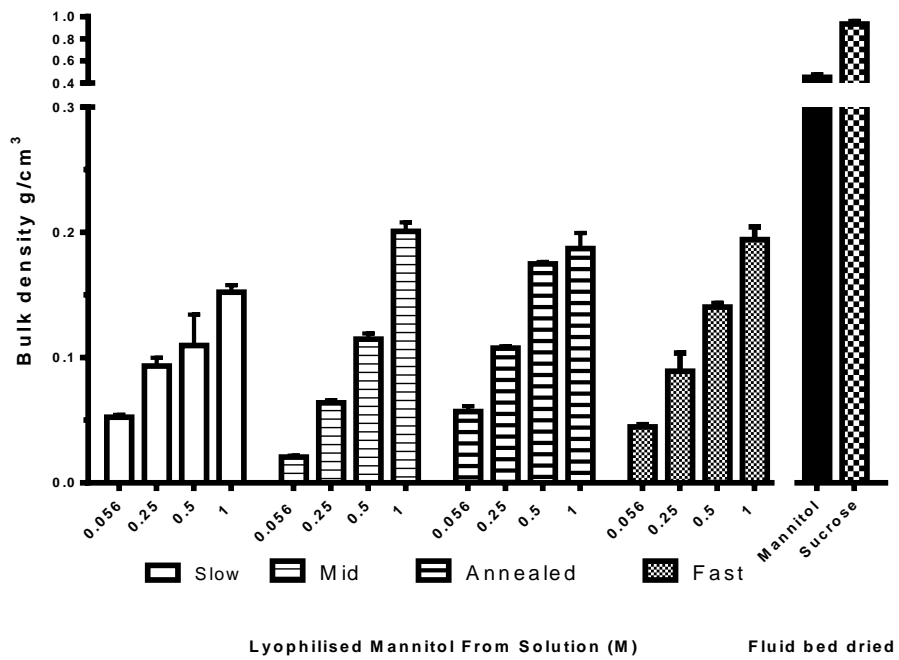
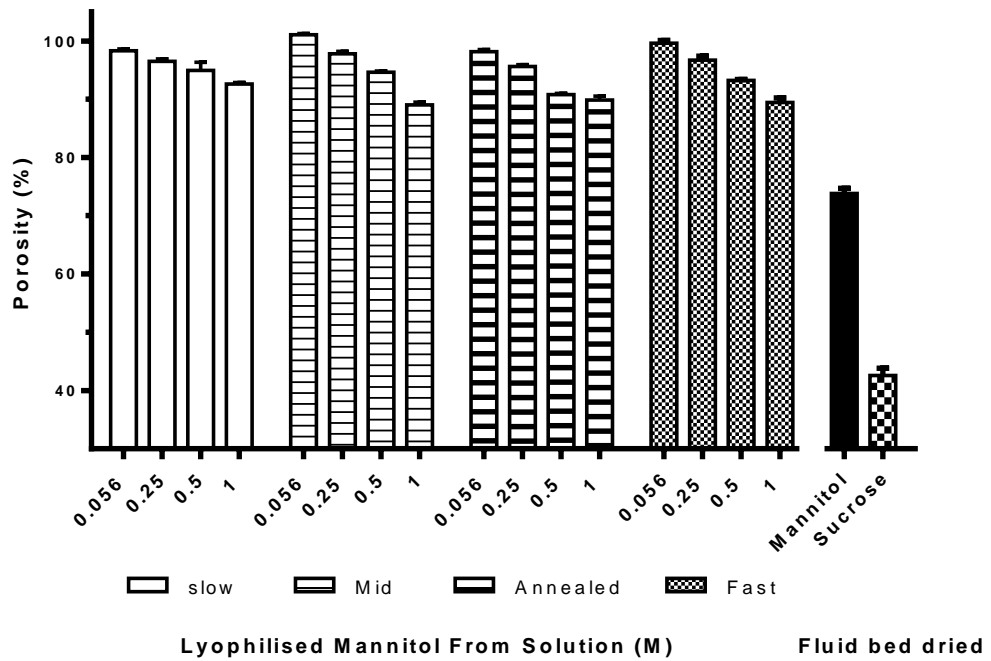


Figure 4.14: Effect of cooling rate and thermal treatment on bulk density ( $n = 3$ ) of bulk freeze dried mannitol from 0.056-1 M solution. Slow = 0.2 °C/min. Mid = 1 °C/min. Fast = freezing rate of 5 °C/min.



**Figure 4.15: Effect of freezing rate and thermal treatment on porosity (n = 3) of bulk freeze dried mannitol from 0.056-1 M solution. Slow = 0.2 °C/min. Mid = 1 °C/min. Fast = freezing rate of 5 °C/min.**

Bulk density (Figure 4.14) and porosity (Figure 4.15) showed densification of powders were achieved from increased solid concentration and appeared not to be generally influenced by freezing rate or thermal treatment during lyophilisation.

#### 4.4.3.6 Particle size analysis

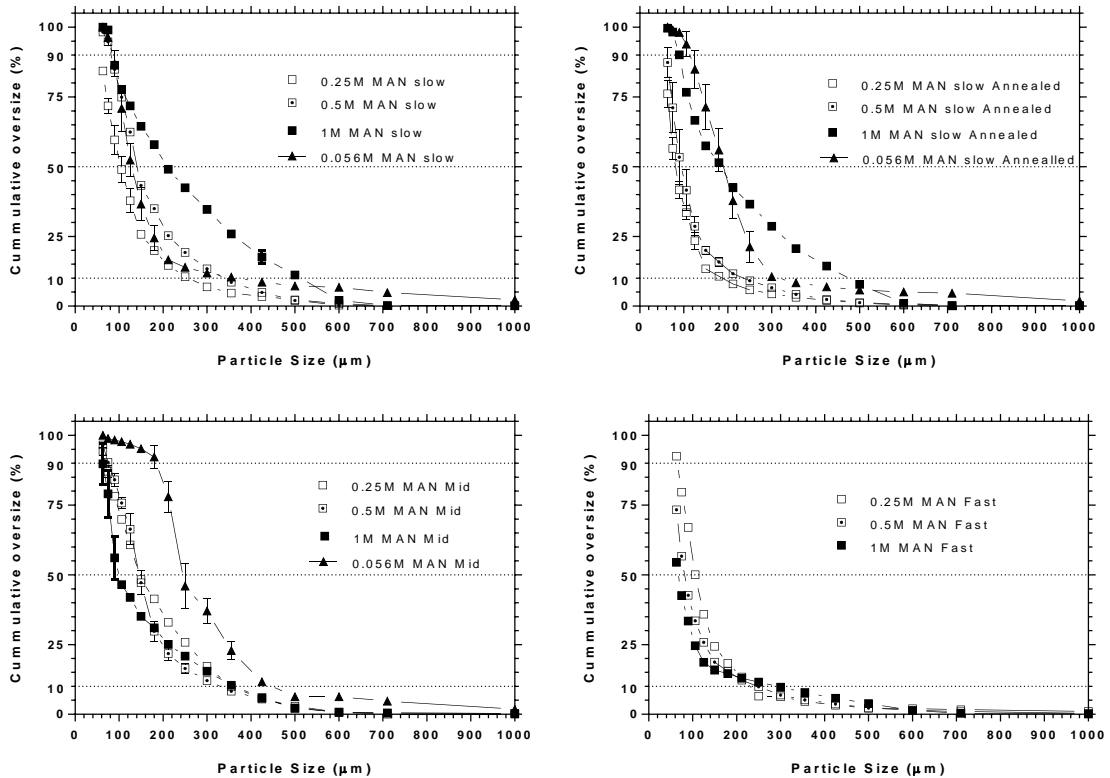


**Figure 4.16: Particle sizing analysis of bulk freeze dried mannitol from 0.056 M (n = 2), 0.25-1 M (n = 3) solutions with varied thermal treatment and powder breaking. Slow = 0.2 °C/min. Mid = 1 °C/min. Fast = 5 °C/min. 0.056 M Fast formed agglomerates on sieving and were invalid.**

Median cumulative particle size ranges were below 250  $\mu\text{m}$  in all samples (Figure 4.16). These were 100-210  $\mu\text{m}$ , 100-240  $\mu\text{m}$ , 60-100  $\mu\text{m}$  and 90-190  $\mu\text{m}$  in slow (2 °C/min), medium (1 °C/min), fast (5 °C/min) and annealed (0.2 °C/min held at -20°C) powders respectively (Figure 4.17). In powders obtained from initial 1 M solute contents, increasing the freezing rate of solutions resulted in a decline in median cumulative particle size from 210  $\mu\text{m}$  to 60  $\mu\text{m}$ . The observed trend in particle size is discussed in relation to the disruption or breaking step (Figure 4.18) later in this chapter.

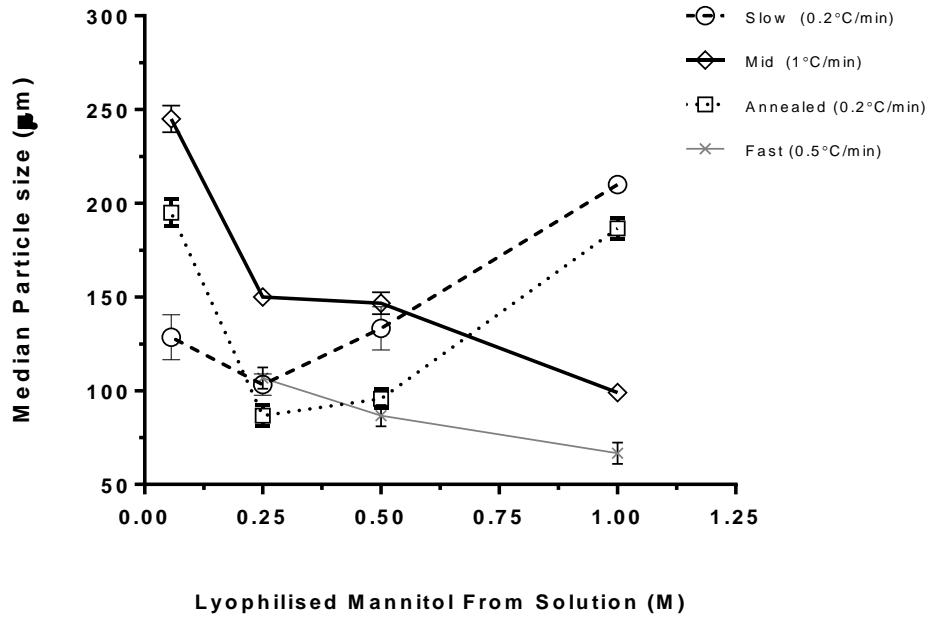


Figure 4.17: Median particle sizes of bulk freeze dried mannitol from 0.056 M (n = 2), 0.25-1 M (n = 3) solutions with varied thermal treatment and powder breaking. Slow = 0.2 °C/min. Mid = 1 °C/min. Fast = 5 °C/min. 0.056 M Fast formed agglomerates on sieving and were invalid.

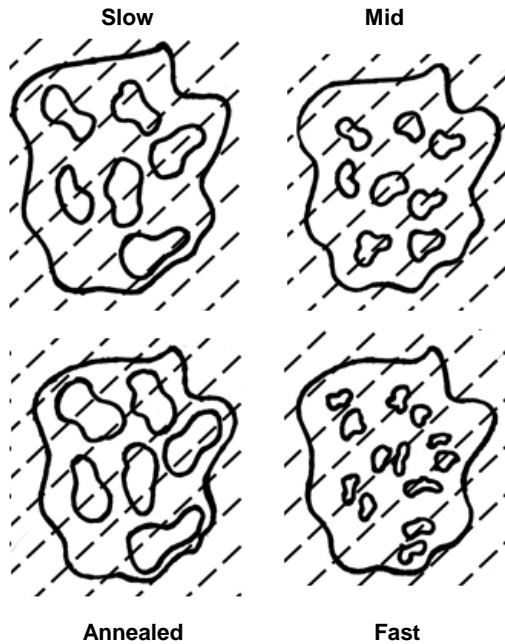


Figure 4.18: Schematic of disruption process of sections of bulk freeze dried mannitol cake dried from solution with varied cooling rates and thermal treatment. Different cooling rates produce cakes of different pore sizes (Order of increasing pore size: Fast, Mid, Slow and Annealed). Dotted lines represent points of fracture within cakes from mechanical agitation of sieves (710-75 µm). Slow = 0.2 °C/min. Mid = 1 °C/min. Fast = 5 °C/min. Annealed = 0.2 °C/min

with  $-20^{\circ}\text{C}$  thermal hold (2 hours). 0.056 M Fast formed agglomerates on sieving and were invalid.

#### 4.4.3.7 Morphology studies-light microscopy

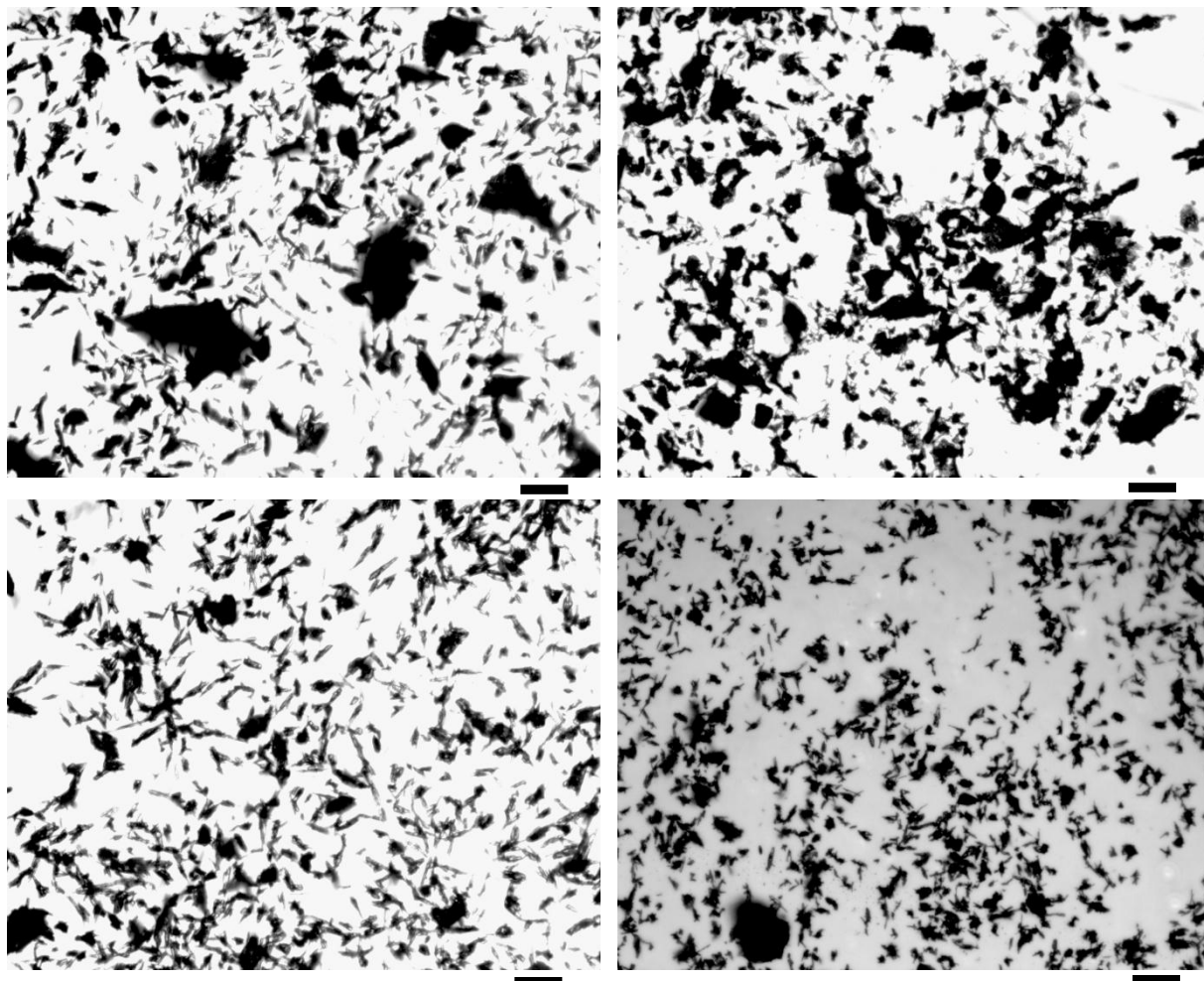
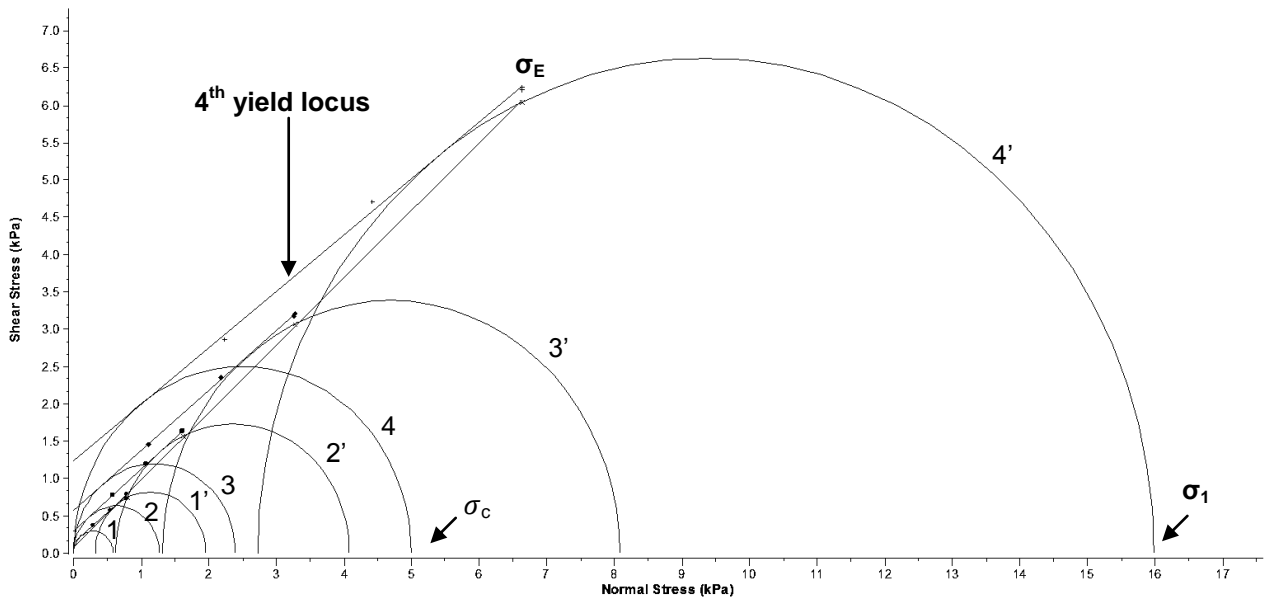


Figure 4.19: Light microscope images at x100 magnification for powders freeze dried from mannitol solutions of Top Left: 1 M (cooled at  $1^{\circ}\text{C}/\text{min}$ , Mid), Top Right: 0.5 M (cooled at  $1^{\circ}\text{C}/\text{min}$ , Mid), Bottom Left: 1 M (cooled at  $5^{\circ}\text{C}/\text{min}$ , Fast) and Bottom Right: 0.5 M (cooled at  $5^{\circ}\text{C}/\text{min}$ , Fast). Scale bar =  $20\ \mu\text{m}$

Optical microscopy revealed irregular, plate like (flaky), angular and needle like morphologies in all powders regardless of cooling rate and thermal treatment (Figure 4.19).

#### 4.4.3.8 Shear Cell



**Figure 4.20: Typical stress data for bulk lyophilised mannitol from 1 M solution at a slow cooling rate of 0.2 °C/min showing effect of consolidation level on 4 yield loci drawn tangentially to each pair of Mohr circles (Small and large). 1 & 1', 2 & 2', 3 & 3' and 4 & 4' form individual pairs of small and large Mohr circles. Flow function curve was derived from a separate plot of major principal consolidation stress ( $\sigma_1$ ) and unconfined yield strength ( $\sigma_c$ ) for each yield locus. 4th yield locus showed ( $\sigma_1$ ) = 15.986 kPa, ( $\sigma_c$ ) = 4.997 kPa strength and consolidation endpoint ( $\sigma_E$ ) = 6.630 kPa.**

Stress data (Figure 4.20) plotted as a function of shear stress to normal stress for samples produced flow function curves (Figure 4.21) which were obtained from resulting yield locus and Mohr circles drawn from stress data.

Lyophilised powders from 0.5 M and 1 M mannitol solutions were cohesive in nature (Figure 4.21). Flowability of bulk solids categorised by a flow function curve worsens in an anti-clockwise order from 'free flowing' to 'very cohesive'. Powders from 1 M mannitol solution frozen at 5 °C/min 1 M Man (Fast) was very cohesive at lower consolidation stress of less than 2 kPa and become cohesive at higher consolidation stresses (Figure 4.21). Its flowability was worse from 2 kPa up to about 10 kPa consolidation stresses. Freeze dried

mannitol from 0.5 M mannitol frozen at 5 °C/min was visually observed as the most cohesive and was adhered the most to the shearing lid vanes of the annular shear tester (Figure 4.22). Fluid bed dried mannitol and sucrose were easy flowing and free flowing respectively.

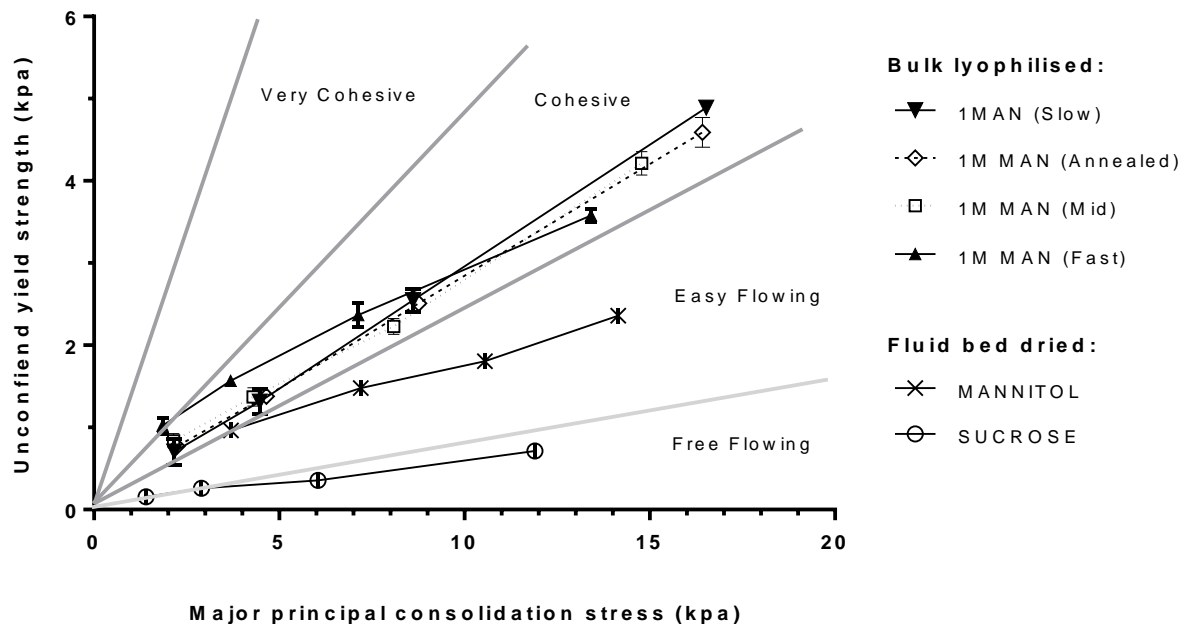


**Figure 4.21: Flow function curve of bulk lyophilised powders (n = 3) from 1 M mannitol solution at different cooling rates compared to fluid bed dried mannitol and sucrose. Slow = 0.2 °C/min. Mid = 1 °C/min. Fast = 5 °C/min.**

Flow index is the slope of the line drawn through the origin of a flow function curve to a yield loci at a given consolidation stress and higher values correspond to poor flowability. The flow index of lyophilised powders from 0.5 M solutions ranged from 0.29 to 0.39 and showed no significant difference in cohesive behaviour (Table 4.3).

All powders from 0.5 M solute content except annealed samples failed to withstand the same level of continuous shear as higher 1 M content powders (See footnote of Table 4.3). Annealed powders from 0.5 M solution and all powders dried from 1 M mannitol solution withstood shear stresses above 6.626 kPa while the former lost strength during the determination of the 3rd yield loci.

**Table 4.3: Flow index determined from shear cell measurements of powders bulk lyophilised from 0.5 M mannitol (Man) solution.**

<b>Bulk lyophilised Powder (Cooling rate, °C/min)</b>	<b>Flow index (°) n = 3 mean (SD)</b>
0.5 M Man (Slow, 0.2 °C/min) *	0.39 (0.04)
0.5 M Man (Mid, 1 °C/min) *	0.29 (0.06)
0.5 M Man (Fast, 5 °C/min) *	0.26 (0.02)
0.5 M Man (Annealed, 0.2 °C/min)	0.29 (0.00)

\* Powder lost strength during determination of 3rd yield locus at stresses above 6.626 kPa.

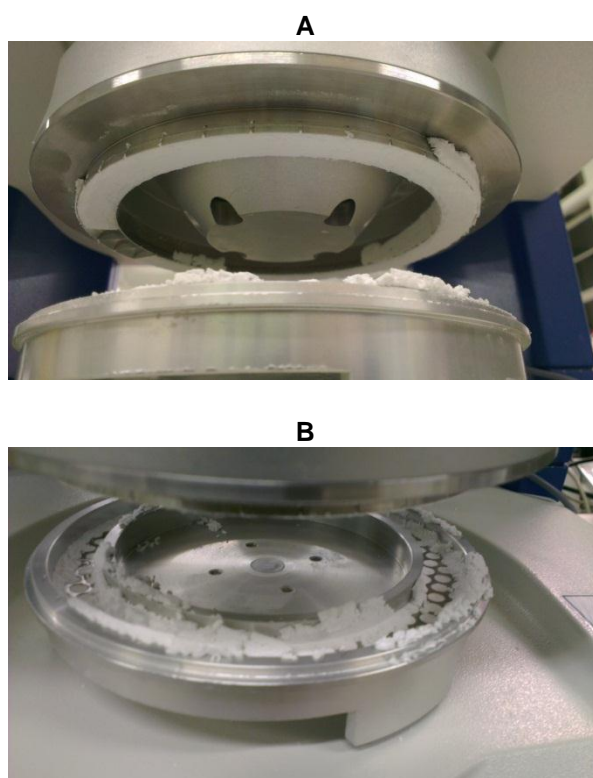


**Figure 4.22: Freeze dried mannitol powder adhered to shear cell. A: Shear cell lid with vanes covered with mannitol powder freeze dried from 0.5 M Mannitol at a shelf cooling rate of 5 °C/min. B: sample trough of shear cell expected to hold all powder under analysis.**

#### **4.4.4 Discussion**

A powder breaking step would be required to disrupt or break large bulk dried cake into loose powder. A different powder breaking step which involved mechanical shaking at an amplitude over time using a standard nest of analytical sieves was used in this chapter. The chapter's previous approach involved the use of a standard tablet friability tester with a rotating drum. Both techniques simulate powder handling through comb or sieve disruption at a commercial level. The rotating drum was operated for a specified number of revolutions with cakes being broken into powder under conditions of avalanche. Sieve disruption was performed to British Pharmacopoeia criteria for completion with all fractions recombined and used.

It was proposed that the use of this method of standard stainless steel sieving would be appropriate, easily reproducible and of a low cost. The use of a standard tablet friability tester needed to be resistant to the build-up of static as the freeze dried powders were seen to easily acquire electrostatic charges when in contact with the plastic surfaces. Either particle-particle or particle-wall collisions and particle fragmentation could have led to charging of the powders (Amidon, 1995). The potential regulatory hurdle envisaged for the use of a sieve system for processing parenterals would be to guarantee absence of metal particulates which may be shed during the mechanical shaking of stainless steel sieves. This is foreseen as a lesser problem for bulk powders intended for oral drug delivery.

##### ***4.4.4.1 Effect of cooling rate and annealing***

Both the cooling rate and freezing rate were found to be similar (Figure A11-A14 in appendix VI on page 261). The freezing rate is the rate of ice growth within a formulation after nucleation and is dictated by the extent of supercooling (Liu, 2006). The number of ice nuclei, rate of ice crystal growth and size of ice crystals are dependent on the degree of

supercooling observed during the cooling stage in freeze drying (Rambhatla et al., 2004, Searles et al., 2001b). The nucleation events during freezing determine the morphology of the final dried cake. At high degrees of supercooling, the nucleation rate is high and freezing rate is faster. The fast freezing rate causes the formation of many small ice crystals with a high surface area while a lower degree of supercooling yields fewer large ice crystals with lower surface area. The ice crystals formed from freezing sublime during primary drying to leave behind pores. The pore size distribution and hence the final porosity within the bulk dried cake are therefore a result of the freezing process.

The use of the annealing step provided additional mechanical strength to freeze dried powders. Formulations dried from a lower concentration of 0.5 M mannitol solution lost mechanical strength at stresses above 6.626 Kpa, while this was not observed in the annealed formulation (Table 4.3). The observation can be attributed to the freezing events during the thermal hold where ice crystal morphology was modified by the annealing treatment. Ice crystals grow during annealing in a phenomenon referred to as Ostwald ripening (Searles *et al.*, 2001a). Annealing also benefits formulations by ensuring the complete crystallisation of mannitol, reducing the propensity for release of moisture during storage. This chapter revealed mannitol had superior flow behaviour over sucrose but also recognises its poorer activity stabilising effect. An annealed formulation's mechanical strength is proposed to improve handling due to a reduction in friability and assisting downstream processing.

#### **4.4.4.2 Flow properties**

The final residual moisture content in the freeze dried samples were below 0.6 %w/w and all negligible (Figure 4.11) in their respective effect on flow as previously discussed (section 4.3.3.2 page 97). Moisture on this scale would penetrate the central core rather than form

liquid bridges which affect flowability (Howard, 2007). Nonetheless moisture levels are an important determinant of final product stability. Acting as a plasticiser, water promotes chemical degradation by depressing the glass transition and induces changes from an initial glassy physical state to a more mobile and less viscous rubbery state (Li *et al.* 2005). Very low moisture levels however do not always favour protein stability and many examples have been cited by Wang (2000). For example bovine serum albumin was found to be more stable at 10 %w/w moisture content than at levels less than 1 %w/w. Stability of the final powdered state from a bulk freeze dried cake is identifiable as a formulation specific parameter not within the scope of this thesis.

Particle size distribution results from mechanical sieving suggested the involvement of three main properties in the observed sizes of final disrupted powder (Figure 4.16). These were the concentration of solute content present, tendency to agglomerate (cohesiveness) and the initial pore size of the cake from which the powder was formed.

We suggest solute content and initial cake pore size influenced the powder breaking or attrition processing. Different cooling rates would produce different amounts and sizes of ice crystals which result in pores of varied sizes after sublimation (Figure 4.18). Pores were therefore expected to be few and large in size for formulations slow cooled at 0.2°C/min. Thermal treatment (annealing) during a slow cooling step would be expected to grow the few but large ice crystals causing them to increase in size. As the cooling and freezing rate increases, the number of pores increases while pore size decreases (Figure 4.18).

Comparing the same area of dried cake in all formulations, the size and number of pores present would influence the cake fracturing process and therefore the final particle size of disrupted powder. For example, in the presence of many small pores in fast cooled (5°C)

cakes when fractured (dotted line on Figure 4.18) across pores would produce the smallest particle sizes (Figure 4.17).

However the initial pore size of the cake was not the only determining factor for powder size distribution because the increased median particle size observed should have followed the increasing order of initial cake pore size (from fast, mid, slow to annealed) across all solute concentrations. This was not the case from solute concentrations of below 0.5 M mannitol content (Figure 4.17). The largest particle sizes would have been produced in the annealed formulations due to the presence of fewest and largest pores (Figure 4.18 and 4.17). The limitation of analytical sieving and particle morphology could explain the higher median size recorded for powders cooled at 0.2°C (Slow) over annealed. Rod like shaped particles could be erroneously sized as they could pass through sieves if vertically oriented.

Below 0.5 M mannitol solute content, increasing cohesive forces increased the tendency for powders to agglomerate and they produced high median particle sizes. This was supported by the visually observed agglomeration of 0.056 M samples cooled at 5°C which was invalid (Figure 4.16). However, at higher mannitol solute concentrations of above 0.5 M increasing mechanical strength afforded especially to the annealed would be expected to make powders less friable and would influence production of larger sized powders during the fracturing process.

The relationship between these observed particle sizes and the cohesive nature of powders observed were related (Figure 4.21). Bulk solids experience inter particulate forces of which a greater proportion are usually Vander Waals forces compared to other forces such as gravitational forces (Visser, 1989). At smaller particle sizes flowability would be expected to decline as particles experience larger magnitudes of Vander walls forces (Visser, 1989).

Size and moisture play synergistic roles in making bulk solids cohesive. Forsyth *et al.*, (2002) found that the critical value of humidity for glass spheres to become cohesive increased with increasing particle size and the cohesive inter particulate forces increased with increasing relative humidity. Larger particles have a greater mass and inertia which require larger forces to impede free flow (Forsyth *et al.*, 2002). A reduced particle size corresponds to an increase in surface area per unit mass which therefore allows cohesive forces to interact with the greater surface area (Fitzpatrick *et al.*, 2004).

#### **4.4.5 Conclusion**

The use of a standard nest of 200 mm sieves (710-75  $\mu\text{m}$ ) produces reproducible powder systems from bulk lyophilised cakes. This was the most appropriate, reproducible and low cost approach for disruption into powder (Section 4.4.4)

Powders with highest flow behaviour correlate with solute concentrations of between 0.25 M and 1 M (Section 4.4.3.3). Mannitol content of formulations optimised for flow should be at a concentration of 0.5 M-1 M.

Bulk formulations intended for further processing should be cooled at rates between 0.2°C to 1 °C/min and cooling rates of 5 °C/min or greater avoided. The latter cooling rate (5 °C/min) yields the most cohesive powders at the least consolidation stresses of 2 kPa from shear cell data and would be most problematic for processing (Section 4.4.3.8). Overall, while annealing showed no benefits for improving powder flowability (From compressibility index and shear cell) when 0.2°C and 1 °C/min cooling rates were compared, the benefits accorded by an added mechanical strength in low solute content formulations would be beneficial for successful adoption of powders for further processing.

## **5 DISPENSING OF BULK LYOPHILATES FOR VIAL OR AMPOULE ENCLOSURE**

### **5.1 Introduction**

Lyophilisation or freeze drying is most common in the food and pharmaceutical industry. In many cases it is the ideal drying process technology for materials liable to thermal degradation. This preference is however, largely due to but not limited to maximised activity recovery, optimum reconstitution times and an ability to confer significant shelf-life on the final powdered state. The trend within the pharmaceutical industry towards large molecule biologic drug substances is well documented. These compounds tend to require injection as the delivery route into the body, and they are not shelf stable in aqueous solution. To avoid the expense (and often impracticality) of cold chain supply, this has led to significant growth in dual chamber reconstitution devices whereby the drug substance is stored as a powder and mixed with the diluent just prior to use. The incumbent system lyophilises the drug substance into a powder cake within a dual chamber device. This process is recognised as being slow and expensive, and limits formulation flexibility.

Few cost analyses of the lyophilisation process have been recorded but drying is known to be financially expensive in comparison with fluid bed or simpler forms of dehydration (Ratti, 2001). Process analytical technology tools (PAT) and quality by design (QbD) provide strategies for shortening cycle times and reducing financial costs while increasing quality and reproducibility. Strategies involving the freezing step include annealing, controlled nucleation and use of aggressive primary drying temperatures have previously been reviewed in relation to final product acceptance and product quality factors (Ekenlebie and Ingham, 2011).

Here we propose a paradigm shift away from conventional drying within the primary container (vial or a dual chamber cartridge) towards bulk or continuous freeze drying to

benefit from the potential cost savings. A potential barrier to adoption of a bulk process will be a requirement for final powder dispensing into a product container.

Bulk drying coupled with a commercially viable dosing system may afford cost savings in the region of 30% (Ekenlebie and Ingham, 2013). These proposed savings were derived from the typical wasted shelf area and hence the volume not used. Wasted volume calculations also considered wall thickness of all glass vials arranged in a hexagonal packing order in comparison to a bulk product in a single tray.

This study investigates the use of commercially available gravimetric and volumetric (pneumatic) dispensing system using freeze dried powders from lyophilised bulk cake. There is limited literature disclosure of dispensing technologies for such powders. Lyophilised bovine vaccine pellets have been recently dosed using a screw conveyor and a vibration chute systems but the specifics of final recovery and important physical attributes of the final dosed units remain ambiguous (Gehrmann *et al.*, 2010). Sanofi disclosed advantages of tray freeze dried vaccine micro pellets for end stage container filling using a commercial dosing technology but falls short of reporting which dosing mechanism is ideal and the physical effects on the dried particulates (Chouvenc and Françon, 2009). The same is true for other published patents where frozen droplets were engineered for subsequent sublimation in lyophilisers without demonstrating how the friable particles would be finally dispensed or aliquoted (Carson *et al.*, 2005, Wende and Jesziorski, 2011, Middlebeek *et al.*, 2009). The possibilities for dosing freeze dried powders disrupted after drying is as yet unclear.

There are a wide range of pharmaceutical powder dispensing technologies available such as augers, dosators and vacuum dosators (Yang and Evans, 2007). These are used in other applications such as capsule fillers and dry powder inhaler filling. Due to the poor powder flow characteristics, volumetric dosing technologies may be unsuitable for dispensing freeze dried powders accurately.

## **5.2 Aim and Objectives**

It was the aim of this chapter to investigate volumetric and gravimetric lyophilised powder dispensing from bulk trays into final container closures using immunoglobulin G (IgG), Beta Galactosidase and Lactate dehydrogenase (LDH) formulations in crystalline and amorphous sugar systems.

An objective was to identify any relationship between constituents or physical form of the loose freeze dried powdered states, known flow behaviour and accuracy of the dispensing system used. A further objective was to investigate if regulatory expectations could be met from the final content uniformity of dosed units. A final objective was to identify the most suitable dispensing approach and key considerations for the successful adaptation of freeze dried powders for powder transfer.

## **5.3 VOLUMETRIC AND GRAVIMETRIC DISPENSING USING ACCOFIL AND QUANTOS DOSING SYSTEM**

### **5.3.1 Materials and Methods**

#### **5.3.1.1 *Materials***

D-mannitol Ph. Eur. and Sucrose BP were supplied as fluid bed dried from Fagron, UK and Fischer, UK. Beta galactosidase was purchased from Sigma UK. Lactate dehydrogenase (LDH) and CombiCoulomat fritless Karl Fischer reagent were obtained from VWR, UK. Ovine sera containing fluorescein isothiocyanate anti bodies (Anti-FIT C) was received as a gift from MicroPharm, UK and IgG was precipitated using caprylic acid and dialysed with 20 mM citrate buffer pH 6.2 using a kvick 30 kDa Nominal molecular weight cut off filter Kwick Lab packet and holder (GE Healthcare, UK). A multi compartment bulk drying tray was designed and machine cut form polystyrene to produce a frame (Trylon UK) and a polyethylene 1 mm base added.

#### **5.3.1.2 *X-ray powder diffraction studies***

The physical form of lyophilised powders were analysed using X-ray powder diffraction (Bruker D2 Phaser, UK) equipped with a 30 kV 10 mA 300 W X-ray source.

#### **5.3.1.3 *Dosing Time***

Time required to dose a single formulation vial was recorded using an automatic inbuilt timer in the mass dispenser or manually kept using a standard laboratory stop watch for the volumetric dispenser.

#### **5.3.1.4 Lyophilisation Process**

Samples were lyophilised in a bench top Virtis advantage freeze dryer in 100 mL volumes in a custom made compartment polyethylene tray system. Vial samples were dried in 5 mL volumes in a tubular type 1 freeze drying vial (Adelphi healthcare, UK). All samples were chilled at 2°C/min from 16°C to -55°C and held for 6 hours. Primary drying was on a -40°C shelf for 36 hours at -75°C condenser and 267 µbar (27 Pascal) vacuum. Secondary drying was at 20°C for 9 hours. Product temperature was monitored as the average reading from K type thermocouples positioned at the bottom edge and centre of each tray compartment (RS Components, UK).

Bulk dried cakes were passed through a funnel into sealed 500 mL bottles for storage. Vials were stoppered in the freeze dryer and aluminium crimped on removal from the chamber.

#### **5.3.1.5 Visual inspection**

Dosed formulations were visually inspected for acceptability.

#### **5.3.1.6 Moisture Content Analysis**

Residual moisture content was determined with a coulometric C20 Karl Fischer titrator (Mettler Toledo, Switzerland) as previously described in materials and methods using a 12 cm hypodermic needle and 10 mL syringe, 2 mL of dry Karl Fischer reagent was drawn from the titration cell into aluminium crimped sample vials.

#### **5.3.1.7 Flowability Characterisation**

Carr's compressibility index was calculated from measurements from a tap density apparatus (Sotax FD2, USA) and bulk density as described in materials and methods chapter (Section 3.4.10.1.2) except for the use of a 10 mL volumetric cylinder.

#### **5.3.1.8 Porosity**

The closest to true sample volume measurements were determined using a helium gas multipycnometer (Quantachrome, USA). Porosity was then calculated for 3 sample replicates from resulting particle density and measured bulk density.

#### **5.3.1.9 Gravimetric and Volumetric dispensing**

Bulk freeze dried powder cakes were broken down into powder using a standard tablet friabilator (Sotax UK) using a fixed 1000 revolutions. Samples in vials were mechanically disrupted with an aluminium paddle of 10 x 2 cm until the powder had visible flow. Powders were then dispensed using either a Quantos (Mettler Toledo UK) mass dispenser or Accofil (Biopharma UK) volume dispensing system. LDH and IgG freeze dried in 15 %w/v mannitol solution was also ball milled (Fritsch Pulverisette 7, Germany) at 300 rpm for 5 minutes and volumetrically dosed. All dosing was conducted at room temperature and pressure.

#### **5.3.1.10 Morphology studies**

Powder morphology was investigated using a light microscope (Carl Zeiss, Scope.A1 Germany) with a camera system at x100-400 magnifications and Axiovision version 4.8 imaging software.

#### **5.3.1.11 Particle sizing by mechanical sieving**

Cumulative over size powder distribution was obtained from measurements using a nest of brass wire woven sieves (Endecotts, UK) and a mechanical sieve shaker (Retsch, AS 200 basic, Germany). A 1000-63  $\mu\text{m}$ , 200 mm diameter sieve nest was used in bulk flow studies and a 16 set 38 mm diameter sieve nest with aperture sizes ranging from 1000-63  $\mu\text{m}$  used in dispensing investigations. Test samples were shaken at an amplitude of 80 mm at 5 minutes interval. The endpoint of the sieving process was determined as previously described in materials and methods.

#### **5.3.1.12 Content uniformity test of dosed units**

IgG activity was determined using fluorescence quenching assay previously described in Section 3.4.9 of materials and methods. An acceptance value was calculated from measured protein activity (British Pharmacopoeia Commission, 2013b).

#### **5.3.1.13 Definitions and pass criteria**

Definitions used in this text include 'Target dose' which refers to the desired final mass the powder dispenser has been programmed to dispense. 'Mean deviation from target dose' is the average mass of all dosed vials expressed as a percentage error from the target dose and is herein used mainly to compare powder behaviour and not as final assessment of compatibility for dosing. 'Over fill' and 'under fill' refers to the dosing device exceeding or failing to meet a target dose and are also represented by positive and negative masses respectively.

Conclusions of the powders compatibility for dispensing were drawn from assessment of final dosed units using the British Pharmacopoeia acceptance value criteria and relative standard deviation (RSD) of a specific dosed formulation batch.

Formulations were passed if an acceptance value (AV) was below 15. None of the passed formulations should fall below 0.75 or 1.25 of the case reference value (M) which was 98.5% or 101.5% or the average of individual dispensed contents expressed as a percentage of the label claim (British Pharmacopoeia Commission, 2013b).

## 5.3.2 Results

### 5.3.2.1 GRAVIMETRIC DISPENSING OF NON-ANNEALED FREEZE DRIED POWDERS (WITH QUANTOS)

Residual moisture content (%w/w) from Karl Fischer analysis was between  $1.30 \pm 0.06$  to  $4.93 \pm 2.38$  (Table 5.1 and Table 5.2).

**Table 5.1: Moisture content (n = 3) of formulations dosed using gravimetric (quantos) and volumetric (accofil) powder dispensing systems.**

Formulation	Moisture content (mean $\pm$ SD)
<b>Fluid bed dried</b>	
Mannitol	$1.40 \pm 0.43$
Sucrose	$1.30 \pm 0.06$
<b>Bulk lyophilised*</b>	
Man 1 %w/v	$4.5 \pm 1.43$
MAN 15 %w/v	$4.72 \pm 1.23$
SUC 1 %w/v	$4.15 \pm 0.86$
SUC 15 %w/v	$4.93 \pm 2.38$
<b>Bulk lyophilised* (Accofil only)</b>	
IgG MAN 1 %w/v	$4.23 \pm 1.68$
IgG MAN 5 %w/v	$4.67 \pm 2.01$
IgG Man 15 %w/v	$5.16 \pm 1.87$
LDH MAN 15 %w/v	$4.28 \pm 2.54$
LDH SUC 15 %w/v	$4.84 \pm 0.98$

\*from solution (%w/v)

**Table 5.2: Moisture content (n = 3) of vial lyophilised formulations dosed using gravimetric (quantos) powder dispensing system. Lyophilised IgG with 18.22 %w/v mannitol (MAN IgG), IgG with 34.23 %w/v sucrose (SUC IgG) and beta galactosidase with 3.42 %w/v sucrose (SUC BGAL). IgG fraction was from 1.7 g/L IgG in 20 mM citrate buffer.**

Vial Lyophilised Formulation	Moisture content (mean $\pm$ SD)
Suc Bgal	$2.3 \pm 0.3$
Suc IgG	$1.9 \pm 0.2$
Man IgG	$2.5 \pm 0.6$
IgG only	$1.8 \pm 0.36$

The observed relative standard deviation (RSD) for the dosed masses of mannitol, sucrose and protein containing formulations was 0.54-7.37% RSD (Figure 5.1). Overfilling of vials was observed for vials of sucrose containing Bgal and IgG.

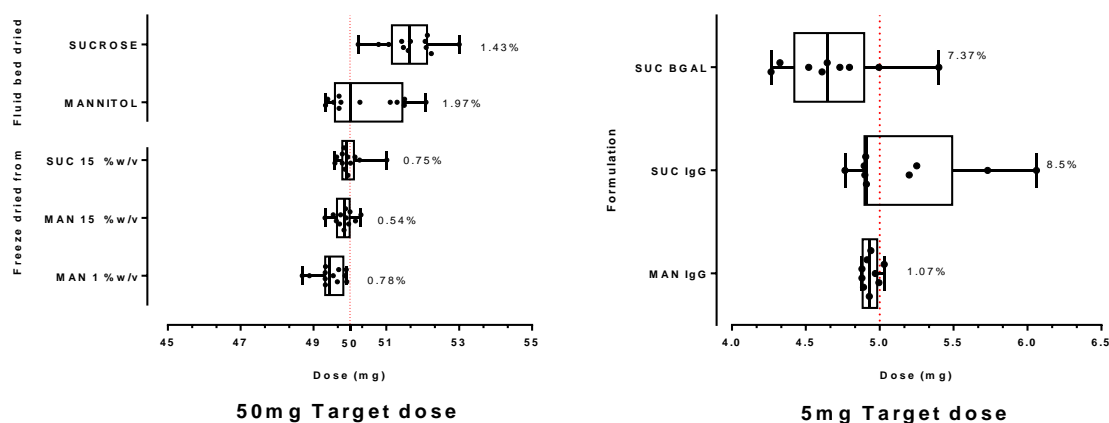


**Figure 5.1: Variation in powder mass transfer using Quantos gravimetric dispenser. Powders were disrupted from non-annealed freeze dried cakes. Box and whisker plot with corresponding RSD of Left: 50 mg target dosing (n = 12) of bulk lyophilised mannitol (MAN) and sucrose (SUC) from 1 %w/v and 15 %w/v solutions. Right: 5 mg target dosing (n = 9) of vial lyophilised IgG with 18.22 %w/v mannitol (MAN IgG), IgG with 34.23 %w/v sucrose (SUC IgG) and beta galactosidase with 3.42 %w/v sucrose (SUC BGAL). IgG fraction was from 1.7 g/L IgG in 20 mM citrate buffer. BGAL fraction contained 2 units/mL. Fluid bed dried mannitol and sucrose are BP, Eur. ph. grade crystalline powders.**

A bulking agent will be required in many cases if a researcher is to consider dosing of a biologic. IgG dried with no bulking agent was not dispensable (Figure 5.2 Left #) neither was 1 %w/v sucrose content. The latter showed very poor flowability resulting in arching or blockage in the dosing reservoir of the powder doser. Increasing solute content showed a trend of improved mean deviations from target in pure crystalline formulations. However, introduction of an amorphous component distorted the observed pattern as seen in 1-34 %w/v sucrose containing formulations (Figure 5.2).

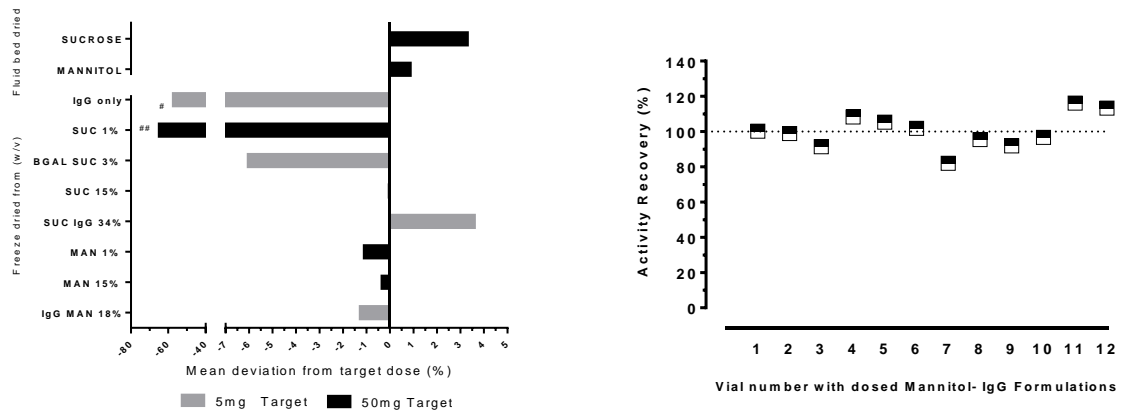


**Figure 5.2:** Left: Mean % deviation (n = 12) from the target dose as dispensed with the Quantos system. Formulation batches are non-annealed bulk lyophilised mannitol (MAN), sucrose (SUC), vial lyophilised (n = 9) mannitol with IgG (MAN IgG), sucrose with IgG (SUC IgG) and sucrose with beta galactosidase (SUC BGAL) freeze dried from different %w/v solutions. IgG fraction contained 1.7 g/L IgG and 20 mM citrate buffer. BGAL fraction contained 2 units/mL. Fluid bed dried mannitol and sucrose are BP, Eur. ph. grade crystalline powders. # Represents n = 3 as subsequent doses were not achieved. # # Represents n = 2 due to an insufficient sample flow into dosing head. Right: Activity (n = 4) ± SD of dosed freeze dried Mannitol IgG. Stock powder was freeze dried from solution containing 1.7 g/L of IgG, 20 mM citrate buffer and 1 M mannitol. Dosed samples were reconstituted with distilled water and quantification conducted with a fluorescence quenching assay. Target dose (dotted grey line) content was 0.5 mg to contain 0.7g/dl IgG. Calculated acceptance value (AV) = 0.16.

The compendia content uniformity (CU) test criteria were met by dosed mannitol IgG formulations using 1 M mannitol solutions. From IgG activity recovery (Figure 5.3) of mass dispensed mannitol from freeze dried 15 %w/w solution, the calculated acceptance value of 0.16 and that none of the dosed units deviated below 0.75 of the reference case (M) or above 1.25M would mean this powder was processed and would be acceptable under the pharmacopeia parameters for content uniformity.

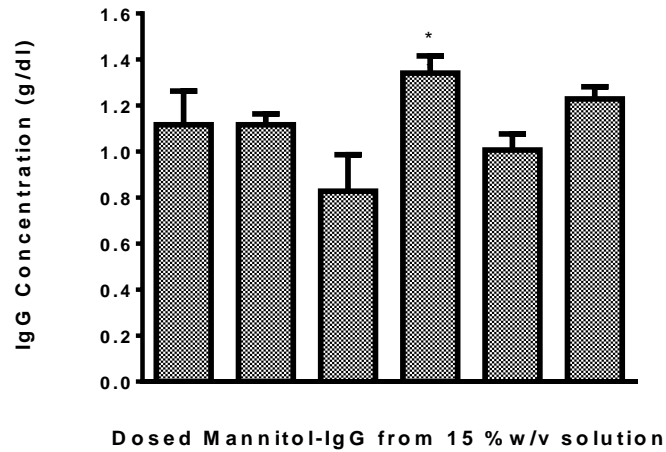


**Figure 5.3: IgG activity recovered (n = 4) of dosed freeze dried Mannitol IgG lyophilised from 15 %w/v solution. Stock powder was freeze dried from solution containing 1.7 g/L of IgG, 20 mM citrate buffer and 1 M mannitol. Dosed samples were reconstituted with distilled water and quantification conducted with a fluorescence quenching assay. \* represents significance at  $p < 0.05$**

The time taken to dose a formulation (Figure 5.4) was found to negatively correlate with the increase in solute content, increases in solute content increase flowability (chapter 4 ) and reduce the time taken to dispense. The time required to dose the masses (50 mg and 5 mg) into vials was below the target of one minute and could be deemed time efficient however a fully automated process may demand further optimisation.

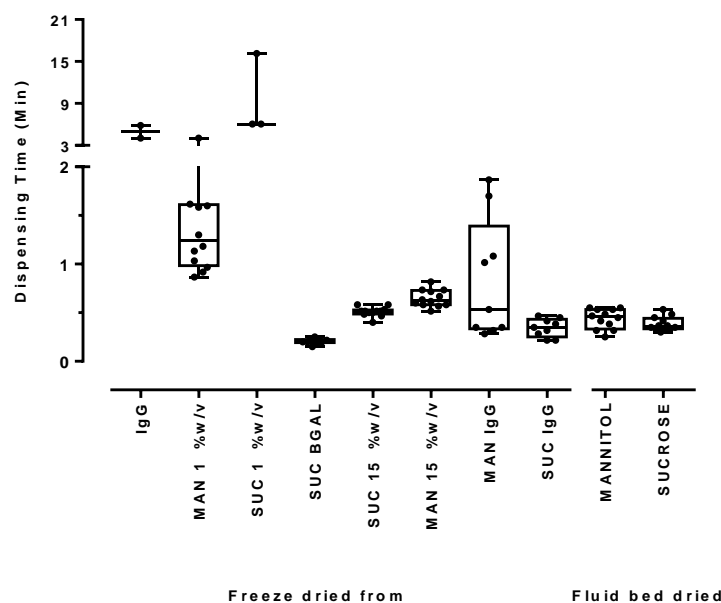


**Figure 5.4: Automated dosing time (n = 12) of bulk lyophilised mannitol (MAN), sucrose (SUC), vial lyophilised (n = 9) mannitol with IgG (MAN IgG), sucrose with IgG (SUC IgG) and sucrose with beta galactosidase (SUC BGAL) from different %w/v solutions. MANNITOL and SUCROSE are fluid bed dried BP grade crystalline powder mannitol and sucrose. IgG fraction contains 1.7 g/L IgG and 20 mM citrate buffer. BGAL fraction contains 2 units/mL.**

### 5.3.2.2 Volumetric dispensing of non-annealed freeze dried powders (with Accofil)

Volumetric dispensing was researched as it provides the main alternative to mass dosing.

Residual moisture content (%w/w) from Karl Fischer analysis was between  $1.30 \pm 0.06$  to  $5.16 \pm 1.87$  (Table 5.1). A comparison of means and standard deviation using one way Anova and Tukey's multiple comparisons test showed no significant difference between the residual moistures observed (Table 5.1 and Table 5.2).

Large variations in the mass transferred were noted for volumetric systems with %RSD values for non-milled freeze dried powders ranging from 1.6%-48.9% (Figure 5.5).

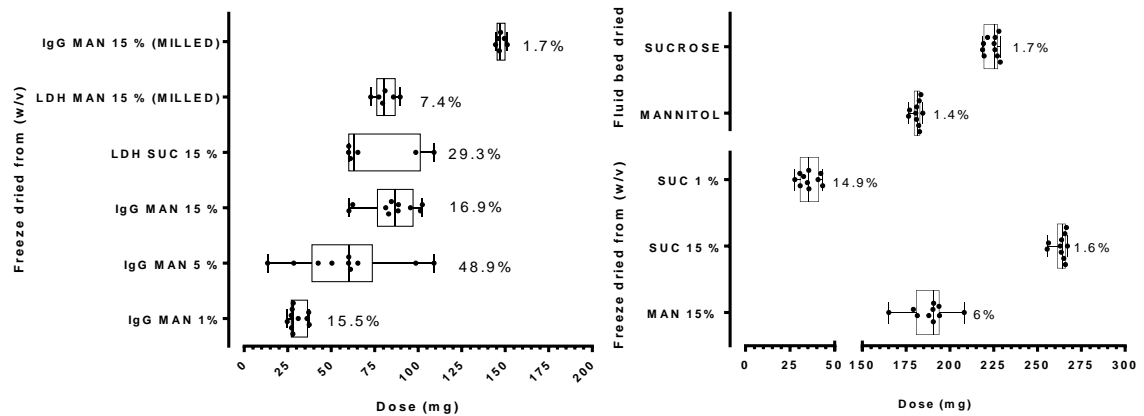


**Figure 5.5: Variation in powder mass transfer using a volumetric dispenser (Accofil). Powders were disrupted from non-annealed freeze dried cakes. Box and whisker plot with corresponding RSD of dosed bulk lyophilised material Left: mannitol (MAN) and sucrose (SUC) from 1 %w/v, 5 %w/v and 15 %w/v solutions containing IgG and LDH (n = 6). Right: mannitol (MAN) and sucrose (SUC) from 1 %w/v and 15 %w/v solutions (n = 6). Fluid bed dried mannitol and sucrose are BP, Eur. ph. grade crystalline powders.**

Dosing was largely affected by bulk density and particle size distribution. More dense formulations resulting from higher solute content were expected to have better particle packing within the dosing die and did show improved reproducibility; a trend seen between IgG freeze dried in 5 %w/v mannitol (IgG MAN 5 %w/v) and in 15 %w/v mannitol (IgG MAN 15 %w/v) as well as sucrose (SUC) freeze dried from solutions in the range of 1-15 %w/v.

Particle size and complete homogeneity in formulations were important parameters that influenced volumetric dispensing. A 10 fold improvement in %RSD was realised in IgG lyophilised in 15 %w/v mannitol (IgG MAN 15 %w/v) when milled with a change from 16.9 to 1.7%. This value was similar to that seen in fluid bed dried mannitol and sucrose which were significantly ( $p < 0.001$ ) bulkier and less porous (Figure 5.6).

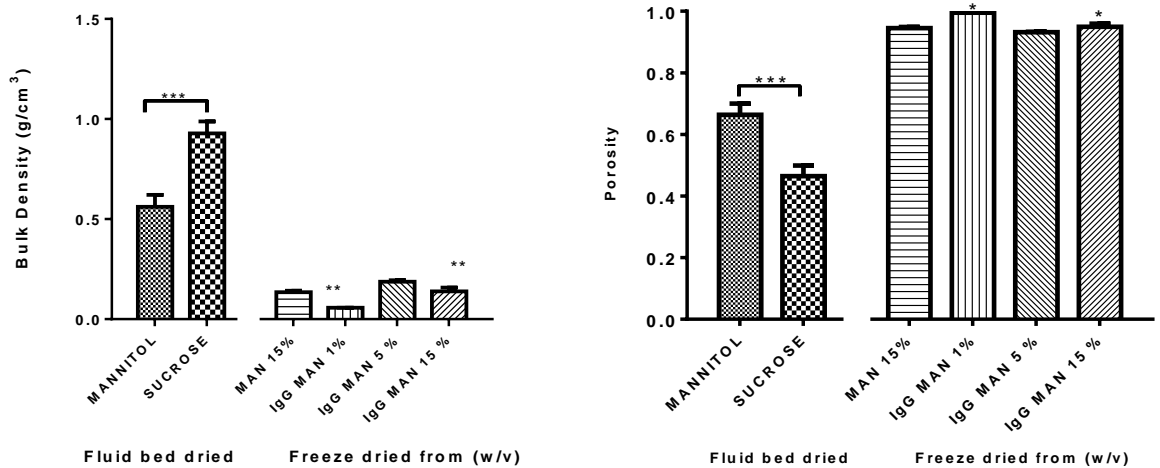


Figure 5.6: Bulk density and porosity of dosed bulk lyophilised mannitol (MAN) and from 1 %w/v and 15 %w/v solutions. Fluid bed dried mannitol and sucrose are BP, Eur. ph. grade crystalline powders. \*\*\* =  $p < 0.001$  from all formulations. \* =  $p < 0.05$ , \*\* =  $p < 0.01$  (one way ANOVA).

Compressibility index for dosed freeze dried mannitol from 15 %w/v solution and IgG dried in 1-15 %w/v mannitol solution (IgG MAN) showed very poor powder flowability (Figure 5.7).

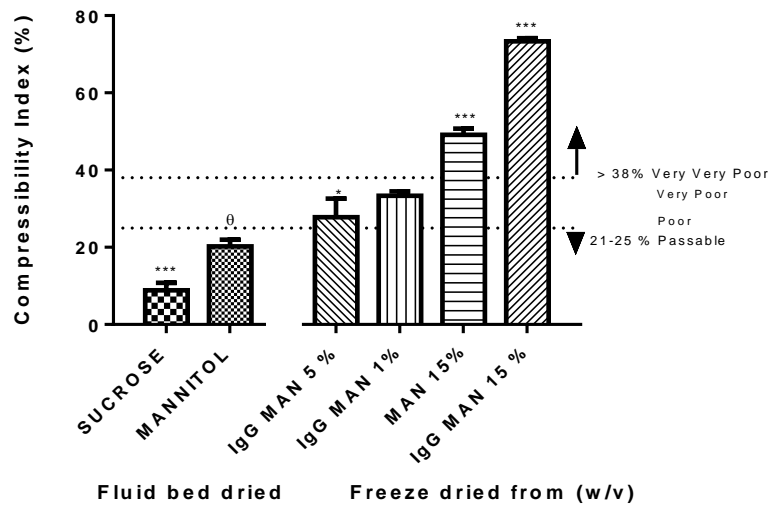
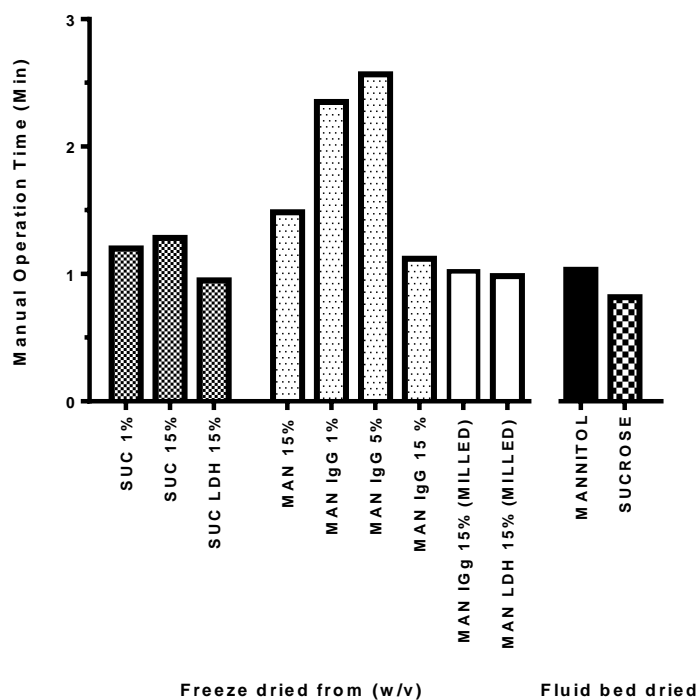


Figure 5.7: Compressibility index ( $n = 3$ ) of dosed formulations freeze dried from different concentrations (%w/v) of mannitol solution. Fluid bed dried mannitol and sucrose are BP, Eur. ph. grade crystalline powders. \*\*\* represents significance at  $P \leq 0.001$  ( $n = 3$ ) ANOVA from all. \* represents significance from MANNITOL at  $p < 0.05$  (ANOVA). Θ represents significance from all formulations at  $p < 0.001$  and  $p < 0.05$  (ANOVA) from Man IgG 5 %w/v.

While the time taken to manually dispense individual formulations cannot necessarily be used to compare formulations because they are dictated by how skilled an operator is in the art, it gave a clear indication of how potentially time efficient the process could be if automated for scaled up powder dispensing (Figure 5.8).



**Figure 5.8: Total manual operation time for dispensing batches (n = 10) of bulk lyophilised mannitol (MAN), sucrose (SUC), IgG and LDH formulations (n = 6).**

Lyophilised IgG in mannitol and sucrose were crystalline and amorphous respectively from XRPD (Figure 5.9). This would be expected to affect flowability and was discussed in chapter 4.

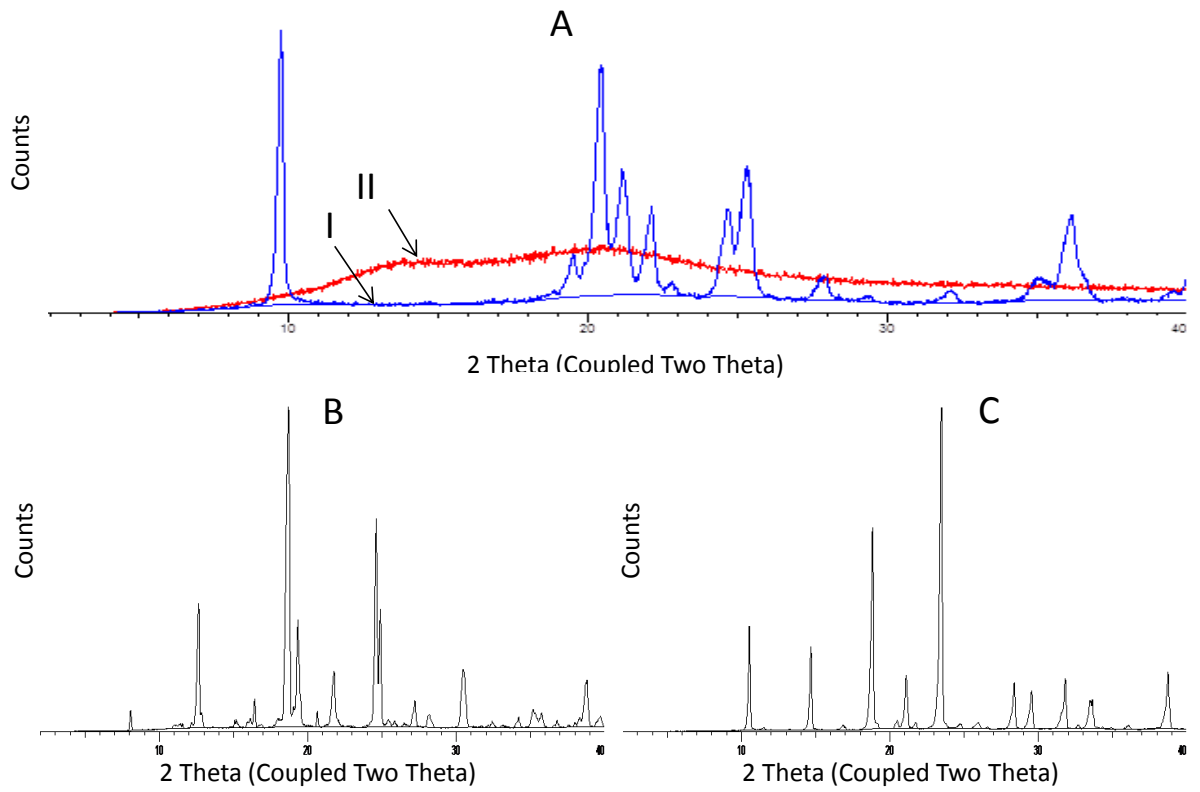


**Figure 5.9: X-ray powder diffractograms for A: IgG freeze dried with mannitol (I) and sucrose (II) showing crystalline and amorphous diffraction patterns. B: fluid bed dried sucrose and C: fluid bed dried mannitol showing crystalline diffraction patterns.**

### 5.3.2.3 Visual appearance of dosed formulations

Powders dispensed volumetrically (Figure 5.10 A&C) showed signs of agglomeration after ejection from the dosing die but were easily broken with gentle agitation of the vial (Figure 5.10 B&D). Powders dispensed using mass filling showed evidence of electrostatic charging and sticking to inner walls of dosing head (Figure 5.11) but with no concern for agglomeration.

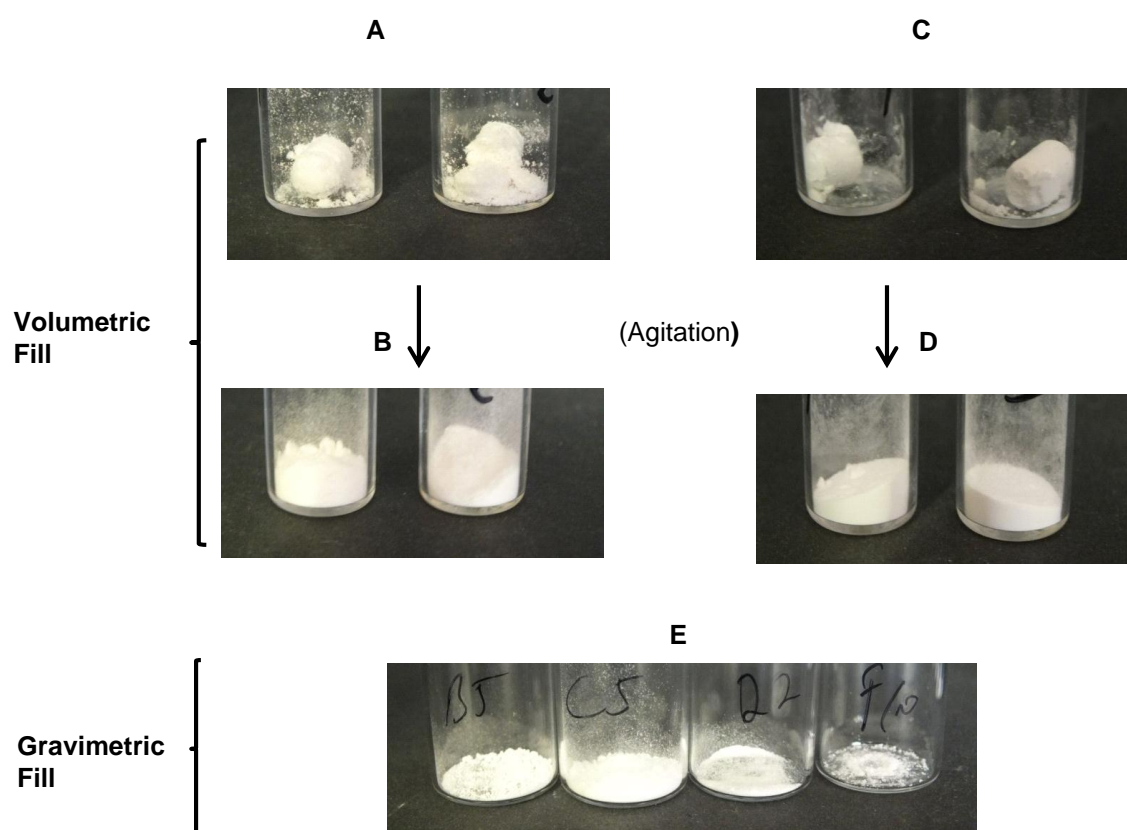


Figure 5.10: Appearance of dosed formulations (A) Lyophilised LDH in Mannitol from 15 %w/v solution\*\*. (B) Dosed sample (A) after agitation. (C) Lyophilised IgG in Mannitol from 15 %w/v solution\*\*. (D) Dosed sample (C) after agitation. (E)\* From left: lyophilised Mannitol from 15 %w/v solution, Lyophilised Mannitol from 1 %w/v solution, fluid bed dried mannitol and lyophilised Sucrose from 15 %w/v solution. \*\* = Dosed with volume dispenser. \* = Dosed with quantos dosing head. Not all dosed using accofil showed agglomeration after dosing.

**A**



**B**



**Figure 5.11: Gravimetric or mass filled lyophilised powder losses due to sticking to inner walls of dosing head (A) and brim of glass vial (B).**

### 5.3.3 Discussion

Two dosing systems employing different mechanisms for dispensing powders have been investigated. The accofil powder dispenser is a volumetric doser working using a pneumatic or pressure control system working in combination with a dosing die (aspirator) to dispense powders. The quantos system uses a dosing head in combination with a stirring and tapping dosing mechanism to powder dispense.

The goal for any dispensing task is to discharge an accurate amount of formulation into individual vials with no or negligible over or under filling (deviations) from the target. The Quantos<sup>®</sup> system was observed to over fill for sucrose powders while producing improved performance with mannitol containing formulations. This was consistent with initial flowability assessments where mannitol was found to be better flowing (discussed in chapter 4). The role of bulking agents on flowability was emphasised by two trends. Dosed accuracy of similar formulations correlated with increased solute concentration of the bulking agent while the absence of a bulking agent resulted in IgG being non dispensable (Figure 5.2). Flowability of freeze dried powder were previously found to benefit from increases in solute content of solutions freeze dried and bulking agent was identified as a necessity for flowability (Studied in chapter 4).

Larger deviations from final target dose were observed using the volumetric dosing system compared to the gravimetric (Figure 5.1 and Figure 5.5). This was due to the differences in the dosing mechanisms. A gravimetric system uses a computerised feedback loop to control the dispensed amounts for more accuracy by opening and closing the outlet of the dosing head. These systems allow operators to control settings to suit a material being dispensed. In this work, the best load cell sensitivity setting was used to acquire the most accurate outcome achievable. The volumetric method however relies solely on proper sample packing into the dosing die or aspirator for subsequent ejection into final containers, although the die volume can be adjusted this is not dynamic.

The quantos gravimetric dosing head was notably prone to blockage with freeze dried powders which belong to the 'very very poor' flow category investigated in this work. This was due to bridging or arching close to the neck of sample reservoir attached to the dosing head. The freeze dried powders experience different stresses within the reservoir which result in consolidation of the powder. A larger shear stress from the head will be required to overcome these consolidation stresses. The absence of a controlled humidity environment during quantos dispensing work may have been contributory to the larger dosing incompatibilities observed particularly in sucrose containing formulations (Figure 5.1 and Figure 5.2) due to the known hygroscopicity of sucrose.

While a standard anti-static kit is available for the quantos system, this was unavailable during this study and freeze dried powders were found to acquire charge. The phenomenon referred to as triboelectrification is due to transfer of electrons between dissimilar materials and is influenced by stresses (in our case from mechanical stirring and tapping), moisture, temperature and adsorbed gas molecules on surfaces (Yang and Evans, 2007). Particle – particle and particle-wall collisions have been previously mentioned as causes of powder charging (Amidon, 1995). We advise that charging of freeze dried powders need to be avoided or reduced to the minimum due to the observed sample losses and therefore concerns of its negative effect on freeze dried powder flow behaviour. This view is reinforced by Staniforth (1982) whose work revealed even powder flow behaviour of free flowing crystalline sugars and cohesive crystalline cellulose charged by friction using air cyclone showed poorer flow compared to the uncharged forms. The charged powders recorded higher angles of repose and 21-84% reduced rates from flow through an orifice characterisation.

We have reported that volumetric powder dispensing is less precise than the gravimetric system for dispensing freeze dried powders. This observation is supported by similar comments on volumetric metering of powders attributing the poorer accuracy to its

dependence on size distribution, powder electrostatics, humidity and packing geometry (Lang *et al.*, 2009). This supports the 10 fold increase in precision observed after milling IgG freeze dried in 15 %w/v mannitol (Figure 5.5). Use of this system is common in capsule filling and the food industry but we do not recommend for dispensing lyophilised biologicals due to the significant irreproducibility illustrated (Figure 5.5).

#### **5.3.4 Conclusion**

The study has demonstrated that lyophilised formulations can be dosed time efficiently while meeting the British Pharmacopeia regulatory expectations for content uniformity (Section 5.3.2.1). Due to the large dosing variations revealed, a gravimetric powder dispensing system utilising a stirring and vibration mechanism was recommended over volumetric methods. The influence of powder flowability on final dosing accuracy was correlated with increases in solute concentration of up to 15 %w/v in gravimetric dosing systems. The bulking agent (mannitol) is indicated in concentrations not less than 5-15 %w/v together with assurances of powder homogeneity. A high amount of amorphous content though necessary for lyoprotection impedes the accurate adaptation of powder dispensing.

Freeze dried powders easily acquired electrostatic charge (Triboelectrification) which could have been caused by stresses induced during handling to include stirring, tapping, mixing or electron transfer between powders and the processing surfaces. This was responsible for sample losses during the dosing process. It is concluded powder electrostatics and environmental humidity should be controlled.

## **5.4 GRAVIMETRIC DISPENSING OF BULK LYOPHILATES USING THE FILL2WEIGHT™ SYSTEM**

### **5.4.1 Background**

The preceding study investigated the use of both volumetric and gravimetric powder dispensing systems for use with bulk dried lyophilates. Conclusions were consistent with the initial postulate that flowability of freeze dried powders influenced all aspects of the dosing process. The gravimetric dosing system was found to be the most suitable for adaptation. In this study the number of formulations studied was narrowed to those containing mannitol or a mannitol:sucrose combination while exploring the use of annealing during the freezing stage. This allowed the number of dosage forms dosed to be increased to 40 dosed units. Annealing was envisaged to enhance the mechanical strength of powders to facilitate accurate dosing while sucrose would serve as lyoprotectant. The new Fill2Weight gravimetric system with a larger throughput and potential for large scale production is investigated for compatibility.

### **5.4.2 Materials and Methods**

#### **5.4.2.1 Materials**

Fluid bed dried D-mannitol Ph. Eur. was purchased from Fagron, UK. Fluid bed dried sucrose BP, reduced nicotinamide adenine dinucleotide (NADH) and sodium pyruvate were from Fischer Scientific, UK.

IgG was obtained from caprylic acid precipitation of ovine sera as previously described in materials and methods (Section 3.1) and was received as a gift from MicroPharm UK (Polyclonal, Wales, Sheep no. 1363 16/02/94). Lactate Dehydrogenase (LDH) and CombiCoulomat fritless Karl Fischer reagent were both purchased from VWR, UK. 100 mM

Sodium phosphate buffer (pH 7.4) was prepared from sodium phosphate monobasic monohydrate from Fischer, UK and sodium phosphate dibasic from Sigma UK.

#### **5.4.2.2 Collapse point and eutectic measurements**

Formulation collapse temperatures were measured using a freeze drying microscopy (Lyostat3, Biopharma UK) as previously described (Section 3.2.1 on page 52).

#### **5.4.2.3 Lyophilisation Process**

Samples were lyophilised in a laboratory scale Virtis advantage freeze dryer. 1.6 mg/mL Immunoglobulin G (IgG) and 0.06 mg/mL lactate dehydrogenase (LDH) formulations were bulk lyophilised in a 3 compartment polyethylene tray system from 100 mL volumes. The freeze dried solution also contained either 1 M or 0.5 M mannitol or sucrose concentrations. Molar ratios of 1:1, 5:2 and 5:1 mannitol-sucrose combinations were formulated to contain 0.09 mg/mL of LDH where mannitol remained fixed at 0.5 M. Samples were equilibrated on a 25°C shelf for 30 minutes, chilled to -55°C (0.5°C/min) and held frozen for 6 hours. Formulations were annealed during the freezing stage to an additional temperature hold at -25°C for 2 hours. Primary drying used a -40°C shelf temperature except for mannitol: sucrose systems which were dried at -25°C and were annealed at -20°C during the freezing stage. A constant -75°C condenser and vacuum of 200 µbar (20 Pa) was used. Shelf was subsequently elevated to 20°C for secondary drying over 9 hours. K type thermocouples were placed at the bottom centre and edge of trays to monitor product temperature during the entire freeze drying cycle. Tray containing bulk dried cakes were transferred into polyethylene bags and into a nitrogen purged isolator (Soloflex, UK). Cakes were passed through a funnel into 500 mL sealed bottles for storage.

#### **5.4.2.4 Moisture Content Analysis**

Residual moisture content determinations were performed using a coulometric C20 Karl Fischer titrator (Mettler Toledo, Switzerland) as previously described in material and methods. Three sample replicates were extracted and sealed into vials. Using a 23G needle, these were reconstituted with 2 mL dry Karl Fischer reagent and 1 mL aliquots were injected into the titration cell.

#### **5.4.2.5 Flowability Characterisation**

Compressibility index was determined using a tap density apparatus (Sotax FD2, USA) as previously described in materials and methods. Bulk density measurement was adapted using a 50 mL cylinder. Samples were passed through a sieve with 1 mm aperture to remove agglomerates formed on storage. The endpoint of the tapped sample was reached when there was no more than a 2 mL change in sample volume. Tapped density was calculated as a ratio of sample weight to tapped volume. Compressibility index was calculated as a percentage of the ratio of the difference between tapped and bulk density to its tapped density.

#### **5.4.2.6 Porosity**

Particle density measurements were made using a helium gas multipycnometer (Quantachrome, MUP- 6DCE, USA). Porosity was then calculated from resulting particle density and measured bulk density as previously described in materials and methods.

#### **5.4.2.7 Gravimetric dispensing of annealed freeze dried powders**

Prior to dispensing, disruption of freeze dried cakes were conducted through mechanical sieving at a vibration amplitude of 80 mm through a 200 mm diameter sieve of 1 mm aperture size where particles greater than 1 mm were removed. Immediately prior to dosing samples were passed through a second 1 mm aperture sieve to break up any agglomerates that may have formed on storage before dispensing using a commercial Fill2Weight (F2W) powder dispensing system (3P Innovation, UK). Powders were conditioned by dry aeration before dosing. Dosing to 10 mg and 150 mg targets were performed in a fixed relative humidity (12.8%-14.5%) controlled with dry compressed air at a 20°C temperature.

#### **5.4.2.8 Particle Morphology studies**

Morphology studies were conducted with a light microscope (Carl Zeiss, Scope.A1 Germany) equipped with a polariser, camera system (AxioCam MRM) and imaging software (Axiovision version 4.8). Magnifications of x10 eyepiece with x10 or x40 objectives were used.

#### **5.4.2.9 Particle sizing**

The size distribution of powders were measured as previously described in materials and methods using a mechanical sieve shaker (Retsch, AS 200 basic, Germany) with a 16 set 38 mm diameter sieve stack (Endecotts, UK) with aperture sizes ranging from 1000-63 µm. Test samples were shaken at an amplitude of 80 mm at 5 minutes intervals. The endpoint of the sieving process was reached when the mass of any of the test sieves was unchanged by more than 5% or 0.1 g of its previous mass (British Pharmacopoeia Commission, 2013a).

#### **5.4.2.10 Protein recovery and activity**

Total protein content was determined using a bicinchoninic acid (BCA) assay kit (Thermo scientific, UK) based on the colorimetric detection of cuprous cations at 526 nm using BCA

LDH activity was determined using a kinetic UV spectroscopy assay conducted at 340 nm on the Multiskan spectrum plate reader (Thermo scientific, UK). These assays were previously described in the materials and methods.

#### **5.4.2.11 Content uniformity test of dosed units**

An acceptance value was calculated from total protein content assays for an enzyme were applicable (British Pharmacopoeia Commission, 2013b).

#### **5.4.2.12 Pass criteria**

Formulations with an acceptance value (AV) below 15 were passed. None of the passed formulations should fall below 0.75 or 1.25 of the case reference value (M) which was 98.5% or 101.5% or the average of individual dispensed contents expressed as a percentage of the label claim (British Pharmacopoeia Commission, 2013b).

### 5.4.3 Results

#### 5.4.3.1 Gravimetric dispensing of freeze dried powders

A lead formulation had been optimised for both protein and flow before being dosed with the high throughput gravimetric F2W powder doser. F2W uses a powder dosing valve which is opened and closed in response to weight feedback. The accuracy is a function of the time taken to dispense the target dose and the consistency of the powder flow properties: Consistent powder flow characteristics are necessary for accurate dosing. Dosing was conducted to meet BP requirements with assessed masses of 40 individual units for 7 batches of freeze dried powder.

Pre-formulation characterisation for collapse point and eutectic using freeze dried microscopy (FDM) showed a collapse temperature of  $-31.7^{\circ}\text{C} \pm 0.6$  for 0.5 M sucrose containing 6-9 mg/100 mL LDH (See Figure 5.12 for typical thermogram). Results for samples containing 0.5 M mannitol and 0.5 M sucrose showed a eutectic melt at between  $-1.7^{\circ}\text{C}$  and  $-1.4^{\circ}\text{C}$ . There was evidence of micro structure collapse between  $-17.7^{\circ}\text{C}$  and  $-21.1^{\circ}\text{C}$ . These values were in agreement with the reported eutectic temperature of  $-1.4^{\circ}\text{C}$  for mannitol (Kim *et al.*, 1998) and  $-32^{\circ}\text{C}$  collapse temperature of sucrose (Pikal, 2007). These critical temperatures were useful in avoiding complete or macro collapse and eutectic melt in formulations by ensuring product temperature was always below these critical temperatures.

Powder dosed for the 10 mg target showed a (-1% to 0.3%) mean deviation from the target while those dosed for 150 mg were dispensed within -2.7% to 1.2% deviations (Figure 5.13). Higher 150 mg target doses showed greater mass variation for the formulations initially dried from a 0.5 M mannitol concentration (Figure 5.13). Fluid bed dried mannitol and mannitol with IgG freeze dried combination (IgG 1 M MAN) showed 2.2% and 1.3% relative standard

deviations at 10 mg mass target dose. The same when dosed at higher 150 mg targets showed 0.8% and 0.79% (Figure 5.14 & Figure 5.15 Left).

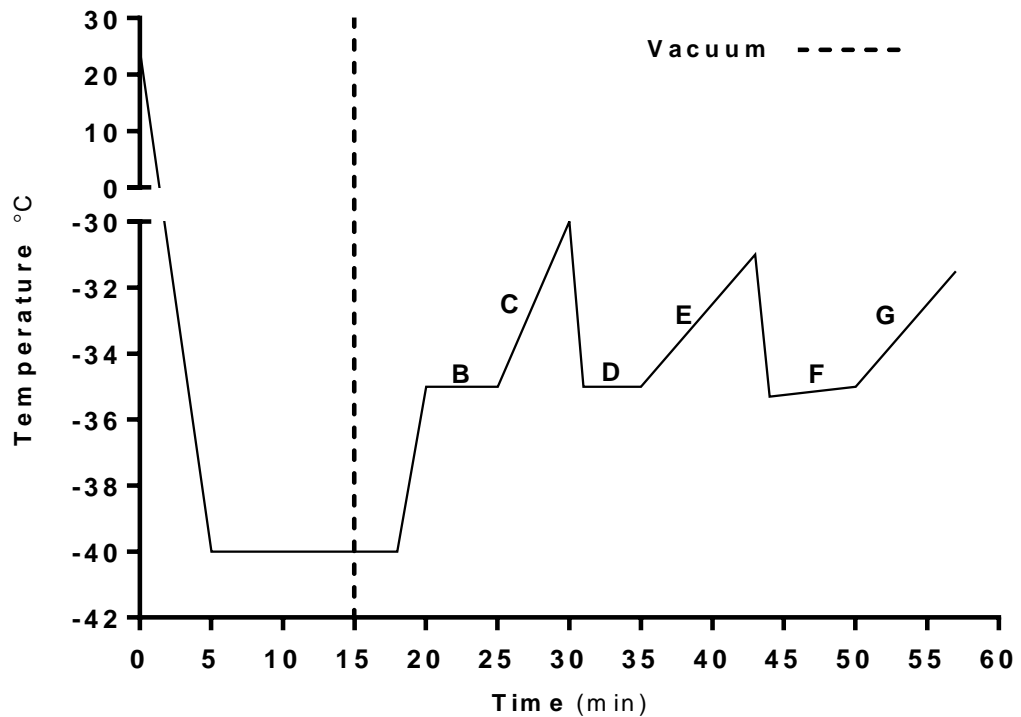
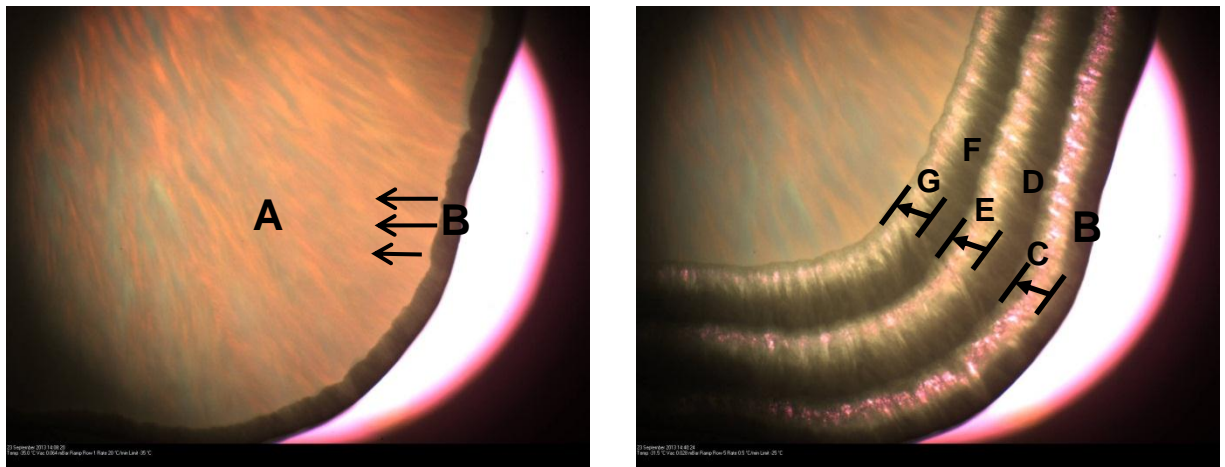


**Figure 5.12:** Typical images and temperature profile from freeze drying microscopy analysis of LDH in 0.5 M sucrose solution. Left: Sample aliquot (1.5  $\mu$ L) containing 1.7 mg/ml frozen from room temperature at  $-20$   $^{\circ}$ C/min to  $-40$   $^{\circ}$ C and held isothermal (A). A sublimation front (B) developed on pulling a 0.064 mbar vacuum. Onset of collapse was initially identified at  $-31.9$   $^{\circ}$ C during product temperature elevation period (C) using a  $1$   $^{\circ}$ C/min temperature ramp with further viscous flow observed over time (C). Decreasing sublimation temperature to  $-35$   $^{\circ}$ C (D) caused a regain in dried structure. Repeated heat cool heat cycles (E-F and G on graph) at a slower ramp rate of  $0.5$   $^{\circ}$ C/min revealed a total collapse temperature of  $-31$   $^{\circ}$ C and  $-32.2$   $^{\circ}$ C.

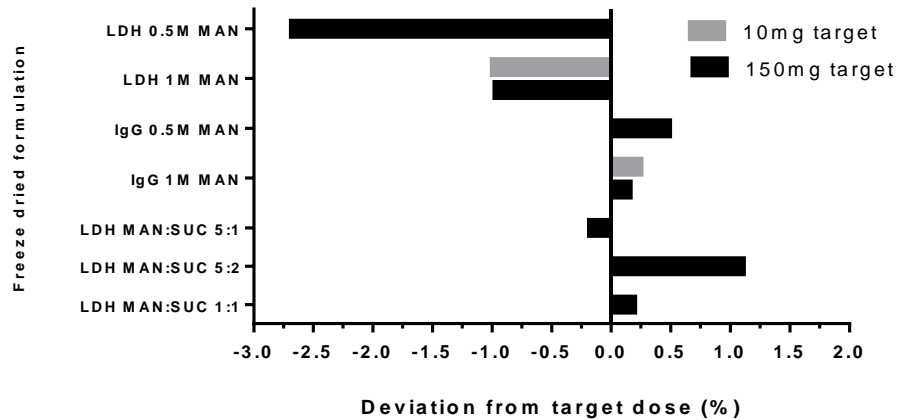


Figure 5.13: Mean deviations from target doses (n = 40) of lyophilised IgG from 0.5 M, 1 M mannitol (MAN) and varied molar ratios of mannitol and sucrose solutions containing lactate dehydrogenase (LDH MAN:SUC).

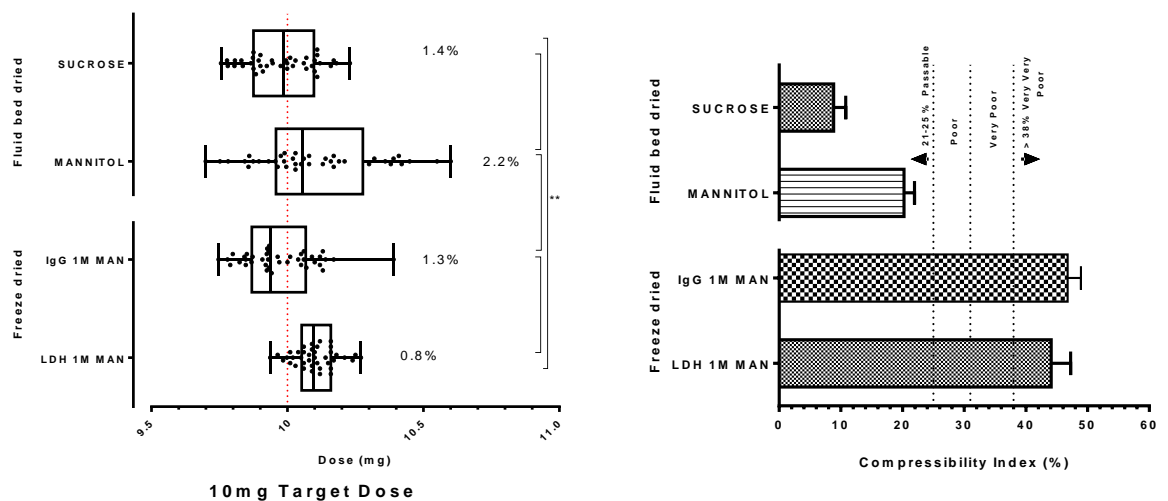
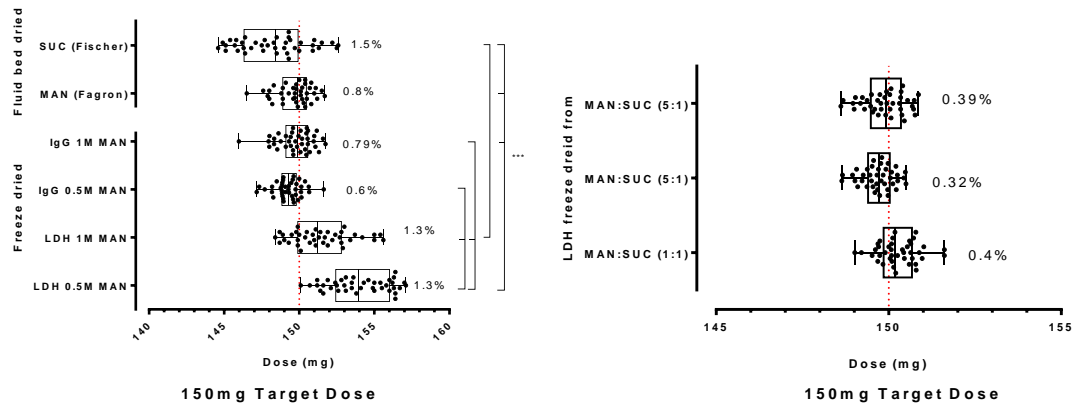
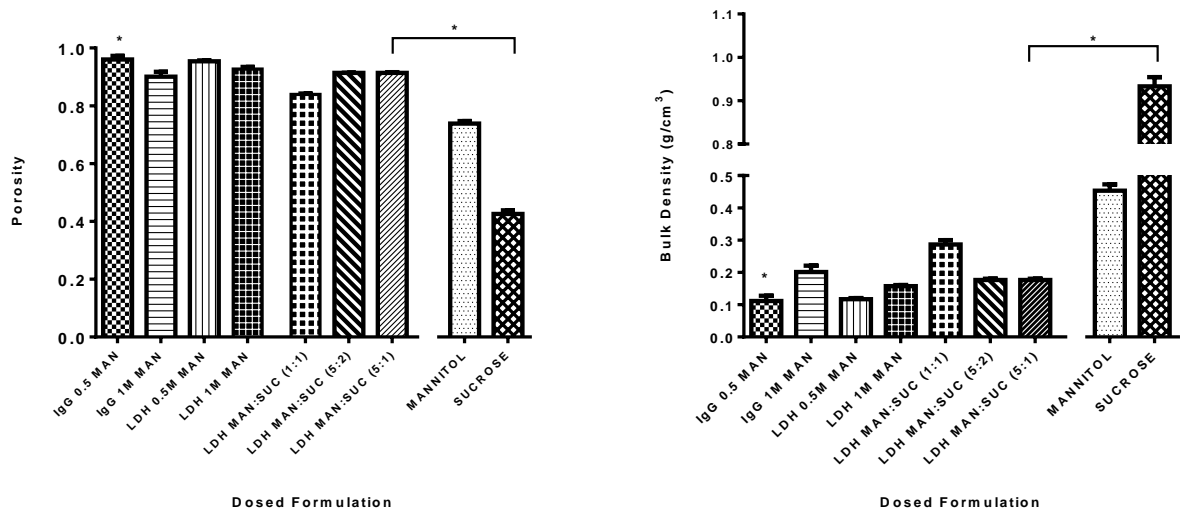


Figure 5.14: Left: Variation in mass of powder transfer (n = 40). Box and whisker plot with corresponding RSD of dosed bulk lyophilised mannitol (MAN) and sucrose (SUC) from 0.5 M, 1 M solutions containing 1.6 mg/mL IgG and 6-9 mg/100 mL LDH. Fluid bed dried mannitol and sucrose are BP, Eur. ph. grade crystalline powders. Target dose = 10 mg \*\*p<0.05 Right: Compressibility index of the same bulk lyophilised formulations (n = 3) of mannitol (MAN) from 1 M solutions containing IgG and LDH.

Solute content above 0.5 M did not significantly make any difference to the accuracy of dosed IgG despite the significant differences in bulk density (p<0.0001) and porosity (p<0.001) of the powders (Figure 5.16).



**Figure 5.15: Variation in mass of powder transfer (n = 40) using Fill2weight gravimetric dispenser. Average dosing time = 7.7 sec per dose. Powders were disrupted from annealed freeze dried cakes. Box and whisker plot with corresponding RSD of dosed bulk lyophilised mannitol (MAN) and sucrose (SUC) from**  
**Left top: fluid bed dried mannitol and sucrose (BP, Eur. ph. grade crystalline powders).**  
**Left bottom: 0.5 M, 1 M solutions containing 1.6 mg/mL IgG and 6-9 mg/100 mL LDH.**  
**Right: varied molar ratios of mannitol (MAN) and sucrose (SUC) solutions containing 9.12 mg/100 mL lactate dehydrogenase (LDH). \*\*\* P < 0.001 (one way ANOVA).**



**Figure 5.16: Porosity (n = 3) and bulk density (n = 3) of dosed bulk lyophilised IgG and LDH from 0.5 M, 1 M mannitol (MAN) and varied molar ratios of mannitol (MAN) and sucrose (SUC) solutions containing 1.6 mg/mL IgG and 6-9 mg/100mL LDH lactate dehydrogenase (LDH). Fluid bed dried mannitol and sucrose are BP, Eur. ph. grade crystalline powders.**

Powders defined as good flowing using BP criteria are expected to be dosed most accurately. Fluid bed dried sucrose had excellent flow properties (Figure 5.14 Right) but

exhibited 1.4%-1.5% RSD across 10 mg and 150 mg target doses suggestive that the individual particle size would be critical to dosed masses (Figure 5.14 & Figure 5.15). The cohesive nature of fluid bed dried mannitol contributed to the largest variation of 2.2% RSD at 10 mg target. We conclude mannitol was most accurately dosed gravimetrically while in its freeze dried form with IgG than from the unprocessed crystalline form.

IgG and LDH dried with 1 M mannitol are significantly different in dosing accuracy depicted by 0.79% and 1.3% RSD values respectively ( $p < 0.001$ ). This is also true when comparing powders of the lower solute (0.5 M) contents of both proteins ( $p < 0.001$ ).

The F2W system displayed a level of high precision for metering a wide spread of powders to include LDH freeze dried in mannitol-sucrose (LDH MAN:SUC) combinations. The latter displayed the best dosing accuracy with a relative standard deviation range of 0.32-0.4% (Figure 5.15 Right). At worst it was less than 1.61 mg over filled and 1.38 mg under filled corresponding to % mean deviations from target mass ranges of -0.18% to 1.1% (Figure 5.13).

Particle distribution through sieving provided no statistical evidence for a difference between amorphous systems expected to freeze dry with freeze drying induced phase collapse and those formulations without freeze dry collapsed solutes. However a 1:1 molar ratio of mannitol to sucrose was significantly bigger in size distribution than those of the 5:1 or 5:2 ratios (Figure 5.17). The median particle size of the freeze dried powders were 100-200  $\mu\text{m}$  ( $p > 0.05$ ) except for a single formulation (LDH MAN:SUC 1:1) which was distinct in its larger 450  $\mu\text{m}$  median size. This same formulation showed no significance ( $p > 0.05$ ) in size distribution from fluid bed dried sucrose. Fluid bed dried mannitol was not any different in size distribution when freeze dried with either IgG or LDH.

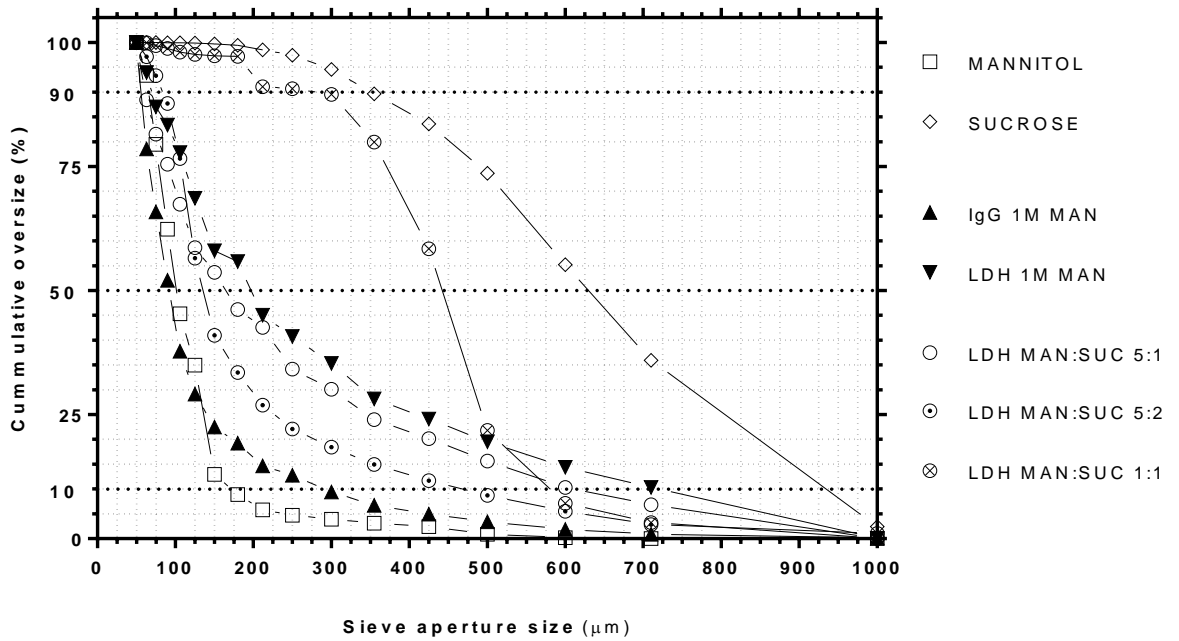


**Figure 5.17: Particle size distribution of formulations (n = 1) freeze dried from 1 M mannitol (MAN) and varied molar ratios of mannitol and sucrose (LDH MAN:SUC). Stock solutions contained 1.6 mg/mL IgG and 6-9 mg/100 mL LDH lactate dehydrogenase (LDH). Fluid bed dried mannitol and sucrose are BP, Eur. ph. grade crystalline powders.**

Polarised light microscopy revealed distinct differences in the morphology of fluid bed dried mannitol as well as IgG and LDH freeze dried in mannitol (Figure 5.18). These distinct differences in particulate morphologies indirectly affect individual powder flow behaviour. Birefringence was observed in all freeze dried samples (Figure 5.18-5.20).

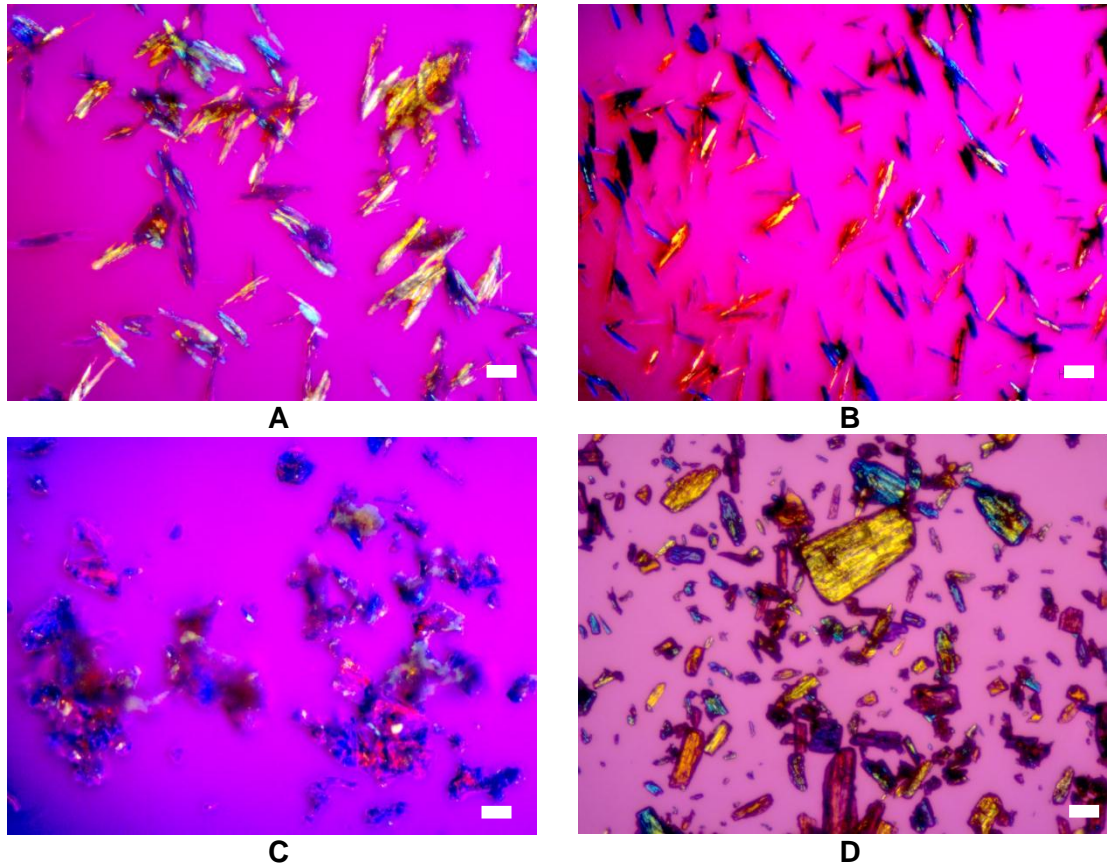


**Figure 5.18: Polarised light microscopy images of F2W gravimetric dispensed powders at x100 magnification A) IgG 0.5 M MAN B) IgG 1 M MAN C) LDH MAN:SUC 1:1 D) Fluid bed dried mannitol. Bold scale bar = 50 microns.**

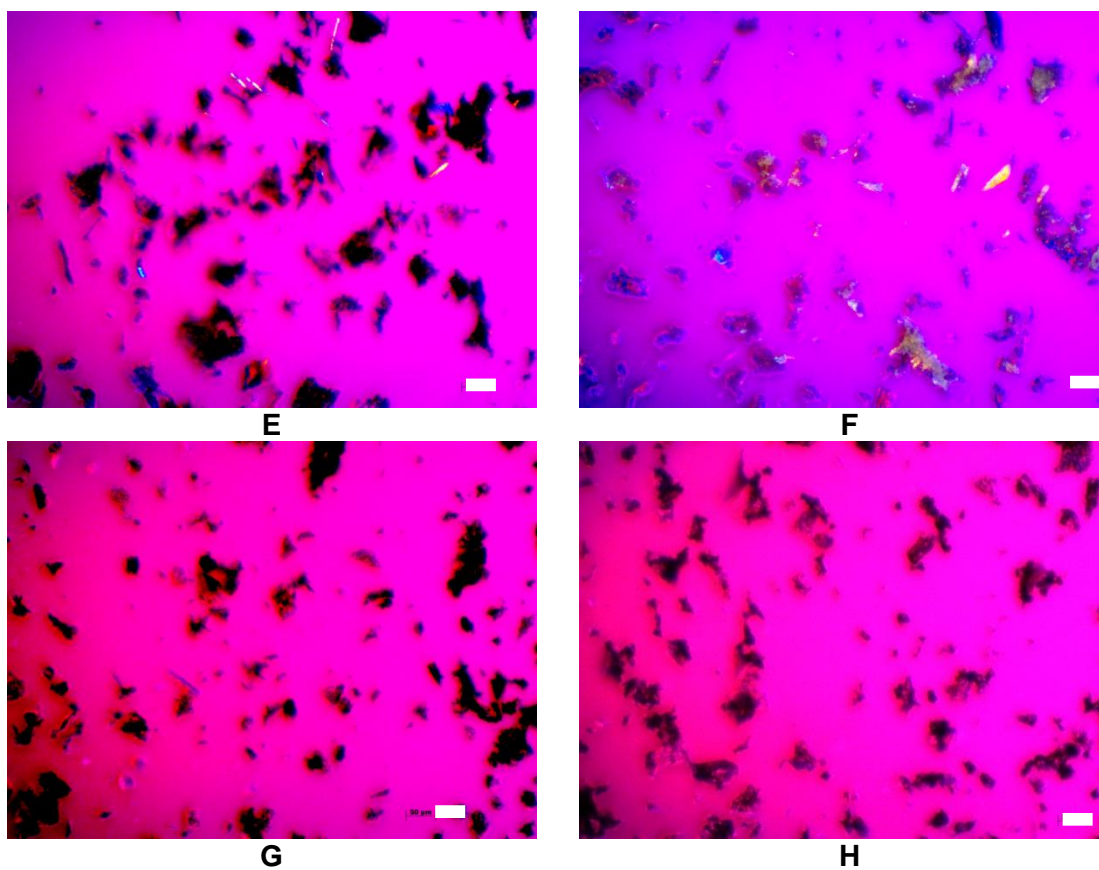


**Figure 5.19: Polarised light microscopy images of F2W gravimetric dispensed powders at x100 magnification E) LDH 0.5 M MAN F) LDH 1 M MAN G) LDH MAN:SUC (5:1) H) LDH MAN:SUC 5:2 Bold scale bar = 50 microns.**

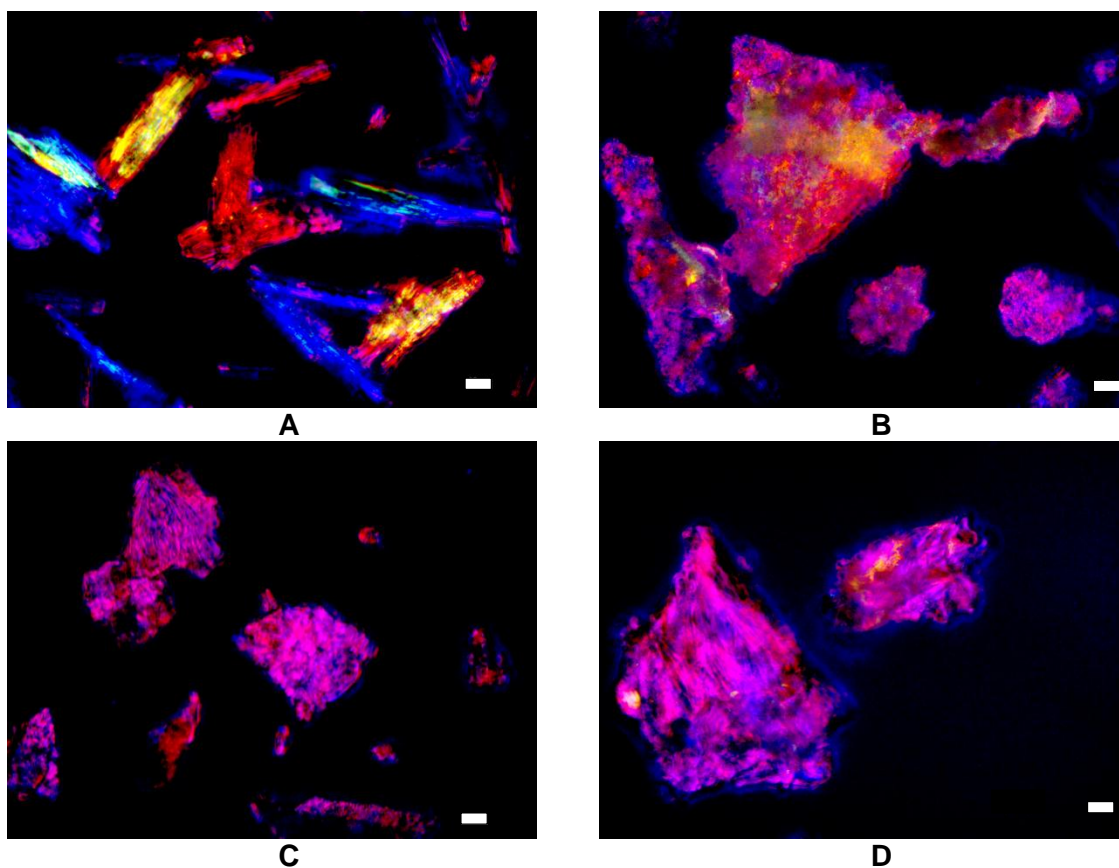


**Figure 5.20:** Polarised light microscopy images of F2W gravimetric dispensed powders at x400 magnification A) IgG 1 M MAN B) LDH 0.5 M MAN C) LDH MAN:SUC 5:2 D) LDH MAN:SUC 1:1. Bold scale bars = 10 microns.

#### **5.4.3.2 Uniformity of Content Assays**

Increasing the amount of bulking agent correlated with an increase in variation of content uniformity observed through the total protein content assay. Content uniformity deteriorated when IgG was substituted with LDH using the same formulation conditions (Figure 5.21). This would indicate that a change of protein type could significantly affect the protein recovery within a specific dosage target. The same trend was seen in 5:1 (13.85% RSD) and 1:1 (15.54% RSD) mass ratios of mannitol:sucrose systems (Figure 5.23).

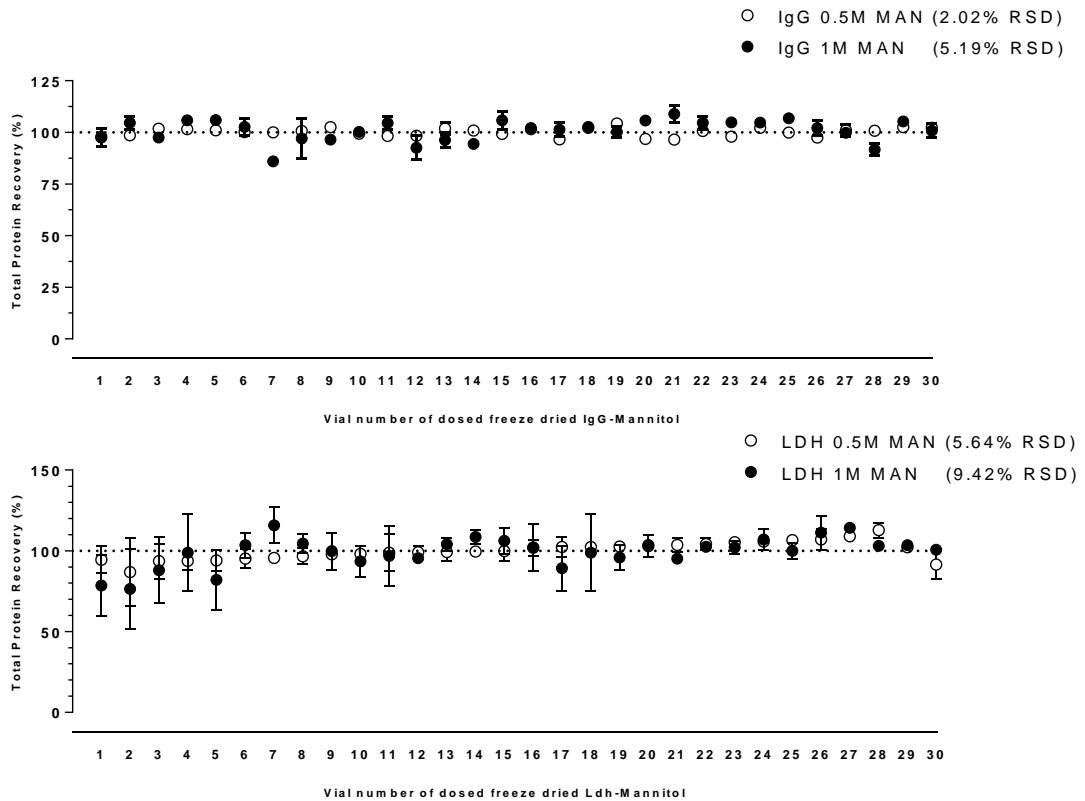


**Figure 5.21: Total protein content (n = 3) with % relative standard deviation (RSD) of Top: dosed Mannitol-IgG Freeze dried. Bulk dry powder was freeze dried from 0.5 M and 0.1 M solutions containing total protein content of 1.6 mg/mL. Bottom: Dosed Mannitol-LDH Freeze dried. Bulk dry powder was freeze dried from 0.5 M and 0.1 M solutions containing total protein content of 6-9 mg/100mL. Samples were reconstituted with 1 mL distilled water and quantified using bicinchoninic acid (BCA) assay. Target dose = 150 mg.**

Increasing the sucrose content in LDH freeze dried in mannitol:sucrose was hypothesised to improve activity recovery but negatively affect flow behaviour and dosing accuracy. This increase did not have any significance on flowability of formulations (Figure 5.22 Left). There was a difference between total protein content and actual activity recovery of LDH in mannitol:sucrose formulations (Figure 5.23). This trend was consistent with the increasing amorphous sucrose content of these formulations protecting the activity. Optimising the

recovery of LDH was not within the scope of this work but has been covered in literature (Anchordoquy and Carpenter, 1996, Anchordoquy *et al.*, 2001, Kawai and Suzuki, 2007). The first 30 LDH Mannitol:sucrose dosed units assayed for both activity and total protein content had a mean dosed mass between 149.7-150.3 mg (0.08-0.2% mean target deviation).

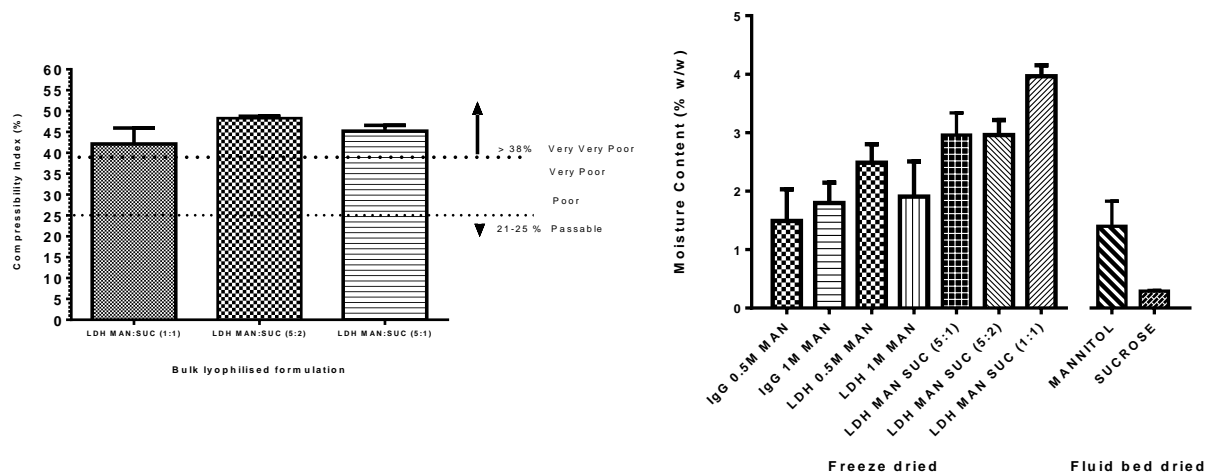


**Figure 5.22: Left: Compressibility index of bulk lyophilised formulation prior to mass dispensing (n = 3). Bulk lyophilised formulations consist of varied molar ratios of mannitol (MAN) and sucrose (SUC) solutions containing lactate dehydrogenase (LDH). Right: Moisture content (n = 3) of bulk freeze dried formulations and fluid bed dried mannitol and sucrose.**

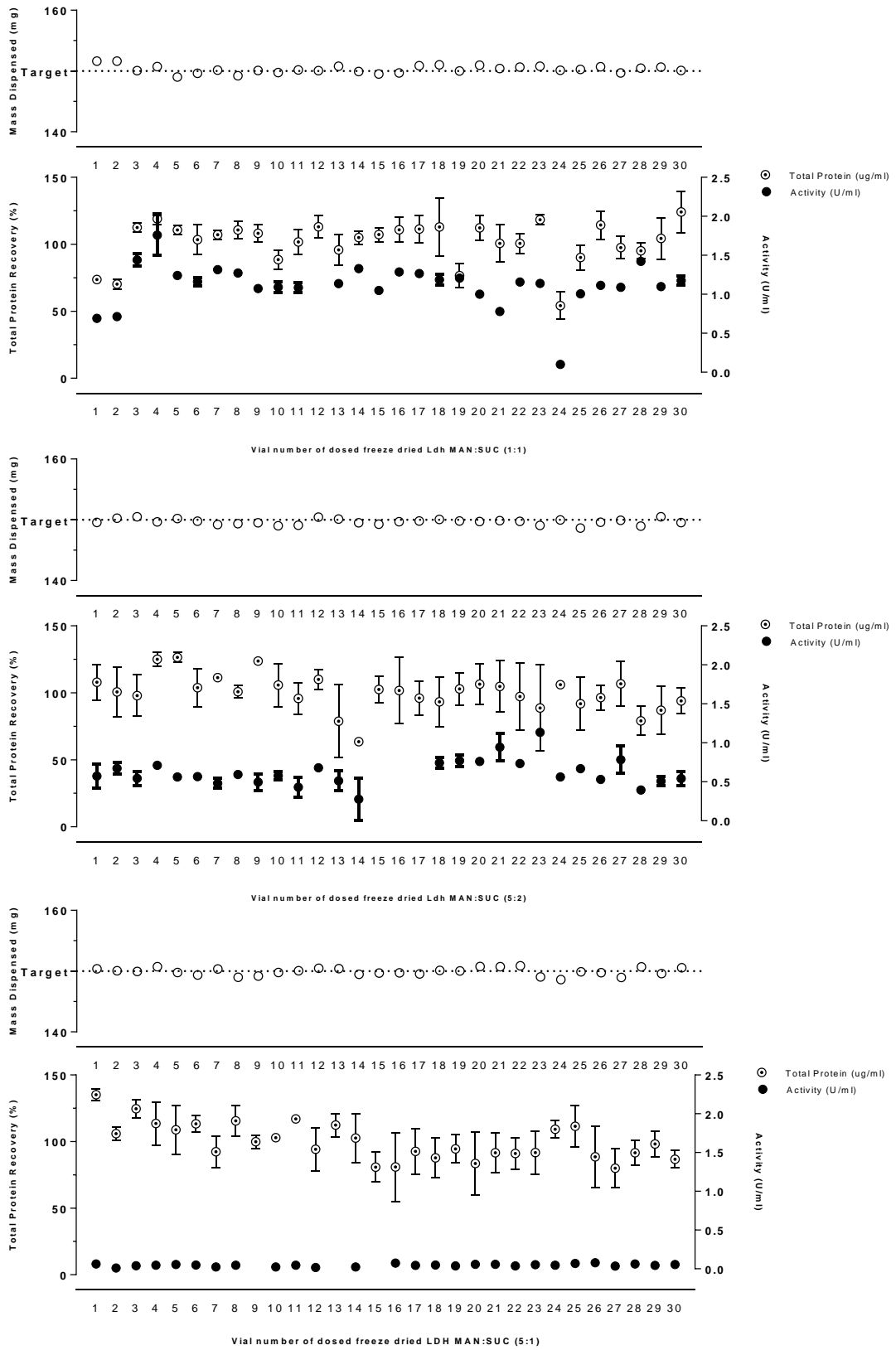


Figure 5.23: Total protein and activity recovery in mass dosed LDH formulations (n = 3). LDH

was bulk lyophilised in molar ratios of mannitol (MAN) to sucrose (SUC) of Top: 1:1 Middle: 5:2 and Bottom: 5:1

Through knowledge of the freeze drying cycle due to a high shelf temperature, there is an expectation the sample would contain micro collapse phases. Thermocouple product recordings confirm samples exceeded the collapse temperatures for the sucrose phase. However, crystalline mannitol would be expected to maintain the macro structure of the bulk cake. The presence of collapse may explain the poor content uniformity (Table 5.3) for mixed sucrose mannitol systems which had poor acceptance values consistent with increasing sucrose collapse. The use of such mannitol and sugar mixtures have been studied and are also present in commercial products (Johnson *et al.*, 2002).

**Table 5.3: Content uniformity and calculated acceptance values (AV) of dosed formulations**

<b>Formulation</b>	<b>Label claim (µg/mL)</b>	<b>% Recovery</b>	<b>SD</b>	<b>Acceptance Value</b>	<b>Comment</b>
LDH 0.5 MAN	35	100.1	2.0	4.0	Pass
LDH 1 M MAN	20	99.4	1.9	3.7	Pass
LDH MAN:SUC 1:1	85	101.7	13.4	27.1	failed
LDH MAN:SUC 5:2	90	100.2	12.0	23.9	failed
LDH MAN:SUC 5:1	70	100.0	9.7	19.4	failed
<b>Formulation</b>	<b>Label claim (mg/mL)</b>	<b>% Recovery</b>	<b>SD</b>	<b>Acceptance Value</b>	<b>Comment</b>
0.5 M MAN IgG	1.9	100.2	0.04	0.1	Pass
1 M MAN IgG	1	101.0	0.05	0.1	Pass

#### 5.4.4 Discussion

Powder flow behaviour influences the compatibility of powders for dispensing in this application. Consistently flowing powders are easier to dose. It is also important for powder transfer from intermediate storage or hoppers to dosing heads for dispensing. Powder arching and rat holing are typical flow problems to avoid. In gravimetric systems, powder feed from a hopper on reaching the dosing head is dispensed by controlling the duration of opening and size of a dosing orifice in response to the dispensed weight and flow rate. It is also common practice to condition the powders before and during the dosing process to encourage flow by aerating them.

Flowability was measured by compressibility index which is an indirect measure of physical properties including size, surface area, shape and moisture (British Pharmacopoeia Commission, 2013c). Cohesive or poor flowing powders tend to be more compressible and display higher compressibility indices (Carr, 1965, Howard, 2007). Freeze dried formulations were cohesive and more compressible (Figure 5.14 Right) and had a general median particle size of 100-200  $\mu\text{m}$  (Figure 5.17). Particles above 250 microns are free flowing while below 100 microns flow problems are eminent due to increased cohesiveness (Staniforth and Aulton, 2007). Observed compressibility indices were in agreement with previous work on freeze dried powders which were classified as having very poor flow behaviour (Chapter 4).

It was observed that excellent flowability did not always guarantee accurate dosing in granular materials. Fluid bed dried sucrose, despite its better flowability (Figure 5.14), showed relatively higher dosed %RSD when compared to freeze dried batches. It is hypothesised that this is due to the larger particle size distributions (median size of 625  $\mu\text{m}$  (Figure 5.17) and significant bulk density (Figure 5.16): this leads to a greater propensity to

overflow during the dosing system's controlled opening and closing of the dosing orifice. A few irregular particulates towards the end of the dosing cycle have the ability to skew the final masses over the target weight. This effect is less apparent for the smaller sized, porous and less dense freeze dried particles.

There was a positive correlation between solute content and final porosity (Figure 5.16). Freeze dried formulations were all very significantly ( $p < 0.0001$ ) porous with lower bulk densities. Bulk densities affect packing of powder within feed hopper and hopper capacity of dosing heads. Hopper replenishing needs to be carefully controlled during repetitive dosing. The height of the powder in the hopper generates a pressure head which alters flow rates and can adversely impact dosing repeatability. It is important therefore to consider the hopper design to include appropriate hopper feed angles and opening dimensions. The F2W system includes in-built stirring and vibration mechanisms which avoid problems such as powder arching and rat holing: these are evident in other systems without these features.

There is a superior compatibility of IgG over LDH when freeze dried in 1 M mannitol for powder dispensing. A difference in particle morphology from light microscopy explains this observation. These distinct differences in particulate morphologies were observed as needle like particulates in IgG (Figure 5.18 A&B, Figure 5.20 A) and more flaky irregular surfaces in LDH (Figure 5.18 C). Rough surfaces cause particles to interlock with each other leading to poorer flow from hopper to dosing pins. No significant differences existed in particle size (Figure 5.17); moisture (Figure 5.22 Right), porosity (Figure 5.16) and flowability of both formulations (Figure 5.14 Right). The very porous nature of freeze dried powders in general means that their flowability is not affected by minute differences in moisture. Moisture in porous and cohesive materials penetrate the core of the particles and no liquid bridges which affect flow are formed (Howard, 2007). This explains why IgG and LDH in 1 M Mannitol (MAN) formulations were not significantly different in flowability despite a 1% non-significant difference in moisture.

Birefringence observed in all freeze dried samples (Figure 5.18) was indicative of crystallinity after freeze drying in mannitol. Generally a more amorphous character was suggestive in the presence of LDH. Such a conclusion would require confirmation using X-ray powder diffraction analysis.

Dosed accuracy also correlated with the amount of solute content present and powder flowability. While this study revealed solute contents above 0.5 M ( $\cong$ 9 %w/v) did not significantly enhance the accuracy of 150 mg target dosing of IgG and LDH formulated in mannitol, previous flowability studies (discussed in chapter 4) of mannitol as a carrier agent revealed that above 5 %w/v of pure lyophilised mannitol there was no significant decrease ( $P>0.05$ ) in compressibility and improvement in flow.

Tendencies to under fill or over fill were evident across both target doses investigated. These are errors attributable mainly to flow behaviour of the powder samples and or systemic errors of the dosing machinery. Systemic errors cannot be detected by replicates of measurements and may be caused by equipment or localised changes in physical properties of the powder affecting flow. In many cases it is responsible for very low or very high values even in replicate determinations (Miller and Miller, 2005).

Though over and under filled container closures were included in these studies, availability of online process analytical technology mean these outliers can be rejected in practice and fed back into bulk feeds to be metered again. This process may require validation and it is envisaged will be easily implemented in gravimetric systems as an integral feedback loop mechanism is already present.

Gehrmann *et al.* (2010) used a gravimetric system composed of a screw conveyor with a vibrating chute to dose 69-199 units of freeze dried pellets and achieved a mean maximum deviation of  $\pm 2$  mg. We have shown smaller maximum deviations at 150 mg target using LDH freeze dried in mannitol and sucrose mixtures (+0.86 mg, -1.39 mg; +0.5 mg, -1.4 mg; +1.61 mg, -0.99 mg). These are in good agreement and indicate similar performance using a non-pelleted formulation. Freeze dried pellets of significantly larger size range of 500  $\mu\text{m}$  fines, 1000-2000  $\mu\text{m}$  as coarse and a mix of both were used by Gehrmann *et al.* Results obtained in our work from non-segregated freeze dried powder mix below 1000  $\mu\text{m}$  and median size of 100-200  $\mu\text{m}$  suggest pelleting may not be a necessity for accurate powder dispensing and optimising ordinary powders could suffice.

Masses dosed accurately do not guarantee content uniformity. Acceptance value calculations determine if batches are to pass or fail (Table 5.3). Excluding mannitol sucrose mixtures, all batches assessed for uniformity passed.

The distribution of protein content within powder particles is believed to be as a result of crystal growth during the annealing process. However, annealing encourages crystal growth and improves the dosing accuracy from preliminary work. The use of an annealing step further encouraged mannitol crystallisation (Hawe and Friess, 2006a) which is recommended for long term stability if continued crystallisation and further release of moisture on storage are to be avoided. Mannitol however provides minimal lyoprotection compared to other non-reducing sugars such as sucrose and trehalose. Mannitol has found use in lyophilisation mainly as a bulking agent to provide an elegant cake appearance. It also provides essential macro structural support in the micro collapse of mannitol:sucrose mixtures where the use of aggressive cycles provide cost savings. It is however important to not unduly add bulk to formulations as this will add to the cost. Bulking agents are important

for flowability of the freeze dried formulations but their addition reduces API density in the final powder and increase target weights. Bulk dried formulations with the same API content and varying amounts of bulking agent would require different dosed masses for same therapeutic effects. Manufacturers must therefore approach dilution of a freeze dried API with care as there is an increase in economic cost associated with the increase excipient mass to be dried.

#### **5.4.5 Conclusion**

Manufacturers of reconstitution injectable formulations who are considering dosing freeze dried powders from bulk need to optimise a number of factors: these include the cake disruption process, the physical form, flowability, process humidity control and also the choice of dosing system. This study has shown this to be practical.

Annealed mannitol bulk content aids dosing accuracy with the gravimetric powder dispenser used (F2W). The type of protein to be dispensed affects morphology of final powders and dosing accuracy due to differences in powder flow behaviour. Bulk mannitol content above 9 %w/v or 0.5 M provide no addition benefits to dosing accuracy or uniformity of content of dosed units. A mannitol solute content of no more than 0.5 M or 9 %w/v in initial freeze dried solution feed is recommended for compatibility with gravimetric powder dispensing. Excess bulk will dilute the API and unduly add to cost of drying.

Further work is required to formulate proteins in a mix of amorphous and crystalline phases which will balance the need for good flow behaviour, dosing accuracy and long term stability. This work shows annealing treatment is required and micro collapse need to be avoided if both crystalline and amorphous bulk phases co-exist to guarantee content uniformity of dosed vials.

The use of a gravimetric dosing system with a process analytical tool to exclude outliers is recommended for freeze dried powder dispensing.

We have demonstrated it is possible to meet current regulatory approval in the illustrated cases using a simple, low cost and reproducible cake disruption process in conjunction with a commercially available powder dosing system.

## **6 X-RAY MICRO COMPUTER TOMOGRAPHY STUDIES OF LYOPHILISED POWDER FOR DETERMINATION OF FLOW CHARACTERISTICS AND DOSE UNIFORMITY OF ACTIVE PHARMAEUTICAL INGREDIENTS.**

### **6.1 Introduction**

Lyophilisation or freeze drying demands adequate characterisation during formulation and cycle development to guarantee the final dried forms are desirable. Attributes desired after freeze drying include but not limited to stability, final physical form, appearance, moisture content, dissolution and morphology. These attributes are quality factors which we defined elsewhere as “ the term given to the individual priorities developers place on distinct aspects of a formulation to define its final acceptance” (Ekenlebie and Ingham, 2011). Various aspects of the product development process need attention to ensure final product acceptance such as freezing, primary drying, thermal treatment (annealing) and final surface area. Many characterisation techniques are therefore available and have been reviewed (Liu, 2006, Devi and Williams, 2013). Selection of a suitable technique is also influenced by duration of analysis, convenience, versatility, cost or simply its availability at the time of research and development.

The final morphology of a freeze dried cake is commonly studied using microscopy. Scanning electron microscopy (SEM) is the most widely used microscopic tool by freeze drying scientists to qualitatively study microstructure. Applications of the various forms of microscopy including SEM, transmission electron microscopy (TEM), environmental scanning microscopy (ESEM) and light microscopy in freeze drying have been reviewed extensively (Overcashier, 2003, Liu, 2006).

It is common practice in microscopy to cut or break glass vials open to access dried cakes. Cakes are subsequently sectioned using razor blades and gold coated if SEM was the choice (Schersch *et al.*, 2010, Liu *et al.*, 2005, Overcashier, 2003). The series of sample

preparation steps involved can be hazardous to the unskilled; tedious if simultaneous control of humidity is required and quite arguable if the true micro structure is indeed revealed due to changes induced by coating and cutting. An interesting approach by Patapoff and Overcashier (2002) involved the use of paraffin wax and a fluorescent dye to enhance imaging of cake cross sections.

Advances in pharmaceutical technology have seen the development of newer quantitative imaging techniques for characterisation of aqueous and dry powder in their various forms. Fu *et al.* (2012) used a computer aided microscopic particle image characterisation device to characterise size and shape of lactose. The device allows dry powder samples between 0.5 microns to 10 mm to be dispersed onto glass slide and images are captured for high through put software analysis of individual particles (Malvern Instruments, 2014). Optical coherence tomography-based freeze drying microscopy has been reported superior to traditional freeze drying microscopy to predict collapse temperatures and also produce three dimension images (Mujat *et al.*, 2012). Davis *et al.* (2013) employed micro flow imaging to study the effect of sub visible particles on stability of lyophilised IgG (Immunoglobulin G). The inner workings of the imaging technique has been described (Protein Simple, 2013).

The use of X-ray radiation has also found newer applications in industry. Its use in freeze drying which was previously limited to characterisation of the final physical form (amorphous or crystalline) via X-ray powder diffraction or freeze drying X-ray powder diffraction (Cavatur and Suryanarayanan, 1998) has recently been demonstrated commercially useful in visual inspection of defects and foreign particles in the range of 40-200 microns in freeze dried cakes within intact glass vials (Prinz, 2012).

X-ray microcomputer tomography (MCT) has aroused interest in pharmaceuticals as a non-destructive technique which requires little or no sample preparation to quantitatively inform

structural attributes of materials. A detailed description of the background and inner workings of MCT together with the subject of tomography was previously described (Section 3.4.12 page 74 & 1.8 page 47). Parker *et al.* (2010) used MCT to quantify pore size distribution, porosity and connectivity in vial lyophilised BSA cakes subjected to a conventional and high temperature aggressive cycles. Authors found a correlation with SEM in observed connectivity.

## **6.2 Aims and Objectives**

Here X-ray microcomputer tomography (MCT) was explored as a versatile quantitative approach to characterising freeze dried cakes and powders. It was the aim of this chapter to identify correlations that exist between traditional techniques and MCT. Objectives were to correlate porosity measurements with gas pycnometry and predict powder flowability from minute sample sizes. Results were compared using regression analysis. New morphometric parameters to freeze drying from three dimensional image analyses as well as creation of three dimensional fly through cross sectional images of powders were investigated. It was a further objective to quantify the distribution of pharmaceutical active ingredients when freeze dried with different cooling rates using a platinum dispersion model.

## **6.3 STUDY OF POROSITY, PACKING AND MORPHOMETRIC PARAMETERS IN BULK LYOPHILISED POWDERS**

### **6.3.1 Background**

It is hypothesised that MCT would allow the use of small sample sizes of freeze dried formulations to be well characterised to inform powder packing and morphology which include porosity, size and shape. Packing and powder morphology are useful indicators of powder flow behaviour. Knowledge of the porosity of the final dried cake or powder influences reconstitution time and duration of primary drying. The porosity of freeze dried cakes can be qualitatively assessed using microscopy. A quantitative approach involves the determination of a material's true density using gas or mercury pycnometry. MCT is capable of quantitatively analysing pore size distribution and porosity of materials. In this section of the thesis MCT technique was compared with the traditional gas pycnometry to investigate any correlations that exist. The use of two different inert gases, nitrogen and helium were initially studied in pycnometric analysis of lyophilised mannitol.

### **6.3.2 Materials and Methods**

#### **6.3.2.1 Materials**

Fluid bed dried D-mannitol Ph. Eur. was purchased from Fagron, UK. Packing straws were obtained from Sainsbury's, UK. Sealing film (Parafilm™) and CombiCoulomat fritless Karl Fischer reagent obtained from VWR, UK. Dental beading wax was from Kemdent, UK.

#### **6.3.2.2 Lyophilisation**

##### **6.3.2.2.1 Bulk dried mannitol powders 1**

Freeze drying of mannitol (100 mL, 5-22.5 %w/v) solutions was in a Virtis Advantage bench freeze dryer using a custom made stainless steel tray as bulk container systems (Material and Methods Figure 3.3 page 57). Samples were chilled at -55°C from room temperature

and held for 6 hours. Primary drying was at a low  $-40^{\circ}\text{C}$  despite the known eutectic temperature of mannitol of  $-1.5^{\circ}\text{C}$  (Kim *et al.*, 1998) for comparative studies not disclosed in this chapter. Secondary drying was at  $20^{\circ}\text{C}$  for 4 hours with a constant  $-75^{\circ}\text{C}$  condenser and pressure at  $200\ \mu\text{bar}$ . K type thermocouples (RS Components, UK) were used to monitor product temperature during the drying process. Trays containing bulk dried cakes were transferred through a funnel into sealed bottles for storage in desiccators over moisture indicating dried silica gel. Cakes were later broken down into powder with the British pharmacopeia tablet friabilator (Sotax USP F2, Switzerland) using a fixed 1000 revolutions in simulation of typical handling.

#### **6.3.2.2.2 Bulk dried mannitol powders 2**

Mannitol solutions (100 mL, 0.056 M-1 M) were freeze dried in a Virtis advantage freeze dryer using a custom made three compartment tray as previously described (Material and Methods, Figure 3.3 on page 57).

Different cooling rates of  $0.2\ ^{\circ}\text{C}/\text{min}$ ,  $1\ ^{\circ}\text{C}/\text{min}$  and  $5\ ^{\circ}\text{C}/\text{min}$  were used. Samples cooled at  $0.2\ ^{\circ}\text{C}/\text{min}$  and  $1\ ^{\circ}\text{C}/\text{min}$  were equilibrated on a  $25^{\circ}\text{C}$  shelf for 30 minutes, shelf temperature was ramped to  $-55^{\circ}\text{C}$  and held frozen for 6 hours. Annealed samples were equilibrated on a  $25^{\circ}\text{C}$  shelf for 30 minutes and cooled to  $-55^{\circ}\text{C}$  ( $0.2\ ^{\circ}\text{C}/\text{min}$ ) with an additional temperature hold at  $-20^{\circ}\text{C}$  for 2 hours. Samples cooled at  $5\ ^{\circ}\text{C}/\text{min}$  were loaded directly onto a  $-70^{\circ}\text{C}$  precooled shelf. Primary drying was at  $-10^{\circ}\text{C}$  shelf temperature. A constant  $-80^{\circ}\text{C}$  condenser and vacuum of  $200\ \mu\text{bar}$  was used. Shelf was elevated to  $20^{\circ}\text{C}$  for secondary drying over 6 hours. K type thermocouples were placed at the centre and edge of trays to monitor product temperature during the entire freeze drying cycle. Tray containing bulk dried cakes were transferred into polyethylene bags and into nitrogen purged isolator (Soloflex, UK). Cakes were passed through a funnel into sealed bottles for storage in desiccators over moisture indication dried silica gel.

Samples were disrupted or broken down into loose powders using a nest of sieves as previously described (4.4.2.2).

### **6.3.2.3 X-ray scans and image processing**

#### **6.3.2.3.1 Bulk dried mannitol powders 1**

Samples were scanned as previously described in materials and methods (section 3.4.12.2 page 75) using a 40 kV X-ray source voltage and 169  $\mu$ A current at a scanning resolution of 3  $\mu$ m. Stage was rotated stepwise at 0.7° with frame averaging and random movement options set to 3 and 4. Images were reconstructed using the Nrecon reconstruction software (version 1.6.4) and quantitatively processed using CT-analyser software.

#### **6.3.2.3.2 Bulk dried mannitol powders 2**

Sample scanning and image preconstruction were performed as previously described in materials and methods. An X-ray voltage source of 36 kV and 200  $\mu$ A current at a scanning resolution of 3  $\mu$ m was used. Stage was rotated stepwise at 0.7° with frame averaging and random movement options set to 3 and 4.

#### **6.3.2.4 Descriptives**

Results and discussion within this chapter make references to common terms used in MCT. These are used through the following sections and definitions are next highlighted from Skyscan (2011). The term 'Pixel' is a square element of an image with a characteristic grey level of the brightness at its particular location. A pixel with a known x, y and z dimensions is three dimensional and referred to as a 'voxel'. A region of interest (ROI) is a selected area within a single two dimensional image slice within an object and the addition of a set of adjacent ROIs forms the volume of interest (VOI) within the selected volume.

### 6.3.3 Results

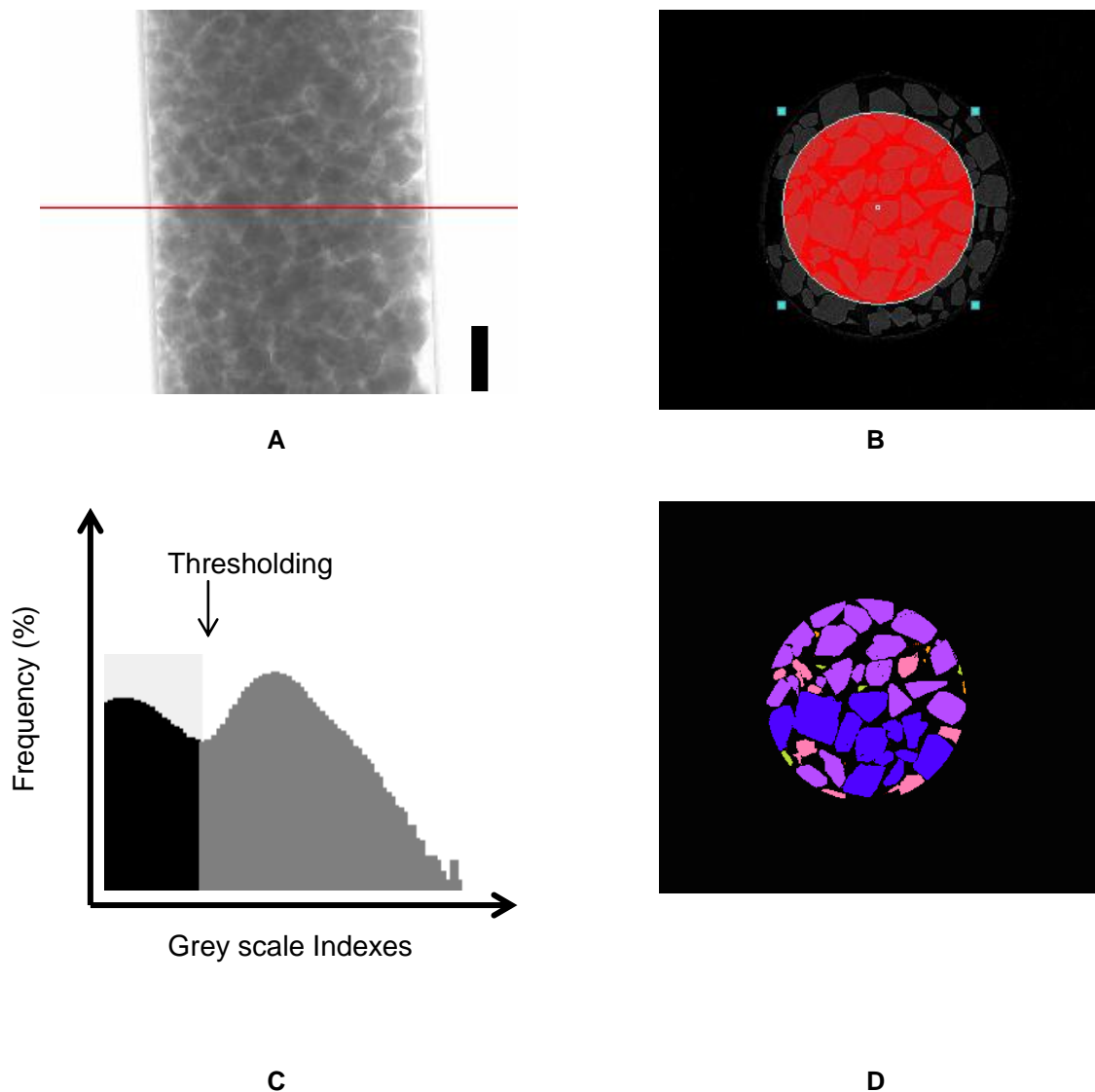


**Figure 6.1: Typical results from MCT scans and 2D morphometric analysis for packed fluid bed dried sucrose** A) Reconstructed image from projected X- ray shadow images after stepwise beam scanning. Red vertical line through packed sample corresponds to a 2D image slice at the location shown as B) the two dimensional binarised image slice. Red circular region within image is the region of interest selected for morphometric analysis. The selected region of interest corresponds to C) grey scale indexes which are segmented into pores (black) and sample (grey) D) Processed 2D coloured size distribution. A collection of image slices from top to bottom make up a volume of interest (VOI) and were analysed to produce 3D morphometric parameters. Black vertical scale bar = 1,000  $\mu\text{m}$ . Total slices = 1099.

All projected X-ray shadow images from scanned samples were successfully processed qualitatively and quantitatively. Qualitative results were obtained from volume rendering

using CTvox software. Typical software processing route for fluid bed dried sucrose illustrates the intermediate results from the methodology involved (Figure 6.1).

### 6.3.3.1 Porosity correlation study 1 (Bulk dried mannitol powders 1)

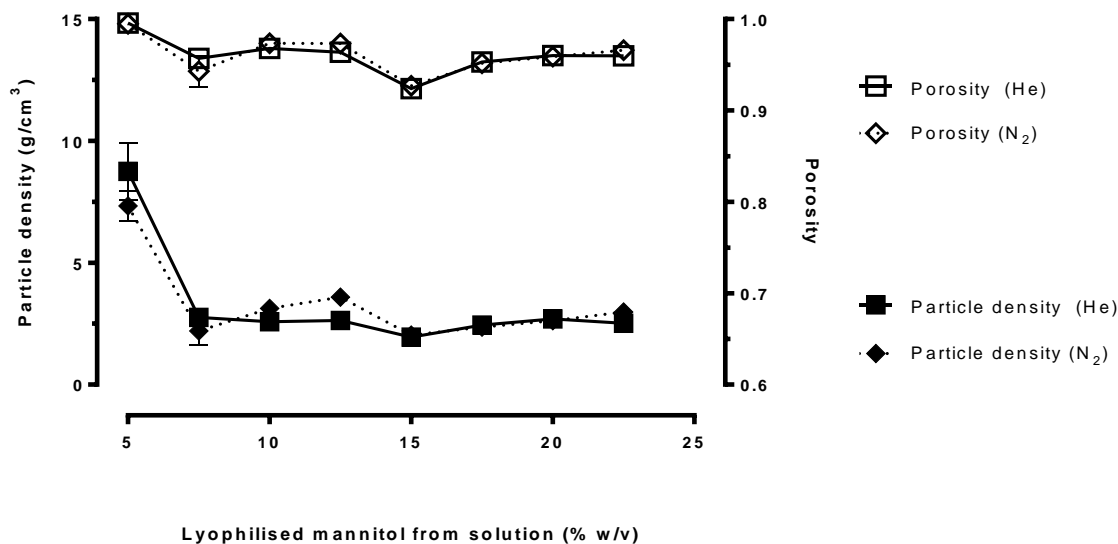


**Figure 6.2: Porosity and particle density of lyophilised mannitol using helium (He) and nitrogen (N<sub>2</sub>) as pycnometric gases (n = 3).**

The use of either helium or nitrogen as inert gas for pycnometric analysis showed no significant differences in measured porosity and calculated particle density (Figure 6.2).

Initial correlation studies comparing helium pycnometry and MCT did not demonstrate any statistically significant correlation (Figure 6.4). MCT measurements were significantly different and lower in value in comparison with pycnometric data (Figure 6.4). While pycnometry measurements showed no significant changes in porosity with increasing mannitol concentration in freeze dried powders from 7.5%-22.5 %w/v; an unexpected increase was observed from MCT measurements from 7.5%-17.5 %w/v suggesting disagreement between the two techniques.

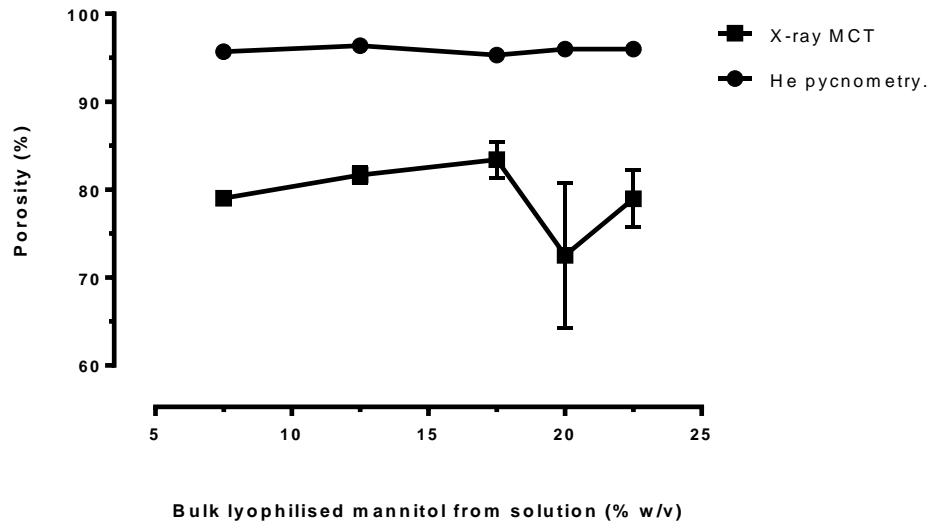


Figure 6.3: Porosity of bulk lyophilised mannitol from solution using X-ray MCT (n = 3, sample volume in volume of interest =  $2.5\text{-}2.59 \times 10^3 \mu\text{m}^3$  and Helium pycnometry (n = 3, sample volume =  $3.9\text{-}4.2 \text{ cm}^3$ ). Samples were tapped gently 3-5 times before measurements.

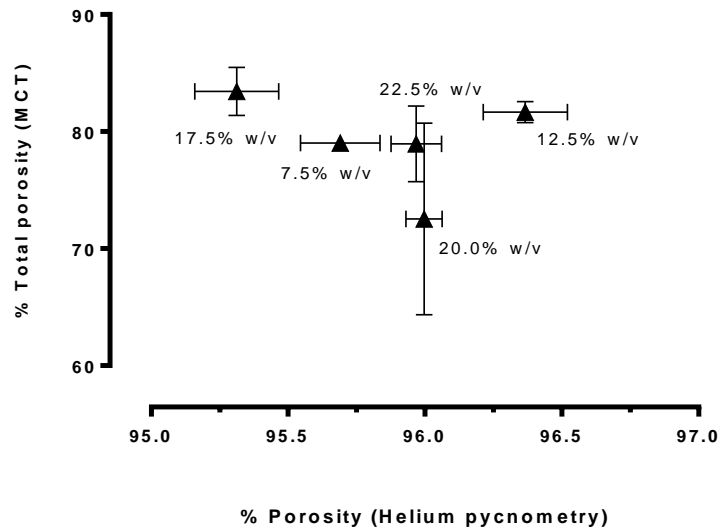
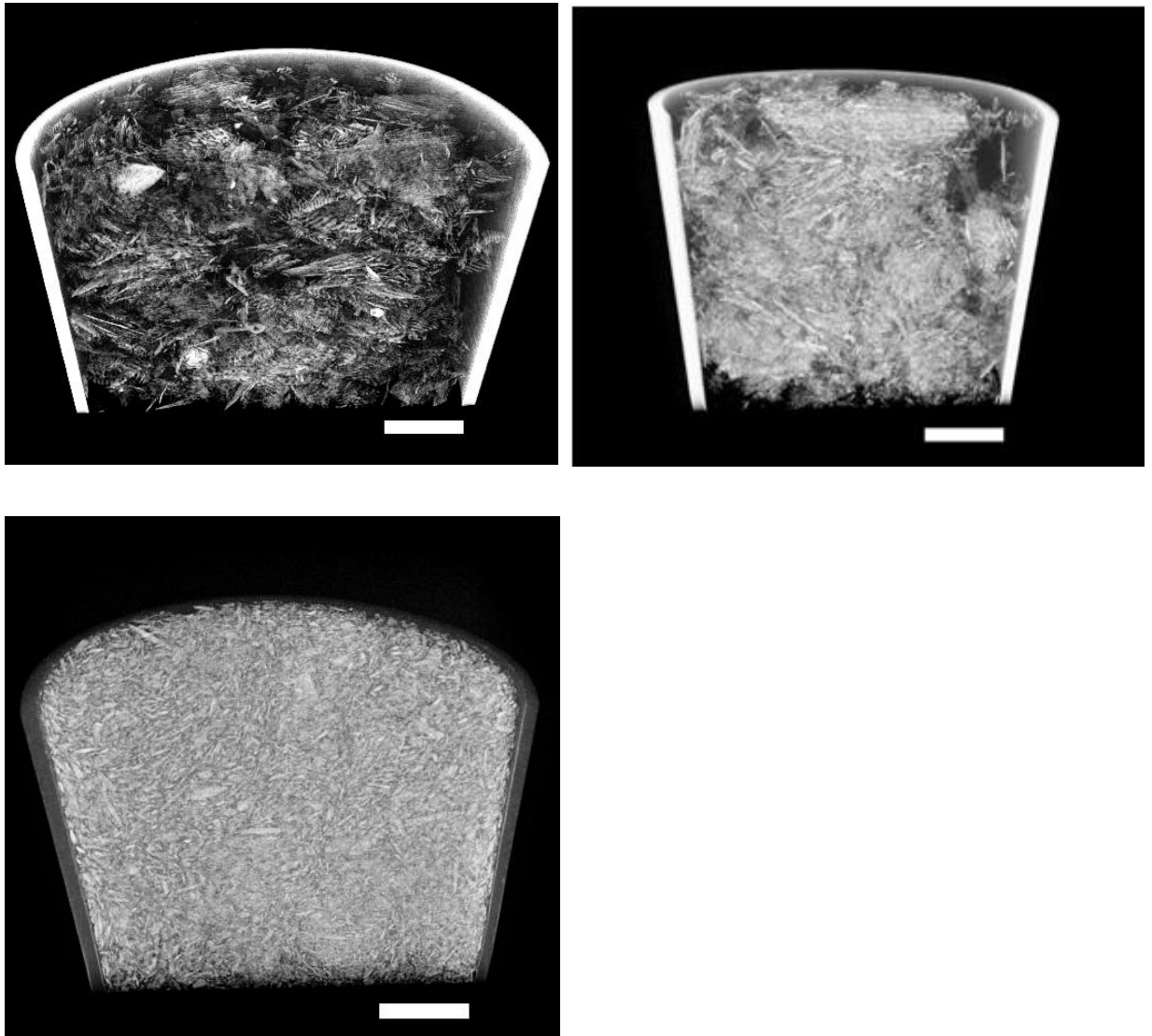


Figure 6.4: Porosity correlation study 1. Correlative plot of helium pycnometry and X-ray microcomputer tomography (MCT) porosity measurements for powders from bulk lyophilised mannitol (n = 3). Mannitol samples were lyophilised from 7.5-22.5 %w/v mannitol solutions.  $R^2$  of linear trend line = 0.0918.

### 6.3.3.2 Powder packing study 1



**Figure 6.5: Three dimensional cross-sectional X-ray MCT into packed powders. Mannitol bulk lyophilised from Top left: 1 %w/v solution and Top right: 15 %w/v solution. Bottom: Fluid bed dried mannitol powder. Scale bar: 1.25 mm.**

Preliminary studies from MCT provided a qualitative assessment of powder packing arrangement. The differences in packing were distinct between the low and high solute content formulations (Figure 6.5). Mannitol bulk lyophilised from an initial 1 %w/v solution was the least densely packed with more air pockets (more aerated) or inter particle packing porosity. Fluid bed dried mannitol showed the most dense packing with the least

inter particulate porosity. These observed trends correlate with pycnometric measurements (See Table 6.1). Volumetric bulk density measurements increased with initial mannitol solute content and inversely with calculated pycnometric true density measurements (See Table 6.1). The true density of fluid bed dried mannitol was therefore expectedly the highest; an expectation for bulk solids with high bulk densities.

**Table 6.1: Bulk and true density measurements of bulk lyophilised mannitol by helium pycnometry in powder packing study 1 (n = 3).**

<b>Bulk freeze dried mannitol</b>				<b>Fluid bed dried</b>
<b>Batch (%w/v)*</b>	<b>1%</b>	<b>5%</b>	<b>15%</b>	
<b>Bulk density (g/cm<sup>3</sup>)</b>	0.030	0.030	0.087	0.455
<b>Standard Deviation (n = 3)</b>	0.00	0.00	0.01	0.02
<b>True density (g/cm<sup>3</sup>)</b>	9.235	4.524	2.275	1.732
<b>Standard Deviation (n = 3)</b>	0.11	1.18	0.09	0.02

\* Expressed batch concentration refers to initial mannitol solute concentration in solution before bulk freeze drying.

### 6.3.3.3 Powder packing study 2

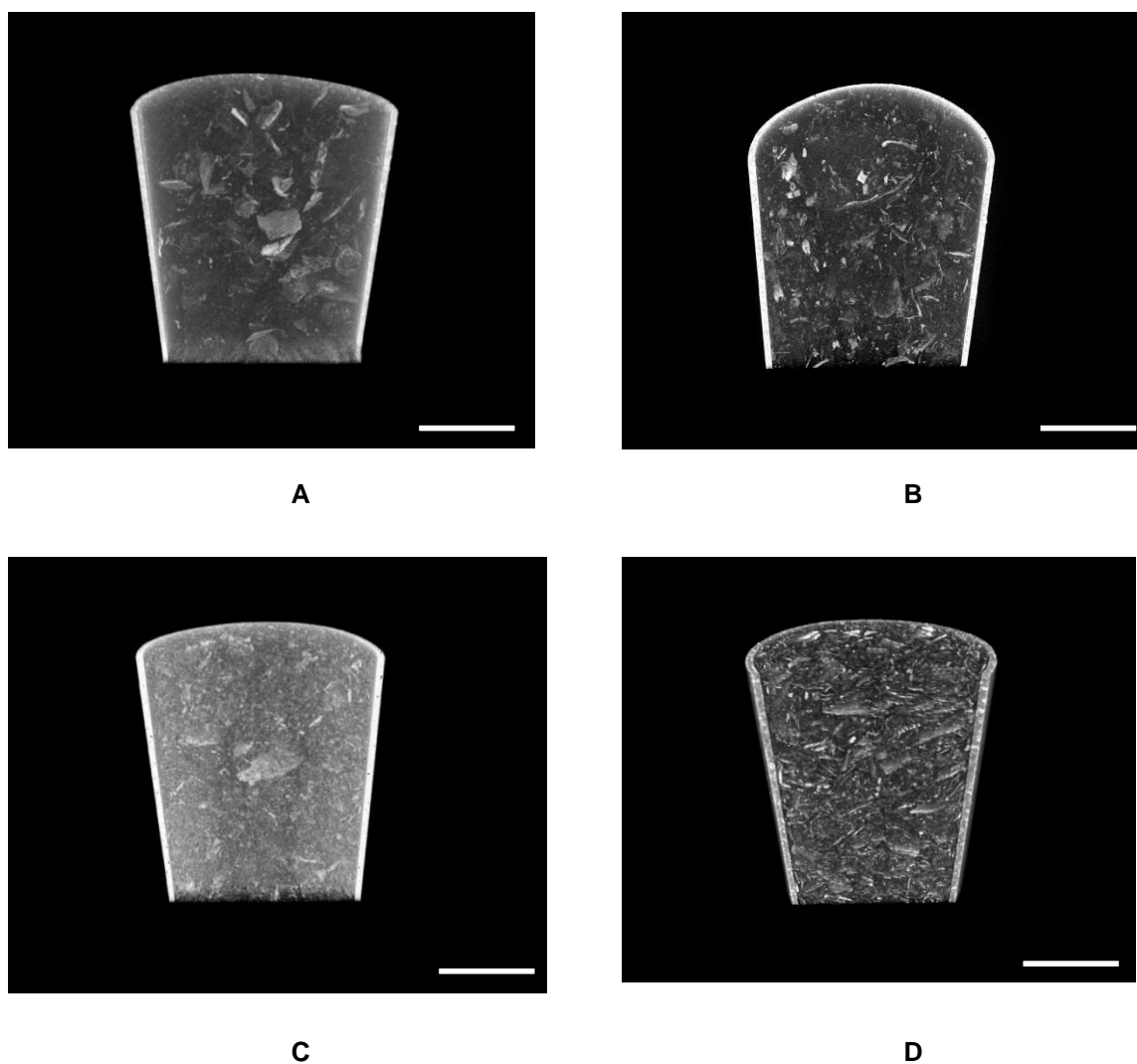


**Figure 6.6:** Three dimensional cross-sectional X-ray MCT images of mannitol lyophilised from solutions of A) 0.056 M B) 0.25 M C) 0.5 M D) 1 M. Samples were cooled at 0.2 °C/min and annealed at -25°C. Scale bar is 2.5 mm. Powder volume was less than 1 mL.

Qualitative three dimensional models of a powdered formulation reconstructed using projected X-ray shadow images can inform differences in packing as earlier observed in (Powder packing study 1). Relevance of this parameter to powder handling and hence flowability is discussed later in this chapter. Differences in packing and bulk density were observed to correlate with increasing solute concentration of mannitol within minute powder

volumes of less than 1 cm<sup>3</sup>. Increasing concentrations from 0.056 M-1 M showed increasing bulk densities which were observed as more solid prominent structures with minimum aeration or air pockets. Fu *et al.* (2006) found particle packing studied using discrete element method (DEM) simulation and MCT to be in agreement but work was restricted to the use of glass beads and micro crystalline cellulose spheres.

### 6.3.3.4 Porosity correlation study 2

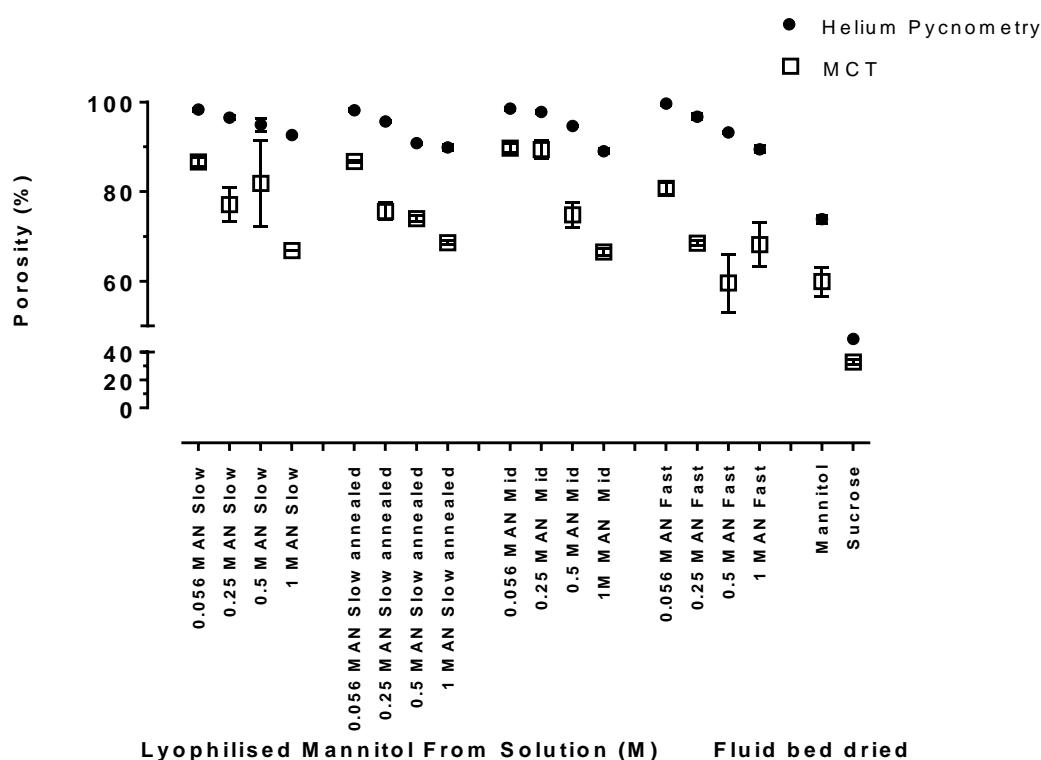
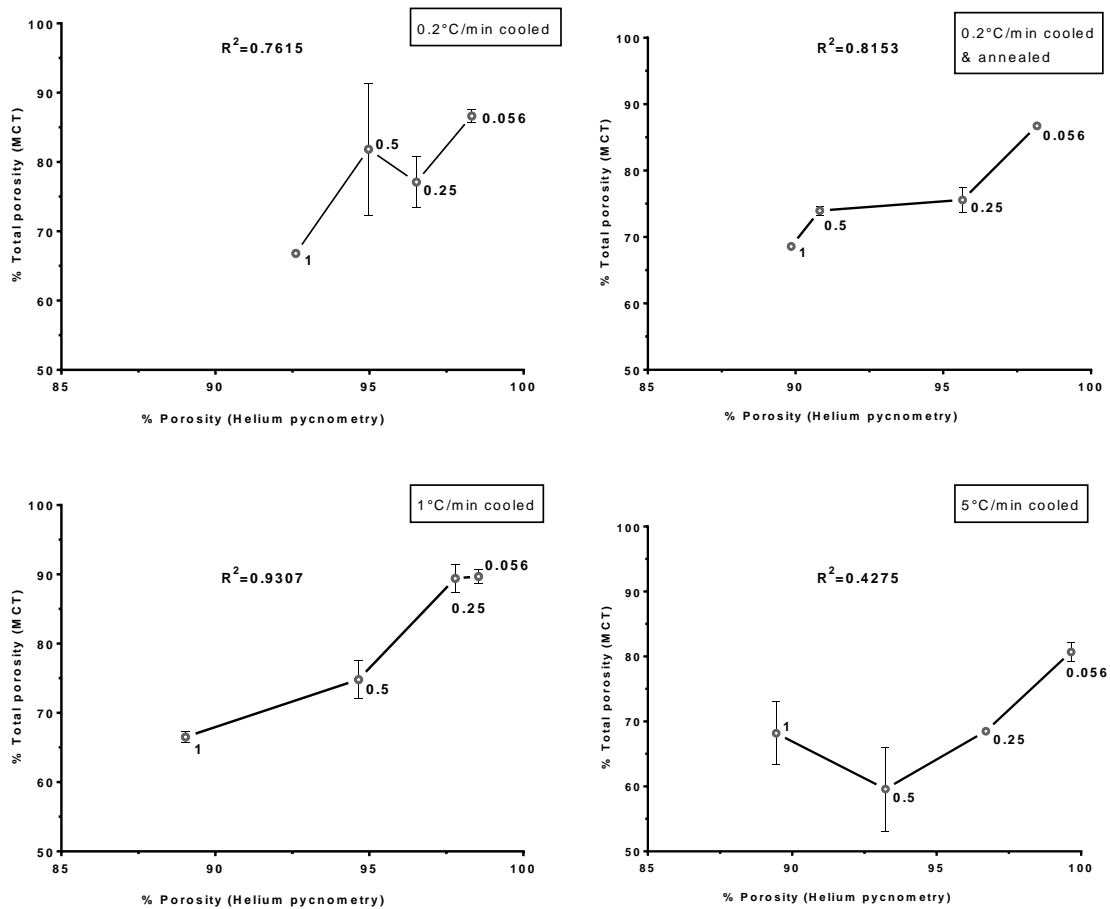


Figure 6.7: Helium pycnometry and X-ray MCT computer tomography porosity measurements for powders from bulk lyophilised mannitol (mean  $\pm$  SD, n = 3). Mannitol was lyophilised from 0.056-1 M mannitol solutions at different cooling rates with or without thermal treatment (annealing) during freezing. Slow: cooled at 0.2 °C/min Annealed: cooled at 0.2 °C/min and held at -25°C (2hrs). Mid: cooled at 1 °C/min. Fast: cooled at 5 °C/min. Samples were tapped 100 times on the laboratory bench prior to measurements.

MCT and pycnometry was repeated in this second study with changes in sample methodology. Here samples were tapped on the bench 100 times from a height of about 2 cm for powder packing repeatability across all samples. An expected trend of decreasing porosity with increasing solute content was observed within all formulations using either helium pycnometry or MCT techniques (Figure 6.7). From reviewing data from MCT across all formulations, it was evident that relatively larger standard deviations were derived compared to helium pycnometry. These resulted in a range of small to large linear patterns of associations informed by regression analysis from calculated correlation squared values. Squared regression constants were 0.4275, 0.7715, 0.8153 and 0.9307 for the various powders analysed (Figure 6.8). The observed correlation is however convincingly strong to demonstrate correlation between the results from both gas pycnometric and MCT techniques.



**Figure 6.8: Porosity correlation study 2. Correlative plot of helium pycnometry and X-ray MCT porosity measurements for powders from bulk lyophilised mannitol (mean  $\pm$  SD, n = 3). Numbers adjacent data points represent concentration of mannitol (M) in solution. Mannitol was lyophilised from 0.056-1 M mannitol solutions at different cooling rates with or without thermal treatment (annealing) during freezing. Slow = 0.2 °C/min. Annealed = 0.2 °C/min and annealed at -25°C. Mid = 1 °C/min. Fast = 5 °C/min. Samples were tapped 100 times on the laboratory bench prior to measurements.**

### 6.3.3.5 Morphology parameters

#### 6.3.3.5.1 Size correlation study

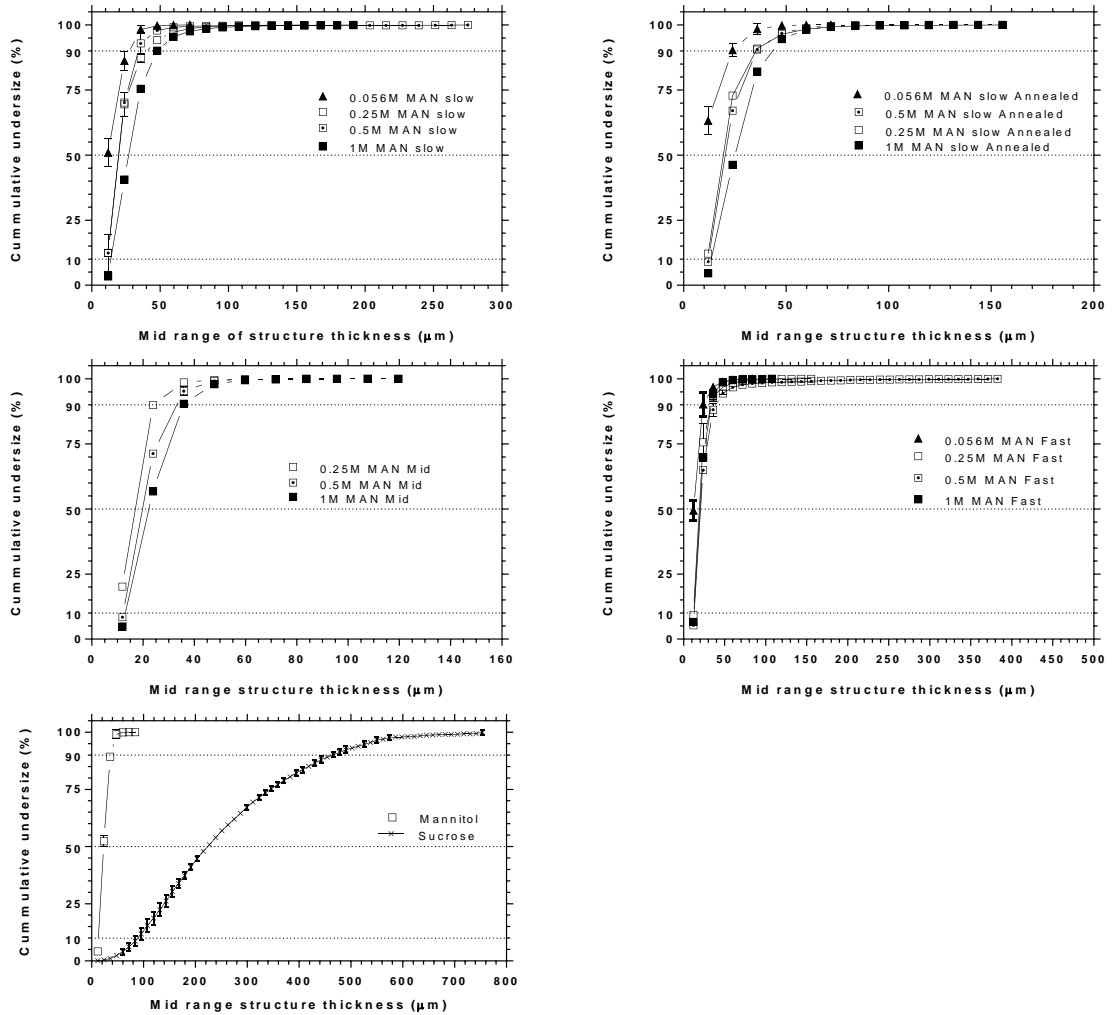


Figure 6.9: Cumulative undersize distribution using structure thickness parameter from MCT (n = 3). Mannitol was lyophilised from 0.056-1 M mannitol solutions at different cooling rates with or without thermal treatment (annealing) during freezing. Slow = 0.2 °C/min. Annealed = 0.2 °C/min and annealed at -25°C. Mid = 1 °C/min. Fast = 5 °C/min. Samples were tapped 100 times on the laboratory bench prior to measurements.

**Table 6.2: Median over size distribution of powder measured from analytical sieving and MCT. Samples differ in cooling rate during freeze drying. Slow = 0.2 °C/min. Annealed = 0.2 °C/min and annealed at -25°C. Mid = 1 °C/min. Fast = 5 °C/min. Samples were tapped 100 times on the laboratory bench prior to measurements.**

Batch (Concentration*)	Median Size	
	Sieve (Mesh size)	MCT (Structural thickness)
<b>Annealed batch</b>		
0.056 M	190	20
0.25 M	90	32
0.5 M	100	34
1 M	180	36.7
<b>Slow batch</b>		
0.056 M	120	25
0.25 M	100	30
0.5 M	140	30
1 M	210	40
<b>Mid batch</b>		
0.056 M	240	-
0.25 M	150	30
0.5 M	150	32.25
1 M	100	35
<b>Fast batch</b>		
0.056 M	-	25
0.25 M	100	30
0.5 M	80	30
1 M	60	30

\* Mannitol was lyophilised from 0.056-1 M mannitol solutions at different cooling rates with or without thermal treatment (annealing) during freezing.

Median particle structural thickness ranged from 20-40 µm for powders analysed (Figure 6.9 and Table 6.2). Particular trends observed were an apparent increase in median volume thickness with increasing concentration of mannitol in initial freeze dried formulation.

### 6.3.3.5.2 Structural model index

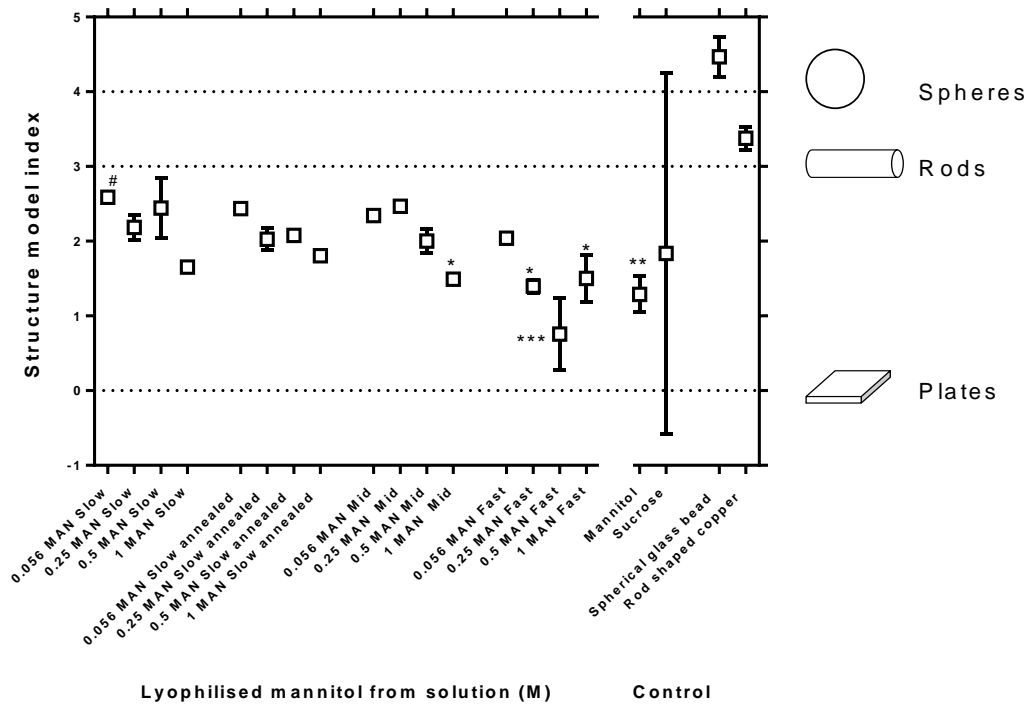


Figure 6.10: Structural model index (SMI) investigations into effect of cooling rate and annealing on the morphology of lyophilised mannitol (MAN) powder. Samples were cooled at different rates. Slow = cooling rate of 0.2 °C/min Mid = cooling rate of 1 °C/min. Fast = cooling rate of 5 °C/min. CCD camera resolution of 6 microns was used. Schematic shapes to the right of main figure correspond to expected values for an ideal sphere, rod and plate. # represents significance from 0.5 MAN Fast ( $p < 0.05$ , one way ANOVA  $n = 3$ ). Significance from rod shaped copper (one way ANOVA  $n = 3$ ) are depicted by \*  $p < 0.05$ , \*\*  $p < 0.001$  and \*\*\*  $p < 0.0001$ . Tukey's multiple test used to compare means.

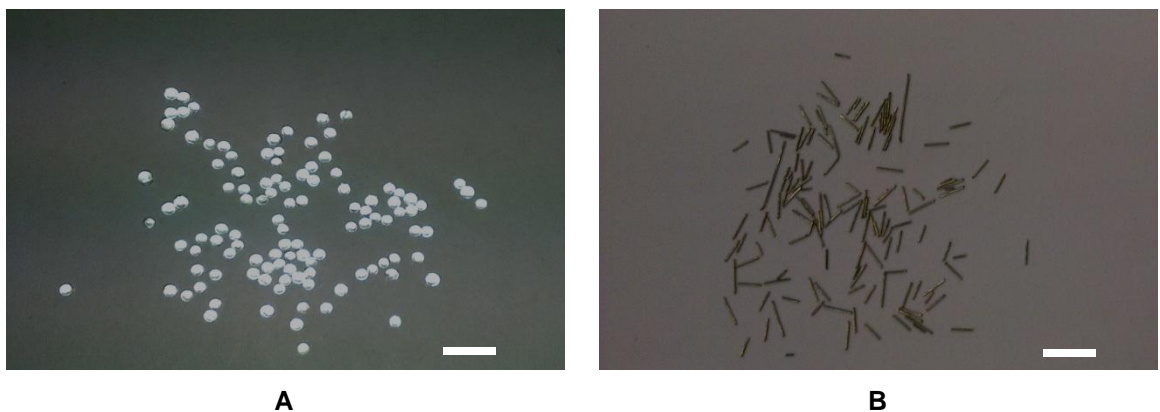
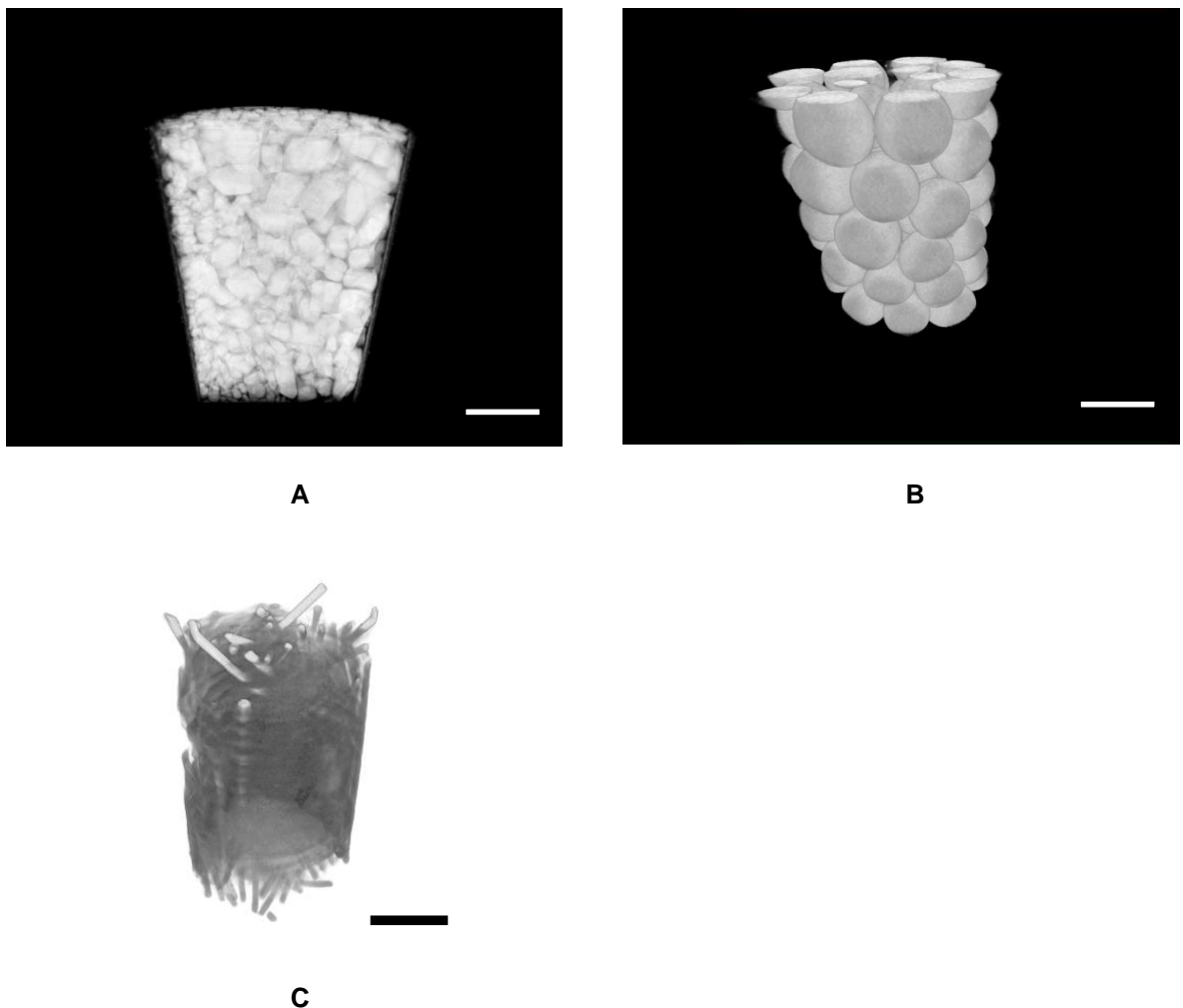
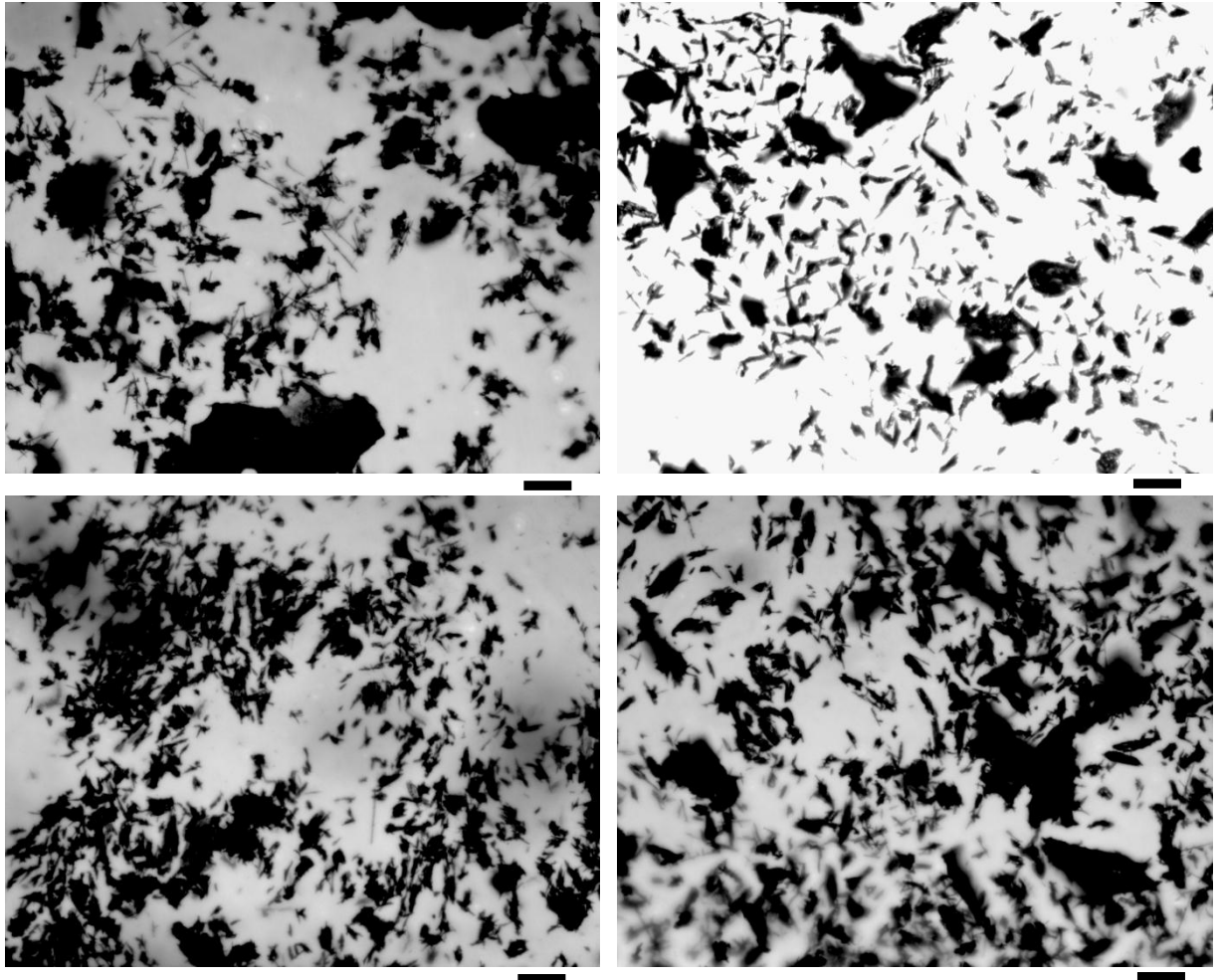


Figure 6.11: Picture of standard shapes used in structural model index morphometric parameter in MCT studies A) spherical glass beads B) rod shaped copper wires. Volume of interest analysed was limited to the protruding rods only. Scale bars = 5 mm.

Structure model index parameter from MCT technique was useful in determining the closeness of individual particulate shapes within formulation powders to known spherical, rod and plate like morphologies. Ideal spheres, rods and plates have SMI values of 4, 3 or 0 respectively dependent on the most dominant shape (Hildebrand and Rügsegger, 1997b). These reference values were in agreement with control samples used in the study. Copper rods and spherical glass beads were used as standard control morphologies for sphere and rods (Figure 6.11 and Figure 6.12 B&C).



**Figure 6.12: Three dimension X-ray tomography models of A) fluid bed dried sucrose B) spherical glass spheres C) Rod shaped copper wires. Volume of interest analysed was limited to the protruding rods only. Scale bars = 2.5 mm.**



**Figure 6.13: Light microscope images at x100 magnification for powders freeze dried from mannitol solutions of Top Left: 0.5 M (cooled at 0.2 °C/min, Slow). Top Right: 0.5 M (cooled at 1 °C/min, mid). Bottom Left: 0.5 M (cooled at 0.2 °C/min, Annealed) and Bottom Right: 0.5 M (cooled at 5 °C/min, fast). Scale bar = 20  $\mu$ m**

Light microscopy images showed flaky (plate like) and elongated needle like morphologies present in all powders (Figure 6.13).

### 6.3.3.5.3 Fragmentation Index

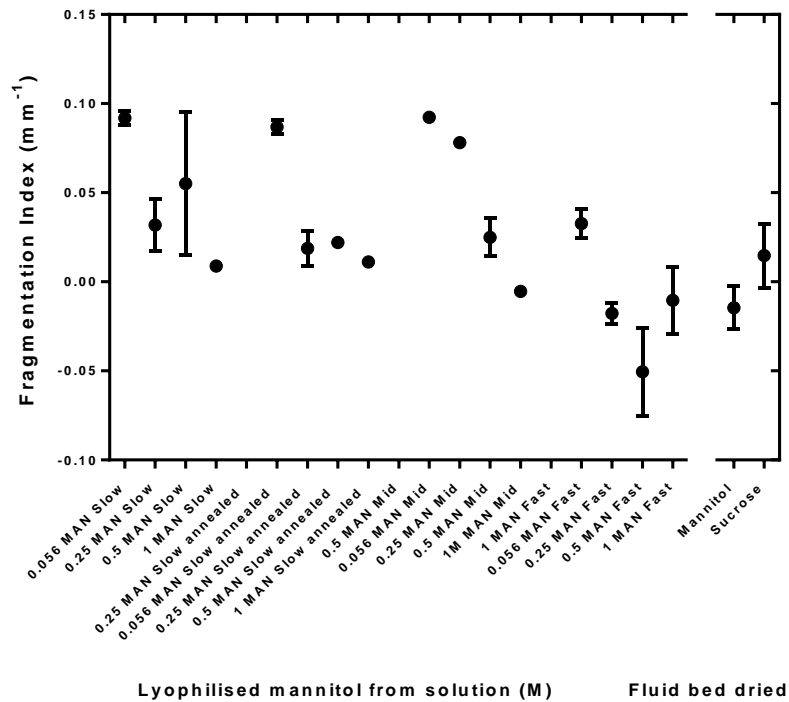


Figure 6.14: Fragmentation index investigation (n = 3) into effect of cooling rate and annealing on fragmentation index of lyophilised mannitol (MAN) powder. Slow = cooling rate of 0.2 °C/min Mid = cooling rate of 1 °C/min. Fast = cooling rate of 5 °C/min. CCD camera resolution of 6 microns.

Fragmentation index is a relative measure of connectivity within compared materials (Hahn *et al.*, 1992) and lower values are representative of better connectivity. Negative values are indicative of the presence of many enclosed cavities and concave surfaces. The trend observed is similar to that seen in SMI due to the similarities in parameter mathematical derivations. Generally, an increased connectedness was observed to correlate positively with increasing mannitol concentration in initial freeze dried formulations.

#### 6.3.3.5.4 Fractal dimension

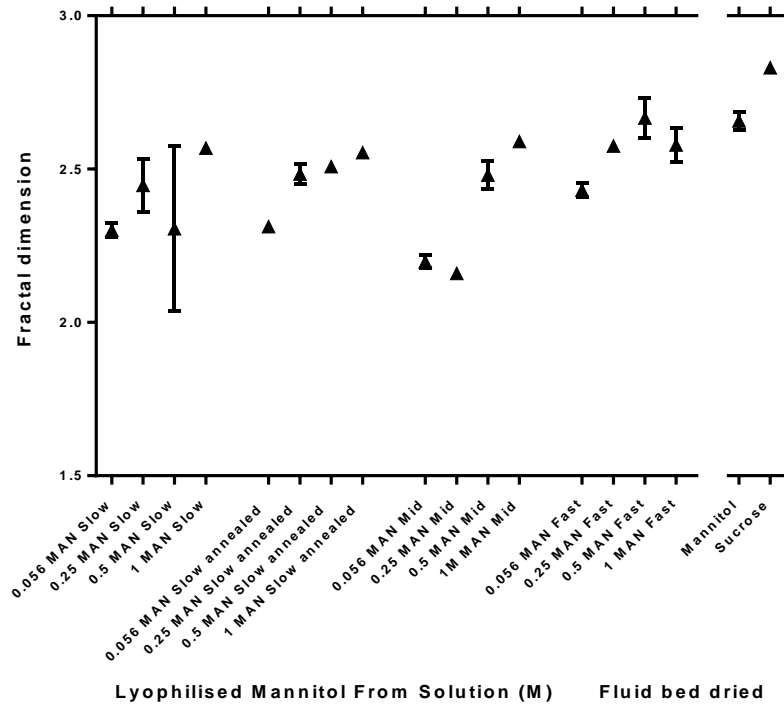


Figure 6.15: X-ray microcomputer tomographic investigation into effect of freezing rate and annealing on fractal dimension of lyophilised mannitol (MAN) powder (n = 3). Slow = cooling rate of 0.2 °C/min. Mid = cooling rate of 1°C/min. Fast = cooling rate of 5°C/min. CCD camera resolution of 6 microns.

Fractal dimension quantifies how an object's surface fills a given space and indicates how complex its surface is (Chappard *et al.*, 2001, Skyscan, 2011). The results show an increase in fractal dimension of freeze dried mannitol in the volume of interest with increasing solute content.

#### 6.3.4 Discussion

Powder particles can be in the form of ideal or irregular shapes. Defining the dimensions of irregular particle can be challenging compared to that for those with closeness to ideal rod or spherical shapes. The influence of particle shape on its size distribution determination has therefore seen the definition of various equivalent diameters which require fitting or relating a particle to an equivalent diameter, volume or surface area of a sphere (Randall, 1995, Washington, 1992). For example, a particle with a fixed volume can be described by either a representative sphere of the same volume or one with the same surface area (Washington, 1992).

The various measurement techniques will generally adapt a size characterisation approach and here we discuss the parameter 'structure thickness' of particles derived from 3D images. Structure thickness estimation from 3D image analysis is a volume based approach which unlike surface based approaches will not overestimate the thickness of particles of irregular or non-ideal structures (Hildebrand and Rügsegger, 1997a). The model is based on the fitting of maximal spheres to particles where they are within the boundaries of the solid surface without assumptions of the type or shape of the structure in question (Skyscan, 2011, Hildebrand and Rügsegger, 1997a).

The SMI parameter is reflective of the ratio of any one of the recognisable shapes within a 3D image based on the volume ratios present in the structure or VOI analysed. Meaning an equal volume of rods and plates will yield a value of 1.5 which is 50% between 3 (100% rods) and 0 (100% plates) (Hildebrand and Rügsegger, 1997b). The results (Figure 6.10) showed a trend of more rod-like morphology for lyophilised particles at low mannitol concentrations and a trend which declined as concentration increased to show greater plate morphologies. This trend without statistical significance appeared more prominent with

increasing cooling rate from slow (0.2 °C/min) to fast (5 °C/min). This was confirmed by the significant difference from rod-like morphology observed at  $p < 0.05$  and  $p < 0.0001$  for powders from fast cooled solutions of 0.25 M-1 M mannitol (Figure 6.10). Fluid bed dried sucrose showed a wide standard deviation across plate, rod and sphere morphologies suggesting there were a variety of shapes present. Negative SMI values inform the presence of more enclosed and concave surfaces (Skyscan, 2011). Optical microscope images showed irregular particle shapes showing plate like (Flaky), elongated, needle like or rod like shapes which was in agreement with SMI parameters (Figure 6.10 and Figure 6.13).

Values calculated for SMI are independent of dimension and Hildebrand and Rügsegger (1997b) found the presence of both plates and rods of equal thickness within a 3D structure to have SMI values between 0 and 3.

Particle morphology is known to influence powder flow behaviour. Irregular particle shapes will cause mechanical interlocking which will impede powder flow.

Calculated SMI parameter allows particulates with sphere, rod and plates shapes to be distinguished (Figure 6.10). There was a good correlation in the observed particle morphology from microscopy and calculated SMI values obtained from 3D image analysis (Figure 6.6). The presence of elongated or rod like morphologies within a given test sample was found not to be statistically different from rod shaped copper wires used as a morphology standard. Hildebrand and Rügsegger (1997b) found minute differences between SMI values to be consistent with 3D images and were adequate at differentiating between either rod like or plate like morphology. For example SMI values of 2.06, 1.65 and 1.05 were found to be consistent with decreasing presence of rods in iliac crest bone biopsies.

Similar mannitol morphologies observed in our study have been reported (Kaialy and Nokhodchi, 2013, Armstrong, 2009a). Kaialy and Nokhodchi (2013) using optical microscopy in combination with a calculated aspect ratio. They found freeze dried mannitol from 5 %w/v solution had the most irregular and elongated shapes compared to commercial and spray dried forms. This was confirmed using SEM and it was emphasised elongated morphology made freeze dried mannitol good carriers for pulmonary delivery. In their study, aspect ratio was obtained from a ratio of particle length to breadth. When crystallised from alcohol, mannitol has been reported to have a morphology described as orthorhombic needles (Armstrong, 2009a).

Hildebrand and Rügsegger (1997b) used SMI to study the presence of rods and plates in osteoporosis where the presence of more rods was a measure of deteriorating disease. This was calculated from the equation:

$$SMI = 6 \left( \frac{S' \times V}{S^2} \right) \quad (6.1)$$

**Equation 6.1: Where SMI is calculated from the surface area (S) of a binarised image with a known volume (V) and a resulting change in surface area (S') after addition of one voxel thickness in a process known as voxel dilation. The surface area and volume were obtained by calculating the total area of triangles that fitted on object surfaces; a process known as surface triangulation.**

Fragmentation index was calculated within the CT analyser software as a ratio of the change in solid surface ( $S_1 - S_2$ ) to change in volume ( $V_1 - V_2$ ) before and after image dilation (Hahn *et al.*, 1992) :

$$Fragmentation\ index = \left( \frac{S_1 - S_2}{V_1 - V_2} \right) \quad (6.2)$$

For powders the parameter was evaluated after compaction by a fixed 100 taps from a height of about 2-5 cm on a laboratory bench. Bulk solids or powders with a low bulk density would be more aerated (have more entrapped air) and particles would show less connectivity. Increased bulk density within a powder bed previously seen in freeze dried powders, result in more connected packing. One would expect powders that show more connectivity to be less compressible as lesser amounts of voids are available for rearrangement in the powder bed. This parameter can therefore be used as an indirect measure of powder's susceptibility to be compacted which in turn can be related to its flow behaviour. Materials which remain relatively less connected after consolidation (fixed number of taps) would be expected to have poorer flowing behaviour. This analogy is similar to that achieved with standard powder tap density experiments except here, the powder's endpoint is not necessarily realised making this approach useful for relative comparisons only. The endpoint in tapped density is said to have been reached when no change in volume is observed with further powder tapping. In standard pharmacopeia volumetric methods this is a change of no more than 2 cm<sup>3</sup> as previously discussed (British Pharmacopoeia Commission, 2013a). While the relative values serve the purpose of comparing scanned objects, its absolute values have little meaning (Skyscan, 2011). Nonetheless powders scanned using the same acquisition modes and sample preparation can be evaluated.

The results from fragmentation index parameter (Figure 6.14) reinforced corresponding porosity data of the same samples (Figure 6.7). The more porous powders were found to be less connected as expected. Parker *et al.* (2010) found connectivity deduced from fragmentation index to agree with SEM. Vial lyophilised BSA cakes which showed 45% porosity and -0.07 fragmentation index had more connected SEM images compared to cakes with 70% porosity and a fragmentation index of 0.01. We here use this parameter with the analogy that similar powders should pack to the same extent.

An alternative approach involving the use of porosity to predict flow was reported by Guerin *et al.* (1999) using an indirect pycnometric approach. The study used the inflections recorded in porograms obtained from mercury extrusion porosity characterisation technique. Guerin and co-workers found flowability to correlate to tap density and some shear cell measurements using 250 mg samples of lactose grades, analgesic and beta blocker powders. Here we show the use of sample sizes of less than 1 mL to predict flow, unlike mercury porosimetry MCT is neither destructive nor involves the use of toxic mercury.

The results for fractal dimension (Figure 6.15) suggested a relationship between the surface complexities of freeze dried powder volumes and increasing concentration of solute. Fractal dimension was found to increase with increasing mannitol concentration. The trend was therefore consistent with the concentration dependence of freeze dried powder flow. An object is fractal if its size when determined using a measured scale displays more detail than when it is measured at higher magnifications (Washington, 1992). Meaning the higher resolution offered by MCT allowed the characterisation of freeze dried powders to reveal an increased surface area. Washington (1992) suggested particles with rough surfaces occupy large volumes and have fractal dimensions of between 2 and 3. A correlation between increased surface area and surface complexity of freeze dried powders was present. CT-analyser software calculated the fractal dimension using a box counting method also known as the Kolmogorov method (Skyscan, 2011). It involved a set of cubes of similar dimensions being overlaid on the volume of interest and the number of cubes encapsulating parts of the powder surface was counted. The fractal dimension was given by the slope of the logarithmic plot of cube number versus cube length.

### **6.3.5 Conclusion**

X-ray microcomputer tomography has been demonstrated as a useful non-destructive tool for characterising bulk freeze dried powders.

Comparison of the porosity results with traditional gas pycnometry showed a strong correlation (Section 6.3.3.4). The use of a fixed number of powder taps about 2-5cm off the bench (100) for uniformity across samples was recommended.

Differences in powder packing of freeze dried powders can be ascertained with sample volumes of less than 1 mL (Section 6.3.3.3). Powder sample used must be representative of the powder stock or batch due to the minute volumes required. Packing and powder porosity have been illustrated as indirect measures for powder flowability (Section 6.3.4).

Morphometric parameters such as size, structural model index, fragmentation index and fractal dimension were useful tools for the relative prediction of flow for freeze dried powders (Section 6.3.3.5). The SMI index provided knowledge of freeze dried particulate shapes but results were restricted to comparison with plate, rod or spherical shapes.

The differences in sample size and methodology did not allow direct extrapolation of sieving data to MCT structural thickness. However, MCT was demonstrated capable of distinguishing between various freeze dried powders which were distinctly different in size to those of equivalent fluid bed dried powders.

## **6.4 INVESTIGATIONS INTO LOCALISATION OF ACTIVE PHARMACEUTICALS IN LYOPHILISED FORMULATIONS**

### **6.4.1 Background**

Content uniformity was earlier studied in chapter 5 for machine dosed formulations from bulk into vials. It was important to have target doses within pharmacopeia acceptance limits to satisfy regulatory approval requirements. The dosing from bulk approach was demonstrated feasible and practical as a result of good content uniformity demonstrated in cases.

An active pharmaceutical ingredient (API) is distributed throughout a formulation during drying and localisation in particular parts of the dried cake may occur depending on the freezing condition used. Localisation of API should therefore be important to scientists looking to adopt bulk drying from fill to finish into container closures. This would typically not be of concern where dried formulations were vial dried and required only reconstitution just before administration.

The use of different freezing rates is known to affect API location in segments of formulation due to induced freeze concentration and phase separation that may have occurred dependent on constituents. This had in the past been demonstrated using destructive techniques which were often chemical assays.

How ice nucleates in a formulation during freezing is important for many reasons. It is responsible for batch to batch variation as it directly affects the size and number of ice crystals formed. Ice crystals grow to different extents after sublimation and leave behind pores. Qualitative analyses of these pores have reported different resulting morphologies in literature. These studies were however not holistic as they used either qualitative two dimensional images limited to small sections of an entire formulation or parts of the dried cake were sectioned using razors and assayed after reconstitution.

Here a mannitol-platinum dispersion model was used as a model to study API localisation. The relationship between API localisation and cooling rate were within complete or whole formulations from top to bottom using three dimensional image analyses.

## **6.4.2 Materials and Methods**

### **6.4.2.1 Materials**

Fluid bed dried D-mannitol Ph. Eur. was purchased from Fagron, UK. Fluid bed dried sucrose BP, platinum powder, analytical grade Glycerol was from Fischer Scientific, UK. Sealing film (Parafilm™), aluminium foil and CombiCoulomat fritless Karl Fischer reagent obtained from VWR, UK. Dental beading wax was from Kemdent, UK. Drying straws were obtained from Macdonalds, UK. Transparent dual cartridges epoxy adhesive and extra flexible single core copper wire RS356-173 were obtained from RS components, UK.

### **6.4.2.2 Optimisation of platinum model**

Platinum powder of 17.7 mg and 56.15 mg were weighed and vortexed for 10 minutes in 25 mL of 10 %w/w mannitol (0.71 mg/mL, Dispersion A) and 31.72 %v/v glycerol (2.25 mg/mL, Dispersion B). Another weighed 7.12 mg and was bath sonicated for 24 hours in 25 mL of 1 M Mannitol (0.29 mg/mL, Dispersion C). Platinum (7.12 mg) was dispersed in 25 mL of 1 M mannitol (0.29 mg/mL, Dispersion D) and 42.44 mg in 50 mL of 1 M mannitol (0.85 mg/mL, Dispersion E). These were probe sonicated at 5 KHz for 60 minutes at 10 minute intervals. Aliquots (3 mL) of dispersions A, B and C were transferred into cuvettes and absorbance measured at 500 nm over 30-120 minutes. Dispersion D and E were left on the bench for 60 minutes and supernatant collected for UV analysis. Supernatant and sediments from dispersion E were mixed and vortexed for a minute. The supernatant was collected after an hour of being undisturbed on the bench. An aliquot (3 mL) was transferred in a cuvette and

analysed. The dispersion or supernatant showing a steady rate of change in absorbance over at least 30 minutes was deemed satisfactory and used for lyophilisation experiment.

#### 6.4.2.2.1 Lyophilisation in straws and preparation of epoxy control

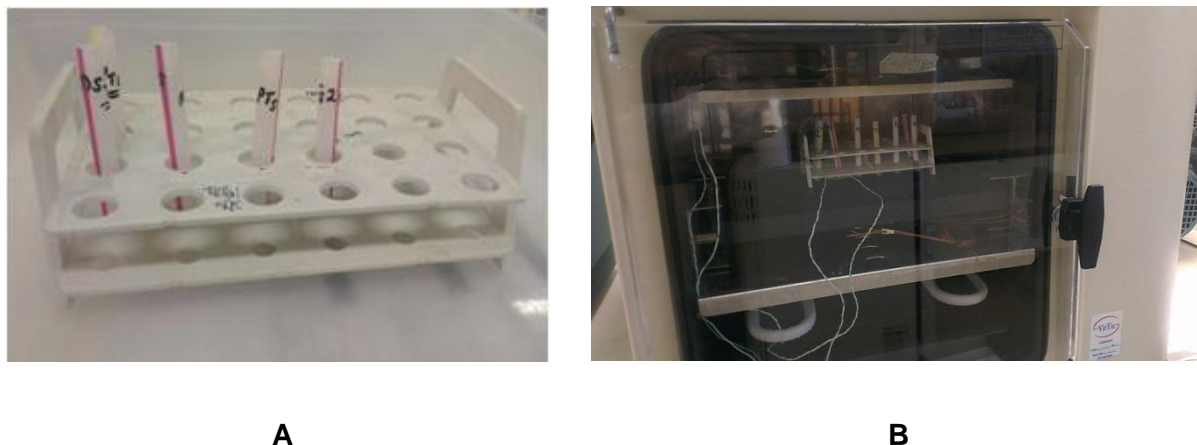


**Figure 6.16: Experimental set up for lyophilisation of optimised 1 M mannitol platinum dispersions filled into straws and supported in A: tube rack placed on a B: Virtis advantage shelf to dry. Product temperature was monitored using K type thermocouples temperature in representative samples.**

Straw samples were chilled to  $-55^{\circ}\text{C}$  ( $0.2^{\circ}\text{C}/\text{min}$  and  $1.5^{\circ}\text{C}/\text{min}$ ) and held for 6 hours. Samples requiring fast cooling were covered in aluminium foil and quench cooled in liquid nitrogen. Foil jackets were removed and samples were transferred onto precooled  $-55^{\circ}\text{C}$  shelf. Primary drying was at  $-10^{\circ}\text{C}$  for 22 hours. Secondary drying was at  $20^{\circ}\text{C}$  for 4 hours with a constant  $-80^{\circ}\text{C}$  condenser and pressure at  $200\ \mu\text{bar}$ . K type thermocouples were used to monitor product temperature during the drying process.

Freeze drying straws were sealed at the base with Sealing film (Parafilm™) and checked for any leakage. Freeze drying of mannitol ( $700\ \mu\text{L}$ , 1 M) at a fill height of 1.97 cm was filled into bottom sealed straws and freeze dried in a Virtis Advantage bench freeze dryer (Figure 6.16).

#### **6.4.2.2.2 *Sample preparation of platinum in epoxy***

700  $\mu\text{L}$  of the optimised 1 M mannitol platinum dispersion in a freeze drying straw was sealed and left to settle over 24hours. The supernatant was discarded and filled to its initial volume with transparent epoxy adhesive. This was stirred with a micro spatula and allowed to set for X-ray scanning.

#### **6.4.2.2.3 *X-ray scanning and image processing***

Sample scanning and image reconstruction were performed as previously described in materials and methods (Section 3.4.12.2). 59 kV X-ray source voltage and 122  $\mu\text{A}$  current at a scanning resolution of 3.94  $\mu\text{m}$  were used. Stage was rotated stepwise at  $0.7^\circ$  with 4 frame image averaging in combination with a 0.5 mm aluminium filter was used. Images were reconstructed using Nrecon software and reconstructed images were analysed for morphometric parameters using CT-analyser software.

## 6.4.3 Results

### 6.4.3.1 Optimisation of platinum model

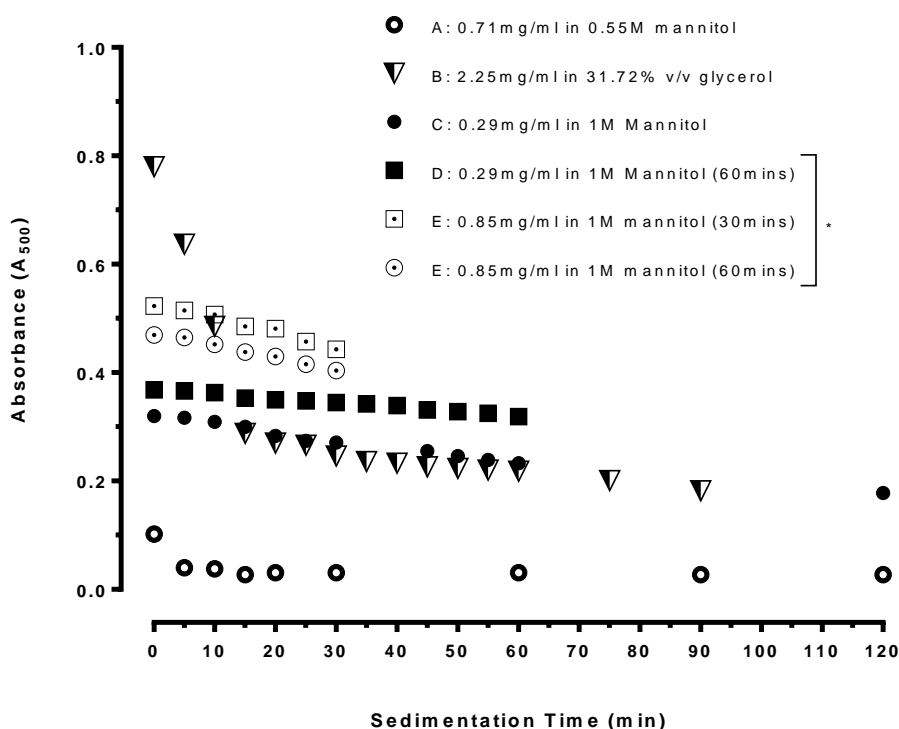


Figure 6.17: Optimisation of platinum dispersion stability for freezing studies with X-ray microcomputer tomography. Initial stock dispersions or supernatants were assayed. Stock dispersions contained A: 0.71 mg/mL in 10 %w/w mannitol; B: 2.25 mg/mL in 31.72 %v/v glycerol; and C: 0.29 mg/mL in 1 M Mannitol. Supernatant dispersions contained D: 0.29 mg/mL in 1 M Mannitol; E: 0.85 mg/mL in 1 M mannitol. \* represents supernatant and the duration allowed before collecting supernatants from sediments are in brackets. Platinum particle size in E:  $X_{90} = 2.43 \pm 0.0 \mu\text{m}$ ,  $X_{99} = 4.28 \pm 0.0 \mu\text{m}$  (from laser light diffraction).

The proposed mannitol-platinum dispersion for use as a model was initially optimised. The focus of optimisation process was to ensure particles did not unduly settle under gravity before adequate freeze concentration and complete solidification during the formulation freezing process. The optimal formulation had to contain the maximum amounts of platinum and viscous enough to control sedimentation rate.

A supernatant collected from 0.85 mg/mL of platinum in 1 M mannitol initially probe sonicated to disperse any aggregates was identified as ideal from  $A_{500}$  sedimentation study over 30 minutes. Success demanded evidence of freeze concentration or complete freezing before 30 minutes. This was confirmed using a slow shelf ramp of 0.2 °C/min (slow, control) and 1.5 °C/min cooling rate steps. Product temperature monitored during the freeze drying cycle is available in Appendix VII on page 264. These are discussed later in detail in relation to the various cooling rates used and the onset of ice nucleation. Nucleation and onset of freezing was confirmed to have occurred before 30 minutes during the freezing stage in the desired formulation (Appendix VII Figure A 16).

#### **6.4.3.2 Localisation of platinum in lyophilised dispersions**

Freeze dryer shelf and freeze dried samples were visually inspected. There was no sign of sample spillage due to leaking container content within the freeze dryer. Samples dried after slow shelf ramp of 0.2 °C/min (Slow) showed a substantial amount of visible black particles at the bottom when viewed from the parafilm covered base. Samples dried after 1.5 °C/min shelf cooling ramp (Mid) showed no visible black deposits when viewed through the parafilm covered base. Both sample cakes were intact with 2 tinny protruding dried bumps or masses on the surface.

Quench cooled samples were intact after drying with a single tinny pointed protruding dry mass on its surface. The base of the sample which was first immersed into liquid nitrogen showed signs of mannitol expansion but no evidence to suggest the ingress of liquid nitrogen into sample which would have been observed as a hollow cavity within the dried cake. Reconstructed images showed no form of ring artefacts which commonly present as concentric rings.

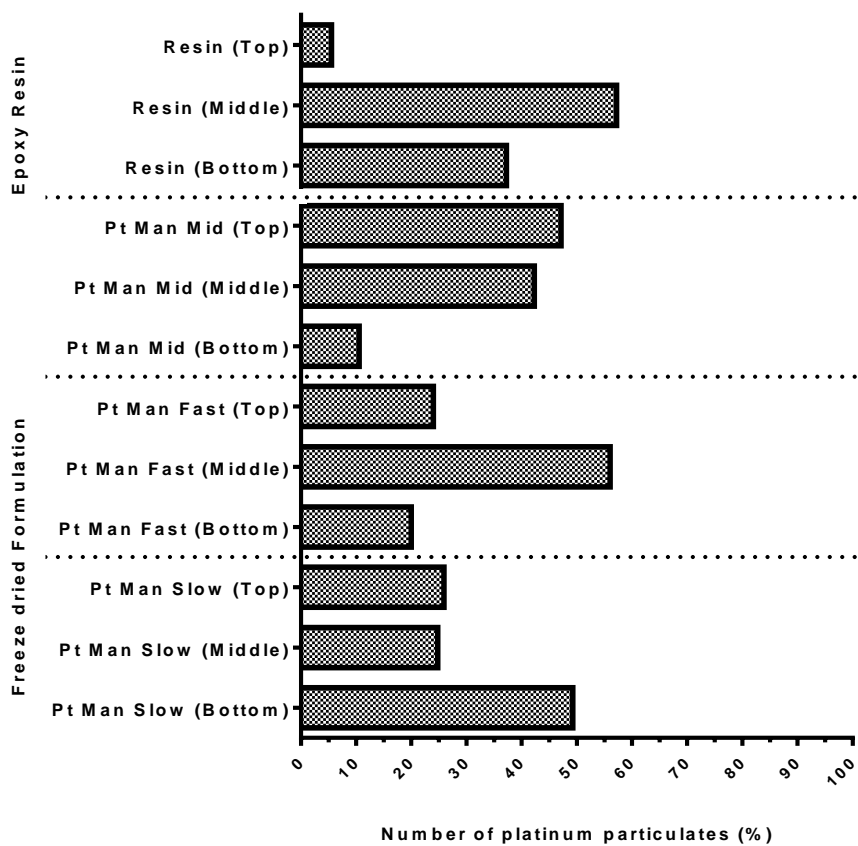
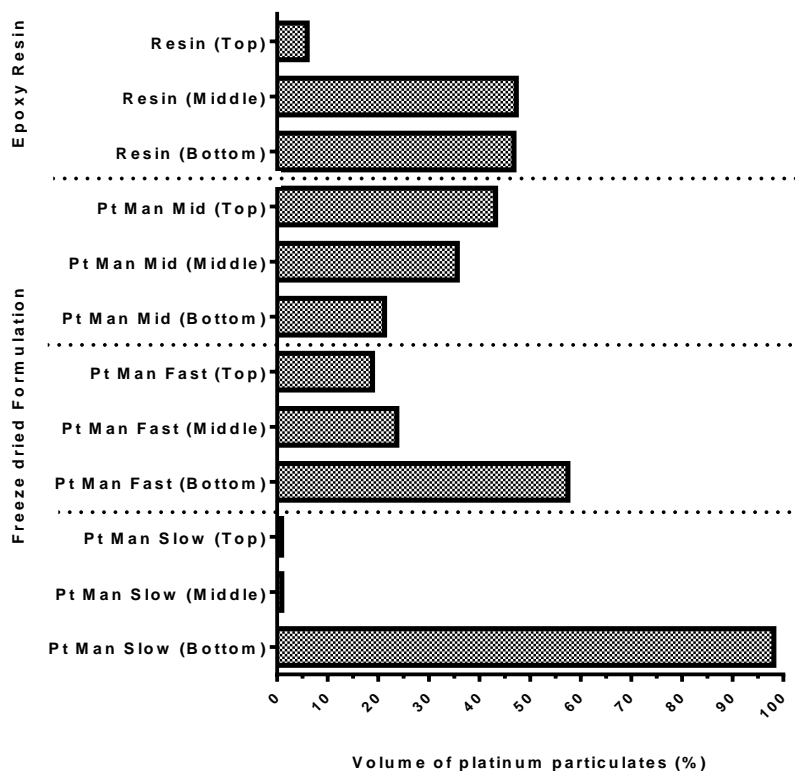


Figure 6.18 : X-ray microcomputer tomographic investigation into effect of cooling rate on number of platinum particulate model localisation in lyophilised mannitol (MAN) cake. Formulations of 1 M Mannitol contain 0.85 mg/mL of platinum. CCD camera resolution was 3.94 microns. Mid = 1.5 °C/min. Slow = 0.2 °C/min. Fast = Quench cooled in liquid nitrogen.



**Figure 6.19: X-ray microcomputer tomographic investigation into effect of freezing rate on volume of platinum particulate model localisation in lyophilised mannitol (MAN) cake. Formulations of 1 M Mannitol contain 0.85 mg/mL of platinum. CCD camera resolution was 3.94 microns. Mid = 1.5 °C/min. Slow = 0.2 °C/min. Fast = Quench cooled in liquid nitrogen.**

Three dimensional binarised image of VOI within top, middle and bottom segments of formulations revealed differences in the volume and number distribution of platinum particles (Figure 6.18 and Figure 6.19). Presence of a large volume of platinum did not necessarily represent or show a large number of platinum particles and vice versa. Platinum particles present were therefore present in different surface areas. A large surface area of many particles or fewer particles with a smaller surface area could equate to the same volume results obtained from analyses.

Platinum mannitol dispersion was shown to be optimised and a valid model. Using a slower cooling rate (Experimental control) that did not guarantee solidification of all phases within

30 minutes caused particulate sedimentation to a very high extent. The use of a slow shelf cooling ramp rate of 0.2 °C/min showed an expectedly high 98% of its particulate volume settled at the bottom of the dried formulation (Figure 5.18) as it took about 3.5 hours for the onset of ice nucleation as per thermocouple reading (Appendix VII Figure A 15). This was in accordance with the initial visual inspecting which revealed many black deposits of platinum at the sample container base.

The use of a relatively faster shelf cooling rate of 1.5 °C/min (Pt Man Mid) was ideal and showed a nucleation event at a nucleation temperature of -4.7°C after 28 minutes of cooling (Table 6.3). Nucleation was completed at -0.65°C with the subsequent onset of solidification (Appendix VII Figure A 16). This was evidence that the dispersion was held below the equilibrium freezing temperature of water or super cooled before the initiation of ice nucleation (Table 6.3).

**Table 6.3: Observed nucleation events and calculated rates for mannitol only and mannitol-platinum dispersions from product freeze drying cycle plots.**

Sample batch	Set shelf cooling rate* (°C/min)	Pre nucleation cooling rate** (°C/min)	Post nucleation freezing rate** (°C/min)	Nucleation temperature (°C)
Mannitol-platinum dispersion	0.2	0.10	0.18	-5.4
Mannitol only	0.2	0.15	0.26	-8.13
Mannitol only	1.5	----	----	-3.29***
Mannitol-platinum dispersion	1.5	1.42	1.79	-4.7

**\*Specified in freeze drying cycle protocol. \*\*Calculated from product temperature cycle plot measured using K type thermocouple in a separate representative sample. \*\*\* A typical prominent nucleation event not observed on thermogram but a distinct inflection in baseline suggested a nucleation temperature around -3.29°C.**

Complete solidification was observed at 44 minutes where the product temperature was at -41.5°C and close to the assigned inlet shelf temperature of -55°C. The use of double folded parafilm as container base may explain the temperature lag due to a poorer thermal transfer than could be expected for other materials such as glass or stainless steel.

Platinum localisation results from epoxy resin samples were expected to be similar to quench cooled samples but not found true in all cases. Within minutes of manual mixing of the 2 component epoxy (resin and hardener) with platinum, the resulting viscous mix hardened. Results for platinum distribution in epoxy resin did not show similar patterns of volume distribution as quench cooled samples (Figure 6.18). Interestingly, similar amounts were found from the calculated percentage number of platinum present in their mid-regions which were 57% and 56% for epoxy resin and quench cooled samples (Figure 6.19). The least volume of platinum particles was present at the top of both epoxy (5.95%) and quench cooled (18.9%) samples (Figure 6.18 and Figure 6.19). The expansion observed at the base of quench cooled sample correlated with the 10.67% difference in volume distribution when the bottom VOIs for quench cooled and epoxy resin samples were compared (Figure 6.19).

While the volume of formulations cooled at 1.5 °C/min (Pt Man Mid) showed increasing volume of platinum from bottom VOI through to the top VOI, the reverse was true for quench cooled formulations (Figure 6.189, Fast). The trend supports the fact that upward particulate migration along the freezing front or ice crystal growth within both sample sets occurred. The number of particulate distribution in the quench cooled sample which was found to be highest in the middle VOI suggested there was particulate migration from the bottom VOI but the fast freezing process did not allow this to proceed much longer and further compared to samples cooled relatively slowly at 1.5 °C/min.

The afore mentioned results involved the use of large VOI corresponding to top, middle and bottom VOI which were analysed for patterns in volume and number of platinum distribution

within samples (Figure 6.18 and Figure 6.19). This was overly generalised and a more detailed approach using many well distributed VOI was investigated. This was aimed at obtaining a more detailed understanding of particulate distribution. The individual large sectioned top, middle and bottom VOI were investigated to ascertain where particulates were distributed along the path from the central core of a cake towards the walls of its container vessel. These sections were shown as centre (CR), ring 1 and ring 2 (See schematic on Figure 6.20 and Figure 6.21). Ring 2 was hence the closest to the container wall and both ring 1 and ring 2 consisted of 8 individual volumes of interest labelled 1-5 along the axes A-D (See schematic on Figure 6.20 and Figure 6.21).

Since the formulation components had mannitol, water and platinum phases present, a platinum-ice-eutectic or partly amorphous mix will form on solidification. Pure ice would sublime to leave behind pores which may be varied in structure dependent on the ice crystal morphology.

A correlation between the concentration or amounts of platinum within the sectioned VOI and nucleation as well as the direction of the freezing front was apparent. This correlation was caused by the method of cooling.

The results for sample shelf cooled at a ramp rate of 1.5 °C/min showed a heterogeneous distribution of particulate volume within the volumes of interest. Observing the volume distribution along the axes A, B, C and D within the volumes of interest showed patterns in volume distribution (Figure 6.21). From the volume distribution within the bottom volume of interest, an irregular pattern of platinum volume was observed from left through the centre to the right container wall along each axis labelled A to D (Figure 6.21 Bottom Left). The observed pattern however for the middle and top volumes of interest generally showed either an increase in volume distribution along any axis A-D or a volume distribution that

increased from outwards (container wall) towards the central core of the dried cake. The amount of platinum present within the central core was highest within the entire cake from top to bottom (Figure 6.21, Right, top to bottom).

The volume distribution pattern observed when sample was quench cooled was found to be generally more orderly within the top to bottom volumes of interest studied. All sections generally followed either an increase in volume distribution along any axis A-D or an increase from the container walls towards the central core. Unlike the shelf cooled sample, the bottom core had the least platinum volume (Figure 6.210).

The impact of this heterogeneous freezing pattern within a shelf cooled sample and the directional freezing in quench cooled samples was demonstrated for visual clarity using a platinum volume distribution map (Figure 6.22).

A coloured scale represented the relative amounts of platinum in any one volume of interest (Figure 6.22). Earlier it was deduced that the freezing front, ice nucleation sites and amount of platinum in any section of a dried cake freeze dried from previously homogenous platinum mannitol dispersion could be made. This postulate was found to be true and clarified by the volume distribution maps.

The observed pattern for shelf cooled formulation suggested heterogeneous nucleation sites with the ice crystal growth or freezing front migrating towards the central core of the formulation. Based on our suggested deduction, the number of nucleation sites was at a minimum where volume distribution was highest within the dried cake.

Applying the same thought process to quench cooled sample showed nucleation was not heterogeneous but localised to any one section of the volume of interest closest to the container wall. This is consistent with the quench cooling process where the entire

formulation was immersed into liquid nitrogen. The freezing front is consistent with the expectation that nucleation will be from the closet point of contact with the cooling medium which were the container walls. For example from Figure 6.22 (Left), the bottom volume of interest of quench cooled sample had the least platinum volume distribution which increased along the A, B and C axes towards the central core of the cake.

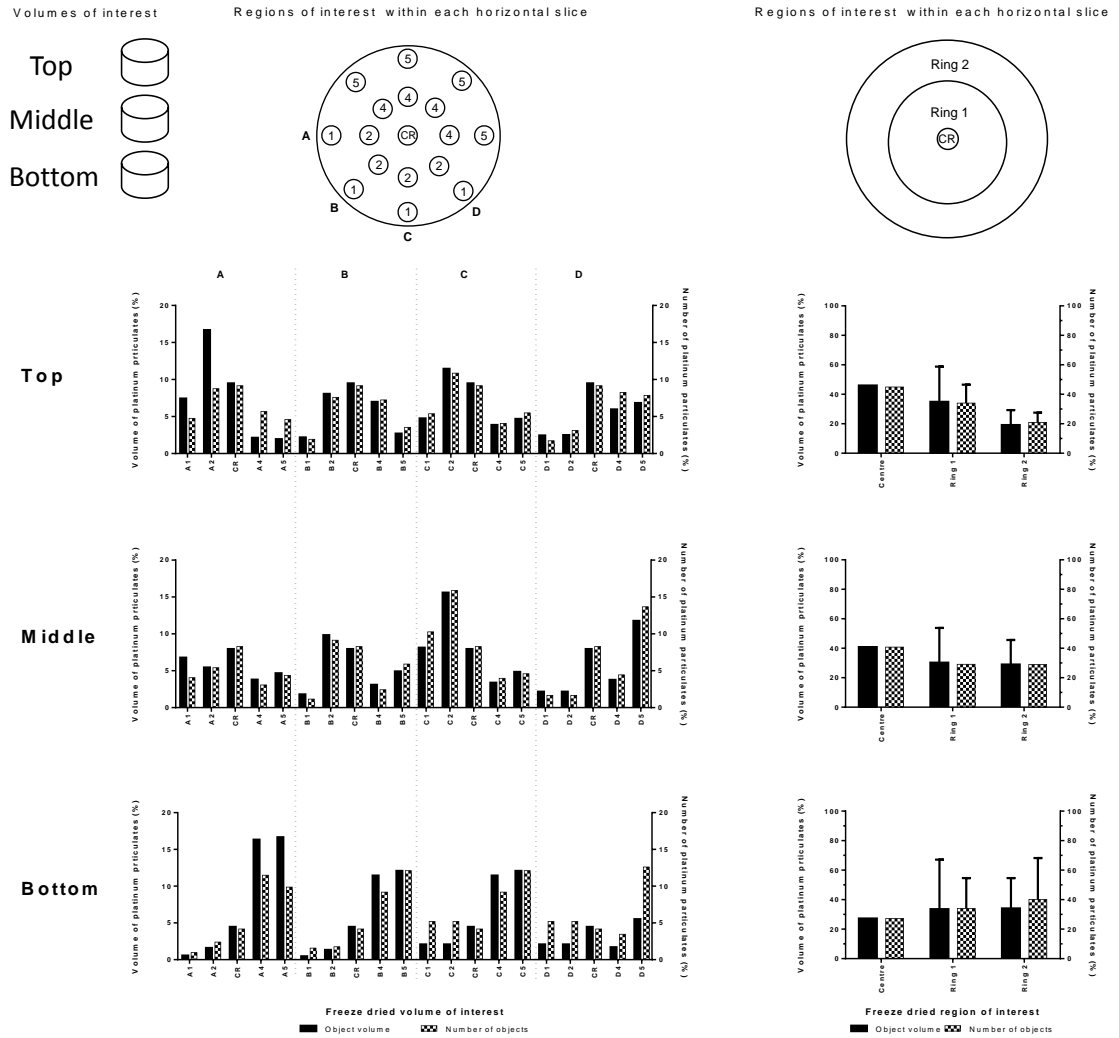


**Figure 6.20: X-ray microcomputer tomographic investigation into effect of quench cooling and fast cooling rate on platinum in lyophilised mannitol (MAN) cakes. Formulations of 1 M mannitol contain 0.85 mg/mL of platinum was optimised for particulate sedimentation rate. CCD camera resolution was 3.94 microns. Samples were sectioned into Left: Top, middle and bottom volumes of interests. Each volume of interest was further sectioned into horizontal slices. Each horizontal slice was further sectioned into regions of interests along the axis A-D. The volume and number of platinum within each region of interest was quantified. Right: sum of platinum volume and number within each horizontal slice.**



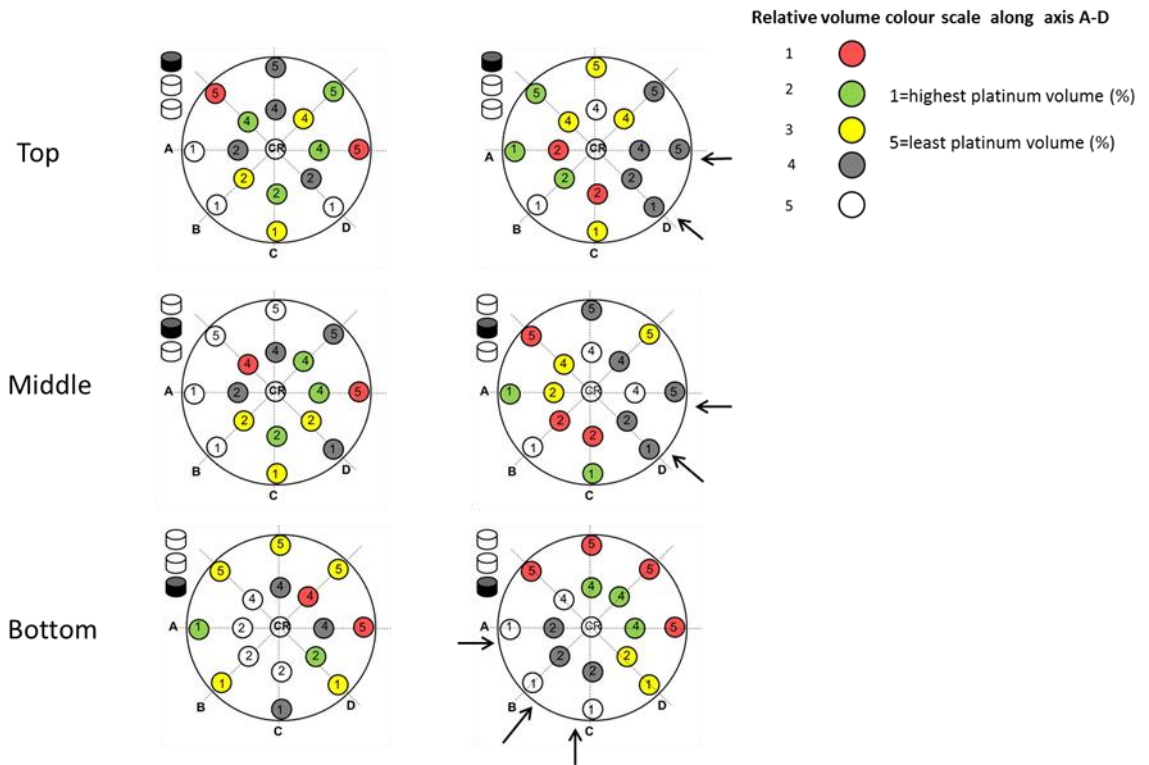


**Figure 6.22: Relative volume colour scale distribution of platinum within freeze dried mannitol along each axis labelled A-D. Left: shelf ramp cooled at 1.5 °C/min. Right: quench cooled samples in liquid nitrogen. Colour scale is relative across each axis. Similar colour scales on different axes do not represent equal volume. Arrows represent suggested path of freezing front.**

#### 6.4.4 Discussion

It was possible to generally predict the likely proximity or the location of nucleation sites or direction of ice crystal growth within the volumes of interest analysed based on platinum distribution within dried cakes. The binarised image thresholding performed allowed the separation of images to include only platinum objects for analysis. X-ray photons are attenuated based on atomic number and density (Baruchel *et al.*, 2000). Unlike monochromatic gamma ray source or synchrotron tomography, the polychromatic X-ray source used in this study can have problems with beam hardening resulting from varied attenuations within samples to produce attenuations from even low energy photons (Baruchel *et al.*, 2000). The concept of X-ray attenuation and background of micro-computer tomography was previously discussed in the thesis (Sections 1.8 and 3.4.12.1).

Because low energy photons experience more attenuation compared to high energy photons, a beam is said to have hardened when the X-ray spectrum shifts towards higher energy in relation to increasing attenuation through a given sample (Zou *et al.*, 2011). A beam hardening correction of 20-30% was ideal and in combination with the 0.5 mm aluminium filter used in this chapter, the noise to signal ratio was minimised. Artefacts introduced by beam hardening are commonly observed as streaks in reconstructed images. These introduce errors when present and quantitative analysis will be erroneous due to the introduction of corrupt pixels.

A limitation with the technique is the rather subjective nature of the thresholding process especially where grey scale indices signals for different material components overlap on the grey scale histogram distribution. This was resolved in our work using the linear binarised scale in combination with deduction of a blank value. A similar study by Koroteev *et al.* (2011) studied the use of MCT to threshold quartz, halite, and calcite mineral powder mix.

The analysed binarised images for the corresponding top, middle and bottom volumes of interest showed differences in volume and number distribution of platinum within the samples analysed (Figure 6.18 and Figure 6.19). The absence of platinum in any one region meant the presence of either a pore and or mannitol in this region. Freeze dried cakes are by nature very porous with pores varied in size and tortuosity (Dawson and Hockley, 1992). It could be inferred that the presence of a pore meant the presence of an ice nucleation site at or within the proximity of the pore in question. The volume distribution within the volumes of interest could therefore be used to a large extent as an indicator of ice nucleation sites and ice crystal growth within a formulation.

The direction of the freezing front and ice crystal growth was also expected to influence platinum volume distributions within the final dried cakes. Since the freezing front and nucleation sites are initially in close proximity, a correlation between these and the amount of platinum distributed within a cake could therefore be made. This was under the assurance that sample solutions prior to freeze drying had a uniform distribution of platinum which was ensured through formulation optimisation studies (Section 6.4.3.1 on page 201).

The observed varied platinum redistribution (Figure 6.19) within the various volumes of interest studied was supported by the rationale that formulation components migrate from the coldest section within a formulation towards the surface when chilled on a freeze drying shelf (Franks, 1990, Dawson and Hockley, 1992). Our results showed a detailed quantitative observation of this trend but migration was to a lesser extent in quench cooled samples (Figure 6.19). The assessment of the dried cake in this study demonstrated the aforementioned phenomenon and showed the trail of resulting concentration gradient created along four planes within formulations (Figure 6.22). The wider implications of this phenomenon would require formulators especially those intending to powder dispense bulk dried formulations to consider the choice of cooling rate. Relating the current results to conclusions from previous powder dispensing studies in chapter 5 (Section 5.3.4 on page

144), the need for powder homogeneity cannot be over emphasised. A homogenous final powder from a reproducible powder breaking step would be required for success.

These observed differences in API homogeneity due to cooling rate suggested homogeneity was influenced by the direction of the freezing front. Here, bottom to top freezing was observed to correlate with API migration from bottom to top. Not all types of freezing follow this pattern and it would be expected that top to bottom freezing which occur in ice fog (Rambhatla *et al.*, 2004) and vacuum induced freezing techniques (Liu *et al.*, 2005) would have API migration follow same.

Thermocouples were placed at the bottom of container vessel of representative formulations but not into the formulations scanned to eliminate thermocouple induced ice nucleation at higher nucleation temperature (Roy and Pikal, 1989). The presence of platinum particulates also in itself could be viewed as nucleating agents. Nucleating agents are useful for modifying the ice nucleation temperature during sample cooling and examples studied in literature include silver iodide and *Pseudomonas syringae* (Searles *et al.*, 2001b, Liu *et al.*, 2005). Searles and co-workers who studied formulations seeded with *Pseudomonas syringae* and silver iodide saw a reduction in nucleation temperature by  $-11.6^{\circ}\text{C}$  (87%) and  $-7.3^{\circ}\text{C}$  (55%).

Evidence of ice nucleation temperature alteration was present to a lesser extent in the freeze dried mannitol platinum dispersions (Table 6.3). From comparing similar formulations containing 1 M mannitol only to that containing platinum showed a  $-2.73^{\circ}\text{C}$  (34%) change in ice nucleation temperature. Searles and Randolph (2000) found 1 mg/2 mL silver iodide particles used in controlled nucleation studies floated at the meniscus before freezing and induced nucleation was detected by external temperature probes. There were no floating particulates visually present on the meniscus of samples in our study and this was because

platinum was denser ( $21.45 \text{ g/cm}^3$ ) compared to silver iodide ( $5.675 \text{ g/cm}^3$ ) (Fischer Scientific, 2012, Acros Organics, 2009).

The observed platinum volume distribution trends (Figure 6.19) resonate with known differences in nucleation events described in literature. For shelf ramped cooling of solutions, the observed results were consistent with Dawson and Hockley (1992) who found the formation of proteinaceous skin layer at the surface of 1 %w/v trehalose containing 5 mg/mL protein when shelf freeze dried at  $1 \text{ }^\circ\text{C/min}$ . Authors found this to be absent when samples were fast frozen and was attributed to migration of formulation components to the surface. The plug or cake had a protein rich surface with most protein within the top fifth (Dawson, unpublished). Franks (1990) observed buffer salt migration towards formulation surface as surface protrusions and was linked to 90% enzymatic denaturation due to pH shifts. Nakagawa *et al.* (2013) however found the activity of bovine serum albumin to be higher at the bottom of a vial which was slow shelf cooled and attributed the observed to the freezing process.

Platinum and mannitol solute migration toward the surface of formulations occurred during the freezing process. Ice crystals growth forming the freezing front can cause the migration of platinum within the formulation. This migration could be confirmed from reviewing the localisation patterns within fast or quench cooled and mid freezing rate frozen samples. Fast frozen formulation where solidified instantaneously from bottom to top as they were dipped into liquid nitrogen. Solute and liquid phases present held the platinum within the ice-eutectic mix. It was also assumed that all formulations contained the same amounts of platinum and were dispersed uniformly within the optimised formulations. From a simple density-mass relationship, the presence of a large volume could be interpreted as the presence of a high

platinum mass. A high platinum volume could also be either made up of a high surface area of many small platinum particulates and vice versa.

#### **6.4.5 Conclusion**

We have demonstrated for the first time a detailed non-destructive application of MCT for quantification of a complete freeze dried formulation to inform API localisation (Section 6.4.3.2).

Using optimised platinum in mannitol dispersions as a model, findings were in agreement with literature and provided the most detailed quantitative report to date of the differences in API localisation in relation to the cooling rate.

Volume and number distribution of platinum was determined by API migration from bottom to top in shelf cooled formulations. While samples cooled at 1.5 °C/min showed a trend of increasing volume of platinum from bottom VOI to top VOI, the opposite was found true for quench cooled samples. This was due to differences in the rate and direction of the freezing front. Freezing front velocity and freezing rate were faster in quench cooling.

The freezing front was responsible for redistribution of API through a formulation. The creation of concentration gradients dependent on this within a formulation was demonstrated along four different planes within three volumes of interest. This was dependent on nucleation events and method of freezing. Quantitative mapping scale for platinum volume distribution demonstrated heterogeneous freezing and solidification fronts in samples dried at 1.5 °C/min. Uniform pockets of API localisation due to directional solidification were revealed in quench cooled formulations due to inward directional solidification of the freezing front from container walls in contact with the cooling medium.

## 7 FINAL CONCLUSIONS AND IMPLICATIONS

This thesis has made important steps in broadening the knowledge that exists for bulk freeze drying and demonstrated this approach to be cost effective, meets regulatory approval and practical. It offers manufacturers and researchers the building blocks for further work and also directs on critical considerations for optimal powder handling and performance.

In the conclusions of chapter 4, it was noted that 23%-34.4% of freeze dryer shelf volume was wasted when compared to the typical vial arrangement in freeze drying. Mannitol and sucrose bulk lyophilised formulations in typical concentration ranges of 1 %w/v to 15 %w/v could be disrupted uniformly to provide free flowing powders with flow classified over the range of 'poor' to 'very very poor'. Techniques were defined that allowed disruption and testing of these highly hygroscopic powders. Cake disruption technique (I) involved the use of a fixed number of rotations by adopting a standard friability tester (Section 4.3.1.2). While the alternate technique (II) involved the use of a nest of standard stainless steel sieves (710  $\mu\text{m}$ -75  $\mu\text{m}$ ) shaken mechanically at an amplitude over time till the powder endpoint was reached (Section 4.4.2.2).

Our initial hypothesis that crystalline bulk content would benefit freeze dried powder flow compared to an amorphous powder was substantiated (Section 4.3.2.2). Crystalline mannitol was found to display superior flow behaviour over amorphous sucrose after freeze drying and disruption to powder. However both agents were still categorised using Carr's classification as 'very very poor'. This meant they were very cohesive and presented with potential handling problems. The concentration-flowability relationship was quantified and related to bulk density and porosity. The main mechanism for improving flowability was to increase the density of the powder which had significant considerations for impedance during the freeze drying process.

Implications of this chapter to our overall objectives were that the identification of poor flow behaviour of bulk freeze dried powders would be a barrier to the successful adoption of powders to a dispensing process. Angle of repose experiments showed occurrence of bridging or arching and powders would require agitation to initiate flow through orifices such as those of commercial hoppers. While the typical residual moisture levels in freeze dried powders were too low to influence its flow, there was a significant need to control humidity during powder disruption and handling.

Formulators hoping to manipulate freeze dried powders would need to avoid mannitol content of less than 5 %w/v. The low concentrations provided no benefit for flow. Although concentrations of up to 15 %w/v showed a relative increase in flow behaviour, further increase in solute content did not benefit flowability. This was limited by solubility in cases and further addition would only add to cost of drying.

In conclusions for investigations into the effect of cooling rate on freeze dried powder flowability (Section 4.4.5), it was revealed that cooling rates of between 0.2 °C/min to 1 °C/min were beneficial in combination with mannitol solute contents of 0.5 M-1 M. It was found that powders treated by annealing benefited from an increased mechanical strength. The previously described cake disruption technique (II) (Section 4.4.2.2) was found as most suitable for powder disruption as a low cost and industrially reproducible approach.

Formulators must avoid cooling rates of 5 °C/min because they produced the most cohesive powders as revealed from compressibility indices and flow function curves (Section 4.4.3.3 and 4.4.3.8).

In the conclusions of chapter 5, larger variations from dosing targets were found to be associated when using volumetric powder dispensing method compared to a gravimetric method due to the differences in their dosing mechanisms. A gravimetric powder dispenser was recommended for dispensing freeze dried powders together with assurances of powder homogeneity.

Freeze dried powders were found to easily develop electrostatic charge during handling (Triboelectrification) and was responsible for sample losses during dispensing. Manufacturers must therefore control triboelectrification.

Powder dispensing of disrupted freeze dried powders in a moisture free and static controlled environment was demonstrated to be practical, time efficient and able to meet regulatory approval in cases. Pharmacopeia acceptance values criteria for dosage uniformity of dosed formulations into container closures determined if samples passed or failed. The presence of micro collapsed amorphous phase in formulations would cause dosed units to fail and must be avoided. The type of protein formulation would influence dosing accuracy because it influences the morphology of the final powders. Annealed formulations with a mannitol solute content of 0.5 M or 9 %w/v was recommended as optimal for use in combination with a gravimetric powder dispenser. The gravimetric dispenser must be equipped with powder stirring and vibration mechanisms.

The use of online process analytical tools to exclude outliers was advised for use with gravimetric dispensers to allow the setting of acceptable weight deviation limits.

It was appreciated that the use of an amorphous and crystalline blend could potentially benefit the requirements for good flow, dosing accuracy and long term stability.

Manufacturers considering dosing freeze dried powders from bulk need to optimise the cake disruption process, the physical form, flowability, process humidity control, powder electrostatics and also the choice of dosing system.

In conclusions for chapter 6, it was demonstrated for the first time the use of X-ray microcomputer tomography (MCT) in informing the flow characteristics of freeze dried powders and finally its API dose uniformity. Sample requirements were less than 1 mL in all cases and was therefore recognised to be potentially useful during early lyophilised product development.

Porosity measurements revealed a strong correlation with traditional helium pycnometric measurements ( $R^2 = 0.93$ ). The combination of porosity, size, structural model index, fragmentation index and fractal dimension analyses as determined by MCT were complimentary attributes which enabled dried powders to be indirectly characterised for flow behaviour. Due to the very small sample volumes used, homogeneous sampling from stock powders was advised.

Scientists intending to inform flow characteristics using MCT need to use a fixed number of bench tapping for uniformity across samples to be analysed. A 100 taps within 2-5cm from the bench was recommended.

It has also been demonstrated a detailed quantitative account of freezing events that occur during freeze drying of an API. Volume and number distributions showed the largest amount of API was localised in the top VOI when cooled at 1.5 °C/min. The evidence showed this was due to API migration during freezing. The freezing front was found to create an API concentration gradient within a formulation dependent on the freezing rate. Heterogeneous freezing and solidification front was revealed in samples cooled at 1.5 °C/min compared to a directional freezing front observed when samples were quench cooled.

## 8 REFERENCES

- ACROS ORGANICS. (2009). *Platinum Materials Safety Data Sheet* [Online]. Available: <https://www.fishersci.ca/viewmsds.do?catNo=AC195210010> [Accessed 21/01/14].
- AMIDON, G. E. (1995). Physical and Mechanical Property Characterization of Powders. In: BRITTAIN, H. G. (ed.) *Physical characterization of pharmaceutical solids*. New York: Dekker.
- ANCHORDOQUY, T. J. & CARPENTER, J. F. (1996). Polymers protect lactate dehydrogenase during freeze-drying by inhibiting dissociation in the frozen state. *Archives of Biochemistry and Biophysics*, 332, 231-8.
- ANCHORDOQUY, T. J., IZUTSU, K. I., RANDOLPH, T. W. & CARPENTER, J. F. (2001). Maintenance of quaternary structure in the frozen state stabilizes lactate dehydrogenase during freeze-drying. *Archives of Biochemistry and Biophysics*, 390, 35-41.
- ARMSTRONG, N. (2009a). Mannitol. In: ROWE, R. C., SHESKEY, P. & QUINN, M. (eds.) *Text Book of Pharmaceutical Excipients*. 6 ed. London: Pharmaceutical Press.
- ARMSTRONG, N. (2009b). Sucrose. In: ROWE, R. C., SHESKEY, P. & QUINN, M. (eds.) *Text Book of Pharmaceutical Excipients*. 6 ed. London: Pharmaceutical Press.
- ASSOCIATION OF BRITISH PHARMACEUTICAL INDUSTRY (ABPI) (2008). *Medicines Compendium*. Surrey: Dataharm Communications Limited.
- AULTON, M. E. (2007). Drying. In: AULTON, M. E. (ed.) *Pharmaceutics: The design and manufacture of medicines*. 3ed. London: Churchill livingstone.
- BAHETI, A., Kumar L., BANSAL A. K., (2010). Excipients used in lyophilization of small molecules. *Journal of Excipients and Food Chemistry*, 1, 41-54.
- BARTLETT, R. L., CHLEWBOWSKI, A. L. & GRECO, P. M. (2013). *Reconstitution device*. WO patent publication W0/2013/0403861.
- BARUCHEL, J., BUFFIERE, J., MAIRE, E., MERLE, P. & PEIX, G. (2000). *X-ray tomography in material science*. Paris: Hermes Science.
- BERGMANN, T. & BRUSTMANN, H. (1994). *Process and container for freeze drying under sterile conditions*. US patent publication 5309649.
- BHAMBHANI, A. & MEDI, B. M. (2010). Selection of Containers/Closures for Use in Lyophilization Applications: Possibilities and Limitations. *American Pharmaceutical Review*, 21-25.
- BOEHRINGER MANNHEIM GMBH. (1994). *Process and container for freeze drying under sterile conditions*. US patent publication 5309649.

- BRITISH PHARMACOPOEIA COMMISSION (2013a). Bulk density and Tapped density of powders. *British pharmacopoeia*. London: The Stationery Office.
- BRITISH PHARMACOPOEIA COMMISSION (2013b). Consistency of Formulated Preparations. *British pharmacopoeia*. London: The Stationery Office.
- BRITISH PHARMACOPOEIA COMMISSION (2013c). Powder Flow. *British pharmacopoeia*. London: The Stationery Office.
- BRITISH PHARMACOPOEIA COMMISSION (2013d). Sieves and Filters. *British pharmacopoeia*. London: The Stationery Office.
- BROOKFIELD ENGINEERING LABORATORIES INC. *Brookfield Powder Flow Tester Operator Manual M09-1200*.
- BROWN, L. & RICHARDS, J. C. (1970). *Principles of powder mechanics: Essays on packing flow of powders and bulk solids*. Oxford: Pergamon Press.
- BUILDERS, P. F., BONAVENTURE, A. M., TIWALADE, A., OKPAKO, L. C. & ATTAMA, A. A. (2010). Novel multifunctional pharmaceutical excipients derived from microcrystalline cellulose-starch microparticulate composites prepared by compatibilized reactive polymer blending. *International Journal of Pharmaceutics*, 388, 159-167.
- BURGER, A., HENCK, J. O., HETZ, S., ROLLINGER, J. M., WEISSNICHT, A. A. & STOTTNER, H. (2000). Energy/temperature diagram and compression behavior of the polymorphs of D-mannitol. *Journal of Pharmaceutical Sciences*, 89, 457-468.
- BURSAC, R., Sever, R., & HUNEK, B. (2009). A Practical Method for Resolving the Nucleation Problem in Lyophilization. *BioProcess international*, 66-72.
- CAO, W., MAO, C., CHEN, W., LIN, H., KRISHNAN, S. & CAUCHON, N. (2006). Differentiation and quantitative determination of surface and hydrate water in lyophilized mannitol using NIR spectroscopy. *Journal of Pharmaceutical Sciences*, 95, 2077-2086.
- CARPENTER, J. F. & CROWE, J. H. (1989). An infrared spectroscopic study of the interactions of carbohydrates with dried proteins. *Biochemistry*, 28, 3916-3922.
- CARR, R. L. (1965). Evaluating flow properties of solids. *Chemical Engineering*, 72, 69-72.
- CARSON, J. K., HILL, H. K., GRAHAM, D. M. & SCHOU, G. B. C. (2005). *Drying process and apparatus*. WO patent publication WO 2005/105253 A1.
- CAVATUR, R. & SURYANARAYANAN, R. (1998). Characterization of Frozen Aqueous Solutions by Low Temperature X-ray Powder Diffractometry. *Pharmaceutical Research*, 15, 194-199.

- CHANG, B. S., KENDRICK, B. S. & CARPENTER, J. F. (1996). Surface-induced denaturation of proteins during freezing and its inhibition by surfactants. *Journal of Pharmaceutical Sciences*, 85, 1325-1330.
- CHANG, B. S. & LIU, R. W. (2011). *Container closure delivery system*. US patent publication 7959600 b2.
- CHANG, B. S. & PATRO, S. Y. (2004). Freeze-drying Process Development for Protein Pharmaceuticals. In: COSTANTINO, H. R. & PIKAL, M. J. (eds.) *Lyophilization of Biopharmaceuticals*. Arlington: American Association of Pharmaceutical Scientists.
- CHANG, B. S. & RANDALL, C. S. (1992). Use of subambient thermal analysis to optimize protein lyophilization. *Cryobiology*, 29, 632-656.
- CHAPPARD, D., LEGRAND, E., HAETTICH, B., CHALES, G., AUVINET, B., ESCHARD, J. P., HAMELIN, J. P., BASLE, M. F. & AUDRAN, M. (2001). Fractal dimension of trabecular bone: comparison of three histomorphometric computed techniques for measuring the architectural two-dimensional complexity. *Journal of Pathology*, 195, 515-21.
- CHO, M., GARYANTES, T. K., GILBERT, H. & JONES, D. F. (1992). *Blood bag for lyophilization*. WO patent publication WO/1992/018058 A1.
- CHOUVENC, P. & FRANÇON, A. (2009). *Process for stabilizing an adjuvant containing vaccine composition*. WO patent publication WO/2009/109550A1.
- COCHRAN, T. & NAIL, S. L. (2009). Ice nucleation temperature influences recovery of activity of a model protein after freeze drying. *Journal of Pharmaceutical Sciences*, 98, 3495-8.
- COELHO, M. C. & HARNBY, N. (1978). Effect of Humidity on Form of Water-Retention in a Powder. *Powder Technology*, 20, 197-200.
- COSTANTINO, H. R. (2004). Excipients for use in Lyophilised Pharmaceutical Peptide, Protein and other Bioproducts. In: COSTANTINO H. R., Pikal M. J. (ed.) *Lyophilization of Biopharmaceuticals*. Arlington: American Association of Pharmaceutical Scientists.
- COSTANTINO, H. R., FIROUZABADIAN, L., HOGELAND, K., WU, C., BEGANSKI, C., CARRASQUILLO, K. G., CORDOVA, M., GRIEBENOW, K., ZALE, S. E. & TRACY, M. A. (2000). Protein spray-freeze drying. Effect of atomization conditions on particle size and stability. *Pharmaceutical Research*, 17, 1374-83.
- COSTANTINO, H. & PIKAL, M. J., (eds.) (2004). *Lyophilization of Biopharmaceuticals*. Arlington: American Association of Pharmaceutical Scientists.
- DATWYLER PHARMA PACKAGING INTERNATIONAL. (2013a). *Closure stopper for pharmaceutical applications*. US patent publication US20130213924.

- DATWYLER PHARMA PACKAGING INTERNATIONAL. (2013b). *Closure for a container and method for carrying out a freeze-drying process*. US patent publication US20130055681
- DAVIS, J. M., ZHANG, N., PAYNE, R. W., MURPHY, B. M., ABDUL-FATTAH, A. M., MATSUURA, J. E., HERMAN, A. C. & MANNING, M. C. (2013). Stability of lyophilized sucrose formulations of an IgG1: subvisible particle formation. *Pharmaceutical Development and Technology*, 18, 883-896.
- DAWSON, P. J. & HOCKLEY, D. J. (1992). Scanning Electron-Microscopy of Freeze-Dried Preparations - Relationship of Morphology to Freeze-Drying Parameters. *International Symposium on Biological Product Freeze-Drying and Formulation*, 74, 185-192.
- DEVI, S. & WILLIAMS, D. (2013). Morphological and Compressional Mechanical Properties of Freeze-Dried Mannitol, Sucrose, and Trehalose Cakes. *Journal of Pharmaceutical Sciences*, 102, 4246-4255.
- EKENLEBIE, E. & INGHAM, A. (2011). Short Cycle Times for Cost-Efficient Processing in Lyophilized Formulations. *American Pharmaceutical Review*, 23.
- EKENLEBIE, E. & INGHAM, A. (2013). Process Optimization of Bulk Lyophilized Bio synthetics: Implications of Powder Rheology. *12th PepTalk Conference on Lyophilisation and Emerging Drying Technologies*. California: Cambridge Healthcare.
- EULYSIS UK LIMITED. (2013). *Container and method of manufacture of container*. WO patent publication WO/2013/026995.
- FAQIH, A., CHAUDHURI, B., ALEXANDER, A. W., DAVIES, C., MUZZIO, F. J. & TOMASSONE, M. S. (2006). An experimental/computational approach for examining unconfined cohesive powder flow. *International Journal of Pharmaceutics*, 324, 116-127.
- FELDKAMP, L. A., DAVIS, L. C. & KRESS, J. W. (1984). PRACTICAL CONE-BEAM ALGORITHM. *Journal of the Optical Society of America A: Optics Image Science and Vision*, 1, 612-619.
- FISCHER SCIENTIFIC. (2012). *Silver Iodide Material Safety Data Sheet MSDS# 20805* [Online]. Available: <https://www.fishersci.ca/viewmsds.do?catNo=S178100> [Accessed 21/01/14].
- FORD, J. L. & TIMMINS, P. (1989). *Pharmaceutical thermal analysis : techniques and applications*. Chichester: Ellis Horwood.
- FRANKS, F. (1990). Freeze-drying - From empiricism to predictability. *Cryo-Letters*, 11, 93-110.

- FRANKS, F. (2007a). Primary Drying: The Sublimation of Ice. *Freeze-drying of Pharmaceuticals and Biopharmaceuticals*. London: Royal Society of Chemistry.
- FRANKS, F. (2007b). Secondary Drying: The removal of unfrozen water. *Freeze-drying of Pharmaceuticals and Biopharmaceuticals*. London: Royal Society of Chemistry.
- FRANKS, F. (2007c). Some Practical Aspects. *Freeze-drying of Pharmaceuticals and Biopharmaceuticals*. London: Royal Society of Chemistry.
- FREEMAN, R. (2007). Measuring the flow properties of consolidated, conditioned and aerated powders - A comparative study using a powder rheometer and a rotational shear cell. *Powder Technology*, 174, 25-33.
- FU, X., HUCK, D., MAKEIN, L., ARMSTRONG, B., WILLEN, U. & FREEMAN, T. (2012). Effect of particle shape and size on flow properties of lactose powders. *Particuology*, 10, 203-208.
- FU, X. W., DUTT, M., BENTHAM, A. C., HANCOCK, B. C., CAMERON, R. E. & ELLIOTT, J. A. (2006). Investigation of particle packing in model pharmaceutical powders using X-ray microtomography and discrete element method. *Powder Technology*, 167, 134-140.
- FU, X. W., MILROY, G. E., DUTT, M., BENTHAM, A. C., HANCOCK, B. C. & ELLIOTT, J. A. (2005). Quantitative analysis of packed and compacted granular system by X-ray microtomography. *Medical Imaging 2005: Image Processing, Pt 1-3*, 5747, 1955-1964.
- GARMISE, R. J., MAR, K., CROWDER, T. M., HWANG, C. R., FERRITER, M., HUANG, J., MIKSZTA, J. A., SULLIVAN, V. J. & HICKEY, A. J. (2006). Formulation of a dry powder influenza vaccine for nasal delivery. *AAPS PharmSciTech*, 7.
- GASSLER, M. & REY, L. (2004). Development of a New Concept for Bulk Freeze-Drying: GORE® LYOGUARD® Freeze-Dry Packaging. In: REY, L. & MAY, J. C. (eds.) *Freeze-Drying/Lyophilization Of Pharmaceutical & Biological Products, Second Edition, Revised and Expanded*. New york: Taylor & Francis.
- GE HEALTHCARE UK LIMITED. (2013). *Container storing freeze-dried biological sample*. WO patent publication WO/2012/101150.
- GEHRMANN, D., FIRUS, A., DAUN, T., MÜLLER, H. K. & WANG, D. (2010). *Sterile freezing, drying, storing, assaying and filling process*. US patent publication US7836606.
- GEIDOBLE, R., KONRAD, I. & WINTER, G. (2013). Can Controlled Ice Nucleation Improve Freeze-Drying of Highly-Concentrated Protein Formulations? *Journal of Pharmaceutical Sciences*, 102, 3915-3919.
- GRANT, Y. (2010). *Engineering the rational design and optimisation of lyophilization processes for biological materials*. Doctor of Engineering, University College London.

- GUERIN, E., TCHORELOFF, P., LECLERC, B., TANGUY, D., DELEUIL, M. & COUARRAZE, G. (1999). Rheological characterization of pharmaceutical powders using tap testing, shear cell and mercury porosimeter. *International Journal of Pharmaceutics*, 189, 91-103.
- HAHN, M., VOGEL, M., POMPESIUS-KEMPA, M. & DELLING, G. (1992). Trabecular bone pattern factor—a new parameter for simple quantification of bone microarchitecture. *Bone*, 13, 327-330.
- HANCOCK, B. C. & DALTON, C. R. (1999). The effect of temperature on water vapor sorption by some amorphous pharmaceutical sugars. *Pharmaceutical Development and Technology*, 4, 125-131.
- HANCOCK, B. C., VUKOVINSKY, K. E., BROLLEY, B., GRIMSEY, I., HEDDEN, D., OLSOFSKY, A. & DOHERTY, R. A. (2004). Development of a robust procedure for assessing powder flow using a commercial avalanche testing instrument. *Journal of Pharmaceutical and Biomedical Analysis*, 35, 979-990.
- HAWE, A. & FRIESS, W. (2006a). Impact of freezing procedure and annealing on the physico-chemical properties and the formation of mannitol hydrate in mannitol-sucrose-NaCl formulations. *European Journal of Pharmaceutics and Biopharmaceutics*, 64, 316-325.
- HAWE, A. & FRIESS, W. (2006b). Physico-chemical lyophilization behavior of mannitol, human serum albumin formulations. *European Journal of Pharmaceutical Sciences*, 28, 224-232.
- HENNIGER, G. (2003). Enzymatic Techniques for Authenticating Food Components. In: LEES, M. (ed.) *Food Authenticity and Traceability*. Cambridge: Woodhead Publishing Limited.
- HILDEBRAND, T. & RÜEGSEGG, P. (1997a). A new method for the model-independent assessment of thickness in three-dimensional images. *Journal of Microscopy*, 185, 67-75.
- HILDEBRAND, T. O. R. & RÜEGSEGG, P. (1997b). Quantification of Bone Microarchitecture with the Structure Model Index. *Computer Methods in Biomechanics and Biomedical Engineering*, 1, 15-23.
- HILL, J. J., SHALAEV, E. Y. & ZOGRAFI, G. (2014). The Importance of Individual Protein Molecule Dynamics in Developing and Assessing Solid State Protein Preparations. *Journal of Pharmaceutical Sciences*, 103, 2605-2614.
- HOWARD, S. A. (2007). Solids:Flow properties. In: SWARBRICK, J. (ed.) *Encyclopaedia of Pharmaceutical Technology*. 3 ed. New York: Informa Healthcare.
- IMAMURA, K., MARUYAMA, Y., TANAKA, K., YOKOYAMA, T., IMANAKA, H. & NAKANISHI, K. (2008). True density analysis of a freeze-dried amorphous sugar matrix. *Journal of Pharmaceutical Sciences*, 97, 2789-2797.

- INTERNATIONAL ORGANIZATION FOR STANDARDIZATION (1988). Test sieving Part 1: Methods using test sieves of woven wire cloth and perforated metal plate. *Test sieving methods*. 1988: International Organization for Standardization.
- IZUTSU, K. I., YOSHIOKA, S. & TERAOKA, T. (1994). Effect of mannitol crystallinity on the stabilization of enzymes during freeze-drying. *Chemical and Pharmaceutical Bulletin*, 42, 5-8.
- JIANG, Y., MATSUSAKA, S., MASUDA, H. & QIAN, Y. (2009). Development of measurement system for powder flowability based on vibrating capillary method. *Powder Technology*, 188, 242-247.
- JIN, T. H., NGUYEN, L., QU, T. & TSAO, E. (2011). Improved formulation and lyophilization cycle for rBCG vaccine. *Vaccine*, 29, 4848-4852.
- JOHNSON, R. E., KIRCHHOFF, C. F. & GAUD, H. T. (2002). Mannitol-sucrose mixtures - Versatile formulations for protein lyophilization. *Journal of Pharmaceutical Sciences*, 91, 914-922.
- JONES, B. E. (2001). The filling of powders into two-piece hard capsules. *International Journal of Pharmaceutics*, 227, 5-26.
- KADOYA, S., FUJII, K., IZUTSU, K.-I., YONEMOCHI, E., TERADA, K., YOMOTA, C. & KAWANISHI, T. (2010). Freeze-drying of proteins with glass-forming oligosaccharide-derived sugar alcohols. *International Journal of Pharmaceutics*, 389, 107-113.
- KAIALY, W. & NOKHODCHI, A. (2013). Freeze-dried mannitol for superior pulmonary drug delivery via dry powder inhaler. *Pharmaceutical Research*, 30, 458-77.
- KASPER, J. C. & FRIESS, W. (2011). The freezing step in lyophilization: Physico-chemical fundamentals, freezing methods and consequences on process performance and quality attributes of biopharmaceuticals. *European Journal of Pharmaceutics and Biopharmaceutics*, 78, 248-263.
- KAWAI, K. & SUZUKI, T. (2007). Stabilizing effect of four types of disaccharide on the enzymatic activity of freeze-dried lactate dehydrogenase: step by step evaluation from freezing to storage. *Pharmaceutical Research*, 24, 1883-90.
- KENTAROU TAKANO & SHINYO GAYAMA. (2013). *S-adenosyl-l-methionine-containing dry yeast composition with excellent storage stability and process for producing same*. European patent publication EP2557151 A1.
- KERLIN, T. W. & JOHNSON, M. (2012). *Practical Thermocouple Thermometry*. 2 ed. ISA.
- KIM, A. I., AKERS, M. J. & NAIL, S. L. (1998). The physical state of mannitol after freeze-drying: effects of mannitol concentration, freezing rate, and a noncrystallizing cosolute. *Journal of Pharmaceutical Sciences*, 87, 931-5.

- KONSTANTINIDIS, A. K., KUU, W., OTTEN, L., NAIL, S. L. & SEVER, R. R. (2011). Controlled Nucleation in Freeze-drying: Effects on Pore Size in the Dried Product Layer, Mass Transfer Resistance, and Primary Drying Rate. *Journal of Pharmaceutical Sciences*, 100, 3453-3470.
- KOROTEEV, D., MUTINA, A. & SASOV, A. (2011). Using X-ray microCT for 3D mineral mapping. *Micro-CT user meeting Abstract book*. Belgium: Skyscan.
- KRANTZ, M., ZHANG, H. & ZHU, J. (2009). Characterization of powder flow: Static and dynamic testing. *Powder Technology*, 194, 239-245.
- KRIEG, A. F., ROSENBLUM, L. J. & HENRY, J. B. (1967). Lactate dehydrogenase isoenzymes a comparison of pyruvate-to-lactate and lactate-to-pyruvate assays. *Clinical chemistry*, 13, 196-203.
- KUMAR, V., KOTHARI, S. H. & BANKER, G. S. (2001). Compression, compaction, and disintegration properties of low crystallinity celluloses produced using different agitation rates during their regeneration from phosphoric acid solutions. *AAPS PharmSciTech*, 2, E7-E7.
- KUMRU, O. S., JOSHI, S. B., SMITH, D. E., MIDDAUGH, C. R., PRUSIK, T. & VOLKIN, D. B. (2014). Vaccine instability in the cold chain: Mechanisms, analysis and formulation strategies. *Biologicals*, 42, 237-259.
- LAMPRECHT. (2013). *Pharmaceutical formulations comprising spherolyophilisates of biological molecules*. WO patent publication WO/2013/041542 A1.
- LANG, R., WINTER, G., VOGT, L., ZURCHER, A., DORIGO, B. & SCHIMMELE, B. (2009). Rational design of a stable, freeze-dried virus-like particle-based vaccine formulation. *Drug Development and Industrial Pharmacy*, 35, 83-97.
- LAVOIE, F., CARTILIER, L. & THIBERT, R. (2002). New methods characterizing avalanche behavior to determine powder flow. *Pharmaceutical Research*, 19, 887-893.
- LI, B., O'MEARA, M. H., LUBACH, J. W., SCHOWEN, R. L., TOPP, E. M., MUNSON, E. J. & BORCHARDT, R. T. (2005). Effects of sucrose and mannitol on asparagine deamidation rates of model peptides in solution and in the solid state. *Journal of Pharmaceutical Sciences*, 94, 1723-1735.
- LIN, L. L., WANG, Z. K., ZHOU, L. P., HU, Q. X. & FANG, M. L. (2013). The influence of prefreezing temperature on pore structure in freeze-dried beta-TCP scaffolds. *Proceedings of the Institution of Mechanical Engineers Part H-Journal of Engineering in Medicine*, 227, 50-57.
- LINDBERG, N. O., PALSSON, M., PIHL, A. C., FREEMAN, R., FREEMAN, T., ZETZENER, H. & ENSTAD, G. (2004). Flowability measurements of pharmaceutical powder mixtures with poor flow using five different techniques. *Drug Development and Industrial Pharmacy*, 30, 785-791.

- LIU, J. (2006). Physical Characterization of Pharmaceutical Formulations in Frozen and Freeze-Dried Solid States: Techniques and Applications in Freeze-Drying Development. *Pharmaceutical Development and Technology*, 11, 3-28.
- LIU, J. S., VIVERETTE, T., VIRGIN, M., ANDERSON, M. & DALAL, P. (2005). A study of the impact of freezing on the lyophilization of a concentrated formulation with a high fill depth. *Pharmaceutical Development and Technology*, 10, 261-272.
- MAA, Y. F., SHU, C., AMERI, M., ZULEGER, C., CHE, J., OSORIO, J. E., PAYNE, L. G. & CHEN, D. X. (2003). Optimization of an alum-adsorbed vaccine powder formulation for epidermal powder immunization. *Pharmaceutical Research*, 20, 969-977.
- MALVERN INSTRUMENTS. (2014). *Morphologi G3 Advanced particle characterization made easy* [Online]. Available: <http://www.malvern.com/en/products/product-range/morphologi-range/morphologi-g3/default.aspx> [Accessed 01/02/14].
- MAYERESSE Y., CUPERE V., VELLION R. & J., B. (2009). Consideration for transferring a bulk freeze drying process from a glass container to a tray. *Pharmaceutical Engineering*, 1-7.
- MELLOR, J. D. (1978). Classical theory of sublimation. *Fundamentals of freeze drying*. Bristol: J.W. Arrowsmith Limited.
- METTLER TOLEDO (2009). *Good Titration Practice in Karl Fischer Titrations*. Schwerzenbach: Markt Support AnaChem.
- MIDDLEBEEK, H. A., KIRKELS, M. & BIEMANS, R. (2009). *Method For Lyophilising Particles Having A Pharmaceutical Compound Contained Therein And A Pharmaceutical Pack Containing Such Particles*. NL patent publication EP 2249810.
- MILLER, J. N. & MILLER, J. C. (2005). *Statistics and chemometrics for analytical chemistry*. Essex: Pearson Education Limited.
- MONKARE, J., PAJANDER, J., HAKALA, R. A., SAVOLAINEN, P., JARVELAINEN, M., KORHONEN, H., SEPPALA, J. V. & JARVINEN, K. (2012). Characterization of internal structure, polymer erosion and drug release mechanisms of biodegradable poly(ester anhydride)s by X-ray microtomography. *European Journal of Pharmaceutical Sciences*, 47, 170-178.
- MORRIS, A. S. & LANGARI, R. (2012). *Measurement and Instrumentation - Theory and Application*. Waltham, MA: Academic Press.
- MOSHARRAF, M., MALMBERG, M. & FRANSSON, J. (2007). Formulation, lyophilization and solid-state properties of a pegylated protein. *International Journal of Pharmaceutics*, 336, 215-232.

- MOUSAVI, R., MIRI, T., COX, P. W. & FRYER, P. J. (2005). A novel technique for ice crystal visualization in frozen solids using X-ray micro-computed tomography. *Journal of Food Science*, 70, E437-E442.
- MUJAT, M., GRECO, K., GALBALLY-KINNEY, K. L., HAMMER, D. X., FERGUSON, R. D., IFTIMIA, N., MULHALL, P., SHARMA, P., PIKAL, M. J. & KESSLER, W. J. (2012). Optical coherence tomography-based freeze-drying microscopy. *Biomedical Optics Express*, 3, 55-63.
- MUMENTHALER, M. & LEUENBERGER, H. (1991). Atmospheric spray-freeze drying - a suitable alternative in freeze-drying technology. *International Journal of Pharmaceutics*, 72, 97-110.
- NAKAGAWA, K., MURAKAMI, W. & HATANAKA, T. (2013). Redistribution of Protein Biological Activity in a Freeze-Dried Cake. *Drying Technology*, 31, 102-111.
- NALLURI, V. R., PUCHKOV, M. & KUENTZ, M. (2013). Toward better understanding of powder avalanching and shear cell parameters of drug-excipient blends to design minimal weight variability into pharmaceutical capsules. *International Journal of Pharmaceutics*, 442, 49-56.
- NEWMAN (2011). X-ray Powder Diffraction in Solid Form Screening and Selection. *American Pharmaceutical Review* [Online]. Available: <http://www.americanpharmaceuticalreview.com/Featured-Articles/36946-X-ray-Powder-Diffraction-in-Solid-Form-Screening-and-Selection/> [Accessed 12/12/13].
- NIAZI K. SARFARAZ (2004). Sterile products. *Hand Book of Pharmaceutical Manufacturing Formulations*. London: CRC Press.
- NOYES, A. A. & WHITNEY, W. R. (1897). The rate of solution of solid substances in their own solutions. *Journal of the American Chemical Society*, 19, 930-934.
- OVERCASHIER, D. E. (2003). Microscopy of Lyophilised Proteins. In: COSTANTINO, H. R. & PIKAL, M. J. (eds.) *Lyophilization of Biopharmaceuticals*. Arlington: American Association of Pharmaceutical Scientists.
- PADILLA, A. M., IVANISEVIC, I., YANG, Y., ENGERS, D., BOGNER, R. H. & PIKAL, M. J. (2011). The Study of Phase Separation in Amorphous Freeze-Dried Systems. Part I: Raman Mapping and Computational Analysis of XRPD Data in Model Polymer Systems. *Journal of Pharmaceutical Sciences*, 100, 206-222.
- PARKER, A., RIGBY-SINGLETON, S., PERKINS, M., BATES, D., LE ROUX, D., ROBERTS, C. J., MADDEN-SMITH, C., LEWIS, L., TEAGARDEN, D. L., JOHNSON, R. E. & AHMED, S. S. (2010). Determination of the influence of primary drying rates on the microscale structural attributes and physicochemical properties of protein containing lyophilized products. *Journal of Pharmaceutical Sciences*, 99, 4616-29.

- PASSOT, S., TRELEA, I. C., MARIN, M., GALAN, M., MORRIS, G. J. & FONSECA, F. (2009). Effect of controlled ice nucleation on primary drying stage and protein recovery in vials cooled in a modified freeze-dryer. *Journal of Biomechanical Engineering*, 131, 074511.
- PATAPOFF, T. W. & OVERCASHIER, D. E. (2002). The Importance of Freezing on Lyophilization Cycle Development. *BioPharm*, 16-20.
- PATEL, S. & PIKAL, M. (2011). Emerging Freeze-Drying Process Development and Scale-up Issues. *AAPS PharmSciTech*, 12, 372-378.
- PATEL, S. M., DOEN, T. & PIKAL, M. J. (2010). Determination of end point of primary drying in freeze-drying process control. *AAPS PharmSciTech*, 11, 73-84.
- PETERSEN, A., SCHNEIDER, H., RAU, G. & GLASMACHER, B. (2006). A new approach for freezing of aqueous solutions under active control of the nucleation temperature. *Cryobiology*, 53, 248-57.
- PFIZER. (2011). *Zithromax iv U.S. Physician Prescribing Information* [Online]. Available: [http://www.pfizer.com/products/rx/rx\\_product\\_zithromax.jsp](http://www.pfizer.com/products/rx/rx_product_zithromax.jsp) [Accessed 4/09/11].
- PIETTE, M., EVRARD, B. & COIA, I. (2013). *Composition and method for treating Hpv*. WO patent publication WO/2013/010942 A1.
- PIKAL, M. J. (2007). Freeze drying. In: SWARBRICK, J. (ed.) *Encyclopaedia of Pharmaceutical Technology*. 3 ed. New York: Informa Healthcare.
- PIKAL, M. J., SHAH, S., ROY, M. L. & PUTMAN, R. (1990). The secondary drying stage of freeze-drying - drying kinetics as a function of temperature and chamber pressure. *International Journal of Pharmaceutics*, 60, 203-217.
- PRINZ, H. (2012). The Final Quality Approach for Freeze dried Products. *5th Annual International Conference on Lyophilization and Freeze Drying*. Bologna.
- PROTEIN SIMPLE. (2013). *MFI™ Technology Principle of Operation* [Online]. Available: [http://www.proteinsimple.com/mfi\\_technology.html](http://www.proteinsimple.com/mfi_technology.html) [01/02/13].
- PYNE, A., SURANA, R. & SURYANARAYANAN, R. (2002). Crystallization of mannitol below  $T_g$  during freeze-drying in binary and ternary aqueous systems. *Pharmaceutical Research*, 19, 901-908.
- QUANTACHROME INSTRUMENTS (2009). Multipycnometer MVP-D160-E Operating Manual P/N 05034 Rev C.
- QUISPE-CONDORI, S., SALDANA, M. D. A. & TEMELLI, F. (2011). Microencapsulation of flax oil with zein using spray and freeze drying. *Lwt-Food Science and Technology*, 44, 1880-1887.
- RAJ SURYANARAYANAN (1995). X-ray Powder Diffraction. In: BRITAIN, H. G. (ed.) *Physical characterization of pharmaceutical solids*. New York: Dekker.

- RAMBHATLA, S., RAMOT, R., BHUGRA, C. & PIKAL, M. (2004). Heat and mass transfer scale-up issues during freeze drying: II. Control and characterization of the degree of supercooling. *AAPS PharmSciTech*, 5, e58.
- RANDALL, C. S. (1995). Particle Size Distribution. In: BRITTAIN, H. G. (ed.) *Physical characterization of pharmaceutical solids*. New York: Dekker.
- RATHORE, N. & RAJAN, R. S. (2008). Current perspectives on stability of protein drug products during formulation, fill and finish operations. *Biotechnology Progress*, 24, 504-514.
- RATTI, C. (2001). Hot air and freeze-drying of high-value foods: a review. *Journal of Food Engineering*, 49, 311-319.
- RELYEA, H. A., VRTIS, J. M., WOODYER, R., RIMKUS, S. A. & VAN DER DONK, W. A. (2005). Inhibition and pH dependence of phosphite dehydrogenase. *Biochemistry*, 44, 6640-9.
- REY, L. & MAY, J. C. (eds.) (1999). *Freeze-drying/lyophilization of pharmaceutical and biological products*, New York: Marcel Dekker.
- ROY, M. L. & PIKAL, M. J. (1989). Process control in freeze drying: determination of the end point of sublimation drying by an electronic moisture sensor. *Journal of Parenteral Science and Technology*, 43, 60-6.
- RUPPEL, J., MULLER, A. K., ALTHAUS, G., DREXEL, C. P. & ZIMMERMANN, I. (2009). The modified outflow funnel - A device to assess the flow characteristics of powders. *Powder Technology*, 193, 87-92.
- SADIKOGLU, H. & LIAPIS, A. I. (1997). Mathematical Modelling of the Primary and Secondary Drying Stages of Bulk Solution Freeze-Drying in Trays: Parameter Estimation and Model Discrimination by Comparison of Theoretical Results With Experimental Data. *Drying Technology*, 15, 791-810.
- SANOPI PASTEUR SA. (2013a). *Heating device for rotary drum freeze-dryer*. WO patent publication WO/2013/050158.
- SANOPI PASTEUR SA. (2013b). *Process line for the production of freeze-dried particles*. wo patent publication WO/2013/050162A1.
- SANOPI PASTEUR SA. (2013c). *Rotary drum freeze-dryer*. WO patent publication WO/2013/050160A1.
- SARCIAUX, J. M., ACAR, L. & SADO, P. A. (1995). Using microemulsion formulations for oral-drug delivery of therapeutic peptides. *International Journal of Pharmaceutics*, 120, 127-136.
- SARCIAUX, J. M., MANSOUR, S., HAGEMAN, M. J. & NAIL, S. L. (1999). Effects of buffer composition and processing conditions on aggregation of bovine IgG during freeze-drying. *Journal of Pharmaceutical Sciences*, 88, 1354-1361.

- SCHERER LTD. (1994). *Improved method for manufacturing freeze dried dosages in a multilaminate blister pack*. WO patent publication WO/1994/012142.
- SCHERSCH, K., BETZ, O., GARIDEL, P., MUEHLAU, S., BASSARAB, S. & WINTER, G. (2010). Systematic investigation of the effect of lyophilizate collapse on pharmaceutically relevant proteins I: Stability after freeze-drying. *Journal of Pharmaceutical Sciences*, 99, 2256-2278.
- SCHIFFTER, H., CONDLIFFE, J. & VONHOFF, S. (2010). Spray-freeze-drying of nanosuspensions: the manufacture of insulin particles for needle-free ballistic powder delivery. *Journal of the Royal Society Interface*, 7 Suppl 4, S483-500.
- SCHNEIDER, L. C. R., SINKA, I. C. & COCKS, A. C. F. (2007). Characterisation of the flow behaviour of pharmaceutical powders using a model die-shoe filling system. *Powder Technology*, 173, 59-71.
- SCHOLZ, E. (1981). Karl-fischer-reagents without pyridine - the accuracy of the determination of water. *Fresenius Zeitschrift Fur Analytische Chemie*, 306, 394-396.
- SCHWEDES, J. (2003). Review on testers for measuring flow properties of bulk solids (based on an IFPRI-Report 1999). *Granular Matter*, 5, 1-43.
- SEARLES, J. A., CARPENTER, J. F. & RANDOLPH, T. W. (2001a). Annealing to optimize the primary drying rate, reduce freezing-induced drying rate heterogeneity, and determine T(g)' in pharmaceutical lyophilization. *Journal of Pharmaceutical Sciences*, 90, 872-87.
- SEARLES, J. A., CARPENTER, J. F. & RANDOLPH, T. W. (2001b). The ice nucleation temperature determines the primary drying rate of lyophilization for samples frozen on a temperature-controlled shelf. *Journal of Pharmaceutical Sciences*, 90, 860-71.
- SHAH, R. B., TAWAKKUL, M. A. & KHAN, M. A. (2008). Comparative evaluation of flow for pharmaceutical powders and granules. *AAPS PharmSciTech*, 9, 250-8.
- SHAH, S. P. & MISRA, A. (2004). Development of liposomal amphotericin B dry powder inhaler formulation. *Drug Delivery*, 11, 247-253.
- SIGMA-ALDRICH. (2012). *Enzymatic Assay of L-Lactic Dehydrogenase (EC 1.1.1.27)* [Online]. Available: <http://www.sigmaaldrich.com/technical-documents/protocols/biology/enzymatic-assay-of-lactic-dehydrogenase.html> [Accessed 28/05/12].
- SKYSCAN. (2011). *Ctan Structural Parameters for Software version 1.0 Revised 5Th November 2011*. [Online]. Available: <http://www.skyscan.be/products/downloads.htm> [Accessed 16/01/12].
- SMITH, P. K., KROHN, R. I., HERMANSON, G. T., MALLIA, A. K., GARTNER, F. H., PROVENZANO, M. D., FUJIMOTO, E. K., GOEKE, N. M., OLSON, B. J. &

- KLENK, D. C. (1985). Measurement of Protein Using Bicinchoninic Acid. *Analytical Biochemistry*, 150, 76-85.
- SP SCIENTIFIC. (2014a). *AdVantage 2.0 BenchTop Freeze Dryer / Lyophilizer* [Online]. Available: [http://www.spscientific.com/Products/Freeze\\_Dryers/\\_Lyophilizers/VirTis/Bench\\_Top\\_Lyophilizers/AdVantage\\_2\\_0\\_BenchTop\\_Freeze\\_Dryer/](http://www.spscientific.com/Products/Freeze_Dryers/_Lyophilizers/VirTis/Bench_Top_Lyophilizers/AdVantage_2_0_BenchTop_Freeze_Dryer/) [Accessed 7/02/14].
- SP SCIENTIFIC. (2014b). *Hull Production Freeze Dryer / Lyophilizer* [Online]. Available: [http://www.spscientific.com/Products/Freeze\\_Dryers/Lyophilizers/Hull/1\\_Clinical\\_Production\\_Lyophilizers/Hull\\_Production\\_Freeze\\_Dryer/](http://www.spscientific.com/Products/Freeze_Dryers/Lyophilizers/Hull/1_Clinical_Production_Lyophilizers/Hull_Production_Freeze_Dryer/) [Accessed 7/02/14].
- SP SCIENTIFIC. (2014c). *Lyophilizers & Commercial Freeze Dryers* [Online]. Available: [http://www.spscientific.com/ProductCategory/100/Lyophilizers\\_Commercial\\_Freeze\\_Dryers/](http://www.spscientific.com/ProductCategory/100/Lyophilizers_Commercial_Freeze_Dryers/) [Accessed 19/02/14].
- STANIFORTH, J. N. (1982). The effect of fractional charges on flow properties of direct compression tableting excipients. *International Journal of Pharmaceutics*, 11, 109-117.
- STANIFORTH, J. N. & AULTON, M. E. (2007). Powder flow. In: AULTON, M. E. (ed.) *Pharmaceutics: The design and manufacture of medicines*. 3 ed. London: Churchill livingstone.
- STRAMBINI, G. B. & GABELLIERI, E. (1996). Proteins in frozen solutions: Evidence of ice-induced partial unfolding. *Biophysical Journal*, 70, 971-976.
- SYMPATEC. (2013). Laser Diffraction Sensors [Online]. Available: <http://www.sympatec.com/EN/LaserDiffraction/LaserDiffraction.html> [Accessed 18/08/13].
- TANG, X. & PIKAL, M. J. (2004). Design of freeze-drying processes for pharmaceuticals: practical advice. *Pharm Res*, 21, 191-200.
- TELSTAR (2010). Isolated lyophilizer loading/unloading system for bulk product. *Pharmaceutical Processing*, 58-60.
- TELSTAR. (2012). *Telstar develops three integrated production lines for Hisun of China Manufacturing Chemist*. [Online]. Available: [http://www.manufacturingchemist.com/news/article\\_page/Telstar\\_develops\\_three\\_integrated\\_production\\_lines\\_for\\_Hisun\\_of\\_China/80787](http://www.manufacturingchemist.com/news/article_page/Telstar_develops_three_integrated_production_lines_for_Hisun_of_China/80787) [Accessed 5/12/13].
- THALBERG, K., LINDHOLM, D. & AXELSSON, A. (2004). Comparison of different flowability tests for powders for inhalation. *Powder Technology*, 146, 206-213.
- TORRADO, S. (2002). Characterization of physical state of mannitol after freeze-drying: Effect of acetylsalicylic acid as a second crystalline cosolute. *Chemical & Pharmaceutical Bulletin*, 50, 567-570.

- TRAPPLER, E. H. (2007). Freeze drying, Scale-Up Considerations. In: SWARBRICK, J. (ed.) *Encyclopaedia of Pharmaceutical Technology*. 3 ed. New York: Informa Healthcare.
- TSI. (2014). *Aero-flow automated powder flowability analyzer 3250* [Online]. Available: <http://www.tsi.com/aero-flow-automated-powder-flowability-analyzer-3250/> [Accessed 10/05/14].
- UMRATH, W. (2007). *Fundamentals of Vacuum Technology*. Cologne: Oerlikon Leybold vacuum.
- VASILENKO, A., GLASSER, B. J. & MUZZIO, F. J. (2011). Shear and flow behavior of pharmaceutical blends - Method comparison study. *Powder Technology*, 208, 628-636.
- VISIONGAIN (2011). *Lyophilisation for pharmaceuticals: technology and services market 2011-2021*. London.
- WALTON, O. R., DE MOOR, C. P. & GILL, K. S. (2007). Effects of gravity on cohesive behavior of fine powders: implications for processing Lunar regolith. *Granular Matter*, 9, 353-363.
- WALTERS, R. H., BHATNAGAR, B., TCHESALOV, S., IZUTSU, K.-I., TSUMOTO, K. & OHTAKE, S. (2014). Next Generation Drying Technologies for Pharmaceutical Applications. *Journal of Pharmaceutical Sciences*, 103, 2673-2695.
- WANG, W. (2000). Lyophilization and development of solid protein pharmaceuticals. *International Journal of Pharmaceutics*, 203, 1-60.
- WARD, K. (2010). *Lyophilisation Technology Product and Process Training Course Book*. Winchester: Biopharma Technology Limited.
- WASHINGTON, C. (1992). *Particle size analysis in pharmaceuticals and other industries: theory and practice*. New York: Ellis Horwood.
- WEBB, S. D., CLELAND, J. L., CARPENTER, J. F. & RANDOLPH, T. W. (2003). Effects of annealing lyophilized and spray-lyophilized formulations of recombinant human interferon-gamma. *Journal of Pharmaceutical Sciences*, 92, 715-729.
- WEBB, S. D., GOLLEDGE, S. L., CLELAND, J. L., CARPENTER, J. F. & RANDOLPH, T. W. (2002). Surface adsorption of recombinant human interferon-gamma in lyophilized and spray-lyophilized formulations. *Journal of Pharmaceutical Sciences*, 91, 1474-1487.
- WENDE, A. & JESZORSKI, M. (2011). *Process for the preparation of essentially spherical lyophilisates*. WO patent publication EP2011/055476.
- WIECHELMAN, K. J., BRAUN, R. D. & FITZPATRICK, J. D. (1988). Investigation of the bichinchonic acid protein assay - identification of the groups responsible for color formation. *Analytical Biochemistry*, 175, 231-237.

- WILLIAMS, J. C. (ed.) (1990). *The storage and flow of powders*. Chichester: John Wiley & sons Ltd.
- WILSON, J. S. (2005). *Sensor Technology Handbook*. Elsevier.
- WOOD, R. (2000). *Lyophilisation Technology Training Course Part 1*. Winchester: Biopharma Technology Limited.
- XU, Y., GROBELNY, P., VON-ALLMEN, A., KNUDSON, K., PIKAL, M., CARPENTER, J. F. & RANDOLPH, T. W. (2014). Protein Quantity on the Air–Solid Interface Determines Degradation Rates of Human Growth Hormone in Lyophilized Samples. *Journal of Pharmaceutical Sciences*, 103, 1356-1366.
- YANG, S. & EVANS, J. R. G. (2007). Metering and dispensing of powder; the quest for new solid freeforming techniques. *Powder Technology*, 178, 56-72.
- YANG, S., YUAN, W. & JIN, T. (2009). Formulating protein therapeutics into particulate forms. *Expert Opinion on Drug Delivery*, 6, 1123-1133.
- YOUXUE, Z. & ZHENGJIU, X. (1995). Atomic radii of noble gas elements in condensed phases. *American Mineralogist*, 80, 670-675.
- YU, L., MILTON, N., GROLEAU, E. G., MISHRA, D. S. & VANSICKLE, R. E. (1999). Existence of a mannitol hydrate during freeze-drying and practical implications. *Journal of Pharmaceutical Sciences*, 88, 196-198.
- ZINGLE, R. & GEORGE, N. (1997). *Vented vial stopper for processing freeze dried products*. US patent publication 5596814.
- ZOU, W., HUNTER, N. & SWAIN, M. V. (2011). Application of polychromatic microCT for mineral density determination. *Journal of Dental Research*, 90, 18-30.

## Appendix I: Standard operating procedure for optimised method for IgG purification using caprylic acid fractionation.

### PRINCIPLE:



Figure A 1: Principle of IgG purification using caprylic acid fractionation.

**METHOD:** Caprylic acid precipitation and filtration based on the principle in (Figure A 1).

### REAGENTS:

- A. Caprylic Acid (n- Octanoic acid); **Sigma Product No. C5038.**
- B. Citric Acid, 99.6%, Anhydrous; **ACROS Organics Product No. 423565000.**
- C. Citric Acid trisodium salt, 99%, Dihydrate; **ACROS Organics Product No. 227135000.**
- D. 20 mM Citrate buffer solution pH 6.2.

(Prepare 10 L in deionised water using Reagent B and Reagent C; Mix 3868.63 mL of 7.74. mM solution of reagent C and 6131.37 mL of 12.26 mM Reagent B).

- E. 0.9 %w/v Saline solution.

(Prepare 2 L in deionised water using Sodium Chloride; **Sigma Product No. S7653**; *weigh 18g and make up to volume*).

- F. 0.1 M NaOH solution.

(Prepare 2L in deionised water using Sodium hydroxide pellets; **Sigma Product No.S5881**; *weigh 8g and make up to volume*).

### MATERIALS:

- 1. Ovine Sera supplied in 1L bottles; **MicroPharm UK.**

2. Glass microfibre filter, Whatman, GF/B 1.0  $\mu\text{m}$  retention, 90 mm; **VWR Product No. 513-5219.**
3. Membrane filter, cellulose acetate, 0.45  $\mu\text{m}$ , 47 mm, **Fischer Product No. FDM-309-110N.**
4. 30 kDa NMWCO (Nominal molecular weight cut off) filter, Kwick Lab packet, **GE Healthcare Product No. 56-4112-08.**

#### **APPARATUS:**

1. Kwick Packet holder, GE Healthcare Product No. 11-0006-70.
2. Peristaltic pump, Watson-Marlow.
3. 50 mL Centrifuge tubes, Polypropylene, Corning Incorporated Product No. 430829.
4. Centrifuge, Baird & Tatlock Mark IV.
5. Spectrometer, Jenway 6405UV/VIS .
6. Vortex-2, Genie, model G560E, Scientific Industries, USA.

#### **PROCEDURE:**

##### **A. SERUM FILTRATION AND CAPRYLIC ACID PRECIPITATION**

1. Thaw about 1 litre of sheep sera raised against Fluorescein Isothiocyanate (Anti-FITC) noting the date, sheep number and volume.
2. Using a suction pump, pre-filter each bottle through a GF/B glass microfibre filter and then filter through a 0.45  $\mu\text{m}$  cellulose acetate membrane filter into glass flask.
3. Weigh filtrate and record the following:
  - a. Weight of glass flask (g)
  - b. Weight of filtered serum + glass flask (g)
  - c. Total weight of filtered serum (g)
4. Take 5 mL aliquot of filtrate for storage in freezer.

5. Dilute the total weight of filtered serum from step 3c by 50% with 0.9 %w/v Saline solution by flashing through filter to recover serum proteins.
6. Record amount of saline added for dilution = 50% x total serum volume from step 3c.
7. Weigh and record the following :
  - a. Final weight of glass flask (g)
  - b. Serum + glass flask (g)
8. Calculate actual weight of saline added (7a-7b).
9. Weigh and add caprylic acid (Reagent A) at 6 %w/w of total weight of serum volume (step 3c). For example add 62.22g of caprylic acid for a 1037g of total weight of serum volume.
10. Note actual weight of caprylic acid added.
11. Vortex continuously for 30 minutes.
12. Record total weight:
  - a. Total weight = Total weight of filtered serum (step 3c) + actual weight of caprylic acid added (step 10) + actual weight of saline (Step 8)
13. Add a further amount of saline. This should be the same amount of saline previously added at step 8 after 30 minutes.
14. Note the following:
  - a. Weight of the expected final volume = Total volume (step 12) + Further amount of saline added (step 13)
  - b. Weight of actual volume added
15. Leave to stand for 1 hour.
16. Split into four or more equal weights into centrifuge tubes.
17. Centrifuge using an appropriate sized holder depending on volume of each split part (step 16) in a Baird & Tatlock Mark IV centrifuge for 60 minutes at 4000 rpm. No

refrigeration is required. Balance tubes in holders with a minimum of two and a maximum of six tubes.

18. Decant supernatant, pool and store at 2-8°C overnight in 1 litre plastic bottle.

19. Hold pellets at 2-8°C until completion of quantifying assay.

### **B. IgG FILTRATION AND FORMULATION IN CITRATE BUFFER**

1. Filter refrigerated supernatant of IgG (from procedure A) through a 0.45 µm filter.

2. A cross filtration set up as shown figure (Figure A 2) will be used. Use a 30 kDa NMWCO membrane filter in membrane cassette holder and perform a pre-treatment :

a. Washing and sanitising with 2L of 0.1 M NaOH for 30 minutes.

b. Flashing with 2L of 0.45 µm filtered purified water.

c. Flash with 2L of 20 mM citrate buffer solution. pH of retentate and permeate must be equal to 5.8-6.2.

3. Operate for 5minutes at 1 bar pressure and no retentate pressure.

4. Reduce flow and concentrate by applying retentate pressure. Keeping inlet pressure at 1bar.

5. Concentrate to 500 mL and diafilter IgG filt against ten 500 mL exchanges of 20 mM citrate buffer solution (Reagent C).

6. Measure pH of permeate after 10 volume exchanges which should read about 6.2

7. Flush with a further 500 mL of 20mM citrate buffer solution and record final weight.

8. Perform a 1:50 dilution by pipetting a 60 µL sample of the concentrated and diafiltered IgG solution and add 2940 µL of citrate buffer.



**Figure A 2: Set up for a Kwick cross filtration kit. Image was taken from instrument manual (GE Healthcare, 2011).**

9. Filter the 1:50 dilution using a 0.45  $\mu\text{m}$  filter and measure optical density ( $A_{280}$ ) at 280 nm with a Jenway spectrometer to estimate protein concentration. The use of a quartz cuvette is recommended.
10. With reference to step 9, dilution factor ( $D$ ) = 50 Use Beer Lambert Law  $A = \epsilon cl$   
Extinction coefficient = 1.5 L/mol/cm

**Table A 1: Measured absorbance and concentration**

Sample	$A_{280}$	Concentration (g/L)	Concentration x D (g/L)
1			
2			
3			
Average			

11. Using the concentration obtained from optical density reading, dilute concentrate to a lower known concentration and note new volume (For example from 28 g/L to 15g/l) and repeat step 9. This is to test for accuracy of optical density readings.
12. Store concentrated and diafiltered IgG over night at 2-8°C.
13. Filter product through a 0.45 µm filter into a sterile bottle and store at 2-8°C.
14. Disconnect Membrane filter and store in appropriate storage solution to prevent damage.

**REFERENCES:**

GE HEALTHCARE. (2011). Membrane Separations Quick Reference Guide 11-0003-81 AD [Online]. Available from [http:// www.gelifescience.com](http://www.gelifescience.com) [Accessed on 21/01/11].

CHERRY, C. (2010). Laboratory book extract. MicroPharm Limited. Wales. UK.

## Appendix II: Standard operating procedure for porosity investigation using helium pycnometry.

### PRINCIPLE:

True density of a sample can be measured by measuring the pressure difference as a result of allowing a known quantity of helium to flow from a precisely known reference volume (VR) into a sample cell. Based on the Archimedes principle of fluid displacement, gas pycnometry measures the particle density (the closest possible to measuring true density) of a sample. The choice of helium as the displacement gas is due to its small atomic dimension which allows open pores approaching one Angstrom to be investigated.

### APPARATUS:

Multipycnometer, Quantachrome instruments, Model number MUP- 6DCE.

### PROCEDURE:

#### A. Particle density



Figure A 3: Photograph of the front panel of multipycnometer (Quantachrome instruments, Model number MUP- 6DCE). Labels A-K corresponds to operation procedure outlined below and is in brackets next to applicable procedure.

NOTE:

Before using the multi pycnometer (Figure A 3) ensure it has been calibrated. To calibrate pycnometer, use the supplied standard calibration spheres. Decontaminate the sample with 10 cycles of helium gas if necessary.

1. Ensure pycnometer is plugged in at the mains and connected to a helium gas cylinder feed.
2. Open the helium gas feed to about 1 bar pressure by turning the regulator knob on the gas cylinder anticlockwise.
3. Turn on the power switch (A) on the pycnometer and allow 15minutes for the pressure transducer to warm up and stabilize.
4. Turn selector valve anticlockwise to "Cell". Using the front panel guide (H) select the desired reference cell volume by closing or opening the toggle valves I and II (I). For example to select the micro reference cell, close both toggle valves I and II.
5. Weigh by difference the sample powder to be analysed into a corresponding sample cell as chosen in step 4. Make sure it is filled to the brim but allow about 1 cm from the brim to allow for easy transfer using forceps in pycnometer kit.
6. Open cover of sample cell holder and insert sample cell into sample cell holder. Use the two white guide marks (C) on cell cover and brim of cell holder to align and properly close cell holder.
7. Raise the "GAS OUT" toggle valve (K) and turn "GAS OUT RATE" valve (J) anticlockwise to open. Wait for a stable zero reading on the display.
8. Adjust reading to zero after stabilising if necessary by turning the zero knob (G).
9. Turn the selector valve (D) to "REF".
10. Raise the "GAS IN" toggle valve (F) and turn "GAS IN RATE" valve (E) anticlockwise to open gas feed. Pressurise to approximately 17 PSIG and close toggle valve to stop flow.
11. Record the pressure displayed as " P1"

12. Turn the selector valve to "CELL".
13. Allow reading to stabilize and record as "P2"
14. Vent the pressure slowly to avoid blowing powder out of cell by raising the "GAS OUT" toggle valve (K) and turning "GAS OUT RATE" valve (J) anticlockwise to open.
15. Repeat steps 5-14 twice.
16. Remove sample cell holder and replace cover as specified in step 6.
17. Turn off pycnometer using the front panel button (A), turn off gas supply at the cylinder valve and turn off pycnometer at the mains.

### CALCULATIONS

Perform calculations manually using the operation equation below and reference values in Table A 3 or using the excel spread sheet file "Helium Pycnometry Template" (See Table A 2) located on electronic file C:\Users\ekenleep\Documents\Aston PhD\Lab work\Pycnometry.

**Table A 2: Helium Pycnometry sample spread sheet**

Date: Sample ID: Reference Cell: Sample cell:			Lab book page:	
Weight (g)	P1	P2	Vp (cm <sup>3</sup> )	Particle density (g/cm <sup>3</sup> )
			Mean	
			S.D.	

**Table A 3: Reference volumes of multipycnometer: Micro cell volume, small cell volume and large reference volumes are reference compartments inside the pycnometer.**

Parameter	Volume (cm <sup>3</sup> )
Micro cell volume	12.030
Micro reference volume	6.397
Small sample cell volume	29.439
Small reference volume	11.578
Large sample cell volume	148.946
Large reference volume	88.685

$$\text{Operating equation: } V_p = V_c - V_r \left( \left( \frac{P_1}{P_2} \right) - 1 \right)$$

A.1

Where:

*P1= Pressure reading after pressurising the reference volume (psig)*

*P2 = Pressure reading after including Vc (psig)*

*Vp = Volume of powder (cm<sup>3</sup>)*

*Vc = Volume of sample cell (cm<sup>3</sup>)*

*Vr = Reference Volume (cm<sup>3</sup>)*

Example

If the small sample cell is used, Volume of powder =  $29.439 - \left( 11.578 \left( \left( \frac{P_1}{P_2} \right) - 1 \right) \right)$

## REFERENCES

QUANTACHROME INSTRUMENTS. (2009). Multipycnometer MVP-D160-E Operating Manual P/N 05034 Rev C.

## Appendix III: Standard operating procedure for lactate dehydrogenase (LDH) enzymatic assay.

### PRINCIPLE:

Time and cost savings associated with the UV method of quantifying proteins or enzymes makes it a widely used in literature alongside its high specificity, simple sample preparation, ease of measurement, high sensitivity and precision (Henniger, 2003).

In the presence of NADH (Reduced Nicotinamide Adenine Dinucleotide) and LDH, Pyruvate is converted to lactic acid (Figure A 4). From measuring absorbance at 340 nm, the amount of NADH consumed can be used to quantify amount of LDH present (Krieg *et al.*, 1967, Grant, 2010).

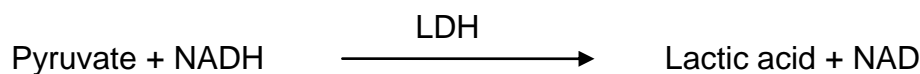


**Figure A 4: Principle of LDH enzymatic assay**

One unit will reduce 1.0  $\mu\text{mole}$  of pyruvate to L-Lactate per minute (Sigma-Aldrich, 2012).

**CONDITIONS:** T = 37°C, pH = 7.4 Wave length = 340 nm, light path length = 1 cm.

**METHOD:** UV absorbance kinetic run determination.

### REAGENTS:

A. Sodium Phosphate monobasic monohydrate **Acros Product No. 207802500.**

(Prepare 0.1 M 200 mL in deionised water using Sodium monobasic monohydrate (mw = 137.99 g/mol); Acros Product No. 207802500; *weigh 2.7598 g and make up to volume*).

B. Sodium Phosphate Dibasic **Sigma product No. S9763.**

(Prepare 0.1 M 200 mL in deionised water using Sodium phosphate dibasic (mw = 141.96 g/mol); Sigma product No. S7907; *weigh 2.8392g and make up to volume*).

C. 100mM Sodium phosphate buffer (SPB) solution pH 7.4.

(Prepare 100mL in deionised water using 19 mL of 0.1 M sodium Phosphate monobasic monohydrate (Reagent A) and 81 mL of 0.1 M Sodium phosphate dibasic (Reagent B solutions).

D. Lactate Dehydrogenase 29.9U, **VWR Product No. A7979001**.

(Weigh 0.001g and make up to 25 mL Volume. Expected activity is 1.196 U/mL.)

E. NADH Fischer Product No. BPE9747500.

**(Only freshly prepared solution should be used for assay. Prepare 0.5 mg/mL weighing 0.005 g and make to 10 mL volume).**

F. Sodium pyruvate Fischer Product No. BP356-100.

(Prepare 10 mg/mL in 100mM sodium phosphate buffer solution (Reagent C) by weighing 0.25g and making to 25 mL volume).

#### **APPARATUS:**

1. UV plate reader, Multiskan Spectrum, Thermo scientific.
2. 96 clear round bottom well plates, **Fischer product FB56412**.

**PROCEDURE:**

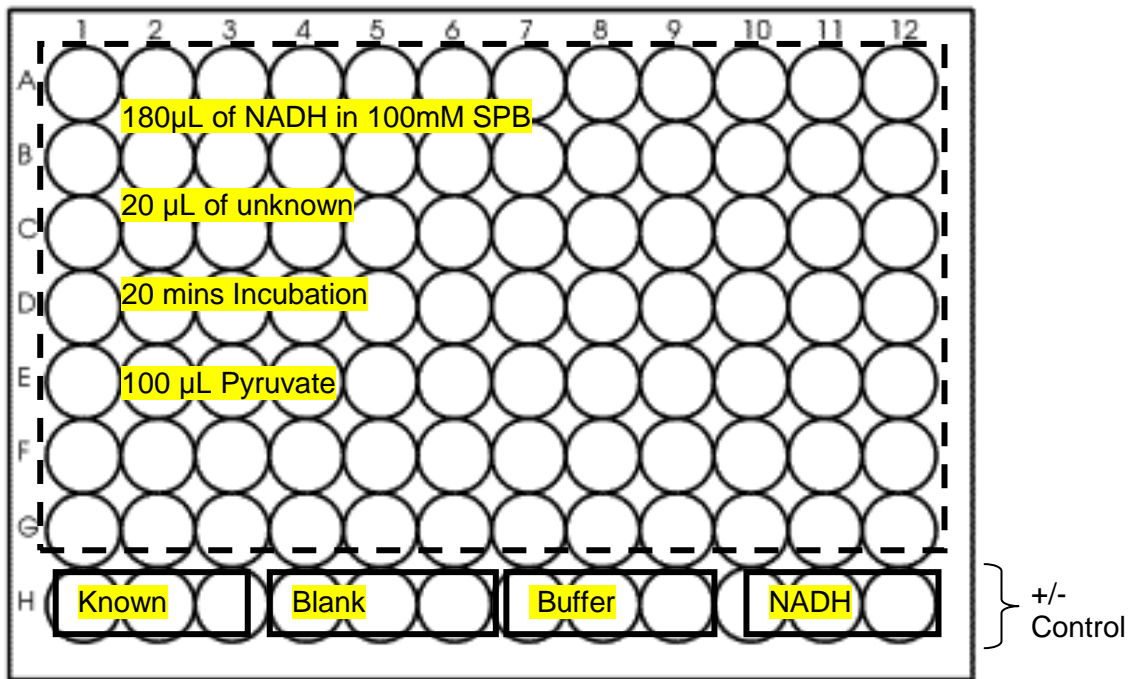


**Figure A 5:** Flat bottom 96 well clear plate (400  $\mu$ L volume) set up for determination of 28 unknowns. [ ] Contains 180  $\mu$ L of prepared NADH (reagent). +/- controls are contained in [ ]

1. Reconstitute unknown lyophilised sample to original or desired volume with distilled water. Dilute 50% of the resulting solution with equal amount of 100mM SPB (Reagent C). Thus making a 1:2 dilution.
2. Pipette the following amounts of Reagents into specified wells (Figure A 5).

Reagent	Volume ( $\mu$ L)	Well
F (NADH)	180	A1-G12 H10-H12
C (SPB)	200	H7-H9
E (LDH)	20	H1-H3

3. Pipette 20  $\mu$ L of unknown sample into Wells A1-G12.
4. Leave to incubate for 20 minutes to allow LDH to uniformly mix with NADH.

5. Pipette 100  $\mu\text{L}$  of sodium pyruvate (Reagent A) into all unknown and known sample wells to initiate reaction.
6. Measure absorbance at intervals of 30 seconds over 20 minutes.

### **CALCULATION**

$$\text{Concentration (M)} = \left( \frac{\text{Change in absorbance at 340 nm per minute}}{\text{Extinction co efficient}} \right) \times \text{Df} \quad (\text{A.2})$$

Dilution factor = 2

Extinction coefficient of NADH =  $6.2 \text{ mM}^{-1}\text{cm}^{-1}$  (Relyea *et al.*, 2005). This is best determined from a calibration curve. Calculate the amount in total volume of assay (0.003 mL).

### **REFERENCES**

- GRANT, Y. (2010). Engineering the rational design and optimisation of lyophilization processes for biological materials. Doctor of Engineering, University College London.
- HENNIGER, G. (2003). Enzymatic Techniques for Authenticating Food Components. In: LEES, M. (ed.) Food Authenticity and Traceability. Cambridge: Woodhead Publishing Limited.
- KRIEG, A. F., ROSENBLUM, L. J. & HENRY, J. B. (1967). Lactate dehydrogenase isoenzymes a comparison of pyruvate-to-lactate and lactate-to-pyruvate assays. *Clinical chemistry*, 13, 196-203.
- RELYEA, H. A., VRTIS, J. M., WOODYER, R., RIMKUS, S. A. & VAN DER DONK, W. A. (2005). Inhibition and pH dependence of phosphite dehydrogenase. *Biochemistry*, 44, 6640-9.
- SIGMA-ALDRICH. (2012). Enzymatic Assay of L-Lactic Dehydrogenase (EC 1.1.1.27) [Online]. Sigma-Aldrich. Available: <http://www.sigmaaldrich.com/technical-documents/protocols/biology/enzymatic-assay-of-lactic-dehydrogenase.html> [Accessed 28/05/12 2012].

## Appendix IV: Standard operation procedure for optimisation of excitation and emission wave lengths for Anti-FITC IgG fluorescence quenching assay

### PRINCIPLE:

A very small Stokes shift if present requires that excitation and emission wave lengths in a fluorescence assay need to be optimised.

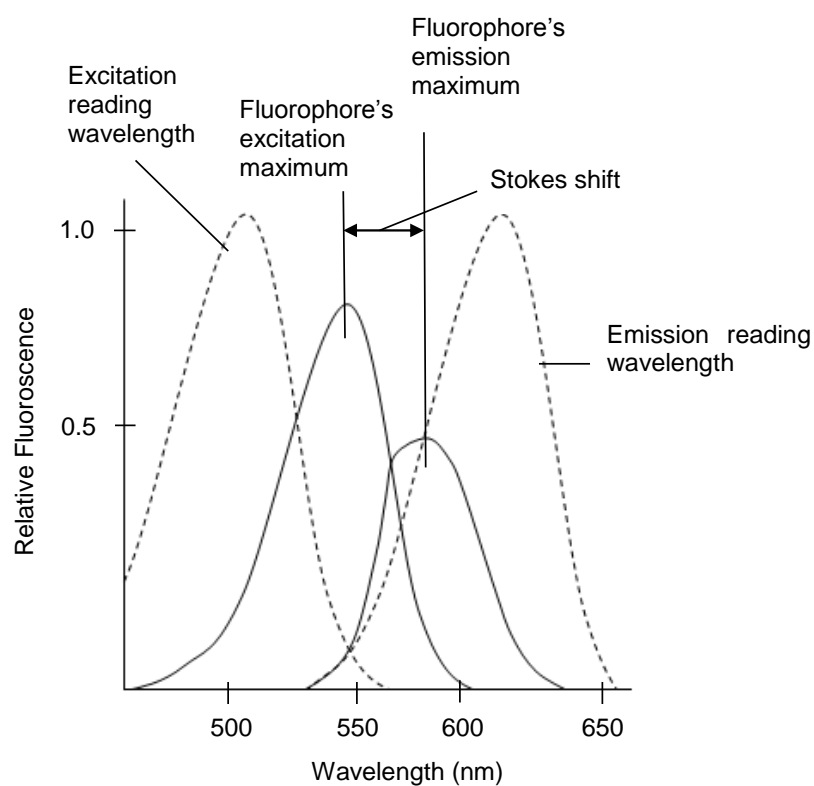


**Figure A 6: Optimised excitation and emission reading wavelengths. Image drawn from Molecular Devices Spectramax Gemini XS Operators Manual.**

In an assay, best results are obtained when the reading wave lengths are not the same wave lengths as that of the fluorophore. Separating the reading excitation and emission

wave lengths allow a smaller amount of excitation light to pass through the emission monochromator onto the photomultiplier tube.

#### **METHOD:**

Spectral scanning to optimise excitation and emission wavelengths.

#### **REAGENTS:**

A. 10mM sodium borate pH 9.2

(Prepare 1L in deionised water using sodium borate, Decahydrate; **Sigma Product No. S9640**; weigh 3.8137g and make up to volume)

B. Bovine gamma globulins, Sigma Product No. G7516-10G

C. Sodium Azide, Sigma Product No. S7653

ABC. Assay diluent buffer solution

(Prepare 10L in deionised water using Reagent A, B and C; weigh 10 mg each of B and C, dissolve in A)

D. Fluorescein sodium, Fluka analytical Product No. 46960

E. 0.01 M NaOH solution

(Prepare 50mL in deionised water using sodium hydroxide, **Sigma Product No. S5881**)

DE. 1 mM Fluorescein stock solution

(Prepare 20mL in Reagent E; Weigh 7.6 mg of Fluorescein (Reagent D) and make up to 20mL volume using 0.01 M NaOH solution (Reagent E).)

#### **APPARATUS:**

1. Fluorescence plate reader, Molecular Devices Gemini, USA.
2. Black 96 well plate, Greiner Product No. 655076

## PROCEDURE:

1. Pipette 10  $\mu$ L of sample and 190  $\mu$ L of 0.8mM fluorescein into well A1 of the 96 black well plate.
2. Pipette 200  $\mu$ L of assay diluent buffer into well B1.
3. Set up the following parameters on the fluorescence plate reader using the SOFTmax PRO software: Spectrum mode, Emission fixed/Ex scan, no cut-off filter and medium PMT (Photo multiplier tube) sensitivity.
4. Set emission wave length of fluorescence to 520 nm.
5. Set excitation wave scan to start and stop from 470 nm to 570 nm in step wise increments of 1 nm.
6. Perform the scan.
7. Note the excitation wave length at the emission peak and the maximum RFU (Relative fluorescence unit) value from the results obtained in step 6.
8. Select the optimum excitation wave length with minimum interference from the assay diluent buffer spectra. If the difference between excitation peak maximum and the emission wave length is less than 80 nm, use the shortest wave length corresponding to 90% of maximal emission.
9. Set up the following parameters on the fluorescence plate reader using the SOFTmax PRO software: Spectrum mode, Ex fixed/Em scan, no cut-off filter and medium PMT (Photo multiplier tube) sensitivity.
10. Set Excitation wave length to the optimum excitation wave length determined in step 8.
11. Set emission wave length scan to start and stop from 520 nm to 570 nm in a stepwise increments of 1 nm.
12. Perform scan and from results choose the wave length giving the maximum emission.

13. Repeat steps 9-12 using an emission cut off filter of 515 nm to block as much residual excitation light as possible without reducing the fluorescence signal.
14. Compare the spectra of the sample containing fluorescein to the spectra of the assay diluent buffer for an estimate of the signal to noise ratio. Repeat step 11 to choose another cut-off filter wave length of significant background noise still persists.
15. The optimum excitation and emission wave lengths are those chosen in step 8 and step 12.

## **GLOSSARY**

Cut-off: blockage of unwanted residual excitation light using filters to minimise background interference.

Emission fixed/Ex scan: Scan with desired emission wavelength kept constant while the excitation wave length is scanned in increments of specified wavelength.

Ex fixed/Em scan: Scan with desired excitation wavelength kept constant while the emission wave length is scanned in increments of specified wavelength.

PMT (Photo multiplier tube): vacuum tube that detects light. Its sensitivity can be set to low, medium and automatic.

## **REFERENCE**

MOLECULAR DEVICES CORPORATION. (2000). Spectramax<sup>®</sup> Gemini XS Operators Manual. Using Spectral scanning to optimise Excitation and emission wavelengths for fluorescence assays. Page 5-8.

## Appendix V: Standard operating procedure for fluorescence quenching assay for Anti FITC IgG.

### PRINCIPLE:

A fluorescence quenching assay offers a simple analytical method for quantifying proteins. When attached to a protein, fluorescein will fluoresce when exposed to an excitation wave length of 491 nm and subsequently emit at 520 nm. If present, Immunoglobulin G raised against fluorescein isothiocyanate (Anti-FITC IgG) will bind to fluorescein in solution and thus quench the fluorescence intensity of fluorescein present (Figure A 7).



**Figure A 7: Principle of Fluorescence quenching assay**

**CONDITIONS:** T = 25°C, Excitation wave length = 485 nm, Emission wave length= 520 nm

**METHOD:** Fluorescence kinetic run determination

### REAGENTS:

A. 10 mM sodium borate pH 9.2

(Prepare 1L in deionised water using sodium borate, Decahydrate; **Sigma Product No. S9640**; weigh 3.8137g and make up to volume)

B. Bovine gamma globulins, Sigma Product No. G7516-10G

C. Sodium Azide, Sigma Product No. S7653

ABC. Assay diluent buffer solution

(Prepare 1L in deionised water using Reagent A, B and C; weigh 1g each of B and C, dissolve in A)

D. Fluorescein sodium, Fluka analytical Product No. 46960

E. 0.01 M NaOH solution

(Prepare 200mL in deionised water using sodium hydroxide, **Sigma Product No. S5881**)

DE. 1 mM Fluorescein stock solution

(Prepare 20mL in Reagent E; Weigh 7.6 mg of Fluorescein (Reagent D) and make up to 20mL volume using 0.01 M NaOH solution (Reagent E).

#### **APPARATUS:**

1. Spectrometer, Jenway 6405UV/VIS
2. Fluorescence plate reader, Molecular Devices Gemini
3. Black 96 well plate, Greiner Product No. 655076

#### **PROCEDURE:**

1. Estimation of the concentration of fluorescein stock solution
1. Take a sample of 100  $\mu\text{L}$  of 1 mM fluorescein stock solution (Reagent DE) and dilute by a 100folds with 9900  $\mu\text{L}$  of 0.01 M NaOH (Reagent E).
2. Test absorbance using spectrophotometer at a wave length of 491 nm and calculate the concentration of fluorescein using published extinction co-efficient,  $\epsilon = 8.72 \times 10^4 \text{ L/mol/cm}$ .

From Beer Lamberts law, Concentration =  $(A/\epsilon) \times \text{dilution factor}$  Where dilution factor = 100

2. Determination of concentration of Anti-FITC IgG

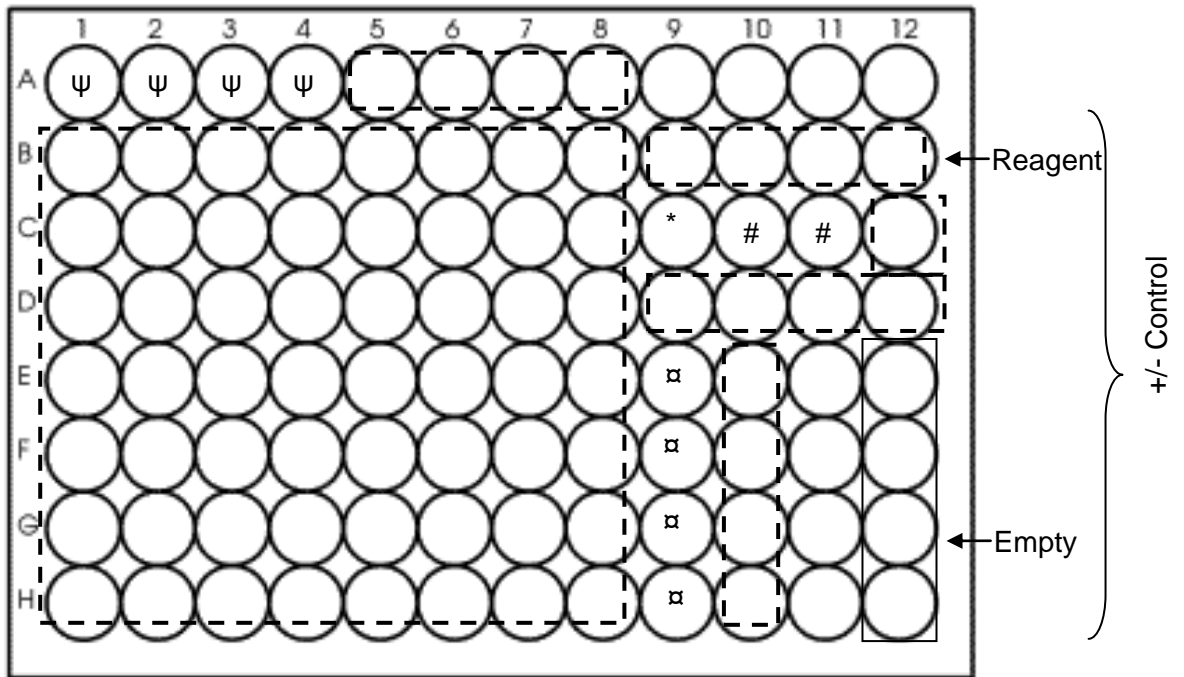


Figure A 8: Black flat bottom 96 well plate (400  $\mu\text{L}$  volume) set up for assay. [---] contains 200  $\mu\text{L}$  of reagent ABC,  $\alpha$  contains 380  $\mu\text{L}$  of reagent ABC,  $\psi$  contains 240  $\mu\text{L}$  of reagent ABC, \* contains 1  $\mu\text{M}$  reagent fluorescein, and # contains 30 nM reagent fluorescein.

1. Pipette the following amounts of assay diluent buffer (Reagent ABC) into the following wells:

Volume ( $\mu\text{L}$ )	Well
380	E9, F9, G9, H9
200	E10, F10, G10, H10, A5-A8, B1-B8 to H1-H2
240	A1-A4

2. Pipette 20  $\mu\text{L}$  of test sample into well E9, F9, G9 and H9.
3. Add 20  $\mu\text{L}$  of unknown sample to E9, F9, G9, H9 to make 20 in 400 i.e. 1: 100 dilution.

4. Pipette 200  $\mu\text{L}$  from E9 in to the adjacent well E10 (10  $\mu\text{L}$  of unknown sample in 400  $\mu\text{L}$  reagent ABC) and repeat for F9, G9 and H9.
5. Pipette 160  $\mu\text{L}$  from E10, F10, G10 and H10 into wells A1, A2, A3 and A4 respectively (4  $\mu\text{L}$  of unknown sample in 400  $\mu\text{L}$  of reagent ABC i.e. making 1:100 dilution)
6. Pipette 200  $\mu\text{L}$  from wells A1 to perform a 200  $\mu\text{L}$  serial dilution down to well H1. Repeat this step for wells A2-A8.
7. Dilute 0.8mM fluorescein (Reagent DE ; Concentration obtained from absorbance measurement) to 1  $\mu\text{M}$  (800times dilution) by taking 10  $\mu\text{L}$  and adding 7990  $\mu\text{L}$  assay diluents buffer (Reagent ABC).
8. Dilute the 1  $\mu\text{M}$  fluorescein solution to 30 nM by making up to volume in a 100mL volumetric flask with assay diluents buffer (Reagent ABC).
9. Add 100  $\mu\text{L}$  of the 30 nM fluorescein to all wells with serial dilutions of unknown sample.
10. Test for fluorescence at 5 minutes intervals for 2 hours using excitation 481 nm and emission 520 nm with 515 nm filter cut off.
11. Plot relative fluorescence intensity versus antibody sample dilutions and determine 50% fluorescence quenching (Figure A 9).

#### **CALCULATION:**

12. Find the final antibody sample dilution that corresponds to 50% quenching of the fluorescein. At this dilution, 5 nM fluorescein is bound to the antibody. Assuming antibody binding sites are saturated with fluorescein, the concentration of bivalent IgG antibody is 2.5 nM.

Molecular weight of Sheep IgG = 160 kDa

Estimated content of specific antibody = 2.5 nM x 160 kDa x dilution factor g/L

E.g. if at 50% quenching D = 1:5000 Then specific antibody = 2 g/L

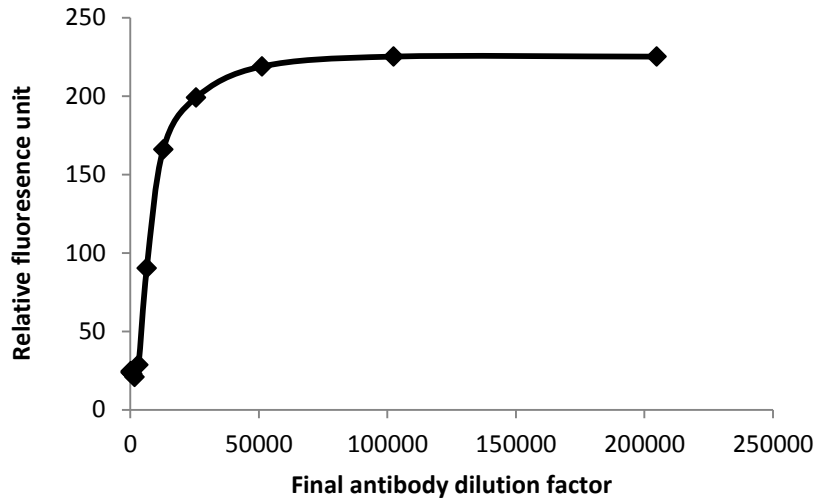


**Figure A 9: Typical fluorescence quenching curve showing specific antibody recovery after 120 minutes quenching.**

**REFERENCES:**

WALKER, D. (1987). A fluorescence technique for measurement of concentration in mixing liquids. *Journal of Physics E: Scientific Instruments*, 20, page 217.

CHERRY, C. (2010). *Laboratory book extracts*. MicroPharm Wales, UK.

## Appendix VI: Typical freeze drying cycle plot for samples studied

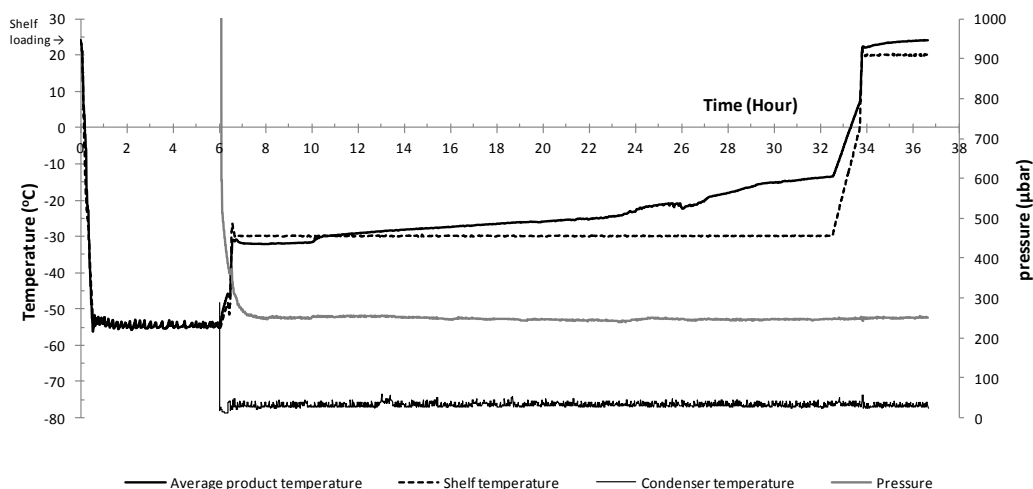
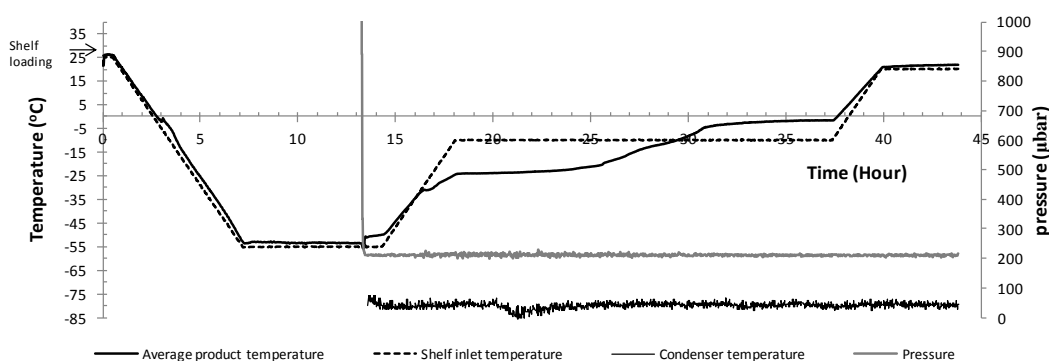
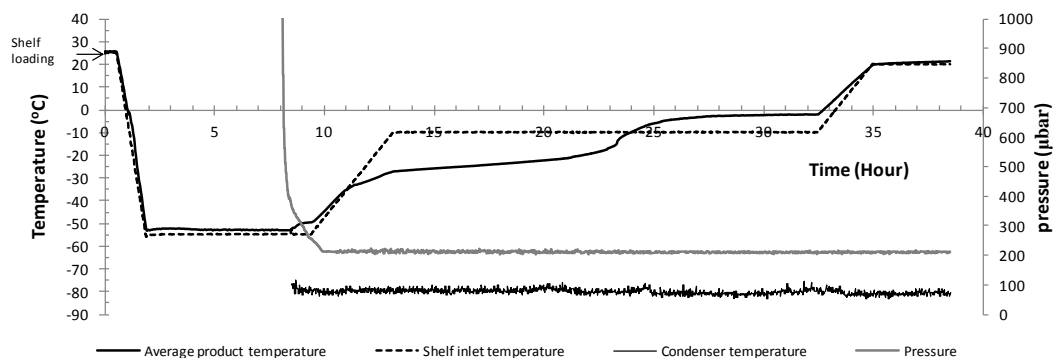


**Figure A 10: Typical thermogram from bulk freeze drying of 1 %w/v mannitol solution. 300mL sample volume was lyophilised in stainless steel tray. Product temperature was measured as an average reading from two k type thermocouples placed at the bottom centre and bottom edge.**



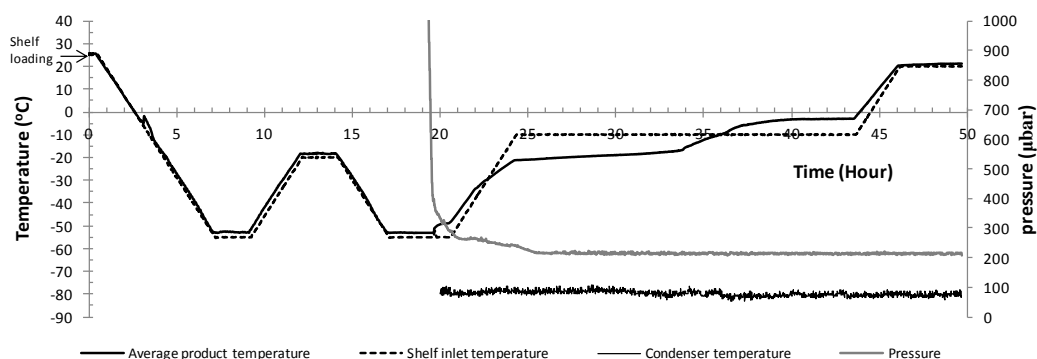
Batch:	0.5M Mannitol				
Fill Vol (ml):	100ml				
Recipe:	GE9				
Parameter	Cummulative time (Hours)	Target Temperature (°C)	Period in stage (hours)	Freezing rate (°C/min)	Pressure (µbar)
Equilibrim	0.5000	25	0.5000	H	-
Freezing	7.1667	-55	6.6667	0.2	-
	13.1667	-55	6.0000	H	-
Primary drying	14.1667	-55	1.0000	H	200
	17.9167	-10	3.7500	0.2	200
	37.1667	-10	19.2500	H	200
Secondary drying	39.6667	20	2.5000	0.2	200
	43.6667	20	4.0000	H	200
Post heat	43.8333	20	0.1667	H	200
				H=Holding	

**Figure A 11: Typical example of freeze drying process cycle of mannitol bulk lyophilised from 0.5 M mannitol solution. Formulation was cooled at 0.2 °C/min. Product temperature was measured as an average reading from two k type thermocouples placed at the bottom centre and bottom edge.**



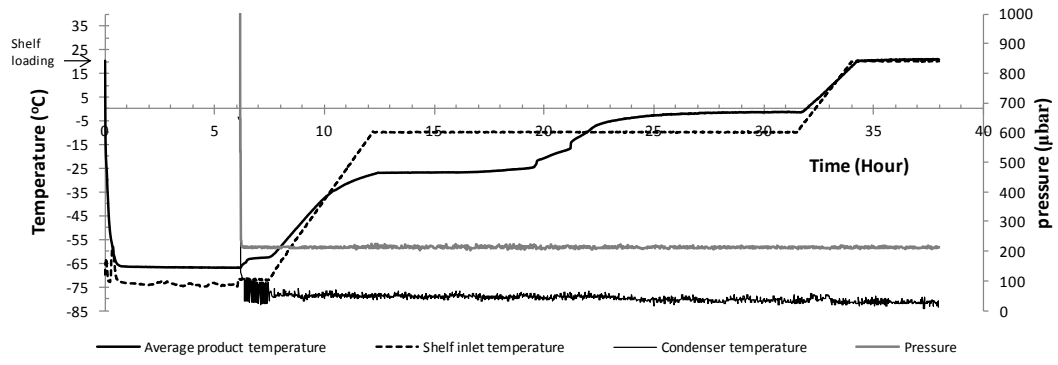
Batch:	0.5M mannitol				
Fill Vol (ml):	100ml				
Recipe:	HE79				
Parameter	Cummulative time (Hours)	Target Temperature (°C)	Period in stage (hours)	Freezing rate (°C/min)	Pressure (µbar)
Equilibrim	0.5000	25	0.5000	H	-
Freezing	1.8333	-55	1.3333	1	-
	7.8333	-55	6.0000	H	-
	8.8333	-55	1.0000	H	200
Primary drying	12.5833	-10	3.7500	0.2	200
	31.8333	-10	19.2500	H	200
Secondary drying	34.3333	20	2.5000	0.2	200
	38.3333	20	4.0000	H	200
Post heat	38.5000	20	0.1667	H	200
				H=Holding	

Figure A 12: Typical example of freeze drying process cycle of mannitol bulk lyophilised from 0.5 M mannitol solution. Formulation was cooled at 1 °C/min. Product temperature was measured as an average reading from two k type thermocouples placed at the bottom centre and bottom edge.



Batch:	0.5M Mannitol				
Fill Vol (ml):	100				
Recipe:	HE 65				
Parameter	Cummulative time (Hours)	Target Temperature (°C)	Period in stage (hours)	Freezing rate (°C/min)	Pressure (µbar)
Equilibrim	0.5000	25	0.5000	H	-
Freezing	7.1667	-55	6.6667	0.2	-
	9.1667	-55	2.0000	H	-
	12.0833	-20	2.9167	0.2	-
	14.0833	-20	2.0000	H	-
	17.0000	-55	2.9167	0.2	-
	19.0000	-55	2.0000	H	-
Primary drying	20.0000	-55	1.0000	H	200
	23.7500	-10	3.7500	0.2	200
	43.0000	-10	19.2500	H	200
Secondary drying	45.5000	20	2.5000	0.2	200
	49.5000	20	4.0000	H	200
Post heat	49.6667	20	0.1667	H	200
				H=Holding	

Figure A 13: Typical example of freeze drying process cycle of mannitol bulk lyophilised from 0.5 M mannitol solution. Formulation was cooled at 0.2 °C/min and annealed at -20°C (2 hours). Product temperature was measured as an average reading from two k type thermocouples placed at the bottom centre and bottom edge.



Batch:	0.056M Mannitol				
Fill Vol (ml):	100ml				
Recipe:	HE81R				
Parameter	Cummulative time (Hours)	Target Temperature (°C)	Period in stage (hours)	Freezing rate (°C/min)	Pressure (µbar)
Freezing	6.0000	-70	6.0000	H	-
Primary drying	7.0000	-70	1.0000	H	200
	12.0000	-10	5.0000	0.2	200
Secondary drying	31.2500	-10	19.2500	H	200
	33.7500	20	2.5000	0.2	200
Post heat	37.7500	20	4.0000	H	200
	37.9167	20	0.1667	H	200
				H=Holding	

**Figure A 14: Typical example of freeze drying process cycle of mannitol bulk lyophilised from 0.056 M mannitol solution loaded onto pre-cooled shelf.**

## Appendix VII: Freeze drying cycle plot for samples studied with x-ray microcomputer tomography.

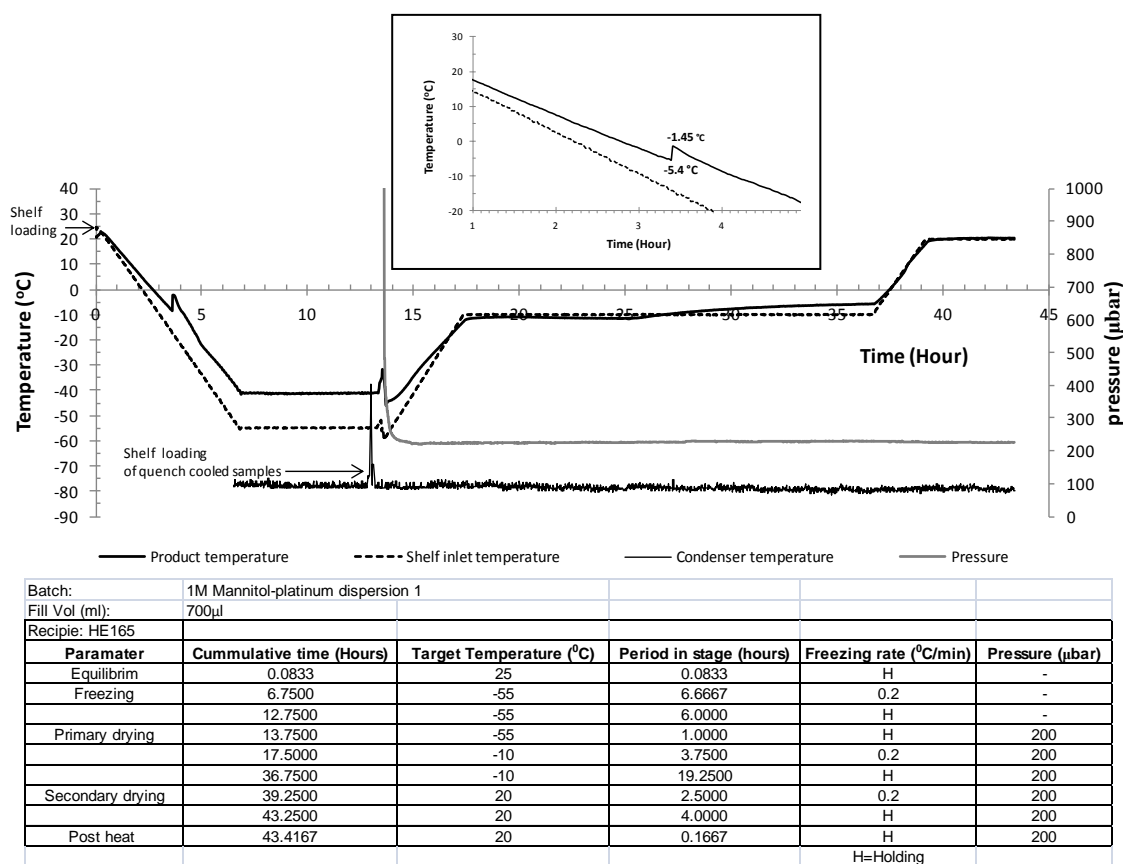
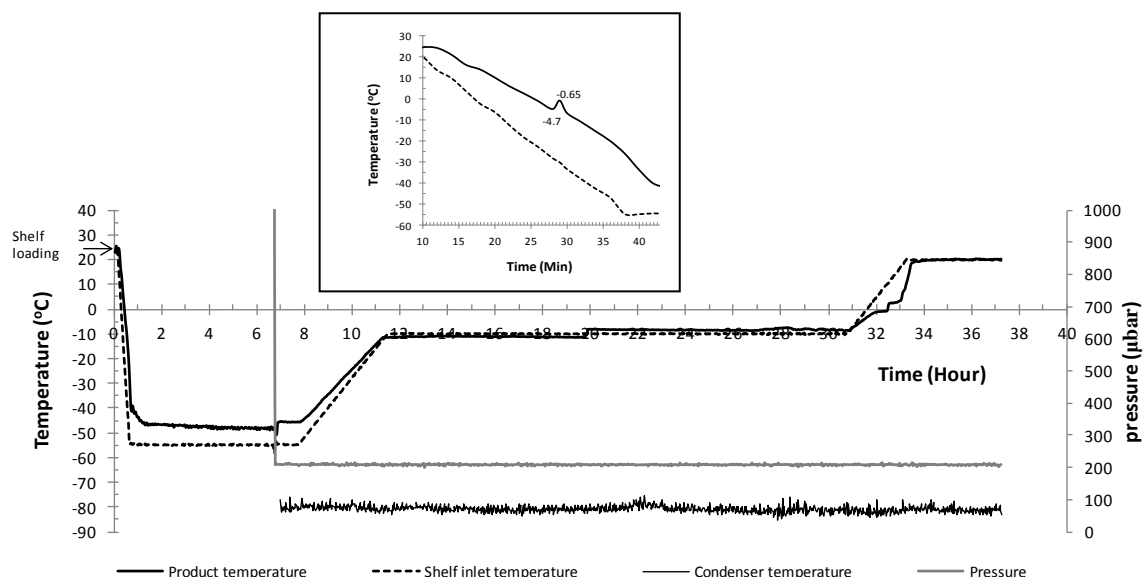


**Figure A 15: Thermograph of freeze dried 1 M mannitol-platinum dispersion 1. Insert: Magnification of observed nucleation event. 700 µL sample volume was freeze dried in straws for microcomputer tomography investigation. Product temperature was measured using a k type thermocouple.**



Batch:	1M Mannitol-platinum dispersion 2				
Fill Vol (ml):	700µl				
Recipe:	HE156R				
Parameter	Cumulative time (Hours)	Target Temperature (°C)	Period in stage (hours)	Freezing rate (°C/min)	Pressure (µbar)
Equilibrim	0.0833	25	0.0833	H	-
Freezing	0.5833	-55	0.5000	1.5	-
	6.5833	-55	6.0000	H	-
Primary drying	7.5833	-55	1.0000	H	200
	11.3333	-10	3.7500	0.2	200
	30.5833	-10	19.2500	H	200
Secondary drying	33.0833	20	2.5000	0.2	200
	37.0833	20	4.0000	H	200
Post heat	37.2500	20	0.1667	H	200
H=Holding					

**Figure A 16: Thermograph of freeze dried 1 M mannitol-platinum dispersion 2. Insert: Magnification of observed nucleation event. 700 µL sample volume was freeze dried in straws for microcomputer tomography investigation. Product temperature was measured using a k type thermocouple.**

## Appendix VIII: Typical MDSC thermographs form pre-formulation characterisation.

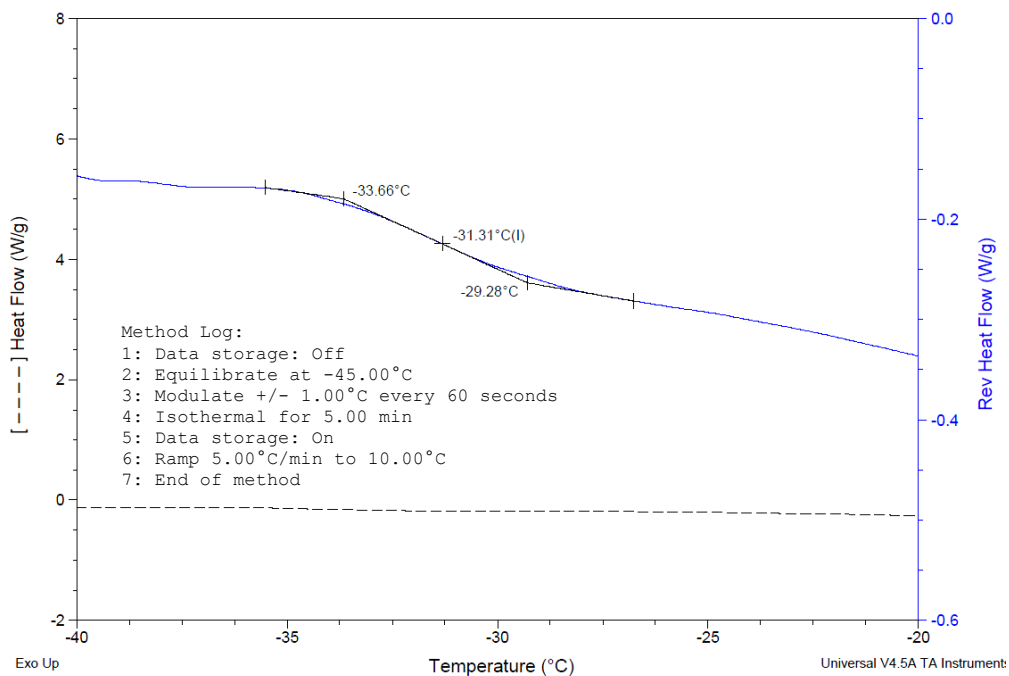
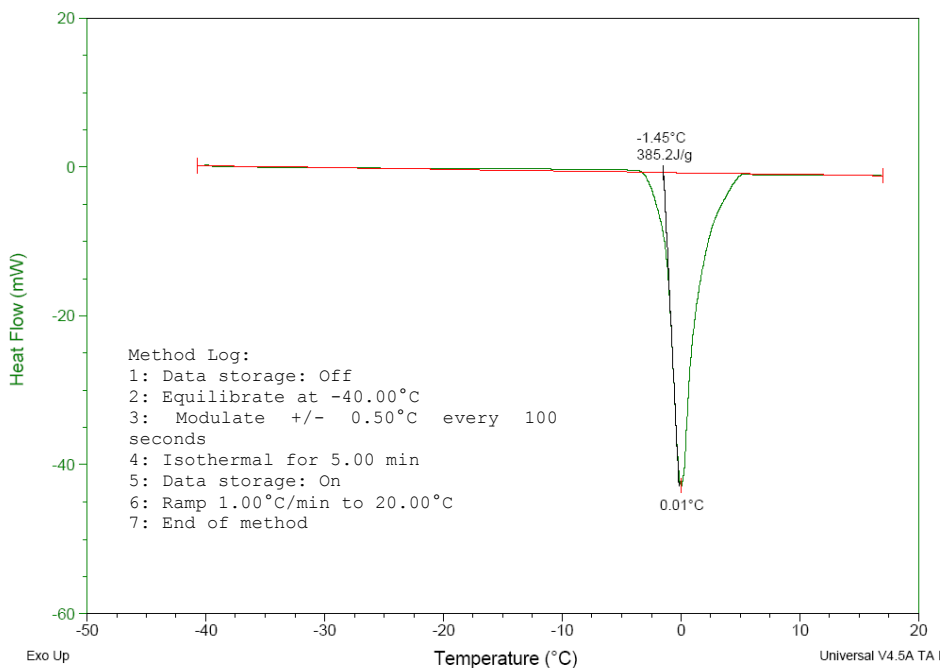


**Figure A 17: Typical MDSC thermographs. Top: 15 %w/v mannitol showing a eutectic melt ( $T_{eu}$ ) at -1.45°C. Bottom: 15% w/v sucrose showing a glass transition ( $T_g'$ ) at -31.31°C.**